MASTER IN CHEMISTRY RESEARCH FOCUS

Preparation, structural investigations and applications of functionalised boroxines as crosslinking nodes for self-healable polymers

WILLEMS, Antoine

Award date:
2022

Awarding institution:
University of Namur

Université de Namur

Faculté des Sciences

Preparation, structural investigations and applications of functionalised boroxines as crosslinking nodes for self-healable polymers

Mémoire présenté pour l'obtention

du grade académique de Master Chimie «Chimie du Vivant et des Nanomatériaux» : Finalité Approfondie

Antoine WILLEMS

Janvier 2022

UNIVERSITE DE NAMUR
Faculté des Sciences
Secrétariat du Département de Chimie
Rue de Bruxelles 61 – 5000 NAMUR
Téléphone : +32(0)81 72.54.44 – Téléfax : +32(0)81 72.54.40
E-mail : enseignement.chimie@unamur.be - www.unamur.be/sciences

Preparation, structural investigations and applications of functionalised boroxines as crosslinking nodes for self-healable polymers

WILLEMS Antoine

Résumé

Ce mémoire est basé sur un ensemble de trois aspects généraux s'appuyant sur l'acidité et la basicité de Lewis ainsi que sur la chimie du bore afin d'obtenir une plateforme dynamique pouvant convenir pour diverses applications telles que les matériaux polymères avec de nouvelles propriétés, des catalyseurs de Lewis très intéressants, etc. Tous ces nouveaux composés sont basés sur un motif identique qui est un cycle formé par la condensation d'acides boronique en une boroxine à la base de ces plateformes dynamiques.

Dans un premier temps, la synthèse de nouvelles boroxines et iminoboroxines a été établie sur des systèmes modèles. Grâce aux différents substituants présent sur le cycle aromatique et sur l'imine, nous modulons l'acidité de Lewis du bore ainsi que la basicité de l'imine modifiant dès lors la formation des adduits de Lewis au sein ces composés. Une étude via DRX, IR et RMN est réalisée donnant des indications sur le nombre d'adduits formés, les longueurs de liaisons et de la structure fine des différentes molécules. La réversibilité des liaisons B-O de ces boroxines coordonnées à l'azote a été vérifiée par hydrolyse et déshydratation dans des conditions douces.

Dans un second temps, ces iminoboronate jouent le rôle de nœuds de réticulation au sein du réseau polymérique PPG-boroxine. Ces nœuds répondent à l'humidité et la chaleur donnant des propriétés d'autoréparation au matériau reformant le polymère après dégradations. Un traitement thermique doux permet le remaniement des liaisons B-O et C=N durant la réparation.

Mémoire de master en Sciences Chimiques à Finalité approfondie

Janvier 2022

Promoteur: G. Berionni, J.-M. Raquez

UNIVERSITE DE NAMUR
Faculté des Sciences
Secrétariat du Département de Chimie
Rue de Bruxelles 61 – 5000 NAMUR
Téléphone : +32(0)81 72.54.44 – Téléfax : +32(0)81 72.54.40
E-mail : enseignement.chimie@unamur.be - www.unamur.be/sciences

Preparation, structural investigations and applications of functionalised boroxines as crosslinking nodes for self-healable polymers

WILLEMS Antoine

Abstract

This master thesis is based on three main aspects based on the Lewis acid/base and boron chemistry to obtain a dynamic platform which can be suitable for diverse applications such as polymeric materials with novels properties, highly interesting Lewis catalysts, macromolecule. All those new compounds are based on the same pattern which is basically a ring formed by the condensation of boronic acid into boroxine which is the building bloc of these dynamic platforms.

The synthesis of novel boroxine and iminoboroxines has been established as model systems. Based on the different substituents present on the aromatic ring and the imine, we modulated the Lewis acidity of the boron and the basicity of the imine modifying the Lewis adduct formation in these compounds. A study *via* XRD, IR and NMR analysis was performed giving clues for number of Lewis acid/base interactions present in the compound, bond lengths and fine structure of the different molecules. The reversibility of the B-O boroxine bonds has been verified with these nitrogen-coordinated dynamic platforms synthetized via hydrolysis and dehydration.

The application of these iminoboronate based boroxines as crosslinking nodes in a PPG-boroxine network previously designed is developed. These dynamic nodes respond to humidity exposure and heating giving self-healing properties to the material reforming the polymer after degradation. The B-O and C=N bond reshuffling are obtained by a mild thermal treatment giving encouraging results as an application for self-healable materials.

Mémoire de master en Sciences Chimiques à Finalité approfondie

Janvier 2022

Promoteur: G. Berionni, J.-M. Raquez

1. Résumé

Ce mémoire est basé sur un ensemble de trois aspects généraux s'appuyant sur l'acidité et la basicité de Lewis ainsi que sur la chimie du bore afin d'obtenir une plateforme dynamique pouvant convenir pour diverses applications telles que les matériaux polymères avec de nouvelles propriétés, les catalyseurs de Lewis très intéressants, diverses macromolécules, etc. Tous ces nouveaux composés sont basés sur un motif identique qui est un cycle formé par la condensation d'acides boronique en une boroxine qui fait office de bloc de construction de ces plateformes dynamiques.

Dans un premier temps, la synthèse de nouvelles boroxines et iminoboroxines a été établie sur des systèmes modèles. Grâce aux différents substituants présent sur le cycle aromatique et sur l'imine, nous modulons l'acidité de Lewis du bore ainsi que la basicité de l'imine modifiant dès lors la formation des adduits de Lewis au sein ces composés. Une étude via DRX, IR et RMN est réalisée donnant des indications sur le nombre d'adduits formés, les longueurs de liaisons et de la structure fine des différentes molécules. La réversibilité des liaisons B-O de ces boroxines coordonnées à l'azote a été vérifiée par hydrolyse et déshydratation dans des conditions douces.

Dans un second temps, sur base de polymers déjà synthétisés, ces iminoboronate ont joué le rôle de nœuds de réticulation au sein du réseau polymérique PPG-boroxine. Ces nœuds répondent à l'humidité et la chaleur donnant un aspect dynamique et des propriétés d'autoréparation au matériau reformant le polymère après d'éventuelles dégradations. Les remaniements des liaisons B-O et C=N permet un traitement thermique doux donnant des résultats encourageants pour une application dans le cadre des matériaux autoréparants. Des tests mécaniques et d'autoréparation sont réalisés afin de confirmer ce comportement où les agents de réticulation sont hydrolysés et condensé pendant le processus de cicatrisation ainsi que l'effet des substituants sur ces propriétés.

2. Abstract

This master thesis is based on three main aspects based on the Lewis acid/base and boron chemistry to obtain a dynamic platform which can be suitable for diverse applications such as polymeric materials with novels properties, highly interesting Lewis catalysts, macromolecule. All those new compounds are based on the same pattern which is basically a ring formed by the condensation of boronic acid into boroxine which is the building bloc of these dynamic platforms.

The synthesis of novel boroxine and iminoboroxines has been established as model systems. Based on the different substituents present on the aromatic ring and the imine, we modulated the Lewis acidity of the boron and the basicity of the imine modifying the Lewis adduct formation in these compounds. A study *via* XDR, IR and NMR analysis was performed giving clues for number of Lewis interactions present in the compound, bond lengths and fine structure of the different molecules. The reversibility of the B-O boroxine bonds has been verified with these nitrogen-coordinated dynamic platforms synthetised via hydrolysis and dehydration.

The application of these iminoboronate based boroxines as crosslinking nodes in a PPG-boroxine network previously designed is developed. These dynamic nodes respond to humidity exposure and heating giving self-healing properties to the material reforming the polymer after degradation. The B-O and C=N bond reshuffling enable to apply a mild thermal treatment giving encouraging results as an application for self-healable materials. Mechanical and healing tests have been performed to confirm this comportment where crosslinkers are hydrolysed and condensate during healing process.

3. Remerciements

Malgré le fait que le mémoire de master en Sciences Chimiques soit un travail personnel, ce dernier implique tout me même l'aide et la contribution de nombreuses personnes afin de mener à la genèse, finalisation et réussite de ce mémoire. Ces remerciements sont là pour exprimer mes sentiments les plus sincères et de remercier toutes ces personnes m'ayant accompagné durant cette année riche en expérience.

Tout d'abord je souhaite remercier le Prof. Guillaume Berionni pour m'avoir chaleureusement accueilli au sein du laboratoire de réactivité et catalyse organique à l'Université de Namur et qui m'a permis de réaliser ce travail avec des débouchées importantes d'un point de vue personnel mais aussi d'un point de vue chimique. Vous m'avez transmis votre passion pour la chimie organique et votre intérêt divers sujets scientifiques de manière générale forgeant mon sens critique et ce depuis 2 ans.

Je souhaite aussi remercier le Prof. Jean-Marie Raquez jouant aussi le rôle de co-promoteur en m'accueillant au Service des Matériaux Polymères et Composites de l'Université de Mons et me permettant de continuer le travail réalisé sur ce sujet. Merci pour votre supervision, vos conseils ainsi que l'encadrement que mis en place pour assurer le bon déroulement d'une partie nécessaire de ce travail.

De la même manière je tiens à exprimer mes plus sincères remerciements au Dr. Aurélien Chardon, tu m'as pris sous ton aile et m'as accompagné tout au long de cette année en tant qu'encadrant, voisin de paillasse mais aussi ami. Tes connaissances en chimie et même sur tous les sujets de manière générale m'impressionne en plus de tes qualités humaines et de ta curiosité scientifique. Tu as été l'un des principaux acteurs de mon évolution, une fois de plus, un grand merci pour tout ça !

De plus, je tiens aussi à remercier Arnaud Osi qui, en tant que second encadrant a aussi joué un rôle important d'un point de vue formation scientifique mais aussi de m'avoir supporté durant un an, de tes interactions et remarques constructives.

Malgré le peu de temps passé au SMPC, je remercie Chiara Magani de m'avoir encadré sur l'aspect polymères de mon travail, de m'avoir initié à méthodes de caractérisation nouvelles

pour un chimiste n'ayant jamais réalisé de polymères, de m'avoir bien intégré au sein de ce laboratoire rendant mon travail encore plus constructif.

Pour leurs contributions nécessaires afin de réaliser mon mémoire, je tiens aussi à émettre une pensée pour le Dr. Nikolay Tumanov pour ses mesures en diffraction de rayons X, Dr. Thu-Hong Doan et Xavier Maes pour leurs expertises en spectroscopie UV-visible mais aussi en spectroscopie stopped-flow. Mais aussi le Dr. Luca Fusaro, l'institut NISM, la plateforme technologique PC^2 et Materia Nova pour la mise à disposition des techniques de caractérisation des molécules.

L'ensemble de l'équipe du laboratoire RCO n'est pas en reste pour les aides ponctuelles et la cohésion régnant dans l'équipe. Et principalement Jennifer, Dorothée et Esteban pour m'avoir accompagné depuis bientôt 5 ans en tant qu'amis malgré les hauts et les bas de la vie. Mais merci à vous pour ces magnifiques années en votre compagnie et de partager avec moi une pléiade de moments en et hors labo.

Ma famille n'est pas en reste, cette dernière m'a permis d'entamer ces études conduisant à la réalisation de ce travail. Merci à mes parents de m'avoir offert une telle éducation ainsi que de m'avoir permis d'évoluer dans les meilleures conditions possibles. Merci du support émotionnel à tout moment des corrections tardives de travaux.

Je tiens aussi à remercier une personne qui se reconnaitra pour faire partie de ma vie, me supporter à tout moment et d'embellir mes journées me permettant de finaliser ce travail de longue haleine.

De manière générale je tiens à remercier tout le monde ayant de près ou de loin participé à la réalisation de ce projet et même de manière générale d'en être arrivé là. Merci !

Antoine

Table of content

4. Background and introduction

Self-healing polymers

Polymers are macromolecules composed of several repeating units ("Poly" = numerous and "Meros" = parts) playing very crucial roles in everyday life from DNA, proteins to synthetic plastics.[1] These natural or synthetic macromolecules are obtained by polymerisation of many organic molecules, also known as monomers. The arrangement of their chains (primary structure) plays a major role on their physical, chemical and thermo-mechanical properties.[2] Their microstructure can be engineered to lead to linear, branched, crosslinked or network polymers. Different scales exist for this material from the sub nanometric to macroscopic length, different arrangement of these polymers is possible forming crystals, semi-crystalline or amorphous polymers determined by the nature of the monomers.[3]

Synthetic polymers have a wide range of applications; their low density make them suitable for large scale weight economy as packaging, vehicles parts. Their unique properties are of high interest for other applications such as biocompatibility, enabling the design of new drug delivery systems, biosensors, adhesives, conductive materials, structural application and so on. This large variety of applications is due to the diversity of the monomeric species and their numerous polymerisation methods .Furthermore, composite could be obtained by non-miscible component (two different polymers and additives) leading to more robust materials with improved stability under certain conditions (light and temperature).[4]

The robustness and longevity of polymers are crucial parameters which allow them to maintain optimal properties and integrity over the time. Thus, in case of rupture of this integrity, the structural application of this polymer is corrupted and more generally the damages of these materials are completely undesirable. Preventing polymers corrupting and damaging is conventionally solved by developing more and more robust materials by increasing the chain interaction, by reticulation of the chains, or adding additives to avoid degradation of the polymers. This method allows to develop robust polymers but suffers from the major drawback that such polymers cannot be recycled due to the irreversible reticulations present in the material.[5]

As in living organisms, these two problems have been solved by the design of a new type of polymers able to repair by themselves also called self-healing polymers. For example, the methylation of guanine bases could be observed with methylating agents, this methylation can deeply change the activity of the DNA without changing the whole sequence.[6] The alkylation could repress the gene transcription if this process is located in a gene promoter. The healing of this DNA is promoted by the protein methyl guanine methyl transferase (MGMT) (*Figure 1*) recovering the structure and the activity of the DNA, the damage induced response of the living organism.

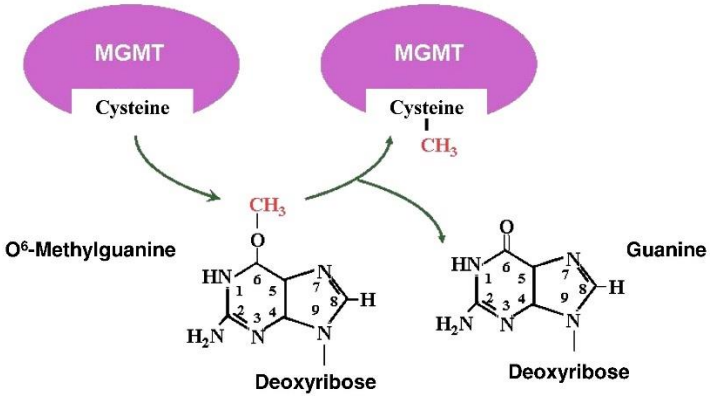

Figure 1 -Repair of O^6-alkylguanine adducts by MGMT[6]

In synthetic self-healable systems, the damage triggers the generation of a mobile phase diffusing to the damaged zone, by physical and/or chemical interaction cover this surface and initiate a healing of the material. The comportment of these polymer allows to increase the materials reliability, longevity and to preserve the thermo-mechanical properties after recycling cycle by avoiding the degradation of the material and ensuring their continuous self-reparation.

Various approaches for self-healing have been described such as physical, physico-chemical and chemical way with specific mechanisms (*Figure 2*). These mechanisms of healing can be mediated by external stimuli such as light, heat, moisture, chemical or others, and the polymer chain structure has to be designed at the molecular level to adapt their behaviours to the chosen stimulus.[7] Early approaches for healing the polymers was only based on the diffusion of polymers chains[8] leading to interfacial interactions/interpenetration with short and flexible chains (*Figure 2*a).

New types of self-healable polymers so called extrinsic self-healing polymer were obtained by using capsules which liberates reactive material when being opened during a damage. By filling the degraded part of the polymer, the material is repaired once the diffused substances reacted, thus, this technique is limited due to reactive material needed at each healing and based on similar concept; cardiovascular networks have been developed where reactive material in contained in capillaries passing through the polymer.[9] Other physico-chemical approaches based on Van der Waals interactions (*Figure 2*c) are also used to induce the healing properties. If these cohesive forces are disturbed by mechanical damage, the system will evolve to energetically favourable state leading to the recovery of these Van de Waals interactions and the healing of the polymers.

Chemical methods related with intrinsic self-healable polymer such as covalent bond formation initiated by free radical combination under UV irradiation or heating represent a straightforward approach for inducing a polymer self-healing. Other reversible covalent bonds forming process (*Figure 2*b) such as C-C bond formed by Diels–Alder, S-S, Se-Se, C=N, B-O bonds are also widespread for the construction of self-healable polymers.[10] Supramolecular chemistry is an alternative approach where weak non-covalent interaction (hydrogen bonding, π-π stacking, metal-ligand coordination, guest-host and ionic interactions) are combined to obtain self-healing materials due to their reversibility, directionality and sensitivity.[4]

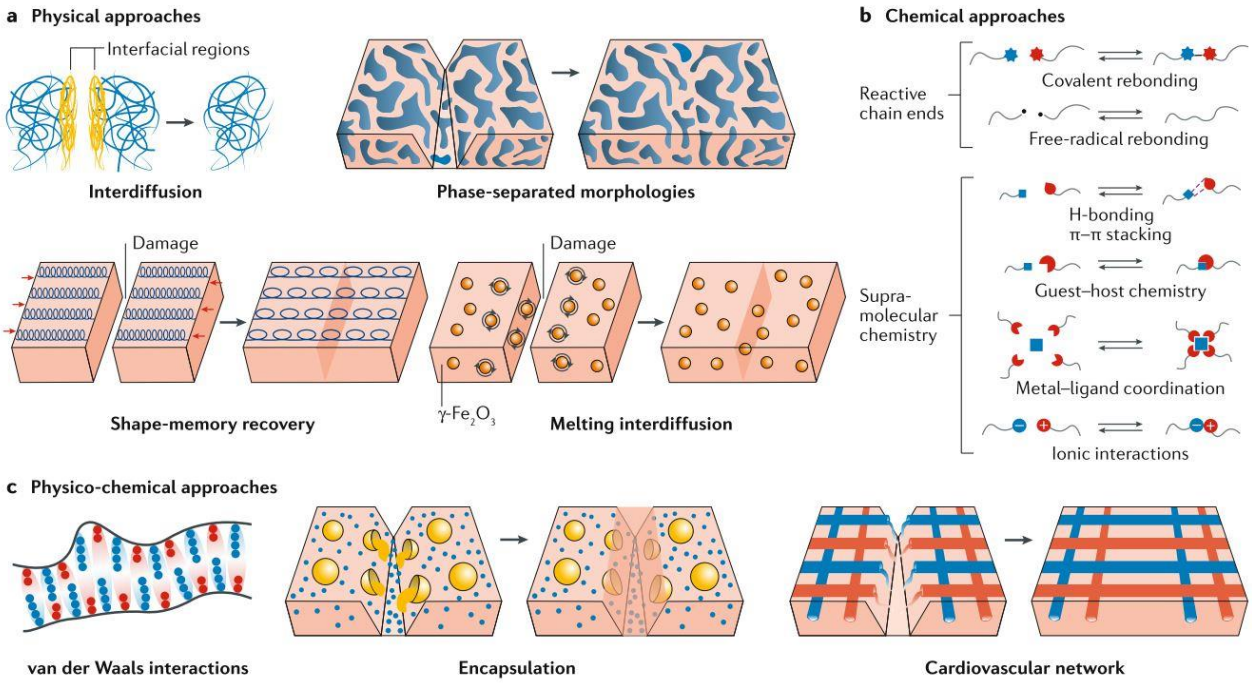

Figure 2 - Self-healing approaches and mechanisms linked for materials[7]

In our case, the chosen chemical approach is based on dynamic covalent bond formation and breaking, a method resulting in more stable polymer than noncovalent ones and avoiding the formation of preferential cleavage points as we can observe in the case of π-π stacked polymers. All of them exhibits specific responsiveness to a healing stimulus (heating, light, water, pH induced, …) and their kinetics are really different related to the bond energies, type and number of species involved.[11]

Among them rapid and efficient healing capacity could be obtained by the formation and cleavage of B-O bonds with boronate esters (*Figure 3*). The cleavage of this bond is induced at low pH while the condensation of the boronic acid (or boric acid) and diol is favoured at the pK_a of this boron species or higher. At low pH the neutral boronic ester forms a strained ring favouriting the hydrolysis of the ester to reform the boronic acid and diol. Whereas the basic boronate ester is more stable toward hydrolysis due to the steric hindrance caused by the substituents and the occupied orbitals avoiding the attack of the water on the boron to initiate this reaction.[12]

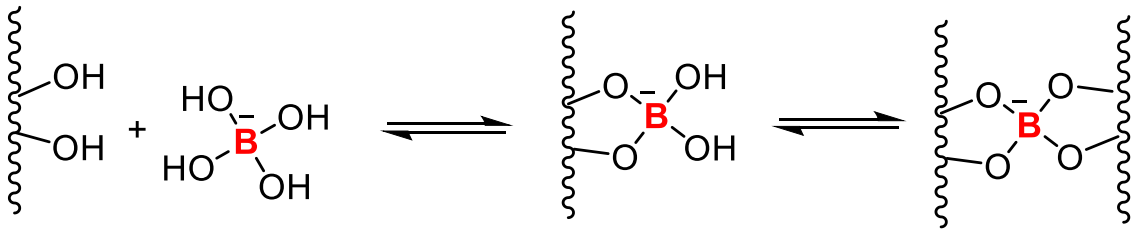

Figure 3 - Boronate ester as reticulation nodes in self-healable polymers

An underexplored method for obtaining pH responsive polymers is to design a material with imines bonds which could undergo a reversible equilibrium between the aldehyde/amine and imine. At neutral or basic pH the reshuffling of these imines[13] is possible at room temperature, reforming the undamaged shape of the polymer while at acidic pH the protonated imine could not access this hydrolysis/recondensation process (*Figure 4*). If this chemistry can be coupled with other reversible covalent bond formation or even with supramolecular interactions, we can obtain powerful tools for the construction of a new generation of self-healing polymers.

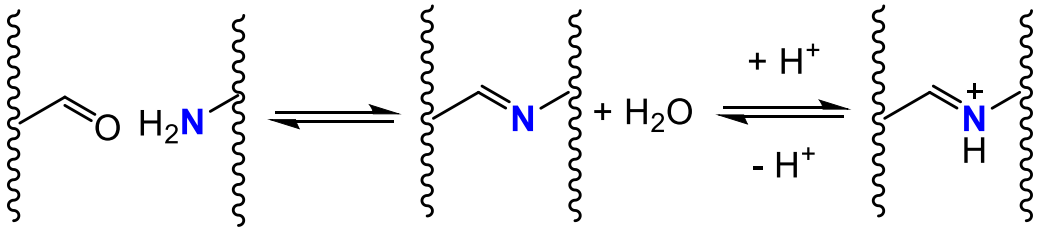

Figure 4 - Imines as reticulation nodes in self-healable polymers

Until today, the reported self-healing polymers suffer from lack of healing capabilities and performances. In this field the major challenge is to obtain reduced healing time, while conserving the properties and reach the highest mechanical properties that we can draw from polymers.

High mechanical properties for polymers are obtained with thermosetting polymers (thermosets) which is irreversibly shaped at the end of the curing. This property results from strong covalent bond and high density of these bonds, more specifically they are obtained by increasing the cross-linkage between the polymers chains. But these irreversible links between the linear chains also induce the impossibility to recycle these materials. One elegant solution for the design of recyclable and self-healable thermosets has been obtained by incorporating reversible cross-linkages in that kind of materials.

In this work, we will combine both the aldehyde/imine and the boronic acid/boroxine reversible linkage. More particularly on the boronic acid/boroxine equilibrium which involves reversible B-O bonds formation and dissociation applied to polymers to design materials with improved healing properties. The coordination of the imine nitrogen atom to the boron to form Lewis adduct will be investigated in details to allow milder healing conditions than when these Lewis acid and base cannot interact together. In this case as the system is sensitive to humidity, the reshuffling of B-O and C=N bonds will mediate the healing process of the material after partial hydrolysis of these bonds without any solvent. The boroxine platform allow the continuous self-healing of the polymer in milder conditions since only a water enriched or even ambient atmosphere is sufficient for healing whereas some polymers require strong acidic treatment, high temperature heating, …

The ultimate objective of this master research work is to obtain polymers with tunable and efficient healing properties, better mechanical and thermal properties. We will tackle this objective by developing polymers containing substituted boroxine nodes which allow to modulate the steric hindrance and the Lewis acidity of the boron atom. The combination of these effects and the influence of the substituents will be investigated quantitatively in order to identify the best candidate as dynamic platform for polymer chemistry.

We also developed practical synthetic methods to obtain boroxines with different substitution patterns (*ortho*, *meta*, *para*) and compared these methods to assess the most efficient to produce boroxines at the multigram scale.

Upon completion of these studies, new iminoboroxine model compounds for dynamic nodes in polymer chemistry will have been developed and will serve as a basis for the future applications in this field and others (*Figure 5*). [14]

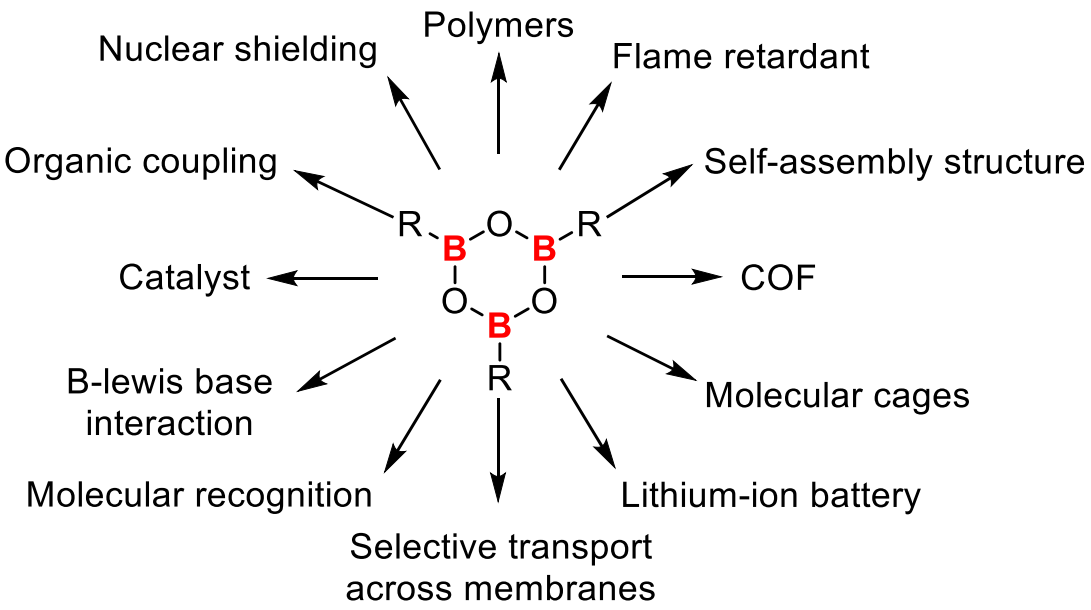

Figure 5 - Boroxine applications in chemistry and material sciences

Boroxine nodes for self-healing PPG polymers

Based on a previous work developed in the J.-M. Raquez laboratory[15], we will focus on star-shaped poly(propylene glycol) bis(2-aminopropyl ether) (PPG) polymers crosslinked by a boroxine building-block with three aldehyde groups, readily forming imines by condensation with amines to form C=N double bonds.[16] This boroxine will act as the crosslinking node of this polymer increasing its rigidity and making it as behaving a dual stimuli-responsive networks to water and heat, allowing self-healing properties.[17] Once the polymer is physically damaged, the hydrolysis of the boroxine will lead to the formation of three boronic acids at the terminal position of the polymers chains, allowing to form afterward a three-dimensional mesh and reform the boroxine node afterward (*Figure 6*). This work focused on the improvement of the healing kinetic of these materials while conserving mechanical properties, on the study of the dynamic mechanism involved at the molecular scale level, of the Lewis interactions and the synthesis of a variety of new iminoboroxines as models to optimise the healing of these materials.

Simple imine is quite sensitive to hydrolysis but different works showed that the boron-imine interaction enhances the exchange kinetics of this C=N bond due to the increased electrophilicity of that double bond. On the other hand, the boroxine hydrolysis is also

prevented by the Lewis adduct formation due to the occupation of the 2p boron orbital, completing its valence shell with nitrogen doublet.

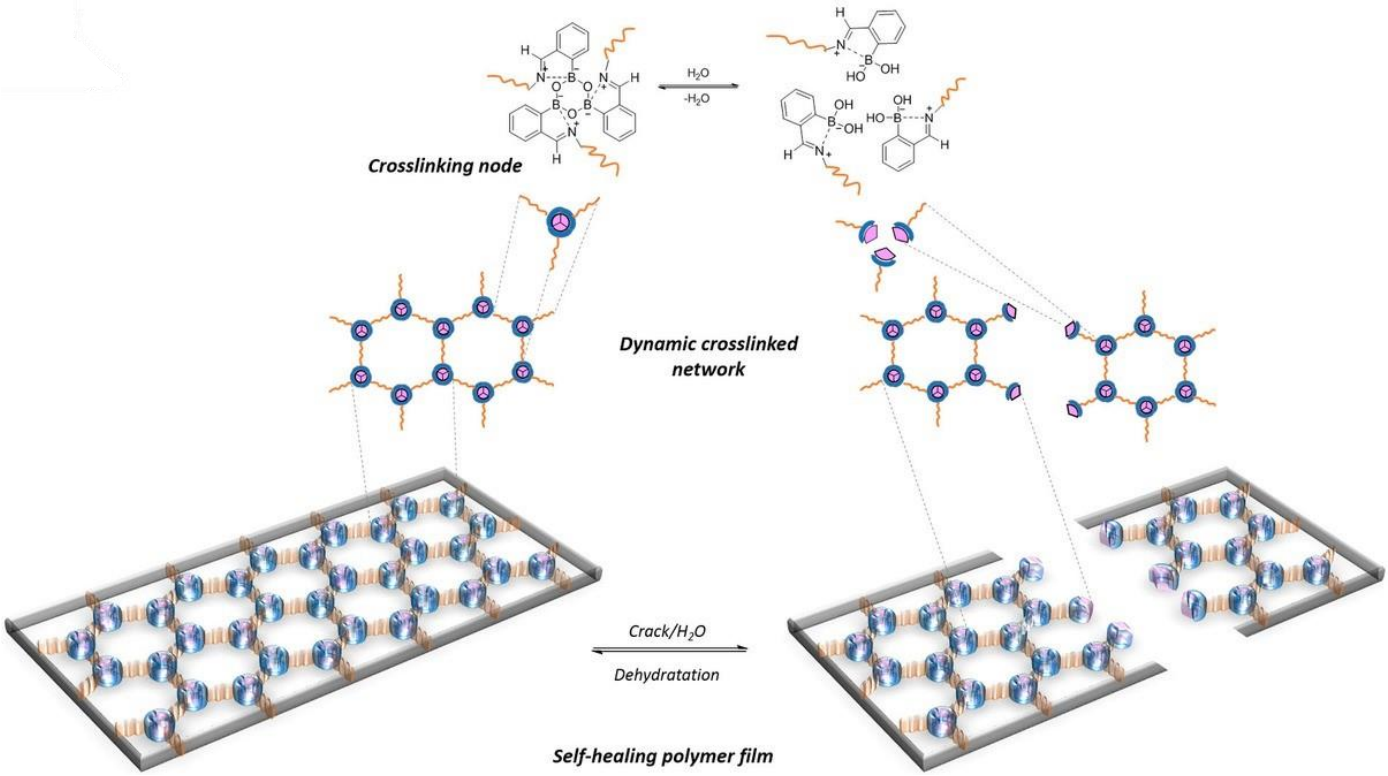

Figure 6 - Self-healing polymer based on boronic acid boroxine equilibrium[15]

Lewis acidity and basicity

The nitrogen atom from the imine and the boron atom from the boroxine will form Lewis acid/base interactions resulting from their respective basicity and acidity in the material. As described in 1923 by Gilbert Lewis, Lewis acidity is described as the thermodynamic tendency of a substrate to accept on electron pair from a donor (Lewis base),[18] thus forming Lewis adducts. On the other hand, the Lewis basicity is based on the donation of electron pair of electrons. Thereby we can increase the Lewis basicity of a molecule by electronically enriching it and for increasing Lewis acidity is obtained by electronically depleting it.

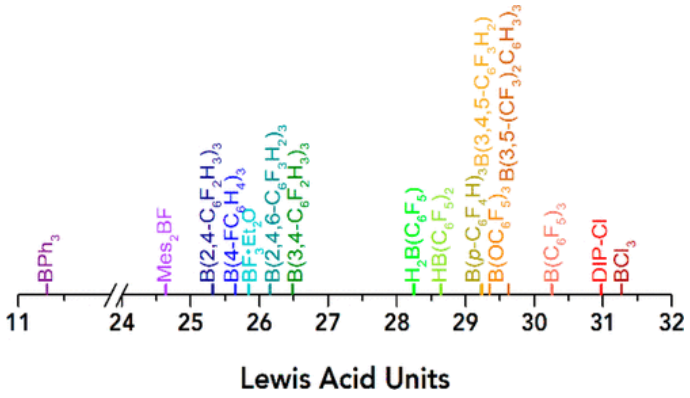

Figure 7 - Scale of the strength of Lewis acidity measured by fluorescence[19]

Different methods are available to characterise this acidity are based on a probe Lewis base which binds to the acid and measuring the energetic or spectroscopic output resulting from this Lewis adduct formation (*Figure 7*). Typical techniques are the following; theoretical studies can be performed such as fluoride ion affinity (FIA)[20] based on enthalpy calculation where fluorine anion is preferred for his small size, the polarizability of the F^- avoiding steric hindrance and this anion avoids π-back-bounding, charge transfer or dispersion.[21]

In this work we used experimental methods such as the Gutmann–Beckett method which is based on the ^{31}P chemical shift of Et_3PO where the oxygen of this probe acts as a Lewis base, changing the phosphorous environment and consequently the ^{31}P chemical shift. When the adduct is formed, the phosphorous atom is deshielded, increasing the NMR shift from 41 ppm (Et_3PO in hexane) which is the reference for this method, allowing the construction of relative scale based on the acceptor number (AN) which is determined by the following equation: $AN = 2.21 \times (\delta_{sample} - 41.0)$.[22] A second experimental method was used based on Infrared (IR) measurement of carbonyl compounds where we observe the variation of the characteristic frequency of this band while the adduct is formed.[23]

Moreover, these Lewis acids are also useful in biochemistry due to this presence in proteins, leading to the possibility of developing new medicines based on the Lewis acid/base association. That is the example of diverse boronic acids which are widely used in pharmacology[24] as antibiotics, blocking the enzyme activity of these organisms. This boron atom accepts a doublet in its free 2p orbital, completing its valence shell. These accepting doublet compounds have also other applications in radiotherapy, targeting certain functions as sensors coupled with fluorescent molecules for example.[25]

5. Results and discussions

A. Strategies and synthesis

For producing the boroxine derivatives, we envisioned a synthesis based on three key steps (*Figure 8*). The first step consists in the synthesis of formyl phenyl boronic acid derivatives by using an organometallic synthetic pathway. The dehydration of these precursors then leads to the generation of substituted boroxines. The boroxines are finally incorporated in the polymer *via* an imine formation by the condensation of the aldehyde present on the boroxine and an amine. The iminoboroxine has been selected for two major reasons, the reversibility of the B-O bond formation, and the expected Lewis acid/base interaction between boroxine and the imine will be crucial for the boroxine ring construction. Once formed the boronic acid and the boroxine undergoes a reversible equilibrium which will be exploited in the poly(propylene glycol) polymer based hydrophobic material (ppg) providing it self-healing properties based on covalent bond cleavage and formation accompanied by the release or capture of three molecules of water.

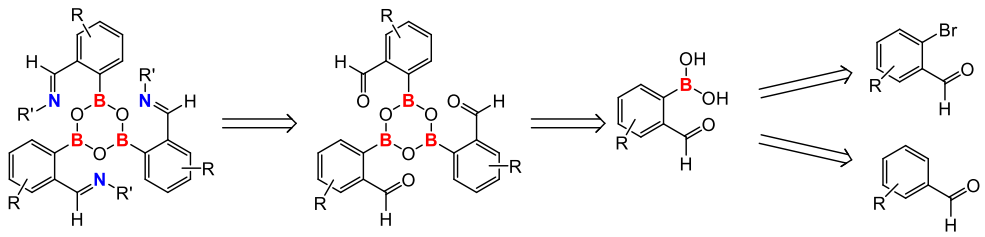

Figure 8 - Proposed retrosynthesis of iminoboronate-based boroxines

B. Boronic acid synthesis

We started by the synthesis of ortho-substituted formyl phenylboronic acids with various substituents on the aromatic ring and by the formation of corresponding imines, in which the nitrogen atom will modify the steric and electronic properties of the -$B(OH)_2$ group, and thus affect the boronic acid/boroxine equilibrium.

After optimising the experimental conditions for the each of the two steps of the reaction from 2-bromobenzaldehyde, we found that the optimal method consists in the initial protection of aldehyde by forming the ethylene glycol acetals **1**-**3** and the subsequent

bromide-lithium exchange with *n*-butyllithium (*Figure 9*) followed by the addition of trimethyl borate and by acidic hydrolysis leading to **4** in good yield and boronic acids **5**-**6**. In the case of electron-deficient or rich systems with fluorine or methyl substituents, the protodeboronation in acidic and basic aqueous solution is fast[26] [27] and the synthesis of diverse boronic acids (**5** and **6**) was problematic due to the required acidic treatment step for removing the acetal protecting group.

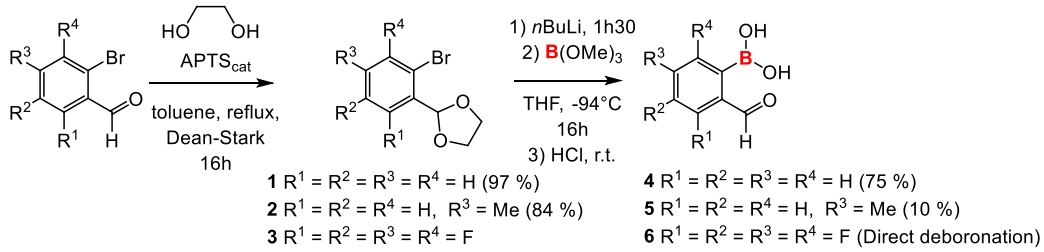

Figure 9 - Synthesis of ortho-substituted formyl phenylboronic acids via cyclic acetal intermediate

A second synthetic method was then investigated based on a recent publication of N. Chatani where direct C-H bond *ortho*-borylation is achieved without acetal formation but *via* a transient imine directing group formation (*Figure 10*). As this method display the advantage of an acidic-free treatment to hydrolyse the imine in aldehyde, and for other reasons (the good regioselectivity of the reaction, the good tolerance of substituents on the aromatic cycle, and usually high overall yield of the complete pathway)[28], it was very promising for the synthesis of the desired boronic acids. The originally described direct borylation and subsequent formation of neopentyl glycol, hexylene glycol and pinacol boronates was not ideal since they are known to be difficult to hydrolyse, and display a protodeboronation process in harsh conditons.[29] Thus, in parallel, the synthesis of glycol boronate esters **10** and **11**, which can be hydrolysed under milder conditions into the desired boronic acid has been developed to avoid the degradation of **4** and **12** owing to the aqueous work up under pH neutral conditions.

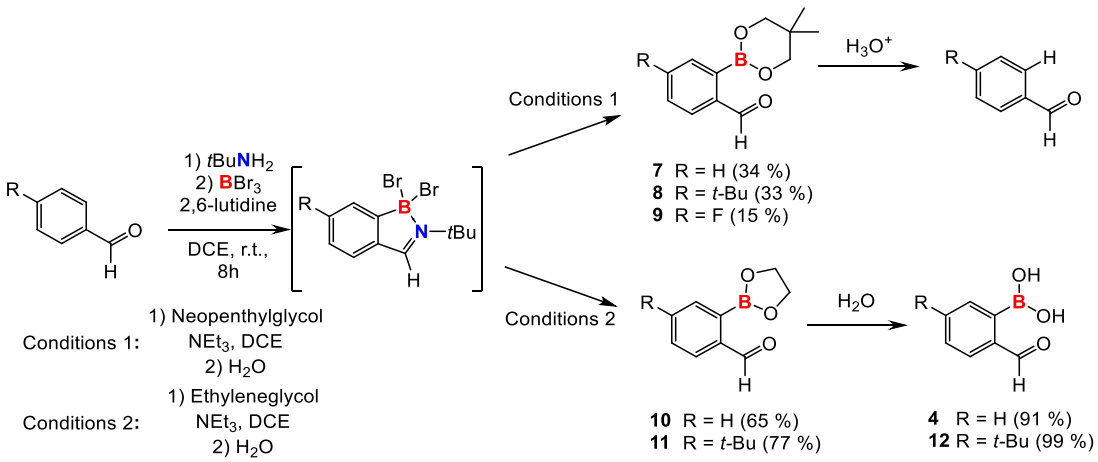

Figure 10 – Synthesis of boronic acid by direct C-H borylation

Thus, the direct *ortho*-borylation reaction of benzaldehydes provided good yields, and tolerated a broader range of substituents, but is yet limited to a smaller scale than the first method, due to the large amount of boron tribromide to be employed in solution. This point will become a limitation when a multigram amount of **4** and **12** will have to be produced for the synthesis of the polymer. Despite the functional group good tolerance of this method, some decomposition has been observed with fluorine on the aromatic ring leading to lower yields. We then turned our attention to another method[30] to ensure the synthesis of these boronic acid derivatives based on the synthesis of acyclic acetal requiring milder deprotection conditions. Acyclic acetals are much more reactive than cyclic ones, which are much more stable against hydrolysis due to the chelating effect. As -OH groups of the acetal are connected to each other in the diol, during the oxonium ion formation, the alcohol from the acyclic acetal stay near to that intermediate and could react directly while water needs to access to the oxonium from the central carbocation.

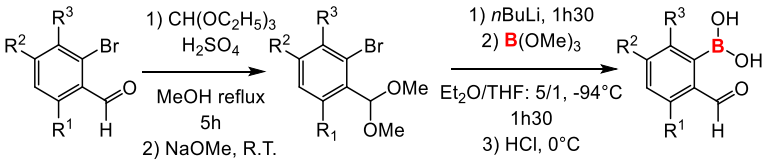

Figure 11 - Synthesis of ortho-substituted formyl phenylboronic acids via acyclic acetal intermediate

This method provided good yield for all steps. Despite the increased reactivity of the acyclic acetal against hydrolysis, a pH neutral treatment did not result in a full deprotection. A slightly

acidic treatment is therefore performed to reach full conversion, but we also saw some protodeboronation (*Figure 11*). For boronic acid **4**, **18** and **19** this side reaction is not occurring. For the boronic acid **17**, the fluorine atom in *ortho* position favours the formation of undesired benzyne during the lithium-bromide exchange when the temperature is too high for the stability of the aryl lithium (*Figure 12*). This aromatic compound is highly reactive due to his strained triple bound leading to the formation of complex mixtures caused by side reactions.

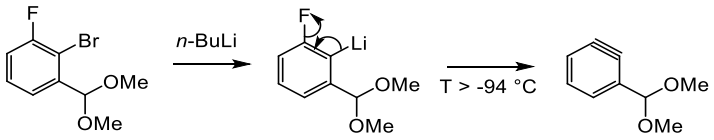

Figure 12 - Benzyne formation during halogen/lithium exchange

Again, it has been showed experimentally[31] and theoretically that *o*-fluoro substituents are especially efficient for assisting the protodeboronation[27] during the acidic treatment (*Figure 13*). With these considerations, we can easily understand why the yield is inevitably reduced compared to the others fluoro formyl phenyl boronic acids. Moreover, the electron donor substituents also facilitate the protodeboronation because the C-B bond is more nucleophilic.

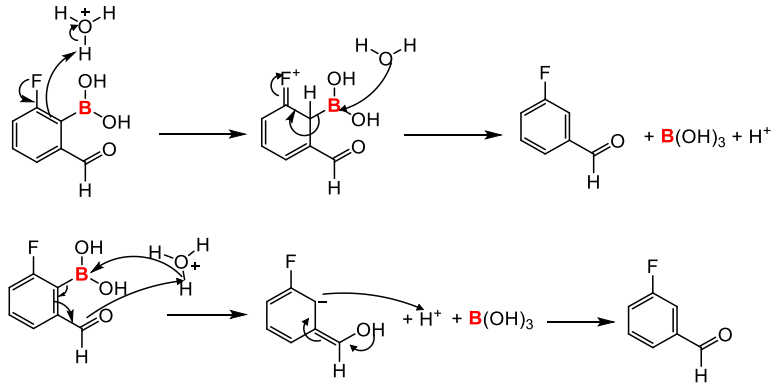

Figure 13 – Protodeboronation of substituted phenyl boronic acids

The following step was the condensation of the boronic acids into boroxines (*Figure 14*). The model boroxine **26** was obtained from **20** by sublimation under reduced pressure with a quantitative yield after optimisation.[32] The other boroxines **21**-**25** were formed and isolated with a high purity by this method, and had to be stored under inert atmosphere to prevent hydrolysis.

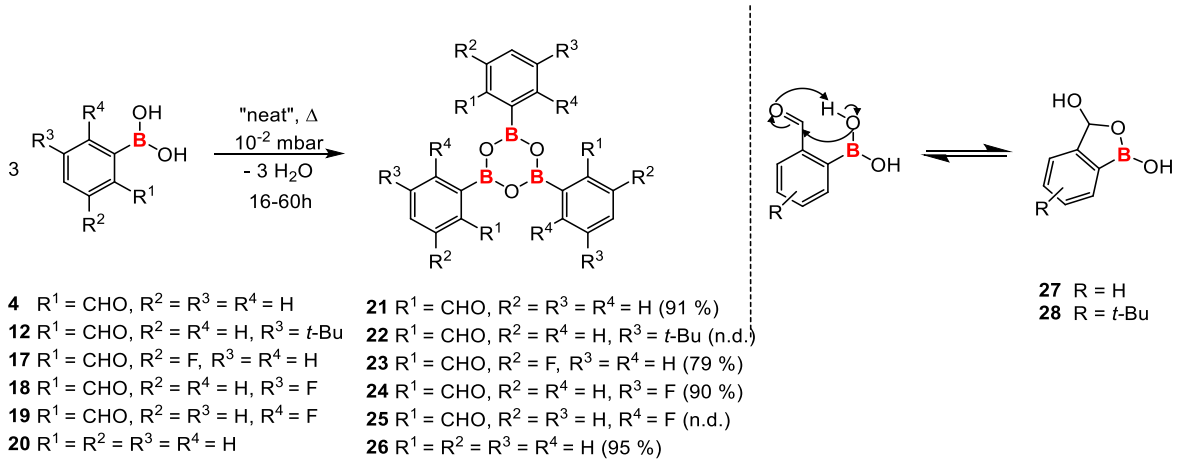

Figure 14 – General synthesis of boroxine from boronic acid (left) and oxaborole formation from boronic acid (right)

This reaction and purification method works well for boroxines **21** and **23** to **26**, although we observed the formation of oxaborole **27** as a side product. The boroxine **22** already decomposed at lower temperature and its isolation was neither possible by this method nor by refluxing in toluene[15] due to the formation of oxaborole **28** and other side products.[33] Milder conditions need to be tested for the formation of this last boroxine using a dehydrating agent such as molecular sieves or $MgSO_4$.

Thus, in the first part of this master research work we successfully implemented a method to obtain functionalised boroxines in good yields and high with purity. Moreover, when the condensation is not complete, we observe the formation of anhydrides via ^1H NMR which can form boroxine after further condensation. The formation of boroxine **25** showed that these conditions are too mild, the temperature need to be slightly higher (75-80°C) to observe the complete transformation of the boronic and anhydrides into the boroxine within a week for a gram scale synthesis. This comportment can be explained by the fact that boronic acid form intrinsic Lewis adduct between fluorine and boron (2.984 Å while the sum of the Van der Waals radius is 3.39 Å) which yield to the occupation of the free orbital of the boron. When this orbital is empty, it assists the formation of the intermediate states as showed in this chart obtained by DFT using B3LYP hybrid function and basic 6-31G(d) set on silver surface which lower the barrier heigh of the reactions.[34] It is therefore normal that boroxine formation from formyl phenyl boronic acid is more difficult due to the occupation of this boron orbital, the Lewis adduct need to be dissociated to form these intermediates and perform the condensations, leading to higher energy transition states (*Figure 15*).

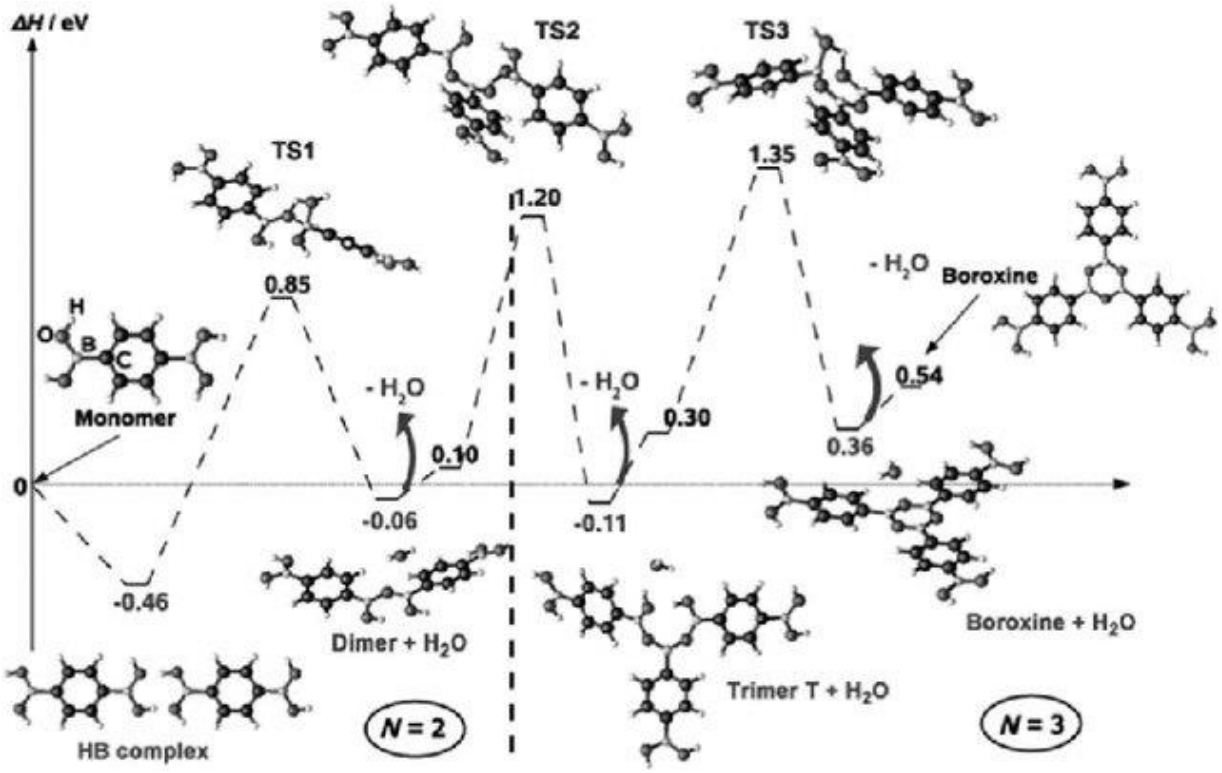

Figure 15 - Boroxine formation reaction mechanism as calculated by DFT on metallic surface[34]

Formation of boroxines Lewis adducts with nitrogen centred Lewis bases

The acidity of the boron species is an important parameter on the reactivity of these species, the study of the Lewis acidity and the adduct formed is a key point to obtain polymers with improved healing properties. Prior to the synthesis of iminoboroxines, we studied the formation of simple Lewis adducts between a boroxine and the strong Lewis base 4-(dimethylamino)pyridine (DMAP). The characterisation of Lewis adducts formed in solution indicated how the B-N bond formed between the boron of the boroxine **26** and the nitrogen atom of DMAP induced a geometrical change from a trigonal planar to a tetrahedral boron atom depending on the size and basicity of the Lewis base and also gives information on the strength of the adduct formed. With one equivalent of DMAP, the mono B-N adduct **29** is formed and the two other boron atoms are free. With two equivalents, we observed a mean peak due to fast exchange in solution between the two occupied boron and the free boron. While with three equivalents, or even with a large excess of DMAP (*Figure 16*) the formation of more than two Lewis adduct was not observed according to ^{1}H and ^{11}B NMR spectra (*Figure 17*). We concluded that with that boroxines will form either one or two Lewis adducts in the iminoboroxines.

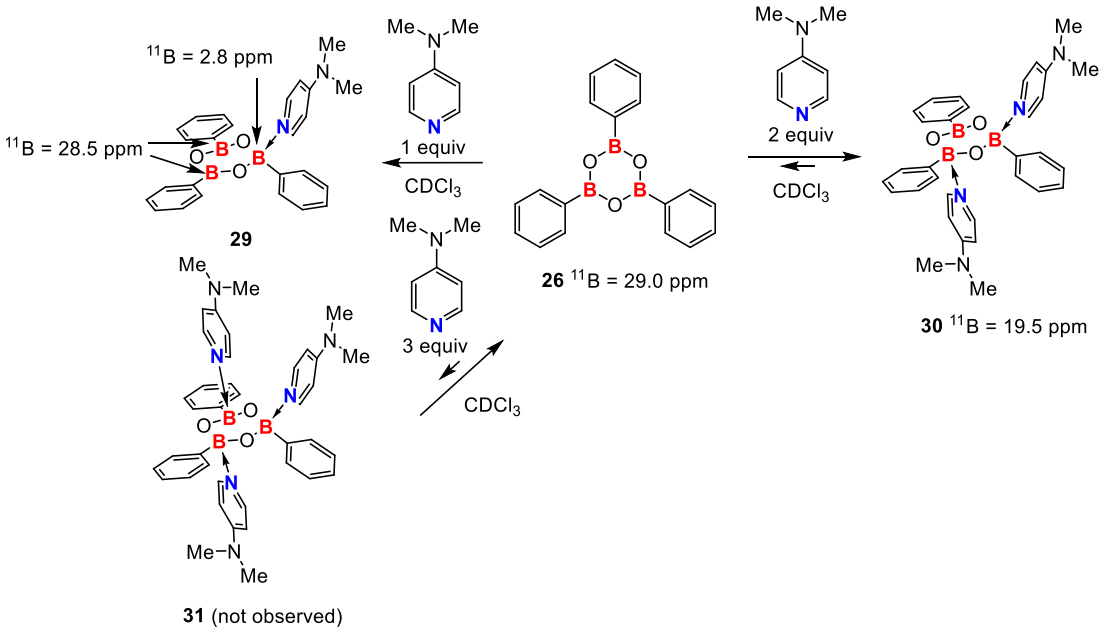

Figure 16 - DMAP/boroxine reversible ligation

Our investigation confirmed recent observations in the literature[35] [36] describing that boroxines usually form one or two Lewis adducts between boron and nitrogen. This can be rationalised by three factors; the steric hindrance around the remaining trivalent boron atoms is increasing at each addition of the Lewis base, the electronic repulsion due to the appearance of partial charges on the boroxine and the decrease of the Lewis acidity of the neighbouring boron is finally decreasing at each formation of Lewis adduct.

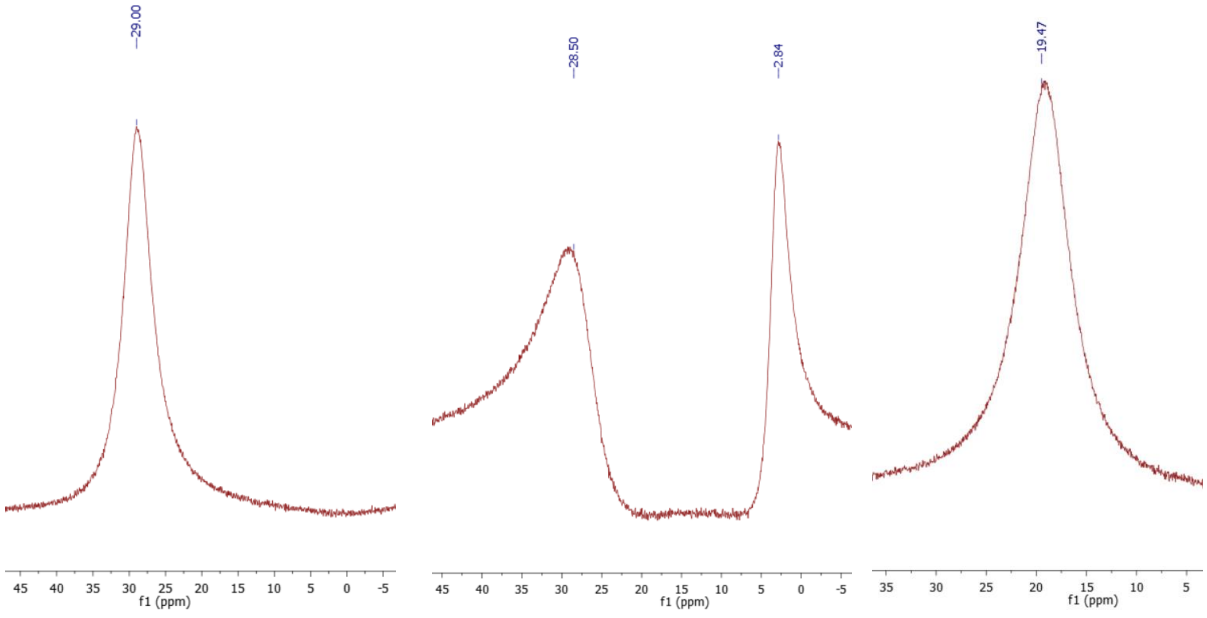

*Figure 17 - ^{11}B NMR spectra of triphenylboroxine **26** (left), with one equivalent of DMAP **29** (middle) and two equivalents of DMAP **30** (right)*

Due to these factors, mostly one Lewis base coordinates on the boroxine cycle and when two Lewis bases add up, each one will attack at opposite face of the boron oxygen six-member cycle. For the boroxine **21** the adduct can also be formed due to the stabilising effect of the aldehyde resulting of the negative mesomeric effect of this adduct and making the boron more acidic.

Synthesis, spectroscopic and structural investigation of iminoboroxines

A way to tune the self-healing properties of the polymer is based on the variation of the imine stereoelectronic properties by modulating the imine and the aryl ring substituents, which will modify the B-N interaction, and at same time the boronic acid/boroxine equilibrium. Thus, the synthesis of a series of functionalised iminoboroxines from the formyl phenylboroxine **21**, **23** and **24** was undertaken. Two methods of synthesis of these iminoboronate-based boroxines are investigated. The first consists in the condensation of three iminoboronic acids to form the boroxine. The second[37] is based on the synthesis of the formyl phenylboroxine and the subsequent formation of the imine. This method works properly for the diverse iminoboroxines synthetised and is the most convenient of the two.

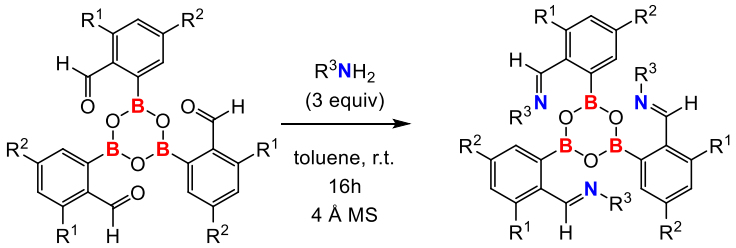

21 $R^1 = R^2 = H$
23 $R^1 = F$, $R^2 = H$
24 $R^1 = H$, $R^2 = F$

32 $R^1 = R^2 = H$, $R^3 = n$-Bu (64 %)
33 $R^1 = R^2 = H$, R^3 = Ph (69 %)
34 $R^1 = R^2 = H$, $R^3 = t$-Bu (60 %)
35 $R^1 = F$, $R^2 = H$, $R^3 = n$-Bu (60 %)
36 $R^1 = F$, $R^2 = H$, R^3 = Ph (63 %)
37 $R^1 = F$, $R^2 = H$, $R^3 = t$-Bu (64 %)
38 $R^1 = H$, $R^2 = F$, $R^3 = n$-Bu (58 %)
39 $R^1 = H$, $R^2 = F$, R^3 = Ph (91 %)
40 $R^1 = H$, $R^2 = F$, $R^3 = t$-Bu (83 %)

Figure 18 – General procedure *for the formation of directly substituted iminoboroxine*

We observed that the variation of the amine substituent R^3 didn't affect the formation of the imine (*Figure 18*) but influenced the interaction between the boron and nitrogen atoms as indicated by the ^{11}B NMR chemical shifts. Due to the stronger B-N interaction than the B-O interactions, the boron atoms in the formyl phenylboroxines **21**, **23** and **24** are more shielded

than in the boroxines **32**-**40**. When increasing imines steric hindrance (*n*-Bu less hindered than Ph and then *t*-Bu), the boron signal is less shielded due to the weaker B-N interaction caused by the bulky R^3 group. And this should also affect the rate of hydrolysis of the boroxine. Despite being the most donor and resulting in the most basic imine, the *t*-butyl substituent is the bulkiest tested and cause a large steric repulsion, leading to a decreased coordination and to a more deshielded chemical shift in ^{11}B NMR (*Table 1*).

Table 1 - Chemical shift in ^{11}B NMR for the formylphenyl boroxines and the corresponding imines

Reacted with	tris[2-formylphenyl]-boroxine **21**	tris[3-fluoro-2-formylphenyl]-boroxine **23**	tris[5-fluoro-2-formylphenyl]-boroxine **24**
-	26.4 (**21**)	25.9 (**23**)	23..9 (**24**)
n-Bu	14.3 (**32**)	13.7 (**33**)	13.9 (**34**)
Ph	17.2 (**35**)	15.3 (**36**)	16.3 (**37**)
t-Bu	20.6 (**38**)	18.2 (**39**)	18.5 (**40**)

Based on the iminoboroxines synthetised, a diamine derived for aniline such as the *p*-phenylenediamine (PPD) was used as a first attempt for the synthesis of a trigonal boroxine-based cage, with 0.5 eq of PPD, both amines of the diamine reacted and bridged two boroxines together **41** and shows this kind of diamine linkers is reactive enough for making boroxine cages based on the iminoboronate interaction and also as polymer chain terminations (*Figure 19*). More attempts for the synthesis of boroxine cages has been realised but the control of the steric hindrance created at each addition of PPD could not lead to the formation of highly ordinated structure. But while we increased the number of equivalences of PPD, we formed highly conjugated systems which could be envisaged as fluorescent compounds with the finely design of the boroxine and the diamine linker.

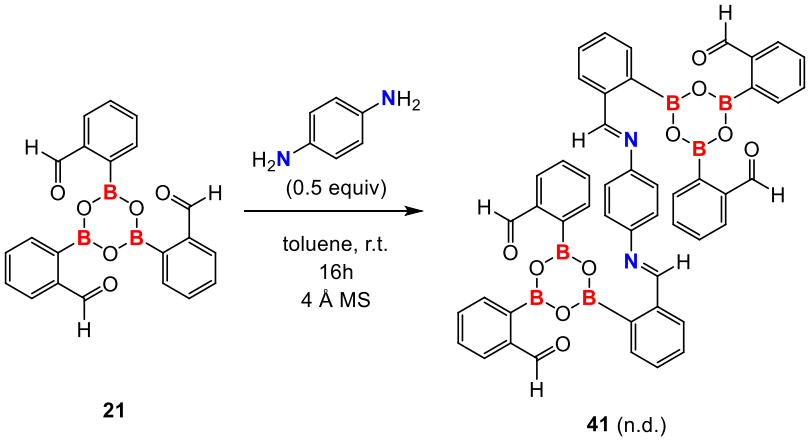

Figure 19 - Synthesis of boroxines linked by diimine

Newer iminoboroxine has been synthetised (*Figure 20*) as models for further applications in the case of conjugated systems with association/dissociation properties. Despite the variation of the substituents on the iminoboroxine **42**, **43** and **44**, we don't observe huge variation on the boron/nitrogen association via liquid ^{11}B NMR. This comportment can be easily explained by the relatively identical steric hindrance caused by the sp^3 carbon acting as a spacer in these compounds minimising the steric hindrance of the substituents. Moreover, the electronic effects of the substituents are also minimised due to the presence of the sp^3 carbon spacer leading to similar chemical environment for the boron atom. As in the case of the iminoboroxine **32**-**40**, the variation of the amine substituent doesn't affect the formation of the imine, showing that synthesis is quite tolerant and is possible with a large variety of substituents with high yields and high purity.

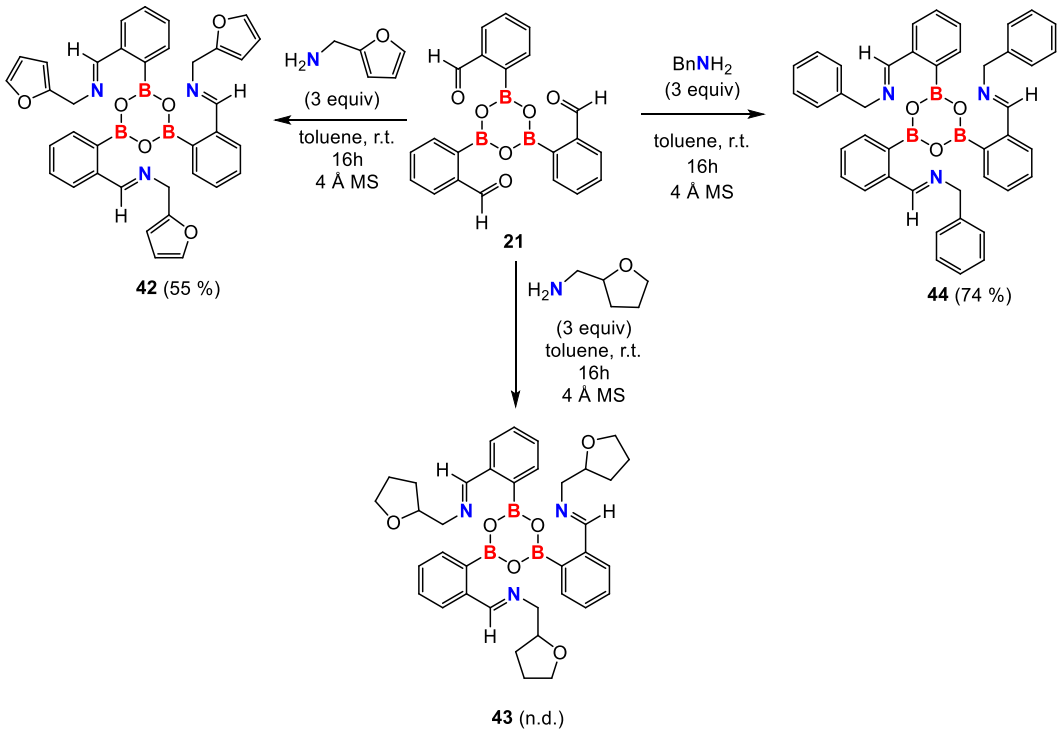

Figure 20 - General procedure *for the formation of substituted iminoboroxine trough imine spacer*

For the fluorinated boroxines event when we increase the Lewis acidity by using fluoro substituted boroxines, we didn't observe more than two Lewis adducts formed. Thus, the steric factor takes precedence over electronic properties causing this comportment, so based on this consideration, we can form iminoboroxines with any substituent while we keep a spacer which don't cause steric hindrance around the boroxine ring. Based on these considerations, we studied the formation of a highly interesting compounds for an eventual application in catalyst for CO_2 conversion.[38]

The pyrene pattern is known to form highly stable π- π interaction with carbon nanotubes (CNT), also with fullerene (C60) and other highly π delocalised systems.[39] Taking into account these properties of this substituent, we wanted to form iminoboroxine containing pyrene and form π- π staking with CNT or C60 as a first study of the possibility to support them for heterogenous catalyst.

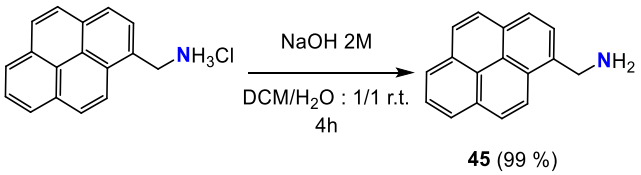

Figure 21 – Deprotonation of pyrene ammonium salt

The commercial pyrene is under the form of ammonium salts needing to be completely deprotonated (*Figure 21*) before the condensation on the aldehydes (*Figure 22*). If in this prior step we observed a major problem, remaining ammonium salts can undergo protodeboronation of the boroxine. In the other hand, this amine **45** is also hygroscopic which is really undesirable because we observe hydrolysis of the boroxine after the addition of this nitrogen containing compound, leading to the formation of the iminoboroxine and the iminoboronic acid. By the way the partial hydrolysis of the iminoboroxine **46** can also be explained by the enhance tendency to react with water generated during the condensation of the aldehyde and the amine. A heating step should be tested to obtain pure iminoboroxine from iminoboroxine/iminoboronic acid mixture but due for sake of time this step could not be tested but we have great confidence against the possibility to form this kind of pure iminoboroxine for further uses such as ones aforementioned.

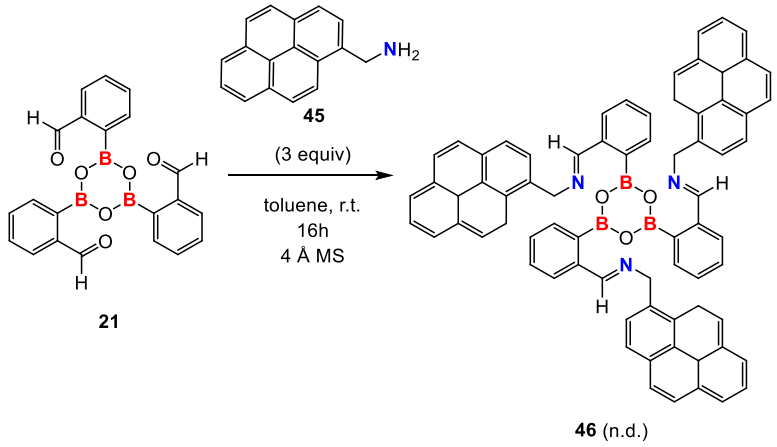

Figure 22 - Pyrene iminoboroxine synthesis procedure

In parallel we also considered the possibility to form the isolated iminoboronic acid **47** with this pyrene substituent keeping the possibility to use that kind of compound as Lewis catalyst since the acidity of the boroxine and boronic acid is relatively identical but we lose the association/dissociation capacity of this catalyst (*Figure 23*). This has been successfully realised in similar condition as the others iminoboroxine previously synthetised and as said before a heating step could be considered for forming the corresponding boroxine. At the end of the reaction, the resulting solid was a mixture of the boroxine **46** and the boronic acid **47**, these results show that these conditions are sufficient for partial dehydration of the system and strengthens us in the possibility of forming the iminoboroxine in mild conditions.

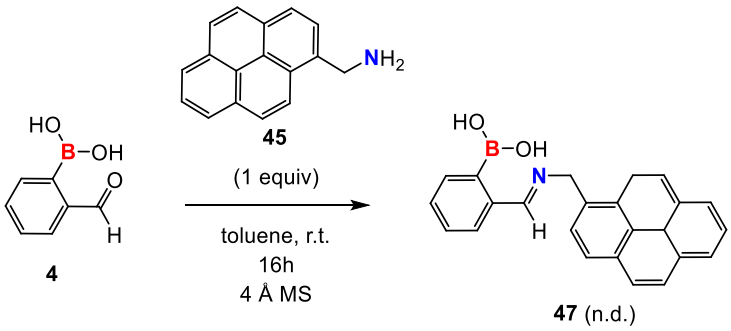

Figure 23 - Pyrene iminoboronic acid synthesis procedure

Structural investigation of boroxines in the solid state

After our detailed investigations of the structures in solution by NMR spectroscopy, we study the effect of the substituents at the atomic level in the solid state by X-ray diffraction analysis. This structural study will provide insights on the optimal substituents required for increasing the stability of the adduct formed. This is of particular importance for the design of self-healable systems having stronger Lewis acid/base interactions.

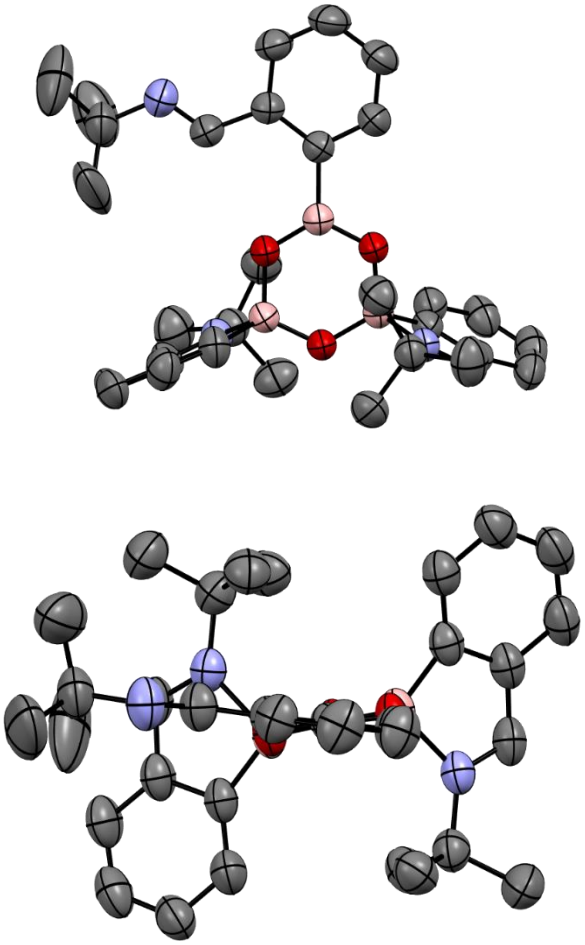

*Figure 24 – Molecular structure of boroxine **34** Ellipsoids are represented at the 50% probability level*

The XDR analysis on single crystal of the iminoboroxine **34** (*Figure 24*) showed that two nitrogen atoms where interacting with two boron atoms from the boroxine *via* opposite faces, forming two spirocyclic 5-membered ring iminoboronate pointing respectively up and down of the boroxine molecular plane. In the solid state the observed B-N lengths are respectively of 1.755 and 1.804 Å in the range of a typical B-N bond, and much shorter than the sum of the Van der Waals radius is 3.47 Å. The remaining uncomplexed imine is under the *E* configuration similarly as the two coordinated ones. This is expected since the *E* diastereomer is thermodynamically more stable than the *Z*, because the steric repulsions between the boroxine faces and *tert*-butyl are minimized.[40] Moreover, the angle of pyramidalization around the boron atom could give information on the B-N interaction strength. In **34**, the angles formed are respectively in each Lewis adducts (ring plane-B-C angle) of: 136.7 and 137.7 °.

For the fluoro substituted boroxine **37**, a similar structure with two intramolecular B-N Lewis adducts and with the *E* imine stereochemistry was observed (*Figure 25*). The *t*-butyl present on

the uncomplexed imine is disordered with a favourite position (94/6 ratio). The B-N bond lengths of 1.762 and 1.794 Å are identical than **34** considering the accuracy limits, showing that fluorine is in *para* position of the imine has not a significant effect. This was expected since the electron withdrawing *para* inductive fluorine effect is small (σ_p = 0.06). The B-O bonds are of similar length in the fluorinated iminoboroxine (1.406 Å) than in the unsubstituted iminoboroxine (1.404 Å). Boroxine **37** the angle formed for the two adducts (ring plane-B-C angle) are the following: 138.0 and 140.4 °.

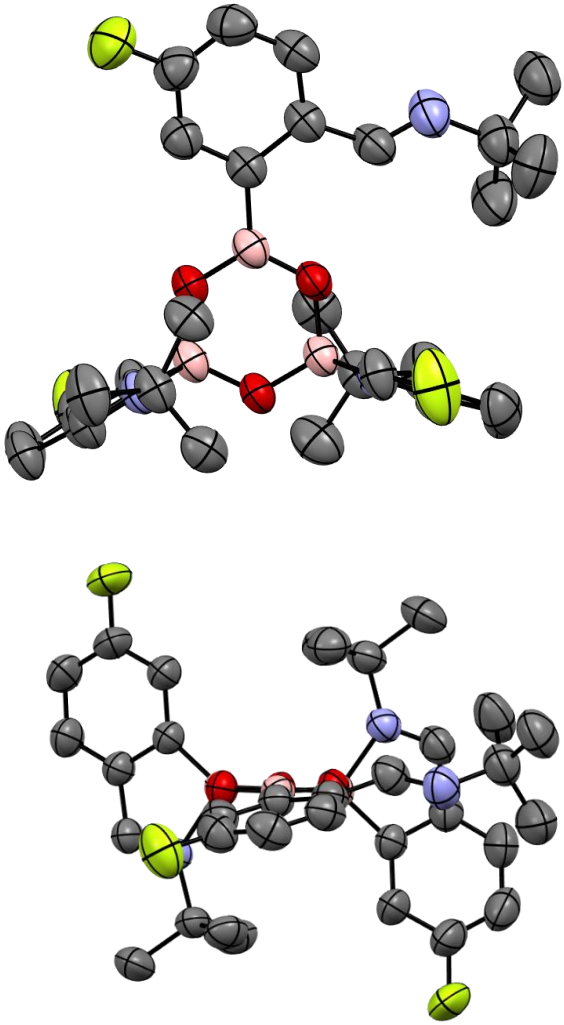

*Figure 25 – Molecular structure of boroxine **37** Ellipsoids are represented at the 50% probability level*

These structural studies are also confronted with infrared spectroscopy which could give be used as a method for the comparison of the acidity of the boron atom in boroxine. This kind of study has been realised by Warren Piers based on the formation of Lewis adduct between carbonyls and boranes to compare the Lewis basicity of the carbonyls.[41] This study showed

that the wavenumber of the C=O bond decrease when the oxygen is in interaction with the boron atom compared to the free carbonyl.

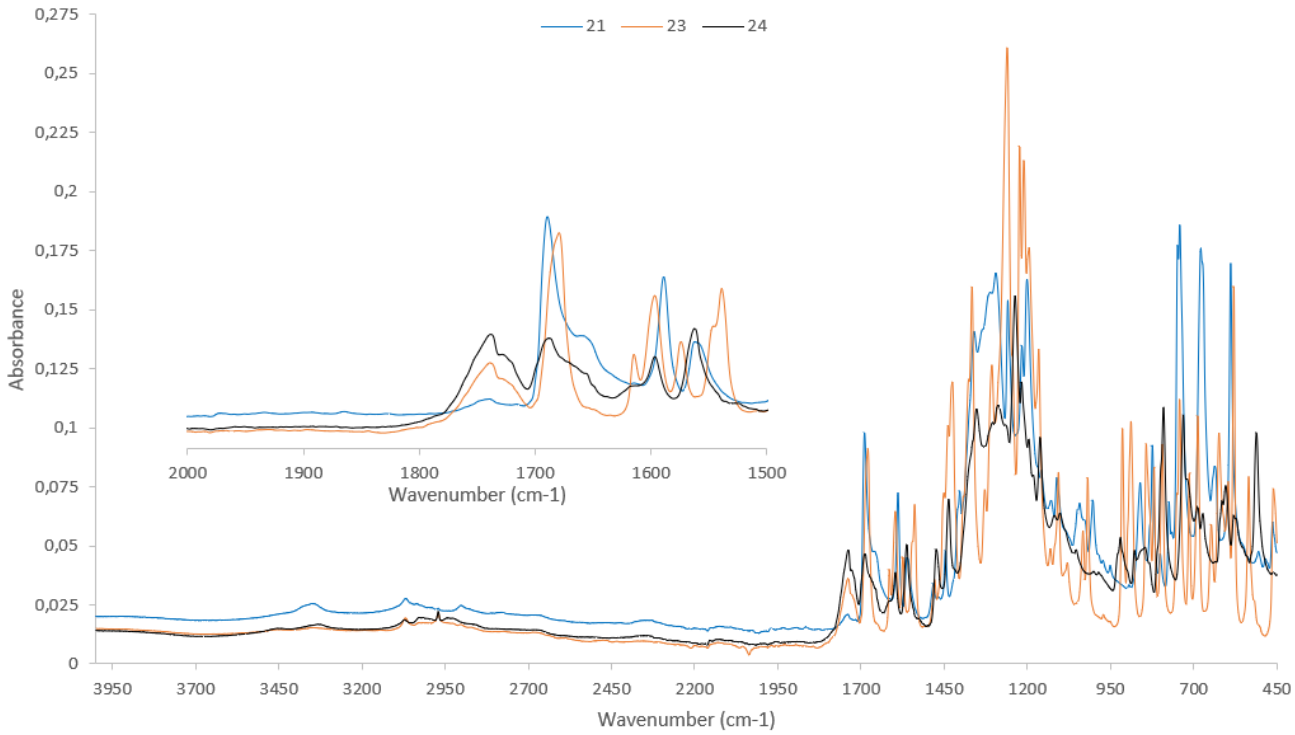

Figure 26 - IR spectra of formyl phenylboroxines with a zoom on the region between 1500 and 2000 cm^{-1}

In the case of formyl phenylboroxine (*Figure 26*) **21**, **23** and **24**, we observed carbonyl-boron interaction but also free carbonyl at two different wavenumbers, respectively at around 1680 and 1740 cm^{-1}. Based on the variation of the wavelength of this adduct, we can construct an acidity scale of the boroxines synthetised which is the following: **21** (1689 cm^{-1}) < **23** (1687 cm^{-1}) < **24** (1679 cm^{-1}). This is due to fluorine atom at the *ortho* position of the aromatic ring which by electron withdrawing inductive effect (σ_n = 0.34) increased the electron defiance of the boron atom making it more acidic. The difference observed between boroxine **23** and **24** could be explained by the proximity of this atom which could explain the lowered density on the carbonyl leading to a decreased interaction between boron and oxygen. For iminoboroxines (*Figure 27*), the range is the following: **34** (1629 cm^{-1}) < **37** (1630 cm^{-1}) < **40** (1631 cm^{-1}), these C=N bonds show less variation when the adduct is formed. These two scales could give indications of the relative Lewis acidity but the variation of these double bond is also linked on the effect of the neighbours functions in completion to the adduct formation.

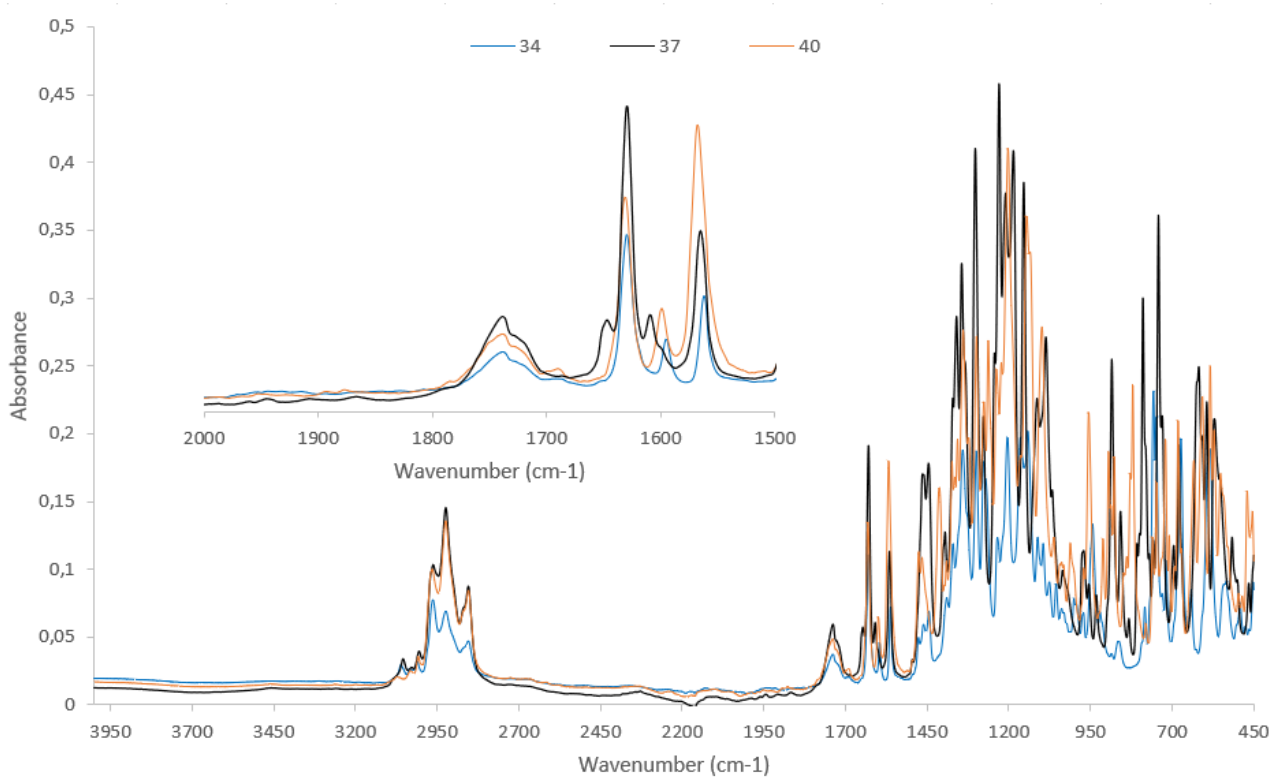

Figure 27 - IR spectra of [2-[(tert-butylimino)methyl]phenyl]-boroxines with a zoom on the region between 1500 and 2000 cm^{-1}

Next, the Lewis acidity of three boroxine were gauged by performing the ^{31}P NMR upon the complexation of $(Et)_3PO$ as in the Gutmann–Beckett method (*Figure 28*). An excess of $(Et)_3PO$ (2 equivalents) was dissolved in CD_2Cl_2 with one equivalent of the boroxine and analysed by ^{31}P NMR spectroscopy. The acidity values order **21** (AN=78.2) < **24** (AN=79.2) < **23** (AN=88.0), is different than the order found in the IR study. As mentioned before, the proximity of the fluorine to the carbonyl that could interfere for the determination of the Lewis acidity by IR spectroscopy. The acceptor number allow us to compare these boroxines to others boron Lewis acids such as $B(C_6F_5)_3$ (AN=78.9) and $Ph_3B_3O_3$ (AN=49).[42]

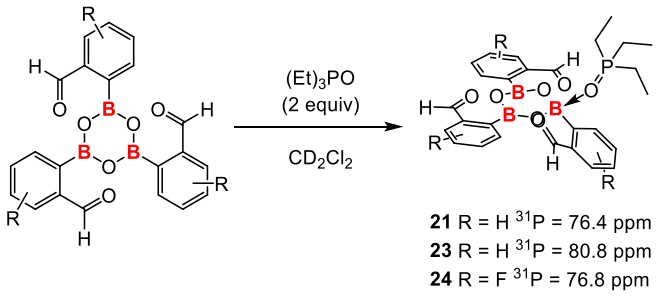

Figure 28 - Gutmann–Beckett method for the Lewis acidity determination af the boroxines

The hydrolysis of the iminoboronate-based boroxine in wet $CDCl_3$ is producing the imino-boronic acid and subsequent evaporation of the solution and heating under reduced pressure successfully yielded the imino-boroxine (*Figure 29*). However, with a large excess of water, we also observed the imine hydrolysis. Thus, the concentration of water needs to be finely controlled in order to avoid the undesired total hydrolysis into boronic acid benzaldehyde derivatives. This parameter is crucial, as if the imines are hydrolysed, there will be a diminution of the reticulation nodes, a loss of the mechanical and healing properties, which is far from being desired. This consideration can be neglected because the thermodynamic stability is enhanced by the bond formed in iminoboronate species which makes the imine product more robust against hydrolysis [43] [44]. This iminoborate has been chosen as bridging group in the polymer due to the possible modulation of the Lewis basicity of this functional group which can control the hydrolysis of the boroxine via the iminoborate bonds and the facile fabrication.

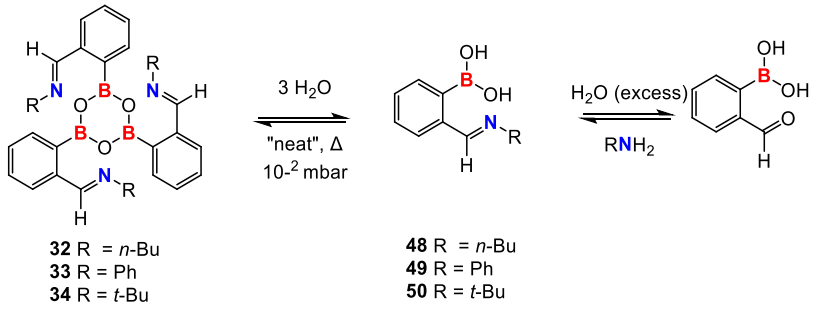

Figure 29 - Iminoboronate-based boroxine/boronic acid equilibrium and the hydrolysis of the imine

As we wanted to have a time resolved evolution of the hydrolysis process the reference boroxine **26** stability has been realised in stopped flow spectrophotometer where the UV-visible spectra have been recorded. Solutions at 1.10^{-3} and 5.10^{-4} M in acetonitrile have been prepared and two main absorption bands where observed at λ_{max}^1 = 224 and λ_{max}^2 = 265 nm which could undergo a blue or red shift during hydrolysis process (*Figure 30*).

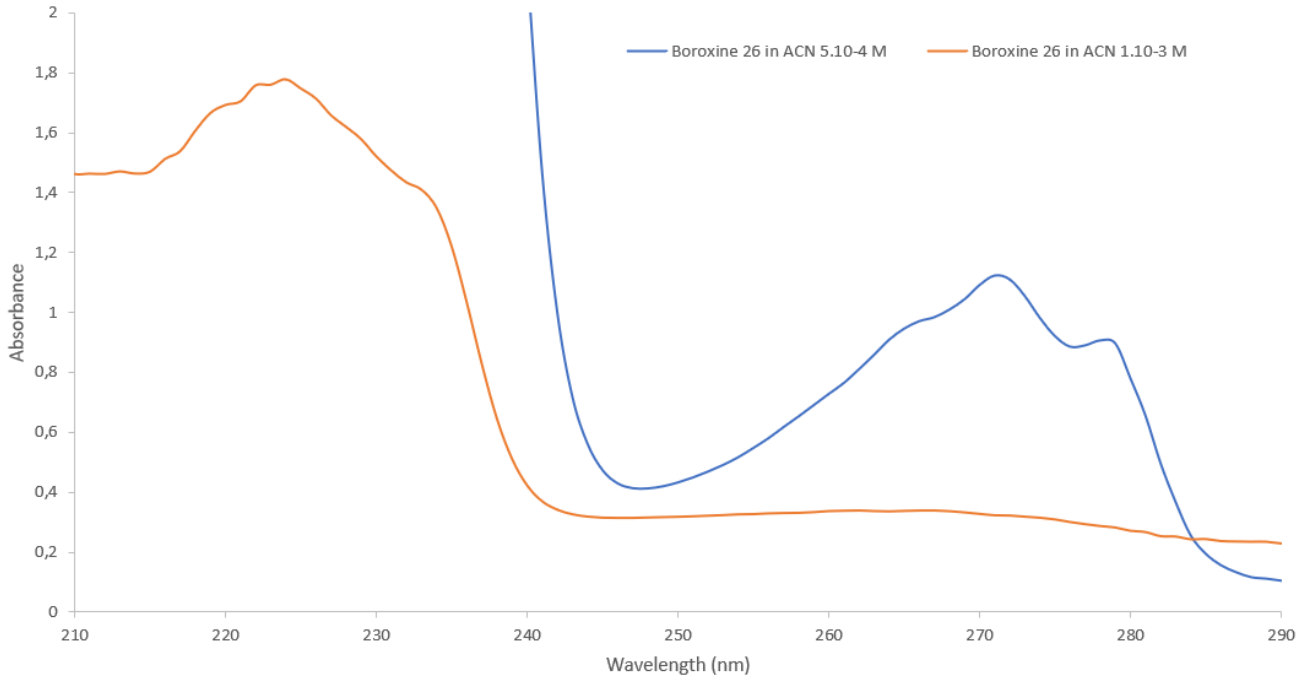

Figure 30 - UV-visible spectra of triphenylboroxine in acetonitrile

Stopped-flow measurement showed that the atmospheric humidity is sufficient to hydrolyse that compound, we were not able to determine the hydrolysis rate *via* this method due to the necessary conditioning of the device which is filled by ambient air. But on the other hand, we were able to obtain the spectra of these solutions by UV-visible spectroscopy in sealed cuvettes for these solutions. A stability test has also been realised and the solution appears to be stable during the interval chosen, this huge difference compared to the stopped flow could be explained by the reduced contact of the solution to the air in the case of the cuvette cells whereas during the stopped flow air has been injected in the solution and hydrolysed the boroxine. But as soon as we add water in the medium, the boroxine at the concentration of 1.10^{-3} M in acetonitrile directly hydrolyse leading to the boronic acid. We can also observe a hypsochromic (265 to 261 nm) effect due to a more energetic electronic transition (*Figure 31*). This difference between the boronic acid and the boroxine is principally due to the partial conjugation in the ring formed by the boron and oxygen which lower the transition state and the energy needed for the electronic transition.

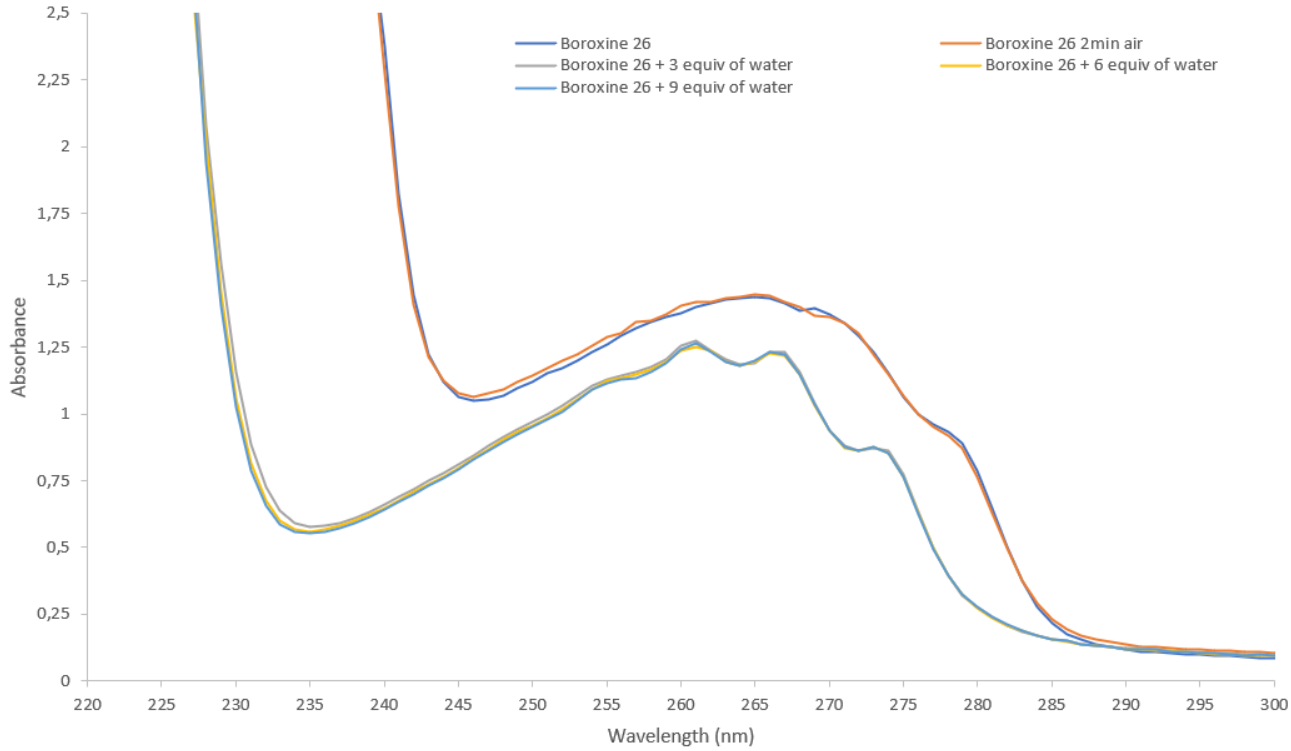

Figure 31 - UV-visible spectra of triphenylboroxine at 5.10^{-4} M in acetonitrile during hydrolysis

Self-healable polymer with boroxine nodes

The boroxines synthetised *via* the methods previously developed in this work will now be employed as reticulation nodes in star-shaped polymers (*Figure 32*). These nodes have two major advantages the first being the reversibility and the dynamic formation of the B-O boroxine bonds which allows the non-permanent reticulation making the recycling of the material possible *via* total hydrolysis/recondensation. This reversibility is also an important parameter to obtain interesting properties such as the self-healing aspect, when the damaged polymer is exposed to humidity, the boroxine slowly hydrolyse, increasing the mobility of the polymeric chains. Due to this increased mobility, the polymer chains will fill the damaged part and after a mild thermic treatment, the healed-polymer with original properties is regenerated.

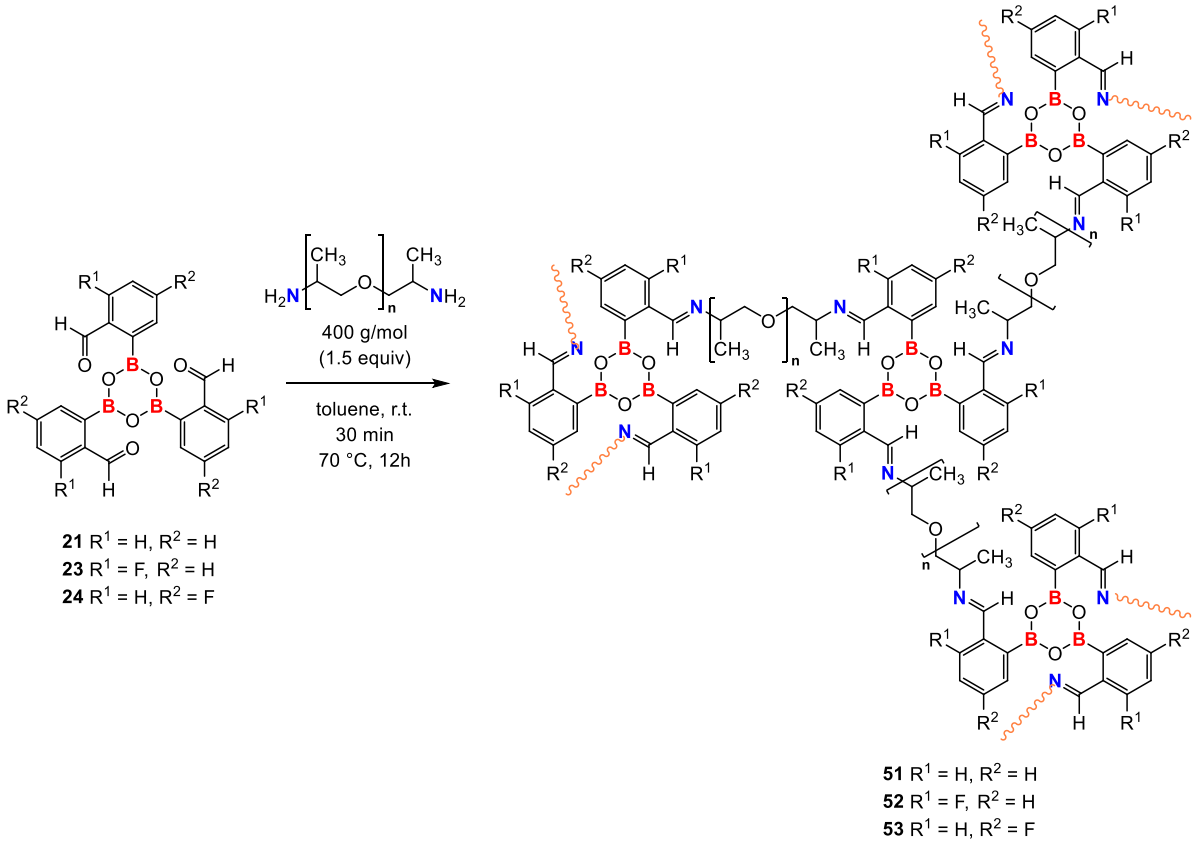

Figure 32 - Synthesis PPG polymer crosslinked by boroxine nodes

Within a PPG polymer, different boroxines are incorporated by condensation reaction between aldehyde and an diamine (1.5 equivalent of 400 g.mol^{-1} poly(propylene glycol) bis(2-aminopropyl ether) leading to the formation of imines, running to the reticulation of the

polymer. This has been successfully realised with the boroxines **21**, **23** and **24** by solubilising the boroxine in dry toluene, adding the PPG amine at room temperature and after 30 minutes of agitation, the solvent was slowly evaporated at 70 °C (solvent casting) during 12h in a petri dish with Teflon film to prevent adhesion of the polymer to the glass. A similar polymer (**54**) has been obtained with a excess (1.75 equivalents) of 400 $g.mol^{-1}$ poly(propylene glycol) bis(2-aminopropyl ether) leaving some free amines in the polymer. With these polymers in hands, healing tests have been performed under three conditions. After an induced cut, we followed the healing under 43 % of relative humidity) at ambient temperature (condition A) and under ambient conditions (35 % of relative humidity at 20 °C) and (conditions B and C). In these ambient conditions we observe partial healing after 48h while humidity enriched conditions showed that we have total healing after same time. The characterisation of the healing is quite spread and convenient, this study gives preliminary indications of the healing efficiency.[12]

*Table 2 - Optical microscopy healing characterisation of the polymers **51** to **54** at 43% of relative humidity (A) and ambient conditions (B and C)*

Polymer	Crack size at 0h (µm)	Crack size at 48h (µm)	Healing ratio (%)
51A	66.940	64.834	3.1
51B	58.116	0	100
52A	50.144	0	100
52B	38.091	0	100
53A	58.653	16.685	71.6
53B	50.301	0	100
54A	72.067	3.701	94.8*
54B	82.754	0	100*
54C	42.435	0	100

Moreover, some of these polymers required a reduced healing time compared to the reference system in same conditions (**51A** and **51B**). Especially the material **52** formed from the boroxine **23**, even showed a complete cicatrisation after 48h while the others showed partial healing (*Table 2*). This comportment can be explained by different factors, firstly an increased healing kinetics for some of these polymers, secondly a deeper cut and lastly the separation of the two polymeric parts can also cause that decreased time. The polymer **54A** in ambient condition also showed a rapid healing, within 24h, the material was almost totally healed and in 48h total healing due to the free imines present in the polymer accelerating the imine C=N exchange reaction, similarly the same polymer **54B** at 43 % relative humidity showed a total healing within 24h.

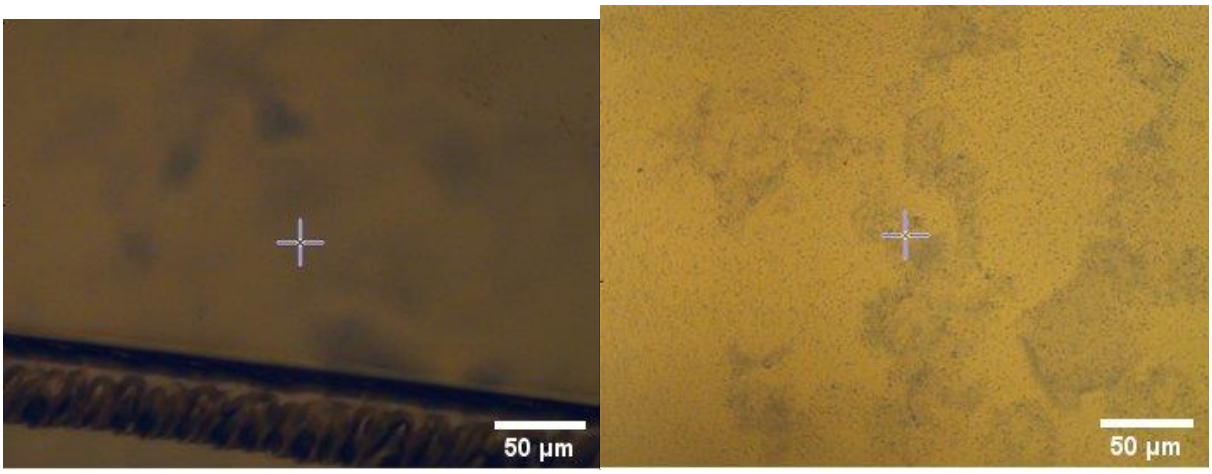

*Figure 33 -Microscope pictures of polymer **52** cut (left) and repaired after 48h exposure to ambient humidity (right) at X20 magnification*

In addition to of the optical measurements (*Figure 33*), we performed Raman measurements both at the undamaged sample surface and at the damaged part in order to follow the healing of the material by monitoring the modifications of the characteristic bands of the boroxine, boronic acid and imine. Unfortunately, this analysis can be prevented by the fluorescence of the analyte as explained in the appendixes. This was the case for the different PPG-boroxine systems synthetised, we only observe large peaks of fluorescence despite the wavelength of the laser source used. We couldn't characterise the healing of the polymer via this analysis method with a 785 nm laser (*Figure 34*) these bands are typically aromatic ring fluorescence in Raman spectroscopy (1367, 1355 and 1385 cm^{-1} for polymers **51**, **52** and **53**). Even with a 532 nm laser, we observed fluorescence bands (1388 cm^{-1} with reference polymer **51**) which can't give information about the healing process of the polymer. Basically, this method is not adequate for these systems but could be highly interesting for less fluorescent nodes in the polymer.

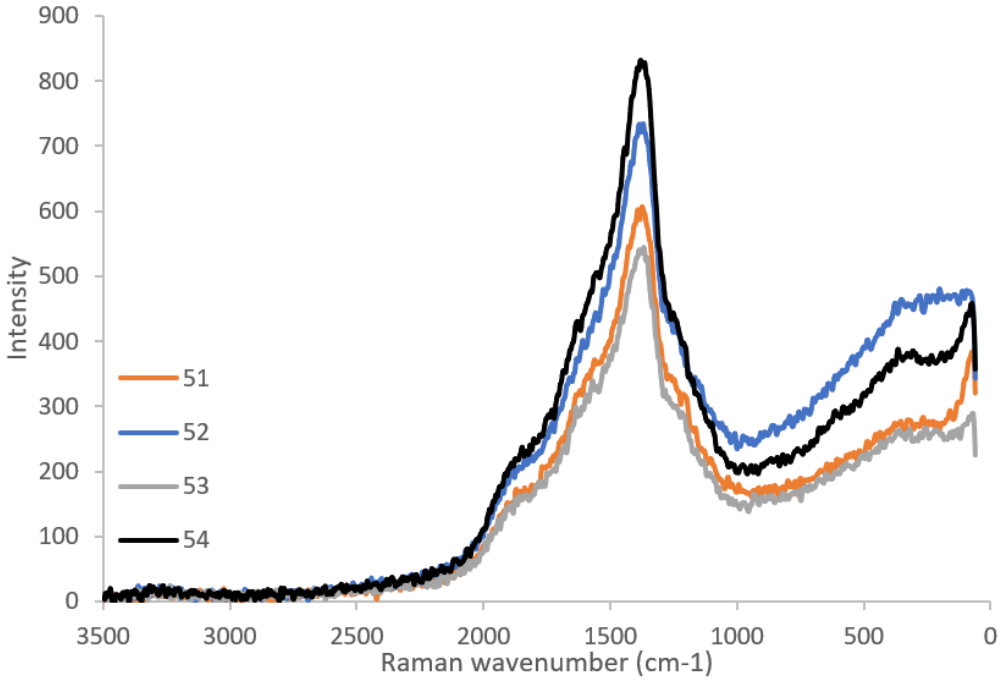

Figure 34 – Raman spectra of iminoboroxine based polymers recorded at 785 nm laser excitation

The IR characterisations was performed to investigate the healing kinetic and the mechanism involved. During the exposition to humidity, slow apparition of broad O-H stretching band around 3450 cm^{-1} were observed. A second spectral modification was the decrease of intensity of the boroxine band at 743 cm^{-1} while a boronic acid band increased (756 cm^{-1}), the ratio between these two peaks evolved with the time. The characteristic amine bands (N-H bending around 1600 cm^{-1} and C-N stretching around 1100 cm^{-1}) and the aldehyde one at 1687 cm^{-1} are not observed despite the hydrolysis, leading us to the conclusion that imine bond remains stable in the polymer due to their improved stability by the formation of the Lewis adduct by the constant intensity of the C=N absorption band at 1750 cm^{-1}.

Moreover, a kinetic study has been performed with the polymer **52**, this measurement showed that in the polymer, a part of this material is partially under the form of boronic acid and a part under the form of boronic acid. The ratio of the IR peaks of boronic acid/boroxine evolves with the time showing that we form boronic acid from the hydrolysis of the boroxine during the exposure to humidity. Three regions have been delineated (*Figure 35*), firstly a plateau is observed during the four first hours and during the two/three next hours we observe a noticeable variation of this boronic acid/boroxine ratio. This comportment is certainly linked to the hydrophobicity of the polymer that prevent the initial condensation of water on its surface and also the hydrolysis at the surface, but as soon as water enter in

contact with the boroxines nodes, the overall hydrolysis is initiated and occurs relatively fast. As soon as the boroxines at the surface are hydrolysed, we observe a second plateau, but the polymer still contains boroxines which are reticulating the material and is present in the polymer deep. This plateau starting at 7 hours could lead to another variation of the ratio boronic/boroxine if the increase mobility of the polymeric chain allows the exposure of these boroxine to the surface.

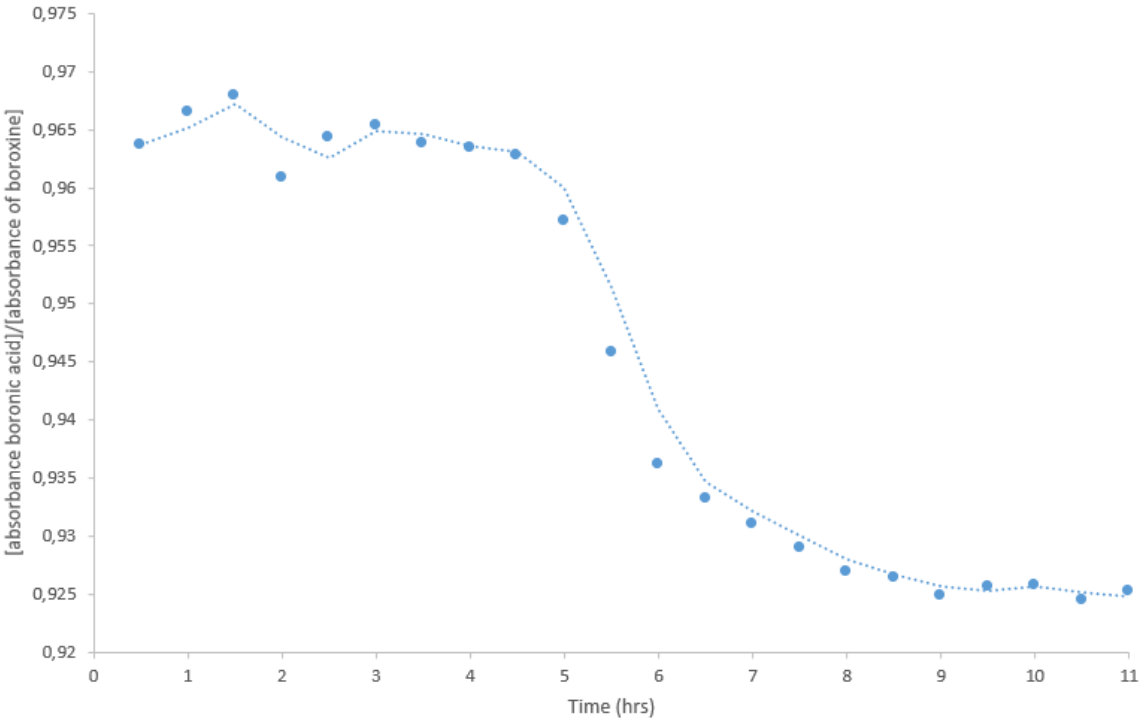

*Figure 35 - IR kinetic study of polymer **52** through the boroxine/boronic acid peaks*

We finally performed thermogravimetric analysis (TGA) and differential scanning calorimetry (DSC) to characterise the temperature stability improvement and the physical transitions of the different polymers.

The TGA analysis will give us information of the boroxine containing polymers and of the corresponding polymer after hydrolysis in ambient conditions (*Figure 36*). With iminoboroxine polymers we observed diverse degradations during the heating process. In every polymer tested we observed a first mass loss between 45 and 100 °C corresponding to the condensation of residual boronic acids present in the polymer.[45] A mass loss occurs at higher temperature (130 °C), which could correspond to residual solvent loss due to the solvent casting present in the polymer. The TGA analysis showed that the introduction of fluorine

substituents leads to a slight diminution of the thermal stability or maintain similar stability and same behaviour when the polymer is heated. Moreover, that analysis show that the thermosets could be used at maximum 200-250 °C without any mass problem and around 250-300 °C as limits of use of this polymer based on this measurement (Table 3).

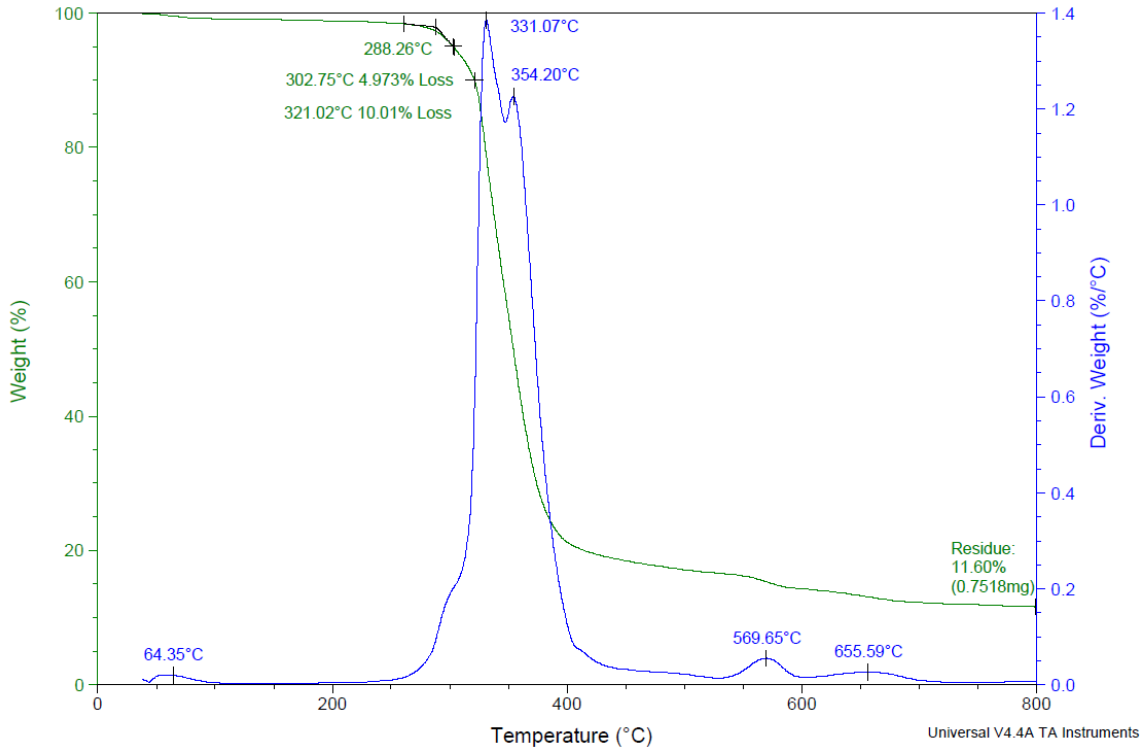

*Figure 36 - TGA curve of the evolution of the polymer **51** mass with the temperature (green) and the first derivative (blue)*

Based on literature data, we can also ensure that the main degradation peak is intrinsic to the polymer[45 46] but, the TGA also showed that even after exposure to ambient humidity during one week, the thermoset is relatively stable. The boroxines present in the polymer are only partially hydrolysed at the surface leading to quite similar overall properties except a slightly decreasing of the thermal properties (main degradation peak, 5% mass lost, …).

*Table 3 – TGA characterisation of the polymers **51** to **54** stored at 70 °C and in ambient conditions during one week (H)*

Compound	Onset (°C)	$T_{5\%\ mass\ lost}$ (°C)	$T_{10\%\ mass\ lost}$ (°C)	Main degradation peak (°C)	Residual mass (%)
51	288	303	321	331 and 354	11.60
51H	282	294	310	320 and 343	9.054
52	275	283	299	348	8.308
52H	248	264	284	340	8.308
53	289	306	321	337 and 356	10.55
53H	292	304	313	324 and 351	8.758
54	280	292	306	354	6.840
54H	279	288	303	353	7.115

The TGA measurement are usually coupled with the study of the change of the heat capacity occurring during the increase of the temperature, leading to the detection of different physical transformations such as melting, glass transition, phase change, crystallisation and curing.

For the polymers **51**-**54**, an endothermic associated to the T_g and is slightly under the room temperature, respectively at 19.9 °C for **51**, 18.4 °C for **52**, 21.8 °C for **53** and 14.1 °C for **54**. These temperatures of glass transition show that the healing test were performed at room temperature was, thus in the at the molten glass state. Mobility of the chains associated with the partial hydrolysis leading were thus optimal for a fast-healing process. No other phase

changes were observed confirming that these polymers are amorphous ad only are in the glass state or molten state. Crystallisation has not been observed (T_c), a process which is exothermic, due to the decrease of mobility in the polymer liberating energy. The melting (T_m) of the material is not occurring in the -80 to 220 °C range, which is an endothermic transformation were the disorder of the material increases during the solid to liquid phase change (*Figure 37*).[3]

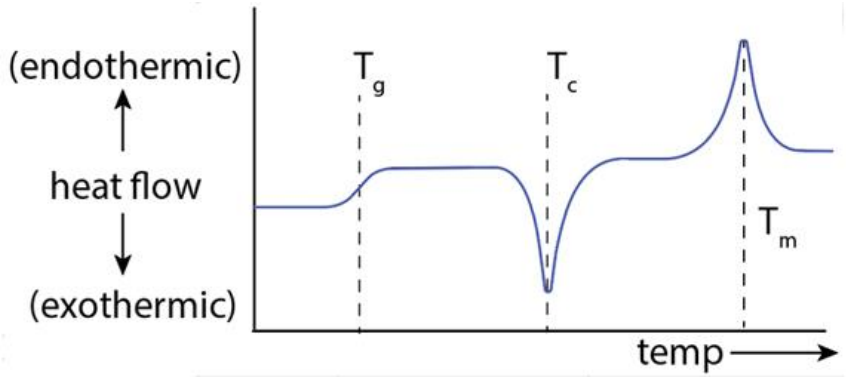

Figure 37 - DSC trace showing multiple phase transitions of a polymer[47]

This boroxine dynamic platform has been firstly used in polymers in 2016[48] for obtaining healing properties for a poly(dimethylsiloxane) (PDMS) polymer. This polymer showed great healing properties and that property has been obtained by wetting the damaged material to generate free boronic acid at the surface and heating it during five hours to obtain high healing efficiencies (95 % recovery of the Young's modulus). This heating at 70 °C has been realised for two reasons, first this step is necessary for the condensation of the boronic acid into boroxine, second this heating lead to the softening of the material (T_g = 65 °C) and increase the chain mobility leading to facilitated healing process. But a notch was still observable after healing (*Figure 38*) and show that the presence of that scar does not affect the mechanical properties so the complete healing (from a visual aspect) is not necessary for mechanical tests. This difference of about 45 °C between the reported polymer and ours is due to the nature and length of polymeric chain used (PDMS versus PPG) modifying the interactions between chains and the thermo-mechanical properties.

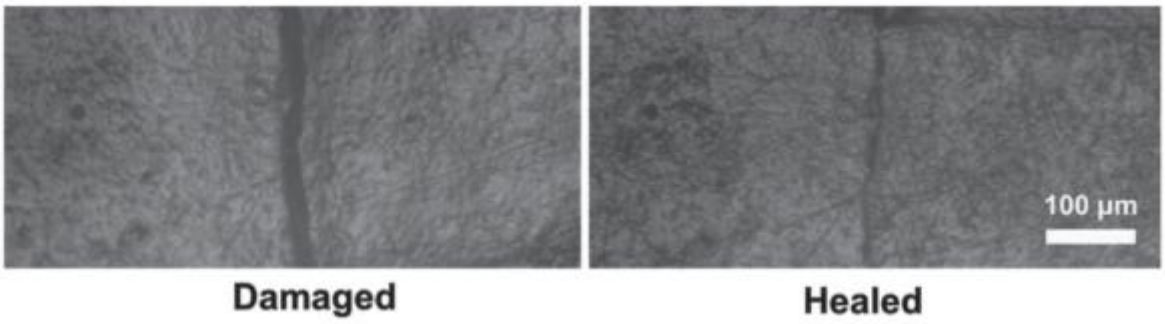

Figure 38 - Microscopic images of a fi lm before (left) and after (right) healing at 70 °C for 5 h[48]

For obtaining improved mechanical and healing properties, aminoboroxine based PPG polymer has been synthetised.[49] Previous studies have shown that the nitrogen-donor compounds, can form Lewis adduct with the boron atom of boroxine to stabilise the ring structure, thereby accelerating the equilibrium between boroxines and boronic acids at room temperature, improving healing kinetic by this interaction which lower the acidity of the boronic acid. This polymer showed a lower T_g than the PDMS-Boroxine (-55 versus 65 °C), due to the use of a PPG instead of a PDMS polymer chain. Compared to polymers **51**-**54**, this aminoboroxine-PPG material showed lower T_g for two major reasons, firstly this temperature should rise while increasing the M_n of the polymer[50] and on the other hand the stronger interaction between amine and boron than the interaction between the imine and boron in our case.

$$T_g = T_{g\infty} - \frac{K}{\overline{M_n}}$$

In the case of this material (*Figure 39*), interesting mechanical properties were observed, mainly due to the molecular mass of the polymeric part, one solution proposed to increase these properties was obtain by developing composite with poly(acrylic acid) (PAA) which form hydrogen bounds with the aminoboroxine-PPG leading up to 112,45 MPa young modulus while iminoboroxine-PPG 400 polymer exhibit Young's modulus at 61 MPa and the boroxine-PDMS have Young's module up to 182 MPa.

Figure 39 - Digital photos of the N-boroxine-PPG sheet being cut into two pieces and being healed at room temperature[49]

6. Perspectives

In this master thesis new molecules have been prepared, boroxines and iminoboroxines, effect of the substituents on the structure and the Lewis acidity has been determined by NMR spectroscopy. X-Ray diffraction analysis on single crystal of these compounds could provide information of this effect of the aromatic rings and imine substituents at the structural level and in addition, acidity measurements (Gutmann-Beckett and IR study) were providing insights on the Lewis acidity of these boroxine derivatives.

Tris[2-[(pyren-1-ylmethylimino)methyl]phenyl]-boroxine **46** and 2-[(pyren-1-ylmethylimino) methyl]phenyl-boronic acid **47** were obtained in mixture despite the use of tris[2-formylphenyl]-boroxine **21** or (2-formylphenyl)boronic acid **4** as starting material. These ambient conditions are not sufficient for obtaining pure iminoboroxine **46**, a heating process is needed and will be tested. A new boroxine containing pyrene could form π- π staking with CNT or C60 as a first study of the possibility to support them for heterogenous catalyst.

Several reactions could be considered with the boroxines, iminoboroxines and even with boronic acid ant iminoboronic acid, these species could be incorporated in boronic acid Mannich, Suzuki reactions and so on. The most interesting boroxine is certainly the tris[2-[(furfurylimino)methyl]phenyl]-boroxine **42** on which a Diels-Alder reaction could be performed to connect other polymer chains and forming copolymers, increasing the interest of the boroxine platform.

Different works reported the formation of boroxines molecular cages which, based on the organoboron, could perform Lewis acid/base interactions to induce a selectivity of the guest molecules in that cage. Based on these considerations, we envisioned the synthesis of iminoboroxine based cages with a small diamine. That kind of iminoboroxine cage could be interesting for the encapsulation of ions of different gases with a possibly reversible trapping of the guest due to the dynamic behaviour of the boroxine platform.

Structural studies are crucial for discovering even better boroxine nodes functionalisation patterns for obtaining self-healable polymers with even better properties. Furthermore, the mechanical tests on these polymers need to be performed to characterise the mechanical improvement and the recovery of the healing efficiency based on the percentage of strain of

the non-cracked and healed material. Moreover, recycling tests could also be considered leading to promising polymer with numerous applications such as self-healable coating, 3D printing of self-healable and recyclable 3D objects, self-healable adhesives, transfer printing, solid polymer electrolytes or piezoresistive sensors able to monitor different body motions.

The versatility of this iminoboroxine platform allow to consider the synthesis of conjugated polymers which take part in portable electronic systems due to the reduced density of polymer and the flexibility of this material. This iminoboroxine electronically conjugated polymer could also as the PPG-iminoboroxines have self-healing properties leading to high interest conductive polymers which could be repaired in ambient conditions once damaged, avoiding the human intervention for miniaturised or inaccessible devises.

7. Conclusions

During this master thesis, the development of a practical and reliable method to synthesise formyl-boroxine and imino-boroxines was achieve. These dynamic platforms have been used for developing self-healing polymers. Promising results have been obtained, such as the reversible iminoboroxine hydrolysis and recondensation on the model system **21**. Also, boroxines with different imines substituents have been prepared for investigating their effects on the boronic acid/boroxine equilibrium for the first time, and for understanding their influence on the structures effect of these substituents.

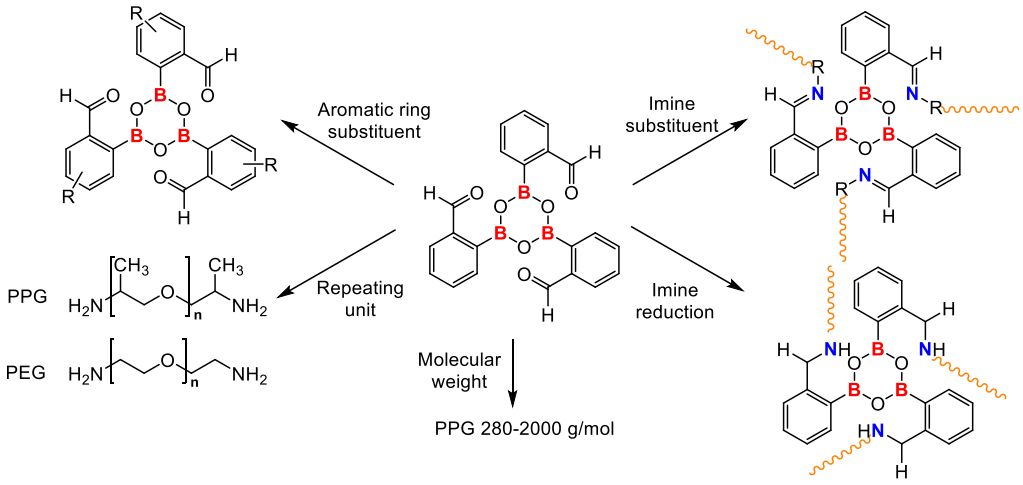

Figure 40 - Considered modifications to adjust the self-sealing properties of the iminoboroxine based polymer

This represents a new approach to optimise the self-healing polymer properties. The modification of the aromatic ring substituents allowed to finely control the hydrolysis rate of the polymer. The repeating unit and the molecular weight of the polymer can be also investigated as a complementary study for self-healing polymers development. Due to the variation of interchain interactions, crosslinking density of the polymer can modify the thermo-mechanical properties (*Figure 40*). We synthetised four self-healing polymers at the SMPC lab and characterised them. Forming polymers with improved healing process and similar thermal stability as previously reported polymers, the healing kinetics for two of them was improved compared to readily reported one in same condition (ambient temperature and humidity), with optical microscopy we observed the total disposition of the damage within 24h (**54**) and 48h (**52**). On the other hand, the thermal degradation of each polymers are similar and the transitions are also similar with a glass transition close to the room temperature (14-22°C).

8. References

1 P. C. Painter and M. M. Coleman, *Fundamentals of polymer science : an introductory text*, Technomic Pub. Co, 1997.

2 N. G. McCrum, C. P. Buckley and C. B. Bucknall, *Princ. Polym. Eng.*, 1997, 84–116.

3 A. T. Lorenzo, M. L. Arnal, J. Albuerne and A. J. Müller, *Polym. Test.*, 2007, **26**, 222–231.

4 K. R. Reddy, A. El-Zein, D. W. Airey, F. Alonso-Marroquin, P. Schubel and A. Manalo, *Nano-Structures and Nano-Objects*, 2020, 23, 100500.

5 R. Brown, *Handbook of polymer testing : physical methods*, Marcel Dekker, 1999.

6 L. D. Moore, T. Le and G. Fan, *Neuropsychopharmacology*, 2013, **38**, 23–38.

7 S. Wang and M. W. Urban, *Nat. Rev. Mater.*, 2020, **5**, 562–583.

8 R. P. Wool, *Soft Matter*, 2008, **4**, 400–418.

9 S. Thomas and A. Surendran, *Self-healing polymer-based systems*, Elsevier, 2020.

10 X. Chen, M. A. Dam, K. Ono, A. Mal, H. Shen, S. R. Nutt, K. Sheran and F. Wudl, *Science.*, 2002, **295**, 1698–1702.

11 W. H. Binder, *Self-healing polymers: From principles to applications*, Wiley-VCH Verlag, 2013.

12 S. Cho, S. Y. Hwang, D. X. Oh and J. Park, *J. Mater. Chem. A*, 2021, **9**, 14630–14655.

13 Z. Q. Lei, P. Xie, M. Z. Rong and M. Q. Zhang, *J. Mater. Chem. A*, 2015, **3**, 19662–19668.

14 A. L. Korich and P. M. Iovine, *Dalt. Trans.*, 2010, 39, 1423–1431.

15 S. Delpierre, B. Willocq, J. De Winter, P. Dubois, P. Gerbaux and J. M. Raquez, *Chem. Eur. J.*, 2017, **23**, 6730–6735.

16 X. Zhang, Y. Zhao, S. Wang and X. Jing, *Mater. Chem. Front.*, 2021, **15**, 5534–5548.

17 W. A. Ogden and Z. Guan, *J. Am. Chem. Soc.*, 2018, **140**, 6217–6220.

18 G. N. Lewis, *Valence and the structure of atoms and molecules,* New York, 1923.

19 J. N. Bentley, S. A. Elgadi, J. R. Gaffen, P. Demay-Drouhard, T. Baumgartner and C. B. Caputo, *Organometallics*, 2020, **39**, 3645–3655.

20 P. Erdmann, J. Leitner, J. Schwarz and L. Greb, *ChemPhysChem*, 2020, **21**, 987–994.

21 J. M. Slattery and S. Hussein, *Dalt. Trans.*, 2012, **41**, 1808–1815.

22 A. Adamczyk-Woźniak, M. Jakubczyk, A. Sporzyński and G. Zukowska, *Inorg. Chem. Commun.*, 2011, **14**, 1753–1755.

23 C. S. Hanson and J. J. Devery, *J. Vis. Exp.*, , DOI:10.3791/60745.

24 A. Adamczyk-Woźniak, J. T. Gozdalik, D. Wieczorek, I. D. Madura, E. Kaczorowska, E. Brzezińska, A. Sporzyński and J. Lipok, *Molecules*, , DOI:10.3390/molecules25040799.

25 M. P. Silva, L. Saraiva, M. Pinto and M. E. Sousa, *Molecules*, 2020, **25**.

26 P. A. Cox, A. G. Leach, A. D. Campbell and G. C. Lloyd-Jones, *J. Am. Chem. Soc.*, 2016, **138**, 9145–9157.

27 P. A. Cox, M. Reid, A. G. Leach, A. D. Campbell, E. J. King and G. C. Lloyd-Jones, *J. Am. Chem. Soc.*, 2017, **139**, 13156–13165.

28 S. Rej and N. Chatani, *J. Am. Chem. Soc.*, 2021, **143**, 2920–2929.

29 R. Bernardini, A. Oliva, A. Paganelli, E. Menta, M. Grugni, S. De Munari and L. Goldoni, *Chem. Lett.*, 2009, **38**, 750–751.

30 K. Kowalska, A. Adamczyk-Woźniak, P. Gajowiec, B. Gierczyk, E. Kaczorowska, Ł. Popenda, G. Schroeder, A. Sikorski and A. Sporzyński, *J. Fluor. Chem.*, 2016, **187**, 1–8.

31 Y. P. Budiman, S. A. Westcott, U. Radius and T. B. Marder, *Adv. Synth. Catal.*, , DOI:10.1002/adsc.202001291.

32 S. Moon, M. Kato, Y. Nishii and M. Miura, *Adv. Synth. Catal.*, 2020, **362**, 1669–1673.

33 S. Luliński, I. Madura, J. Serwatowski, H. Szatyłowicz and J. Zachara, *New J. Chem.*, 2007, **31**, 144–154.

34 M. Sassi, V. Oison, J. M. Debierre and S. Humbel, *ChemPhysChem*, 2009, **10**, 2480–2485.

35 S. Saha, R. K. Kottalanka, T. K. Panda, K. Harms, S. Dehnen and H. P. Nayek, *J. Organomet. Chem.*, 2013, **745–746**, 329–334.

36 A. Torres-Huerta, M. D. J. Velásquez-Hernández, D. Martínez-Otero, H. Höpfl and V. Jancik, *Cryst. Growth Des.*, 2017, **17**, 2438–2452.

37 A. Adamczyk-Woźniak, I. Madura, A. H. Velders and A. Sporzyński, *Tetrahedron Lett.*, 2010, **51**, 6181–6185.

38 Y. Song, J. R. C. Junqueira, N. Sikdar, D. Öhl, S. Dieckhöfer, T. Quast, S. Seisel, J. Masa, C. Andronescu and W. Schuhmann, *Angew. Chemie Int. Ed.*, 2021, **60**, 9135–9141.

39 C. Carati, N. Gasparini, S. Righi, F. Tinti, V. Fattori, A. Savoini, A. Cominetti, R. Po, L. Bonoldi and N. Camaioni, *J. Phys. Chem. C*, 2016, **120**, 6909–6919.

40 M. M. Utecht, F. Zhao, H. Kulla and S. A. Kovalenko, , DOI:10.1002/chem.201404649.

41 D. J. Parks, W. E. Piers, M. Parvez, R. Atencio and M. J. Zaworotko, *Organometallics*, 1998, **17**, 1369–1377.

42 M. Jakubczyk, A. Adamczyk-Woźniak and A. Sporzyński, *Chapter 4 Acceptor number of organoboron molecules-quantitative determination of Lewis acidity*, .

43 A. Bandyopadhyay, K. A. McCarthy, M. A. Kelly and J. Gao, *Nat. Commun.*, 2015, **6**, 6561–6561.

44 A. Bandyopadhyay and J. Gao, *Chem. - A Eur. J.*, 2015, **21**, 14748–14752.

45 A. Adamczyk-Woźniak, E. Kaczorowska, J. Kredátusova, I. Madura, P. H. Marek, A. Matuszewska, A. Sporzyński and M. Uchman, *Eur. J. Inorg. Chem.*, 2018, **2018**, 1492–1498.

46 Y. Xia, H. Yao, Z. Miao, Y. Ma, M. Cui, L. Yan, H. Ling and Z. Qi, *RSC Adv.*, 2015, **5**, 50955–50961.

47 Thermal Transitions and Differential Scanning Calorimetry | MATSE 202: Introduction to Polymer Materials, https://www.e-education.psu.edu/matse202/node/845, (accessed 17 December 2021).

48 J.-C. Lai, J.-F. Mei, X.-Y. Jia, C.-H. Li, X.-Z. You and Z. Bao, *Adv. Mater.*, 2016, **28**, 8277–8282.

49 C. Bao, Y.-J. Jiang, H. Zhang, X. Lu and J. Sun, *Adv. Funct. Mater.*, 2018, **28**, 1800560.

50 L.-P. Blanchard, J. Hesse and S. Lal Malhotra, *Can. J. Chem.*, 1974, **52**, 3170–3175.

51 K. Unapumnuk, T. C. Keener, M. Lu and S. J. Khang, *J. Air Waste Manag. Assoc.*, 2006, **56**, 618–627.

52 R. Comesaña, M. A. Gómez, M. A. Álvarez and P. Eguía, *Thermochim. Acta*, 2012, **547**, 13–21.

53 R. B. Prime and D. J. Mrnczel, *Thermal Analysis of Polymers: Fundamentals and applications*, 2009.

54 S. Tanaka, *Thermochim. Acta*, 1992, **210**, 67–76.

9. Material and methods

Analytical method

NMR spectra were recorded on 400 or 500 MHz NMR JEOL spectrometers. The observed signals are reported in parts per million (ppm) relative to the residual signal of the non-deuterated solvent for ^{1}H and ^{13}C NMR spectra. The external references considered as 0,0 ppm are borontrifluoride etherate ($BF_3.Et_2O$) for ^{11}B NMR, trichloromonofluoromethane ($CFCl_3$) for ^{19}F NMR and H_3PO_4 (85%) for ^{31}P NMR.

The following abbreviations are used to describe multiplicities s = singlet, d = doublet, t = triplet, q = quartet, quin = quintuplet, br = broad, m = multiplet.

Flash chromatography was performed using silica gel Silica Flash® 40-63 micron (230-400 mesh) from Sigma-Aldrich. TLC detection was accomplished by irradiation with a UV lamp at 265 or 313 nm.

Melting points were determined on a Büchi B-545 device and are not corrected.

Infrared spectra were recorded on a PerkinElmer FT-IR Spectrometer Spectrum TWO.

Stopped flow spectroscopy was performed on a SFM 3000 from BioLogic equipped with a TIDAS E base diode-array spectrophotometer and high-power UV-vis fiber light source from Hamamatsu.

UV-visible spectra were obtained on a Bio-Tek Uvikon XS UV-visible spectrophotometer in quartz cells with 1 cm light path.

Molecular structures have been obtained by single crystal x-ray diffraction on an Oxford Diffraction Gemini Ultra R system with CuKα radiation.

Thermogravimetric analysis (TGA) was performed on samples with a weight of ~10 mg on platina pan using TGA Q5000 TA Instruments under nitrogen atmosphere (10,0 mL/min for the balance and 25,0 mL/min for the sample) and with a heating rate of 20 °C/min from 25 °C to 800 °C. These measurements could determine applications of the polymers related to the surrounding temperature such as fire retardant, high temperature resistant material, and so

on. The most known ones are the following: Teflon (PTFE) used in reactors for example, polybenzimidazole (PBI) used in the space industry, polyetherimide (PEI) used for medical devices and aerospace industry, all of these polymers are thermoplastics as the polymers that we are forming based on the iminoboroxine platform. Moreover, these properties could be intrinsic to the polymer synthetised but could also reached by adding additives to it such as flame retardants and antioxidants. For example, the flame retardants process endothermic reactions and endothermic transitions dehydration liberating water which will absorb heat from the medium, typical agents used for this retardant property are metal hydroxides, silica-based material and boron containing compounds. Antioxidants are also used for avoiding the degradation of the polymer where the thermal oxidation can result to the chain scission (*Figure 41*) or even forming new crosslinking in the material causing an increase of the molecular weight, the brittleness and reduced elongation. Typical antioxidants used are the following hindered phenols forming quinones while trapping radicals formed, thioesters, hindered amines, hydroxylamines and so on are also widespread.

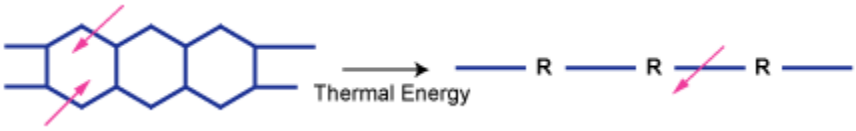

Figure 41 – Thermal induced degradation of molecules[51]

Basically, the synthetised polymers combined the molecular design of the polymer to obtain thermosets due to the high number of reticulation nodes, but the polymer also present boron containing compound which could act as flame retardant by endothermic transition but also endothermic reaction if some traces of boronic acid are present in the polymer forming boroxine.

The principle of the thermogravimetric analysis is relatively simple, the mass of a sample is measured over temperature changes, which can give information of chemical (thermal decomposition, oxidation, reduction, chemisorption, …) and physical (phase transition, absorption and desorption) phenomena. The analyser is a high precision balance coupled with furnace controlled by a thermocouple sensor under controlled atmosphere and is useful for the analysis of characteristic decomposition patters of materials (*Figure 42*).

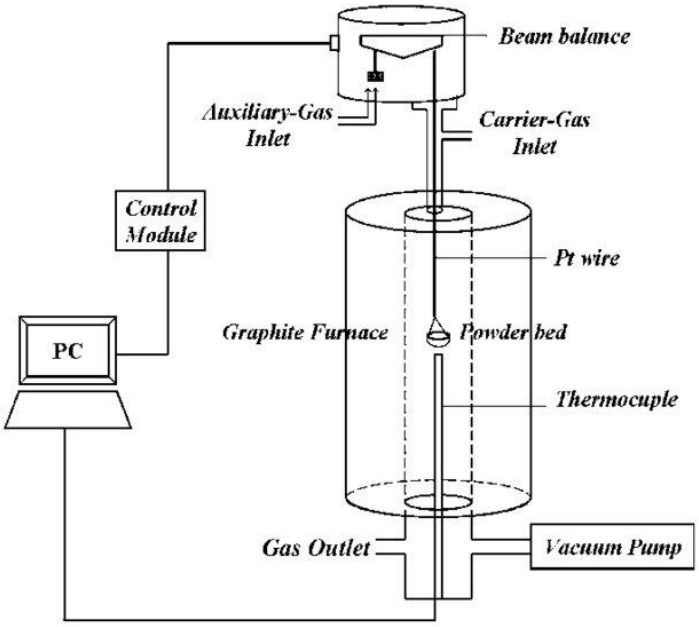

Figure 42 - Schematic diagram of TGA[51]

For ensuring an accurate and reproductible measurement, different parameters have to be finely controlled such as the type of gas, gas flow, heating speed, type of pan used and mass of sample. The type of gas used could lead to inert (N_2, Ar) or reactive conditions (O_2, CO_2) leading to reactive thermal degradation or only thermal degradation. The flow of this gas could also influence the results since a low flow does not extract gas formed during the degradation but an important flow could also destabilise the pan and distort the mass. The heating speed also modify the fingerprint of the TGA as the thermal events are kinetics, a fast heating will lead to a thermal lag (degradation at higher temperature) due to thermal equilibrium which is not reached.[52] The type of pan use is also important, they have limits in temperature range of use due to melting, degradation too and also catalytic activities but the thermal conductivity is also important to reach the thermal equilibrium. Moreover, the mass of analysed compound is also crucial, the limit of the resolution of the balance can be exceeded if we analyse small mass but on the other hand high quantity of that compound could also lead to pronounced thermal gradient.[53]

Differential scanning calorimetry (DSC) measurements were carried out using DSC Q2000 TA Instruments with modulated heat/cool/heat program from -80 °C to 220 °C. Samples (~ 10 mg) were encapsulated in non-hermetic Tzero aluminium pans and tested under nitrogen atmosphere (50,0 mL/min). The method was the following: cooling to -80 °C, isothermal (1

min), heating ramp (10 °C/min) up to 220 °C, isothermal (1 min), cooling ramp (10 °C/min) up to -80°C, isothermal (1 min), heating ramp (10 °C/min) up to 220 °C, isothermal (1 min). In the case of heat flux DSC, the temperature of the sample and reference contained in the same unit is modified and the differences between these two cells is measured as a function of temperature. The use of a reference (empty pan) is used to remove the contribution of this container on the thermal measurement. For the power compensation DSC, the difference of thermal energy needed to equalise the temperature between the sample and the reference is measured and the temperature of the unit is also varied in parallel.[54] For this method the signal recorded correspond to the thermal energy (q) which could be linked to the variation of enthalpy and also of heat capacity:

$$\frac{dH}{dt} = C_p.\frac{dT}{dt} = \frac{q}{m.dT}.\frac{dT}{dt} \leftrightarrow q = \frac{dH}{dt}.\frac{dt}{dT}.m.dT = \frac{\Delta T}{R}$$

Most of materials exhibit some sort of phase transition, this method is easily applied in many industries such as for the study of the purity of compounds, characterisation of polymers transitions. This method is important for the determination of glass transition in polymers (T_g) which correspond to the reversible transition from hard and brittle to viscous or rubbery state of amorphous material while the temperature is increased. That transition will appear in DSC as step change in the baseline due to the change of heat capacity caused by the increased mobility in the polymer. That transition is also the best indicator of the material's properties, differences in degrees of polymerisations or use of additives change that heat capacity change changing the step size and position. This parameter is really important, the permeability of the polymer is related to his state and in the case of molten glass, this property is increased leading to non-hermetic polymers which could be undesired.[53]

Optical microscopic images and micro-raman spectra were carried out on Bruker Senterra equipped with 532 and 785 nm lasers under a 20x magnification. Spectroscopy techniques are widespread in applied sciences for routine control, structure investigation, kinetics studies and so on. These studies rely on the response of the matter (absorption, diffraction, …) and electromagnetic radiation. Most commonly used in chemistry are the following; infrared spectroscopy, ultraviolet-visible spectroscopy and nucleus magnetic resonance which are used for aspects previously mentioned. The Raman spectroscopy is one of these spectroscopic

methods used to characterise materials and has been more and more spread in research induced by the development of lasers making that analysis easier and faster due to the possibility to obtain powerful light sources at a defined wavelength. This type of analysis is based on visible light as following; when a photon of visible light is too low in energy to allow an electronic transition in matter, it is inelastically scattered. Three scattering modes are possible such as the elastic one (Rayleigh), removing energy (anti-Stokes scattering) from the vibrational energy of the molecule or giving it (Stokes scattering) (*Figure 43*).

Typically, when a molecule is exposed to an electric field (E), an electric dipole moment (p) is induced. In the case of Raman spectroscopy, an electromagnetic radiation causing an oscillating electrical field (ν_0 the vibrational frequency of the electromagnetic radiation).

$$p = \alpha . E_0 . \cos(2\pi . \nu_0 . t)$$

That polarizability being function of the shape and the dimensions of the chemical bound, while the molecule vibrates, the chemical bounds change including the modification of the polarizability. Since then, the polarizability tensor (α) is function of the normal coordinates of the molecule (Q) with a phase angle (φ_ν) and for the ν^{th} vibration mode the polarizability tensor is the following:

$$\alpha_\nu = \alpha_0 + \alpha'_\nu . Q_{\nu 0} . \cos(2\pi . \nu_0 . t + \varphi_\nu)$$

The dipole moment can be defined as

$$p = \alpha_0 . E_0 . \cos(2\pi . \nu_0 . t) + \alpha'_\nu . E_0 . \cos(2\pi . \nu_0 . t) . Q_{\nu 0} . \cos(2\pi . \nu_0 . t + \varphi_\nu)$$

And modified to become

$$p = \alpha_0 . E_0 . \cos(2\pi . \nu_0 . t) + \frac{1}{2} . \alpha'_\nu . E_0 . Q_{\nu 0} . \cos(2\pi . (\nu_0 + \nu_\nu) . t + \varphi_\nu) + \frac{1}{2} . \alpha'_\nu . E_0 . Q_{\nu 0} . \cos(2\pi . (\nu_0 - \nu_\nu) . t - \varphi_\nu)$$

And be generalized as a function of the vibrational frequencies of the molecule (ν_ν) and of the incident radiation (ν_0):

$$p = p(\nu_0) + p(\nu_0 + \nu_\nu) + p(\nu_0 - \nu_\nu)$$

This comportment is only possible if we have a variation of the polarizability of the molecules with the vibration induced in the molecule and is a selection rule to determine the Raman active modes:

$$\alpha'_v = \left(\frac{\partial \alpha}{\partial Q_v}\right)_0 \neq 0$$

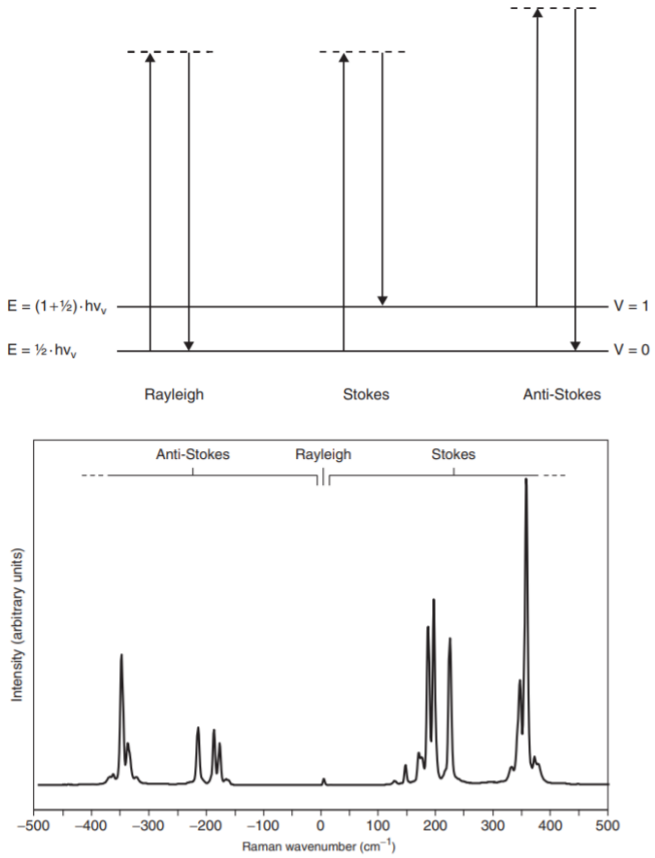

Figure 43 - Idealised model for the dispersion of light by molecules (left) and Raman spectrum of the mineral realgar (As4S4) in the anti-Stokes region, Rayleigh line and Stokes region (right)[53]

But this method can be affected by different factors, firstly, amorphous materials are more likely to obtain broad bands in the Raman spectrum. The difference of chemical environment causes a slightly different force constant of chemical bonds inducing that band broadening.

On the other hand, the absorption of the incoming light source could be observed if the energy on the incident radiation allowing the excitation of molecules to higher states. The transitions could be toward electronic states (UV-visible radiation) or vibrational state (IR absorption) released as heat (radiationless transitions) or transferred to the environment. Changing the

wavelength of the laser can minimise or even reduce that kind of interference, moreover the Raman scattered light can also interact with the matter making this measurement difficult.

Fluorescence also poses a problem in Raman spectroscopy, the molecule is excited to upper energy state, this molecule can decay to lower energy state by radiationless transition. This compound can go down to fundamental level while emitting fluorescence radiation, this comportment can be avoided by using a lower energy light source (*Figure 44*).

These interferences could also conduct to the thermal decomposition induced by the heating radiationless transitions but also the photodecomposition destructing the fluorophore group especially for short wavelength laser where the energy of them can correspond to bonding energy.

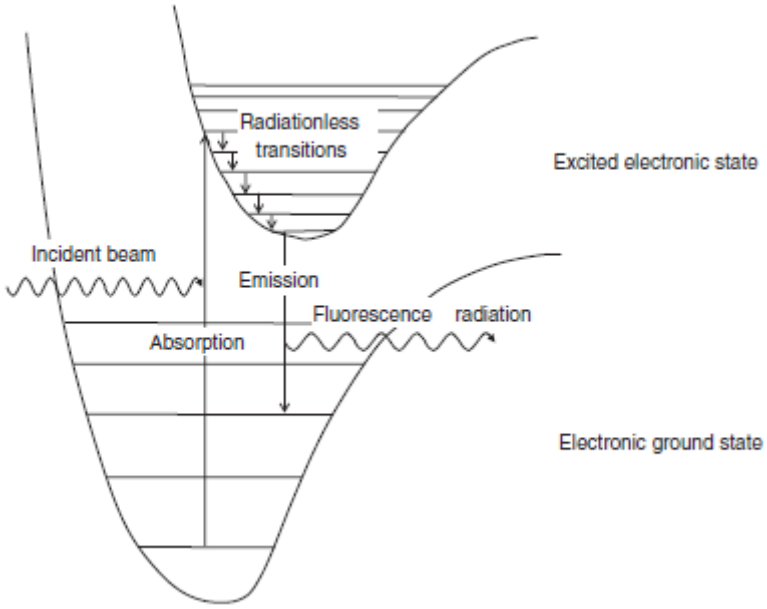

Figure 44 - Energy diagram of the fluorescence effect[53]

This Raman spectroscopy could be coupled with optical microscope to obtain micro-Raman spectroscopy which enable to obtain molecular information at the micrometer scale. There the mapping of the material to detect the inhomogeneities is possible when they are smaller than the measured volume. In this case the Raman spectra are recorded while the relative position of the laser is changed at each measurement.

Material

4 Å Molecular sieves were dried at 400 °C under high vacuum for 3 days and stored in a glove box. Diethylether, tetrahydrofuran, toluene and dichloromethane were dried with an MBraun solvent purification system and stored under argon. CD_2Cl_2 was dried over preactivated 4 Å molecular sieves and stored in a glovebox, all others solvents were dried over CaH_2, distilled and stored over preactivated 4 Å molecular sieves in a glove box prior to use. Others reagents and chemicals were purchased from Sigma-Aldrich, Alfa Aesar, TCI and Fluorochem and used without further purification.

Unless otherwise stated all the reactions were performed under an atmosphere of argon using classical Schlenk line technique or in a high-performance glovebox.

2-(2-bromophenyl)-1,3-dioxolane **1**:

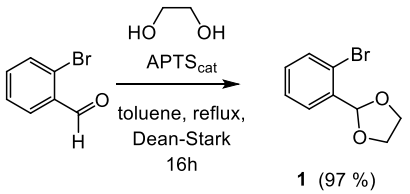

1 (97 %)

Ethylene glycol (8.0 mL, 143 mmol, 4.8 equiv) was added to 2-bromobenzaldeyde (3.2 mL, 30 mmol, 1.0 equiv) in toluene in presence of APTS·H_2O (1.01 g, 5.74 mmol, 0.19 equiv) and the resulting mixture was heated at reflux in a Dean-Stark apparatus during 16h. After 16h, the organic phase was washed with saturated sodium bisulphite aqueous solution (2x100 mL) and with brine (1x100 mL), the organic phase was dried by magnesium sulphate, filtered and the solvent was then evaporated. The ^{1}H NMR data are consistent with those reported in the literature.

Yellow oil (6.6 g, yield = 97 %).

^{1}H NMR (500 MHz, CDCl3) δ (ppm) = 7.59 (dd, *J* = 7.7, 1.3 Hz 1H), 7.55 (d, *J* = 8.0 Hz, 1H), 7.33 (t, *J* = 7.5 Hz, 1H), 7.24-7.18 (m, 1H), 6.09 (s, 1H), 4.35-3.86 (m, 4H).

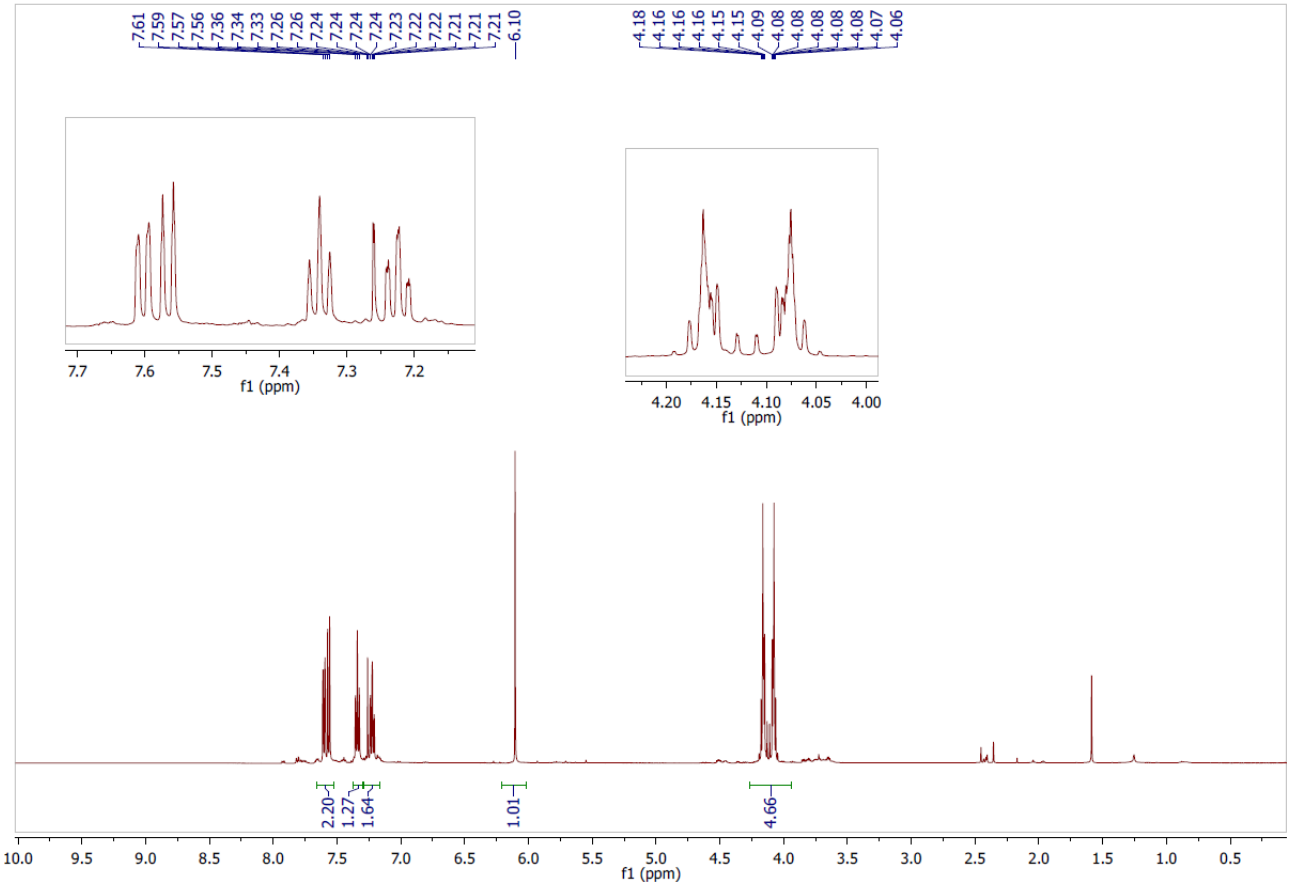

2-(2-bromo-4-methylphenyl)-1,3-dioxolane **2**:

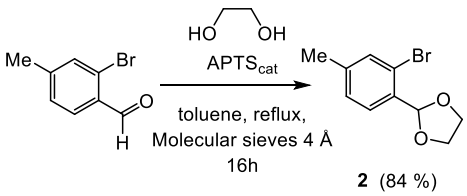

Ethylene glycol (12 mL, 215 mmol, 10 equiv) was added to 2-bromo-4-methylbenzaldehyde (4.15 g, 21 mmol, 1.0 equiv) in toluene in presence of catalytic APTS·H_2O (0.80 g, 4.2 mmol, 0.20 equiv) and the resulting mixture was heated at reflux over molecular sieves during 16h. The organic phase was washed with saturated sodium bisulphite aqueous solution (2x100 mL) and with brine (1x100 mL), and then dried by magnesium sulphate, filtered and the solvent was then evaporated. The crude was purified by flash column chromatography (hexane/AcOEt,95:5). The ^{1}H NMR data are consistent with those reported in the literature.

Yellow oil (4.3 g, yield = 84 %).

^{1}H NMR (500 MHz, CDCl3) δ (ppm) = 7.46 (d, *J* = 8.0 Hz, 1H), 7.38 (s, 1H), 7.33 (t, *J* = 7.5 Hz, 1H), 7.12 (d, *J* = 7.6 Hz, 1H), 6.05 (s, 1H), 4.44-3.46 (m, 4H).

2-(5,5-dimethyl-1,3,2-dioxaborinan-2-yl)benzaldehyde **7**:

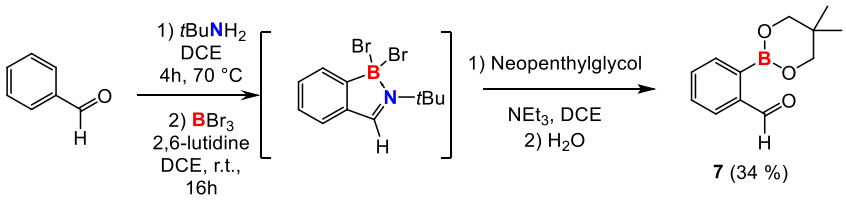

*t*BuNH$_2$ (1.05 mL, 10 mmol, 4 equiv) is added to distilled benzaldehyde (0.25 mL, 2.5 mmol, 1 equiv) in dry DCE and heated at 70 °C during 4h under Ar atmosphere. The solvent was then removed under vacuum, and the mixture was then backfilled with Ar. DCE was added to solubilise the intermediate followed by lutidine (0.58 mL, 5 mmol, 2 equiv) and BBr$_3$ (1M in CH_2Cl_2, 5.0 mL, 5.0 mmol, 2 equiv). After 16h at room temperature, the reaction was quenched with neopentyl glycol (0.52 g, 5 mmol, 2 equiv) and triethylamine (3.4 mL, 25 mmol, 10 equiv) and stirred during 2h under Ar at room temperature and then diluted with water. The aqueous phase was extracted by AcOEt (3x50 mL), the organic phases were reunited, dried with $MgSO_4$, filtered and solvent evaporated. The crude was purified by flash column chromatography (hexane/AcOEt 8:2) and solvent evaporated. The title compound partially decomposed over silica gel, accordingly no characterisation was possible.

4-(tert-butyl)-2-(5,5-dimethyl-1,3,2-dioxaborinan-2-yl)benzaldehyde **8**:

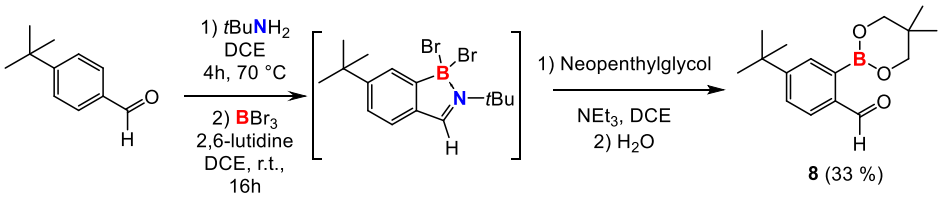

*t*BuNH$_2$ (1.10 mL, 10.4 mmol, 4 equiv) is added to benzaldehyde (0.42 mL, 2.5 mmol, 1 equiv) in dry DCE and heated at 70 °C during 4h under Ar atmosphere. The solvent was then removed under vacuum, and the mixture was then backfilled with Ar. DCE was added to solubilise the intermediate, followed by lutidine (0.58 mL, 5 mmol) and BBr$_3$ (1M in CH_2Cl_2, 5.0 mL, 5.0 mmol). After 16h at room temperature, the reaction was quenched with neopentyl glycol (0.52 g, 5 mmol, 2 equiv) and triethylamine (3.4 mL, 25 mmol, 10 equiv) and stirred during 2h

under Ar at room temperature and then diluted with water. The volatiles were removed and the aqueous phase was extracted by AcOEt (3x), the organic phases were reunited, dried with $MgSO_4$, filtered and solvent evaporated. The crude was purified by flash column chromatography (hexane/AcOEt 8:2) and solvent evaporated.

Colourless oil (226 mg, yield = 33 %).

^{1}H NMR (500 MHz, $CDCl_3$) δ (ppm) = 10.3 (s, 1H), 7.84 (d, *J*= 8.2 Hz, 1H), 7.78 (s, 1H), 7.53 (dd, *J* =8.2, 2.0 Hz, 1H), 3.81 (s, 4H), 1.33 (s, 9H), 1.08 (s, 6H).

^{11}B NMR (160 MHz, $CDCl_3$) δ (ppm) = 26.6 (br)

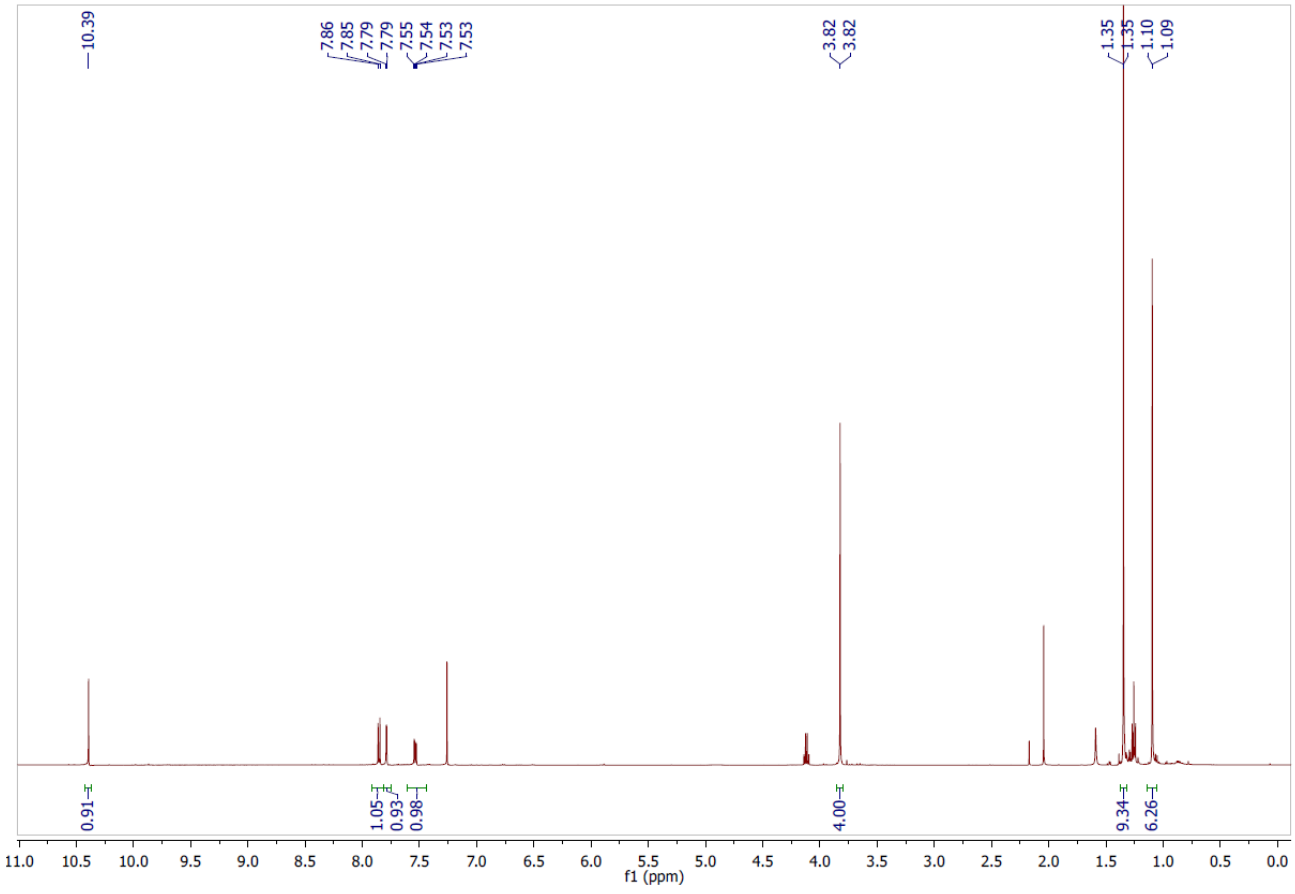

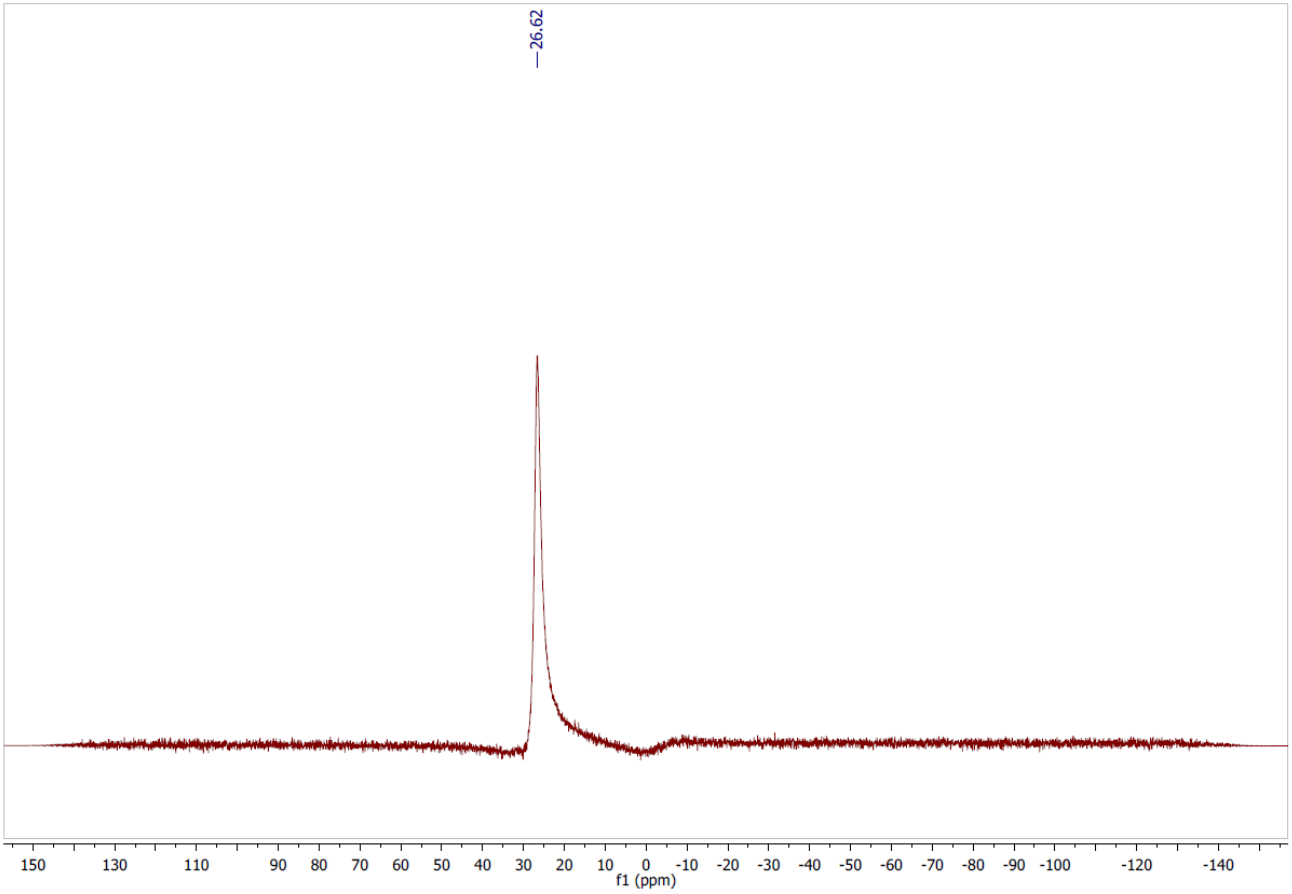

2-(5,5-dimethyl-1,3,2-dioxaborinan-2-yl)-4-fluorobenzaldehyde **9**:

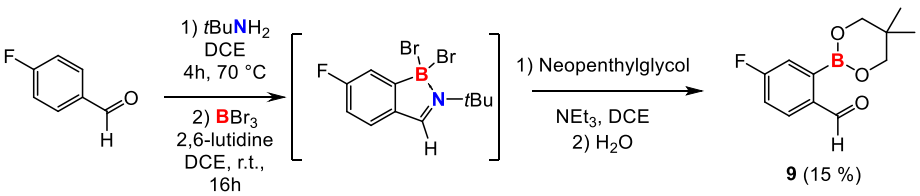

*t*BuNH$_2$ (1.10 mL, 10.4 mmol) is added to benzaldehyde (0.26 mL, 2.5 mmol) in dry DCE and heated at 70 °C during 4h under Ar atmosphere. The solvent was then removed under vacuum, and the mixture was backfilled with Ar. DCE was added to solubilise the intermediate followed by lutidine (0.58 mL, 5 mmol) and BBr_3 (1M in CH_2Cl_2, 5,0 mL – 5,0 mmol). After 16h at room temperature, the reaction was quenched with neopentyl glycol (0.52 g, 5 mmol, 2 equiv) and triethylamine (3.4 mL, 25 mmol, 10 equiv) and stirred during 2h under Ar at room temperature. The volatiles were removed and the mixture was solubilised in EtOAc/water 1:1 and the phases were separated. The aqueous phase was extracted by AcOEt (3x100 mL), the organic phases were reunited, dried with $MgSO_4$, filtered and solvent evaporated. The crude

was purified by flash column (hexane:AcOEt 8/2) and solvent evaporated. The title compound partially decomposed over silica gel, accordingly no characterisation was possible.

2-(1,3,2-dioxaborolan-2-yl)benzaldehyde **10**:

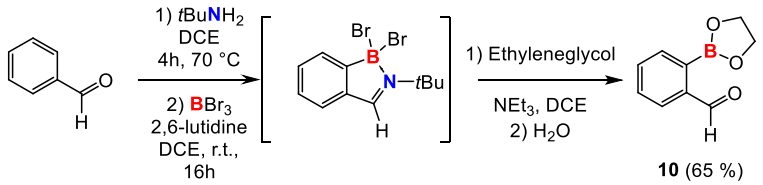

*t*BuNH$_2$ (1.10 mL, 10.4 mmol, 4 equiv) is added to distilled benzaldehyde (0.25 mL, 2.5 mmol, 1 equiv) in dry DCE and heated at 70 °C during 4h under Ar atmosphere. The solvent was then removed under vacuum, and the mixture was backfilled with Ar. DCE was added to solubilise the intermediate followed by lutidine (0.58 mL, 5 mmol, 2 equiv) and BBr_3 (1M in CH_2Cl_2, 5.0 mL, 5.0 mmol, 2 equiv). After 16h at room temperature, the reaction was quenched with ethylene glycol (1.4 mL, 25 mmol, 10 equiv) and triethylamine (3.4 mL, 25 mmol, 10 equiv) and stirred during 2h under Ar at room temperature. The volatiles were removed and the mixture was solubilised in EtOAc/water 1:1 and the phases were separated. The aqueous phase was extracted by AcOEt (3x100 mL), the organic phases were reunited, dried with $MgSO_4$, filtered and solvent evaporated. The crude was purified by flash column (cyclohexane:AcOEt 8/2). The title compound partially decomposed over silica gel.

4-(tert-butyl)-2-(1,3,2-dioxaborolan-2-yl)benzaldehyde **11**:

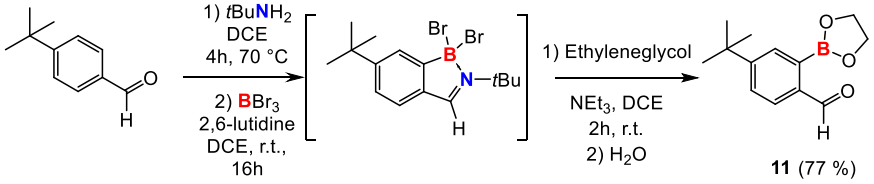

*t*BuNH$_2$ (1.10 mL, 10.4 mmol, 4 equiv) is added to benzaldehyde (0.42 mL, 2.5 mmol, 1 equiv) in dry DCE and heated at 70 °C during 4h under Ar atmosphere. The solvent was then removed under vacuum, and the mixture was backfilled with Ar. DCE was added to solubilise the intermediate followed by lutidine (0.58 mL, 5 mmol) and BBr_3 (5.0 mL, 5.0 mmol). After 16h at room temperature, the reaction was quenched with ethylene glycol (1.4 mL, 25 mmol, 10 equiv) and triethylamine (3.4 mL, 25 mmol, 10 equiv) and stirred during 2h under Ar at room

temperature. The volatiles were removed and the mixture was solubilised in EtOAc:water 1/1 and the phases were separated. The aqueous phase was extracted by AcOEt (3x100 mL), the organic phases were reunited, dried with $MgSO_4$, filtered and solvent evaporated. The crude was purified by flash column chrommatography (cyclohexane:AcOEt 8/2). Brown oil (417 mg, yield = 77 %). The title compound partially decomposed into the corresponding boronic acid over silica gel, accordingly no characterisation was attempted.

(5-(tert-butyl)-2-formylphenyl)boronic acid **12**:

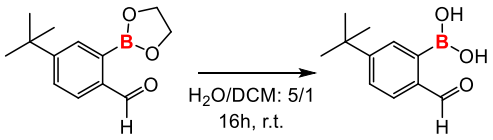

11 **12** (99 %)

The 4-(tert-butyl)-2-(1,3,2-dioxaborolan-2-yl)benzaldehyde 11 (0.29 g, 1.3 mmol) was solubilised in H_2O/DCM 5:1 solution and stirred at room temperature during 16h. The phases were separated, the aqueous phase was extracted with DCM (3x10 mL) and the organic phases reunited washed with brine. The organic phase was dried with $MgSO_4$, filtered, solvent evaporated, the boronic acid was obtained by precipitation in pentane and washed with pentane.

Slightly brown solid (yield = 99 %).

(2-bromophenyl)methanediol **13**:

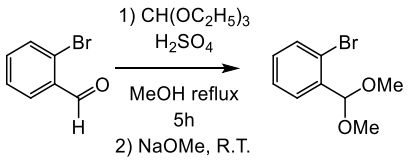

13 (92 %)

Triethyl orthoformate (2.6 mL, 16 mmol, 1.3 equiv) has been added dropwise to a methanolic solution of 2-bromobenzaldehyde (1.5 mL, 13 mmol, 1 equiv) and catalytic H_2SO_4 (0.1 mL, 2 mmol) the resulting solution was heated at reflux during 5h. The solution was brought to pH = 11 with a 2 M sodium methoxide methanolic solution and the solvent was evaporated. The solid formed was washed with pentane and the filtrate obtained was evaporated. The ^1H NMR data are consistent with those reported in the literature.

Colourless oil (2.7 g, yield = 92 %).

^{1}H NMR (500 MHz, $CDCl_3$) δ (ppm) = 7.61 (dd, *J* = 7.7, 1.8 Hz, 1H), 7.56 (dd, *J* = 8.0, 1.2 Hz, 1H) 7.61 (td, *J*= 7.5, 1.1 Hz, 1H), 7.23-7.15 (m, 1H), 5.56 (s, 1H), 3.39 (s, 6H).

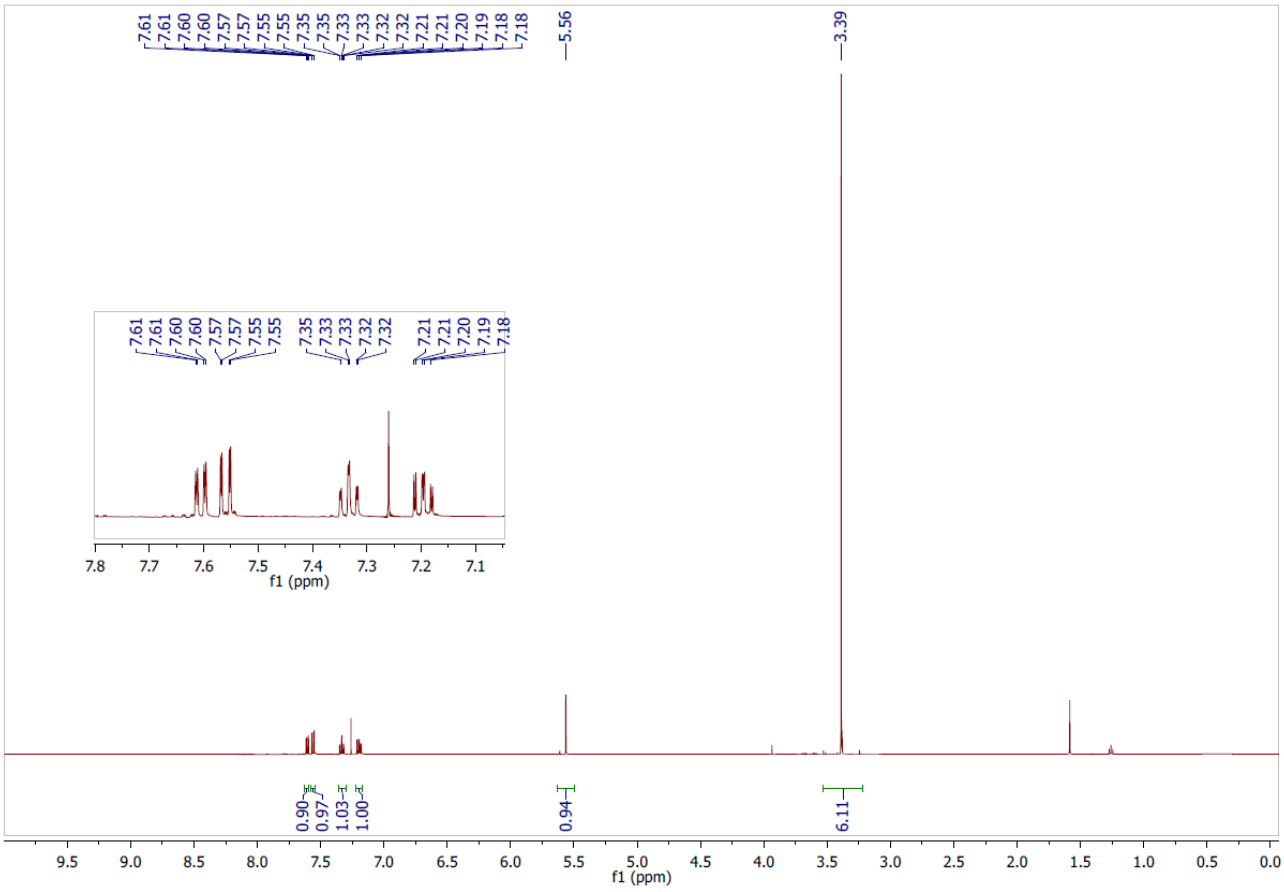

1-bromo-2-(dimethoxymethyl)-3-fluorobenzene **14**:

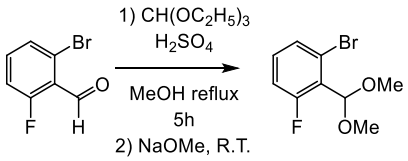

14 (85 %)

Triethyl orthoformate (2.2 mL, 14 mmol, 1.4 equiv) has been added dropwise to a methanolic solution of 2-bromo-6-fluorobenzaldehyde (1.99 g, 9.81 mmol, 1 equiv) and catalytic H_2SO_4 (0.1 mL, 2 mmol), the resulting solution was heated at reflux during 5h. The solution was brought to pH = 11 with a 2M sodium methoxide methanolic solution and the solvent was evaporated. The solid formed was washed with pentane and the filtrate obtained was evaporated. The ^{1}H and ^{19}F NMR data are consistent with those reported in the literature.

Colourless oil (2.0 g, yield = 85 %).

^{1}H NMR (500 MHz, $CDCl_3$) δ (ppm) = 7.37 (dd, *J* = 8.0, 1.0 Hz, 1H), 7.17 (td, *J* = 8.2, 5.6 Hz, 1H) 7.61 (ddd, *J*= 10.3, 8.3, 1.1 Hz, 1H), 5.71 (s, 1H), 3.49 (s, 6H).

^{19}F NMR (476 MHz, $CDCl_3$) δ (ppm) = -111.2 (dd, *J* = 10.2, 5.6 Hz)

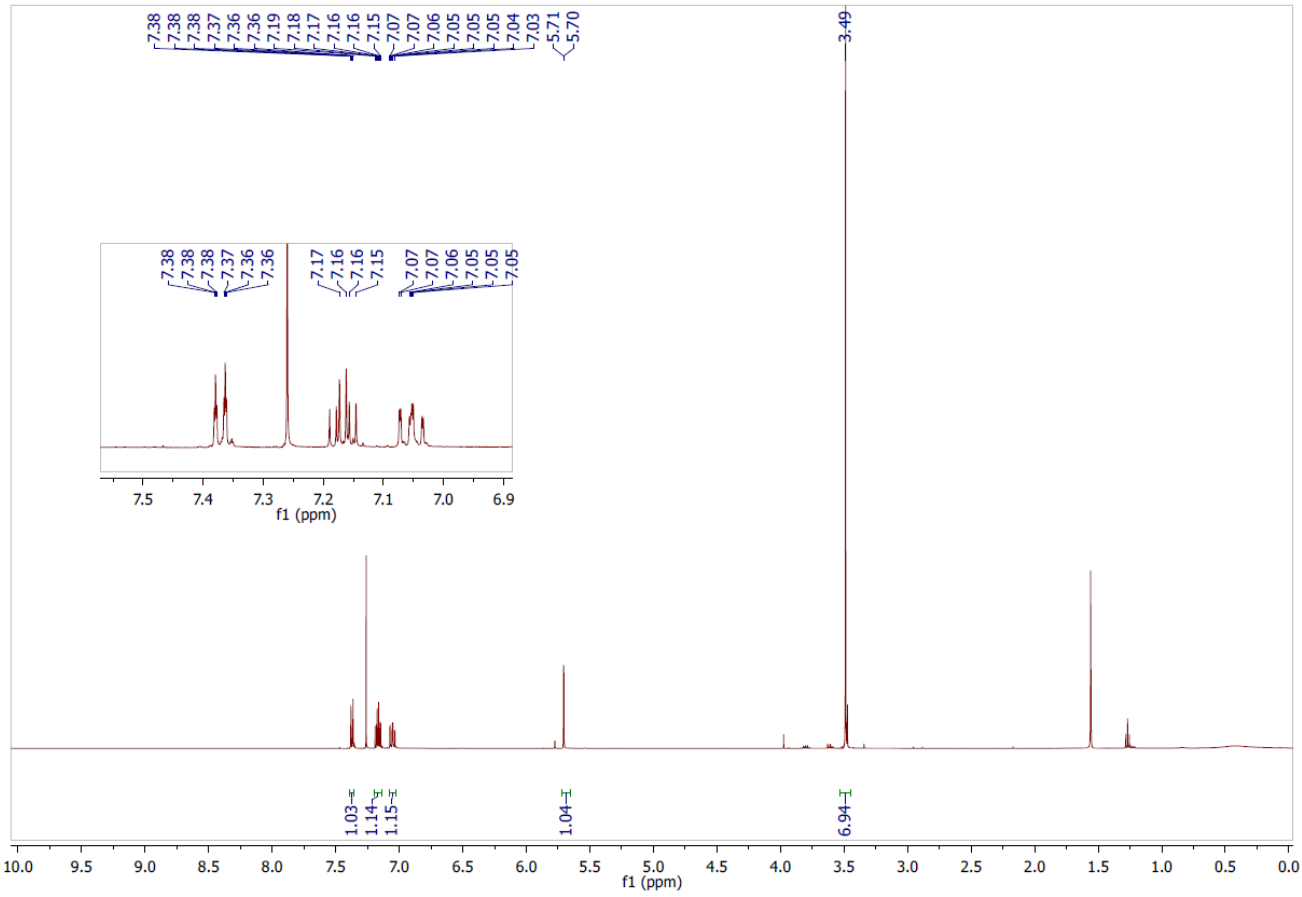

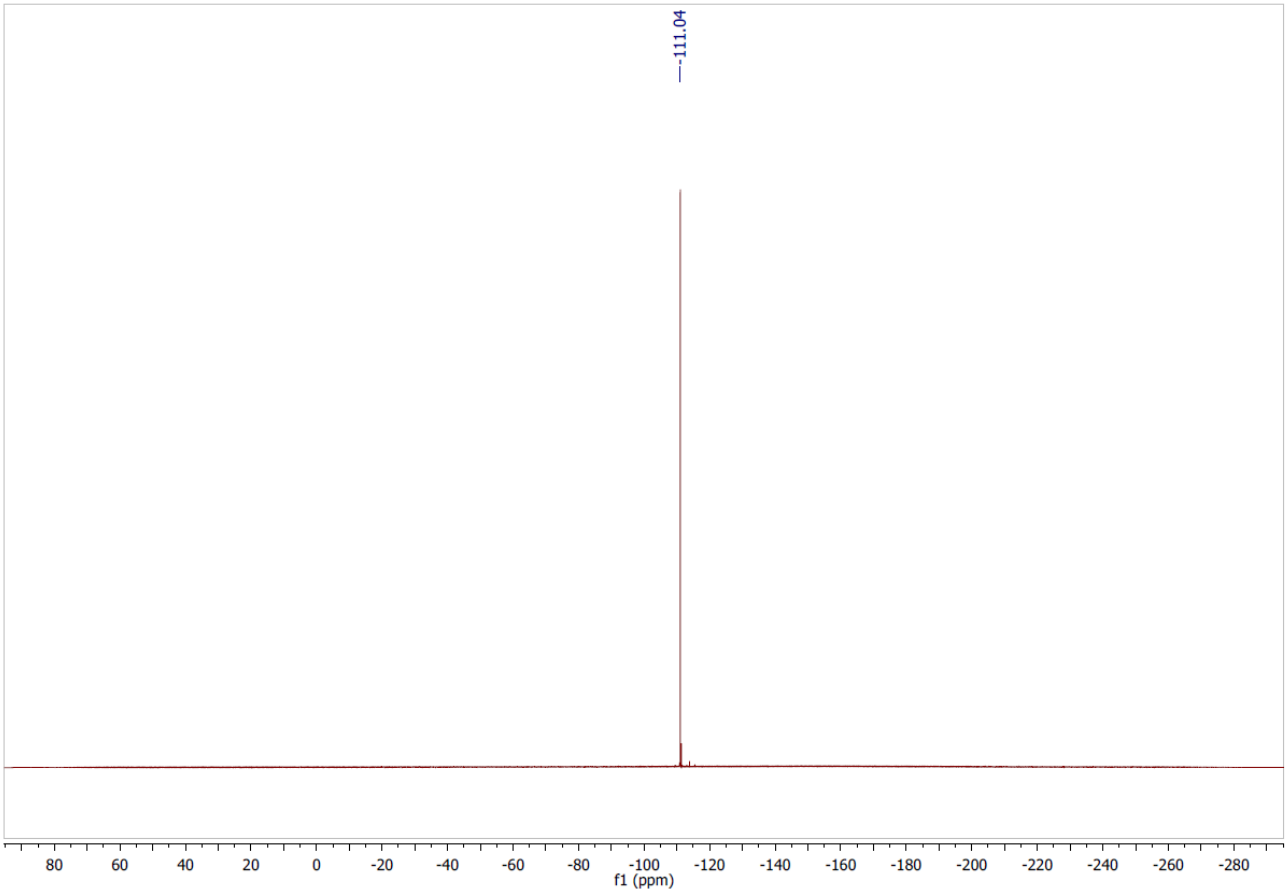

2-bromo-1-(dimethoxymethyl)-4-fluorobenzene **15**:

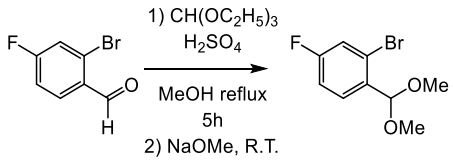

15 (88 %)

Triethyl orthoformate (2.2 mL, 14 mmol, 1.4 equiv) has been added dropwise to a methanolic solution of 2-bromo-4-fluorobenzaldehyde (1.99 mL, 9.81 mmol, 1 equiv) and catalytic H_2SO_4 (0.1 mL, 2 mmol) the resulting solution was heated at reflux during 5h. The solution was brought to pH = 11 with a 2 M sodium methoxide methanolic solution and the solvent was evaporated. The solid formed was washed with pentane and the filtrate obtained was evaporated. The ^{1}H and ^{19}F NMR data are consistent with those reported in the literature.

Slightly yellow oil (2.1 g, yield = 88 %).

^{1}H NMR (500 MHz, $CDCl_3$) δ (ppm) = 7.59 (dd, *J* = 8.7, 6.2 Hz, 1H), 7.31 (dd, *J* = 8.2, 2.6 Hz, 1H) 7.05 (td, *J*= 8.3, 2.6 Hz, 1H), 5.52 (s, 1H), 3.36 (s, 6H).

^{19}F NMR (476 MHz, $CDCl_3$) δ (ppm) = -111.2 (dd, *J* = 14.5, 7.9 Hz).

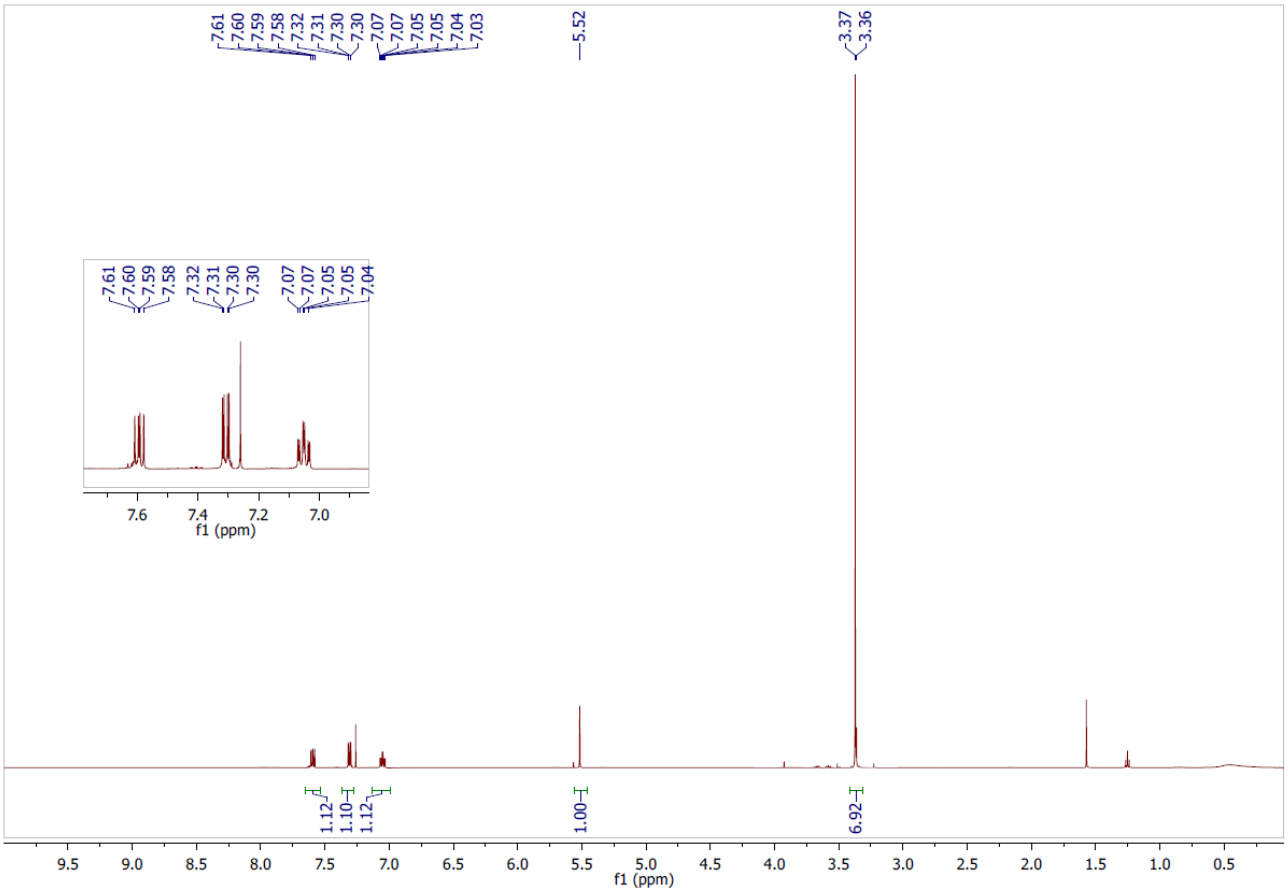

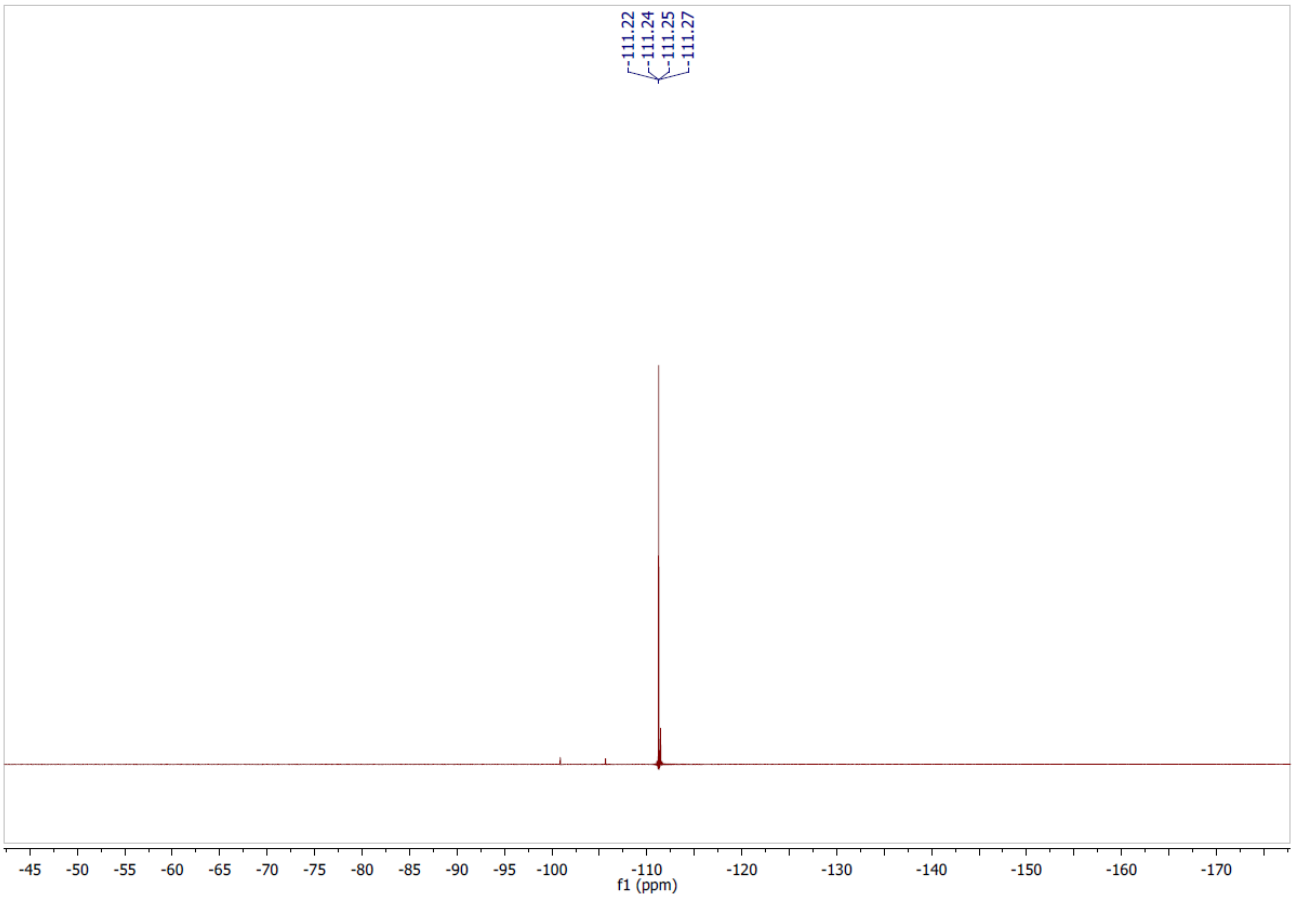

2-bromo-1-(dimethoxymethyl)-3-fluorobenzene **16**:

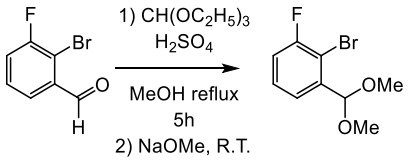

16 (85 %)

Triethyl orthoformate (2.2 mL, 14 mmol, 1. 4 equiv) has been added dropwise to a methanolic solution of 2-bromo-3-fluorobenzaldehyde (1.99 mL, 9.81 mmol, 1 equiv) and catalytic H_2SO_4 (0.1 mL, 2 mmol), the resulting solution was heated at reflux during 5h. The solution was brought to pH = 11 with a 2M sodium methoxide methanolic solution and the solvent was evaporated. The solid formed was washed with pentane and the filtrate obtained was evaporated. The ^{1}H and ^{19}F NMR data are consistent with those reported in the literature.

White solid which slowly liquefied upon storage (2.1 g, yield = 85 %).

^{1}H NMR (500 MHz, $CDCl_3$) δ (ppm) = 7.41 (d, *J* = 7.8 Hz, 1H), 7.36-7.28 (m, 1H) 7.05 (td, *J*= 8.3, 1.5 Hz, 1H), 5.57 (s, 1H), 3.39 (s, 6H).

^{19}F NMR (476 MHz, $CDCl_3$) δ (ppm) = -105.4 (dd, *J* = 8.3, 5.5 Hz)

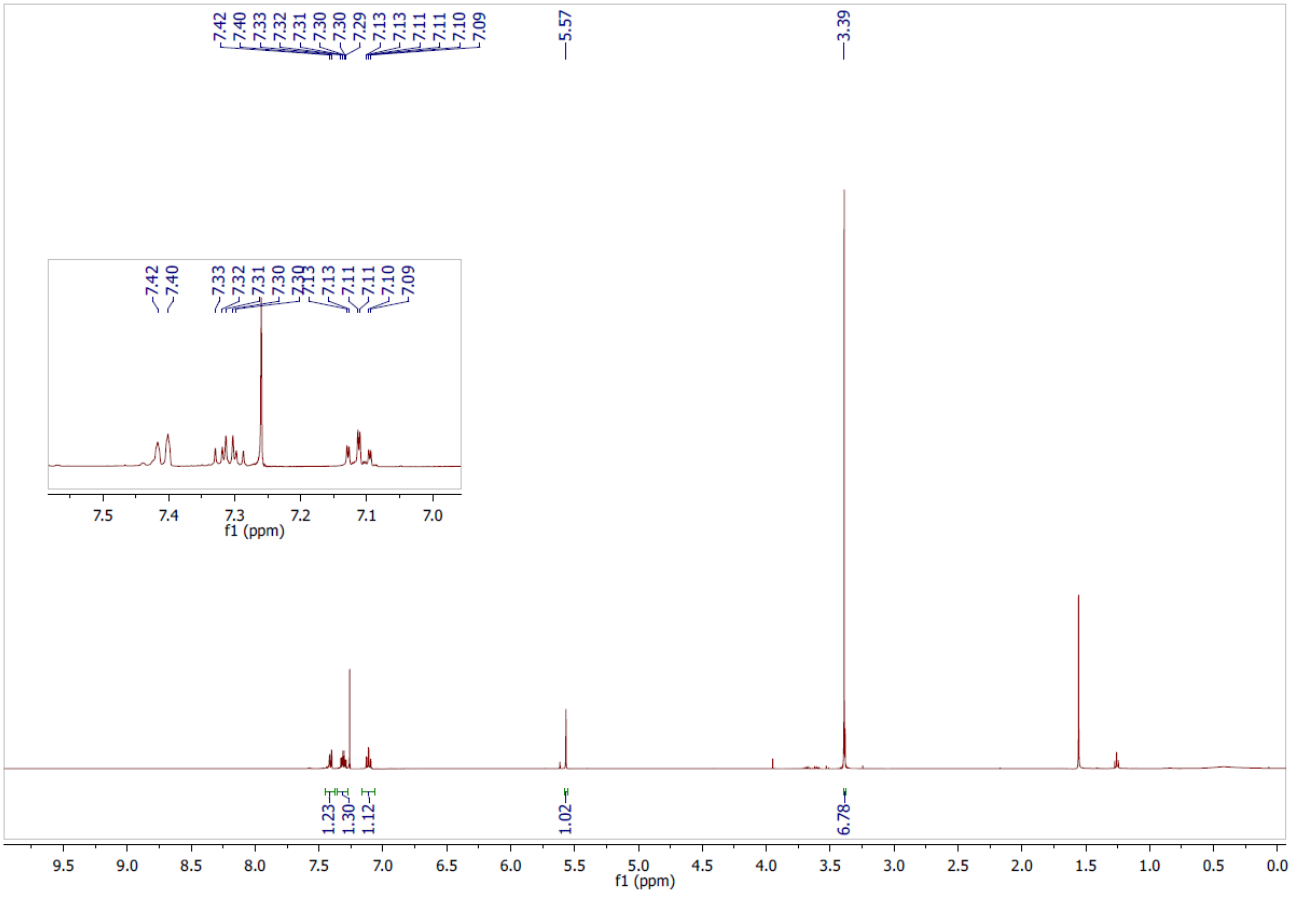

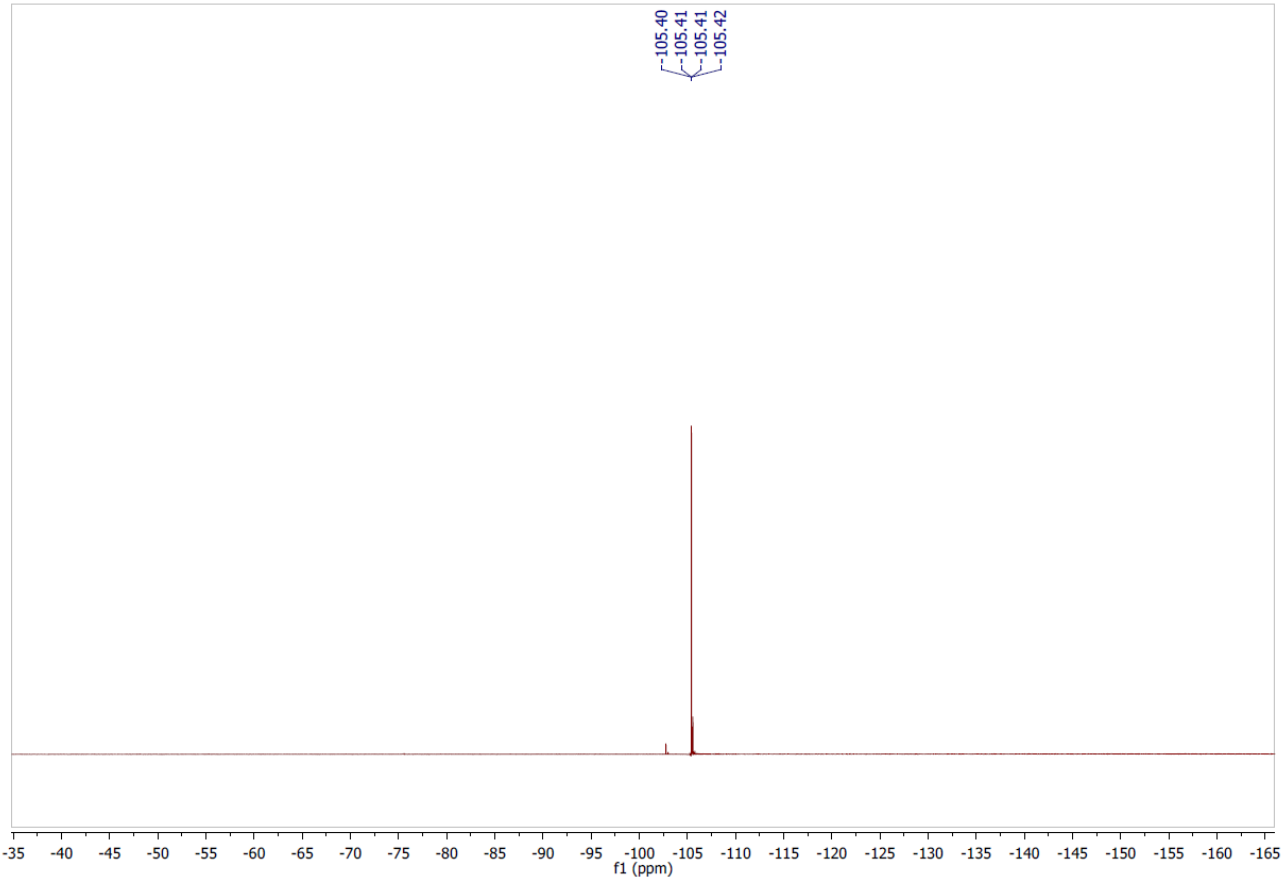

(2-formylphenyl)boronic acid **4**:

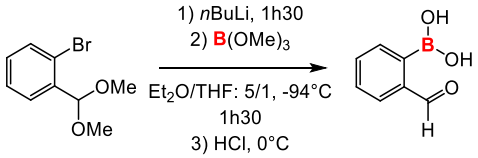

13 **4** (47 %)

*n*BuLi (2.5M in hexanes, 5.2 mL, 13 mmol, 1.1 equiv) was added dropwise on (2-bromophenyl)methanediol **13** (2.73 g, 11.8 mmol, 1 equiv) in a Et_2O/THF 5:1 anhydrous solution under Ar atmosphere at -94 °C. After 1h30 at -94 °C $B(OMe)_3$ (1.5 mL, 13 mmol, 1.1 equiv) was added dropwise and after 1h30, the solution was slowly brought to 0 °C during acidification (pH = 3) of the mixture with 3 M HCl solution. The phases were separated and the aqueous phase was extracted with Et_2O (2x50 mL) and the reunited organic phases was extracted with brine. The organic phase was dried with magnesium sulphate, filtered and the solvent was then evaporated, the solid formed was washed with pentane. The ^1H NMR data are consistent with those reported in the literature.

White solid (831 mg, yield = 47 %).

M.p. (pentane): 95-104°C

^{1}H NMR (500 MHz, $CDCl_3$) δ (ppm) = 9.93 (s, 1H), 8.31 (dd, *J*= 5.6, 3.1 Hz, 1H), 8.07-7.79 (m, 1H), 7.81-7.66 (m, 2H), 7.58 (s, 2H).

(2-fluoro-6-formylphenyl)boronic acid **19**:

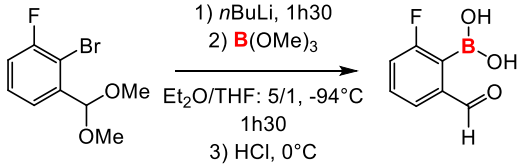

16 **19** (29 %)

*n*BuLi (4.8 mL, 12 mmol, 1.1 equiv) was added dropwise on 1-bromo-2-(dimethoxymethyl)-3-fluorobenzene **16** (2.73 g, 11.0 mmol) in a Et_2O/THF: 5/1 anhydrous solution under Ar atmosphere at -94 °C. After 1h30, at -94 °C and under Ar atmosphere, $B(OMe)_3$ was added dropwise (1.4 mL, 12 mmol) and after 1h30, the solution was slowly brought to 0 °C during acidification (pH = 3) of the mixture with 3 M HCl solution. The phases were separated and the aqueous phase was extracted with Et_2O (2x50 mL) and the reunited organic phases was washed with brine. The organic phase was dried with magnesium sulphate, filtered and the solvent was then evaporated, the solid formed was washed with pentane.

White solid (532 mg, yield = 29%).

^{1}H NMR (500 MHz, $CDCl_3$) δ (ppm) =10.5 (s, 1H), 8.00 (d, *J* = 7.4, 1H), 7.32 (ddd, *J* = 8.3, 7.5, 5.4 Hz 1H), 7.30 (ddd, *J* = 11.3, 8.3, 1.2 Hz, 1H), 7.13 (br, 1H)

^{11}B NMR (160 MHz, $CDCl_3$) δ (ppm) = 27.3 (br)

^{13}C NMR (126 MHz, $CDCl_3$) δ (ppm) = 193.0 (d, *J* = 14.1 Hz), 138.0 (d, *J* = 10.0 Hz), 133.6 (d, *J* = 4.0 Hz), 127.3 (d, *J* =2.8 Hz), 118.2 (d, *J* = 22.1 Hz).

^{19}F NMR (476 MHz, $CDCl_3$) δ (ppm) = -117.8(br)

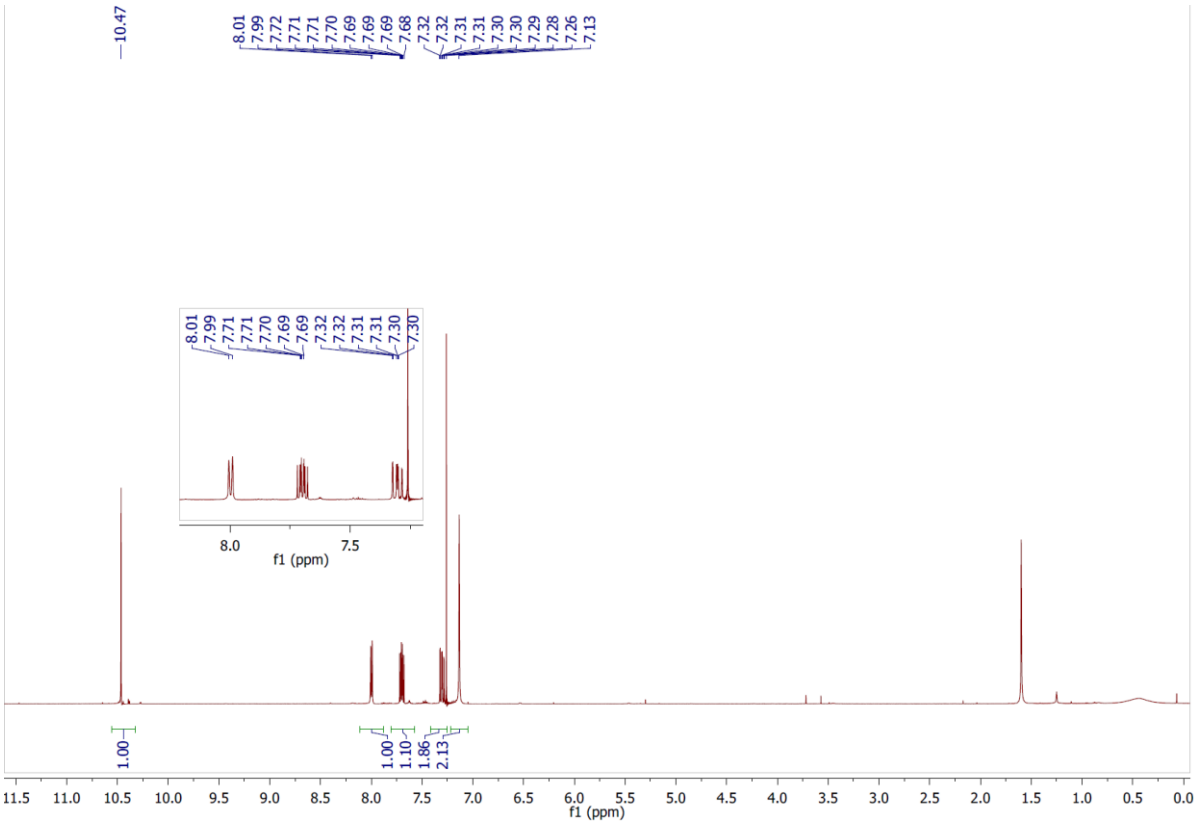
10.47
8.01
7.99
7.72
7.71
7.71
7.70
7.69
7.69
7.69
7.68
7.32
7.32
7.31
7.31
7.30
7.30
7.29
7.28
7.26
7.13
8.01
7.99
7.71
7.71
7.70
7.69
7.69
7.32
7.32
7.31
7.31
7.30
7.30
8.0
7.5
f1 (ppm)
1.00
1.00
1.10
1.86
2.13
11.5 11.0 10.5 10.0 9.5 9.0 8.5 8.0 7.5 7.0 6.5 6.0 5.5 5.0 4.5 4.0 3.5 3.0 2.5 2.0 1.5 1.0 0.5 0.0
f1 (ppm)

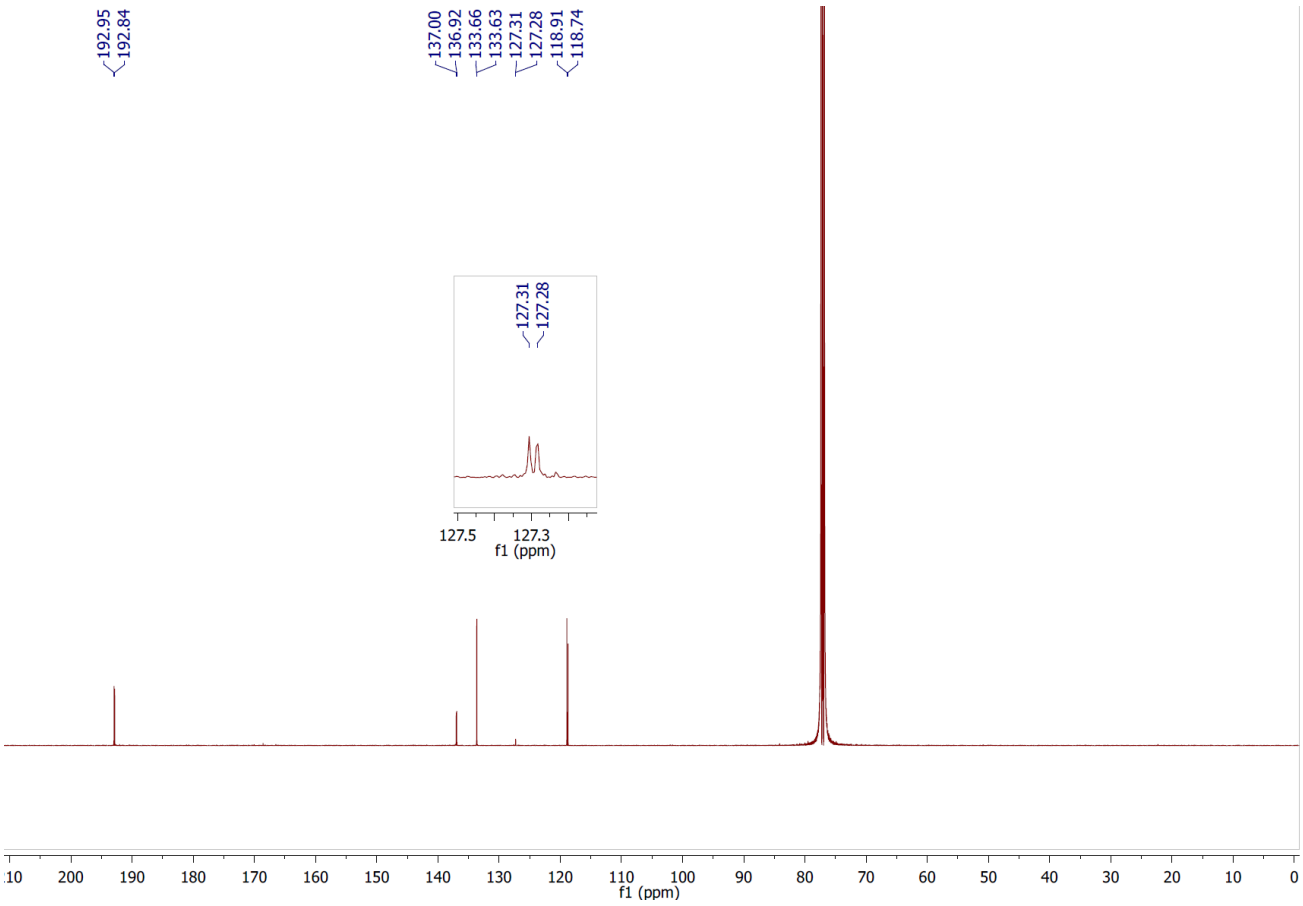
192.95
192.84
137.00
136.92
133.66
133.63
127.31
127.28
118.91
118.74
127.31
127.28
127.5
127.3
f1 (ppm)
210 200 190 180 170 160 150 140 130 120 110 100 90 80 70 60 50 40 30 20 10 0
f1 (ppm)

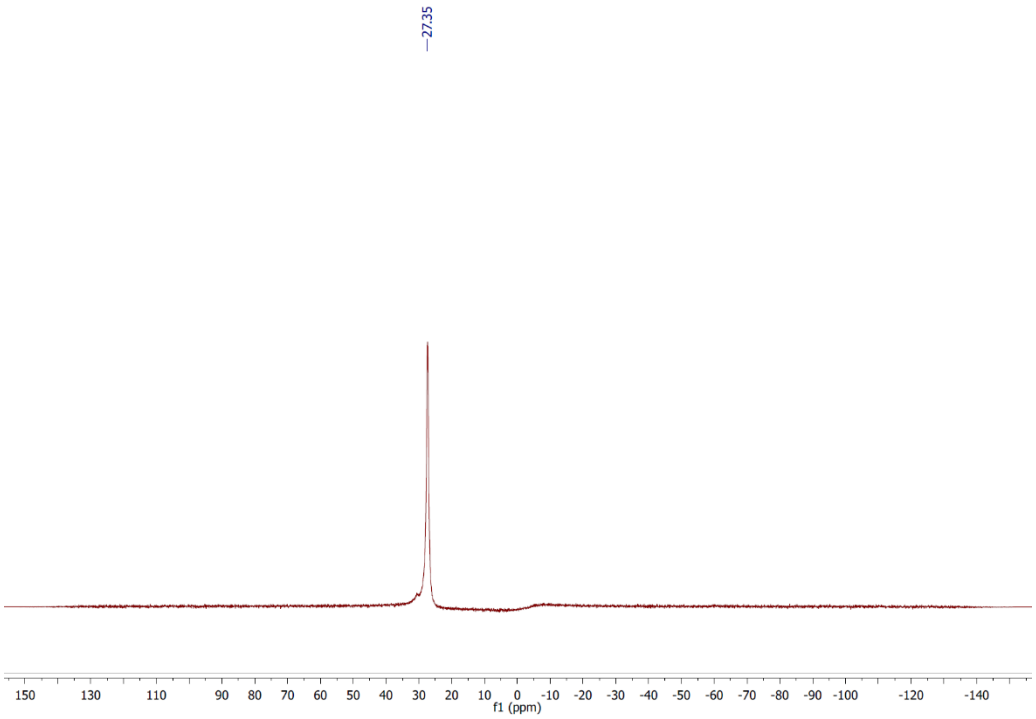
27.35
150 130 110 90 80 70 60 50 40 30 20 10 0 -10 -20 -30 -40 -50 -60 -70 -80 -90 -100 -120 -140
f1 (ppm)

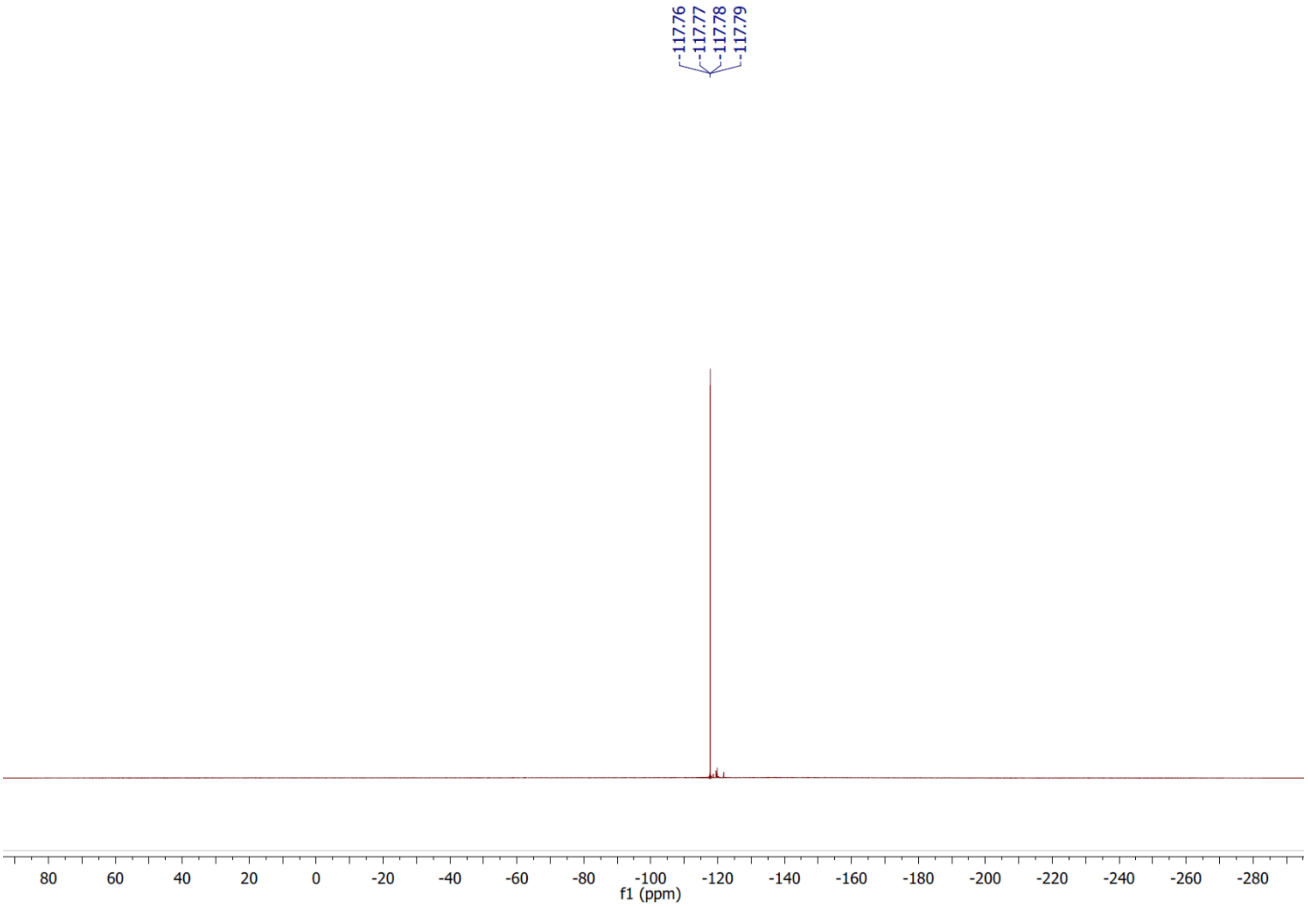
-117.76
-117.77
-117.78
-117.79
80 60 40 20 0 -20 -40 -60 -80 -100 -120 -140 -160 -180 -200 -220 -240 -260 -280
f1 (ppm)

(5-fluoro-2-formylphenyl)boronic acid **18**:

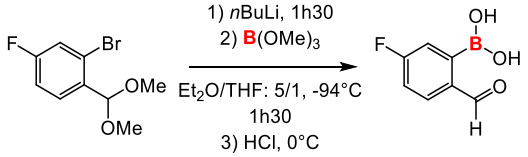

15 **18** (86 %)

*n*BuLi (2.5M in hexanes, 3.8 mL, 9.5 mmol, 1.1 equiv) was added dropwise on 2-bromo-1-(dimethoxymethyl)-4-fluorobenzene **15** (2.16 g, 8.70 mmol, 1 equiv) in a Et_2O/THF 5:1 anhydrous solution under Ar atmosphere at -94 °C. After 1h30 at -94 °C and under Ar atmosphere, $B(OMe)_3$ (1.1 mL, 9.7 mmol, 0.97 equiv) was added dropwise and after 1h30, the solution was slowly brought to 0 °C during acidification (pH = 3) of the mixture with 3 M HCl solution. The phases were separated and the aqueous phase was extracted with Et_2O (2x50 mL) and the reunited organic phases was washed with brine. The organic phase was dried with magnesium sulphate, filtered and the solvent was then evaporated, the solid formed was washed with pentane. The ^{1}H and ^{11}B NMR data are consistent with those reported in the literature.

White solid (yield = 86 %).

M.p. (pentane): 95-100°C

^{1}H NMR (500 MHz, $CDCl_3$) δ (ppm) = 9.88 (s, 1H), 8.05-7.86 (m, 2H) 7.36 (ddd, *J*= 8.4, 7.5, 2.7 Hz, 1H), 7.29 (s, 2H).

^{11}B NMR (160 MHz, $CDCl_3$) δ (ppm) = 26.8 (br)

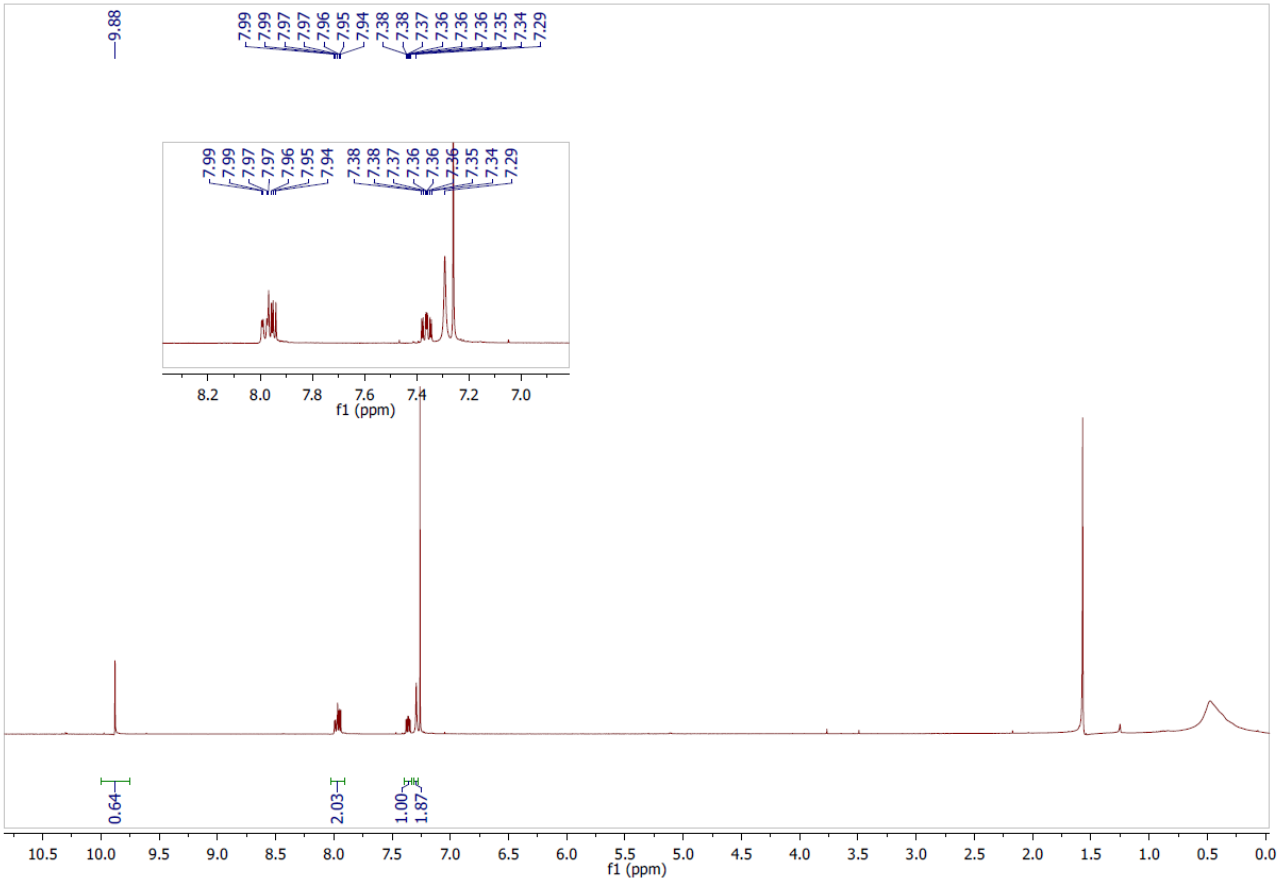
9.88
7.99
7.99
7.97
7.97
7.96
7.95
7.94
7.38
7.38
7.37
7.36
7.36
7.36
7.35
7.34
7.29
0.64
2.03
1.00
1.87
f1 (ppm)

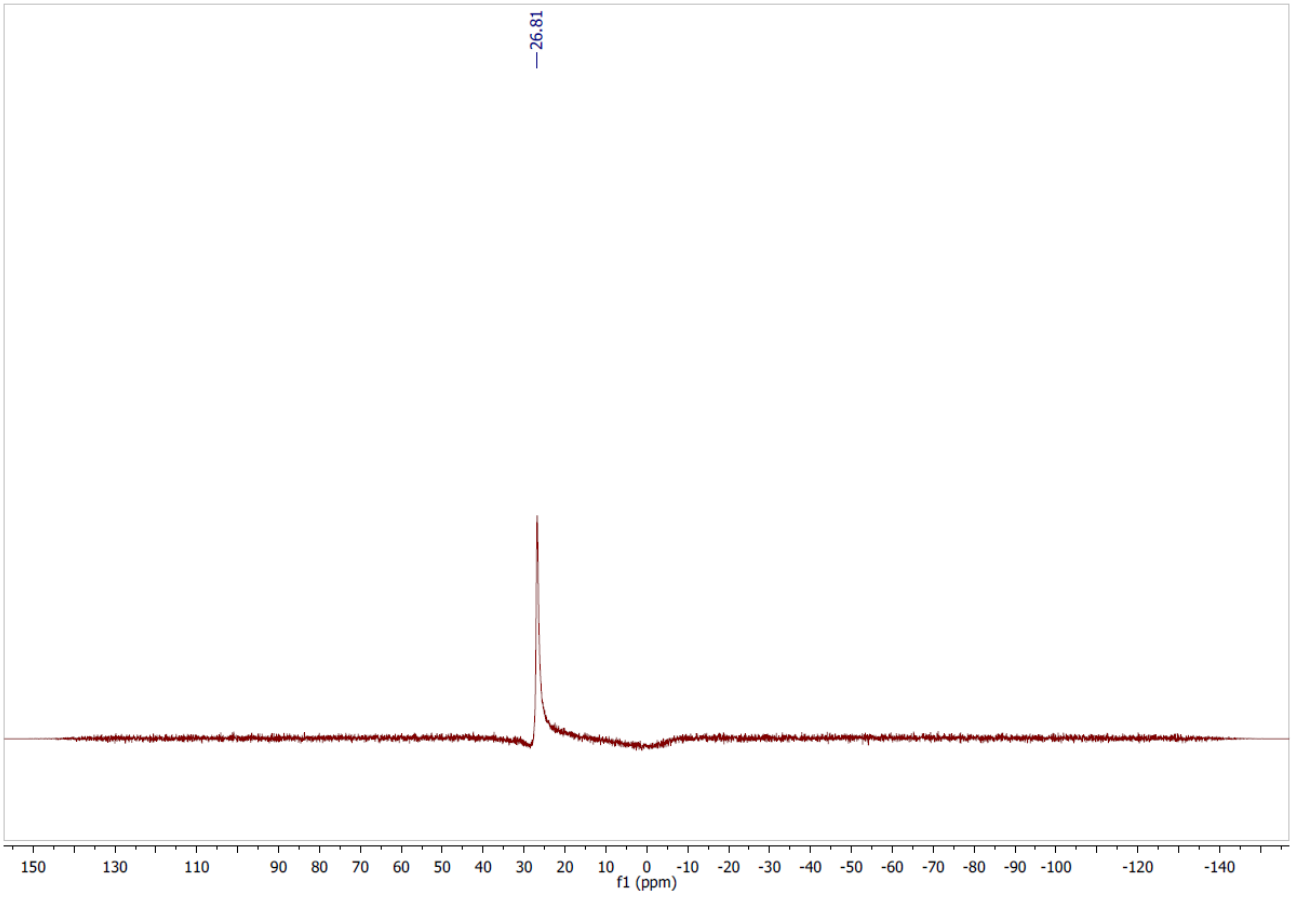
26.81
f1 (ppm)

(3-fluoro-2-formylphenyl)boronic acid **17**:

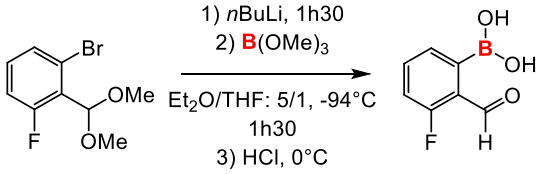

14 **17** (67 %)

*n*BuLi (2.5M in hexanes, 4.0 mL, 10 mmol, 1.1 equiv) was added dropwise on 2-bromo-1-(dimethoxymethyl)-3-fluorobenzene **14** (2.34 g, 8.99 mmol, 1.0 equiv) in a Et_2O/THF 5:1 anhydrous solution under Ar atmosphere at -94 °C. After 1h30 at -94 °C and under Ar atmosphere, $B(OMe)_3$ (1.1 mL, 9.7 mmol, 0.97 equiv) was added dropwise and after 1h30, the solution was slowly brought to 0 °C during acidification (pH = 3) of the mixture with 3 M HCl solution. The phases were separated and the aqueous phase was extracted with Et_2O (2x50 mL) and the reunited organic phases was extracted with brine (1x). The organic phase was dried with magnesium sulphate, filtered and the solvent was then evaporated, the solid formed was washed with pentane. The ^{1}H ^{11}B NMR and ^{19}F NMR data are consistent with those reported in the literature.

Off-white solid (1.0 g, yield = 67 %).

M.p. (pentane): 107-114°C

^{1}H NMR (500 MHz, $CDCl_3$) δ (ppm) = 10.0 (s, 1H), 7.69 (d, *J* = 7.5 Hz, 1H) 7.59 (td, *J*= 7.9, 5.5, 1H), 7.37-7.31 (m, 1H).

^{11}B NMR (160 MHz, $CDCl_3$) δ (ppm) = 28.4 (br)

^{19}F NMR (476 MHz, $CDCl_3$) δ (ppm) = -104.3 (br)

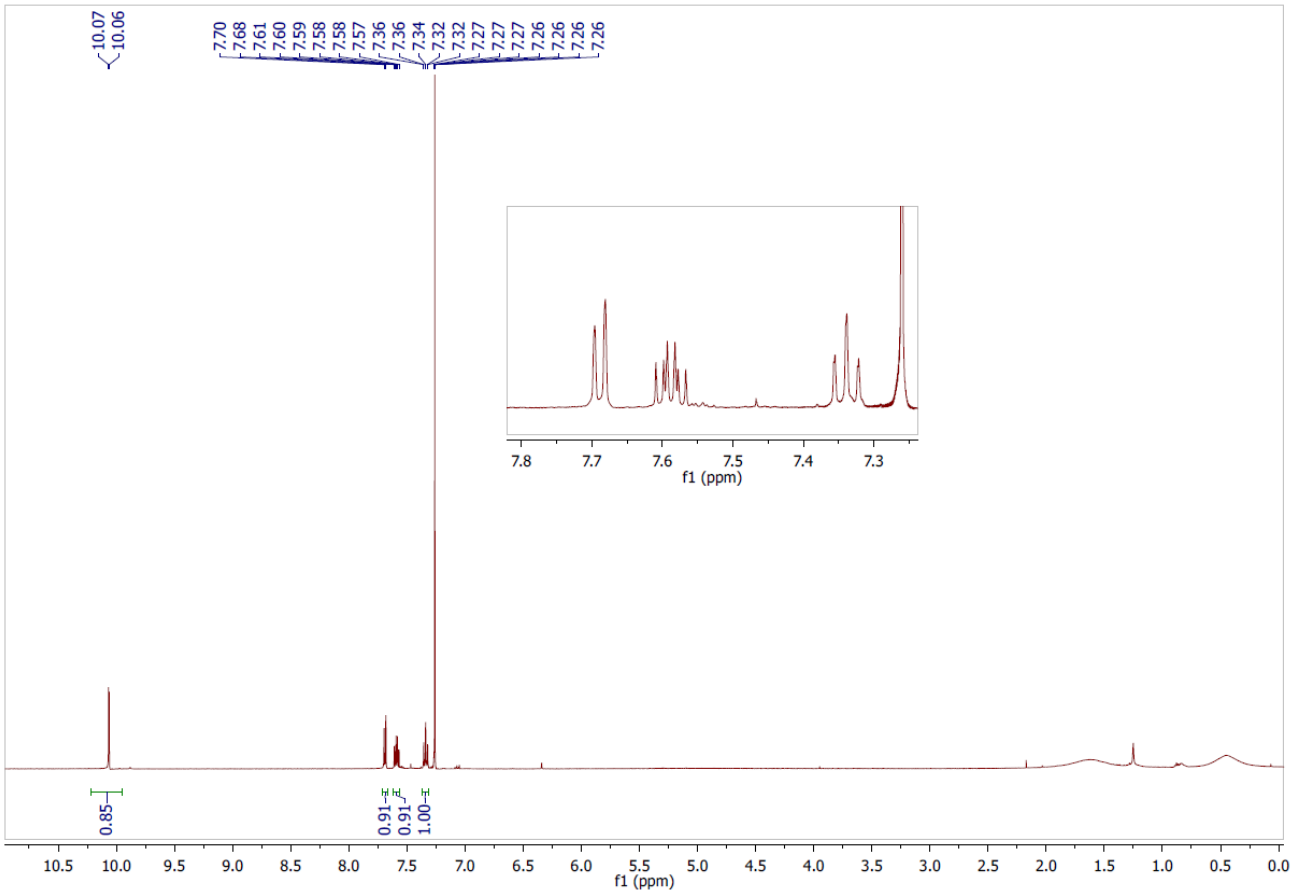
10.07
10.06
7.70
7.68
7.61
7.60
7.59
7.58
7.58
7.57
7.36
7.34
7.32
7.27
7.27
7.26
7.26
7.26
7.26
0.85
0.91
0.91
1.00
f1 (ppm)

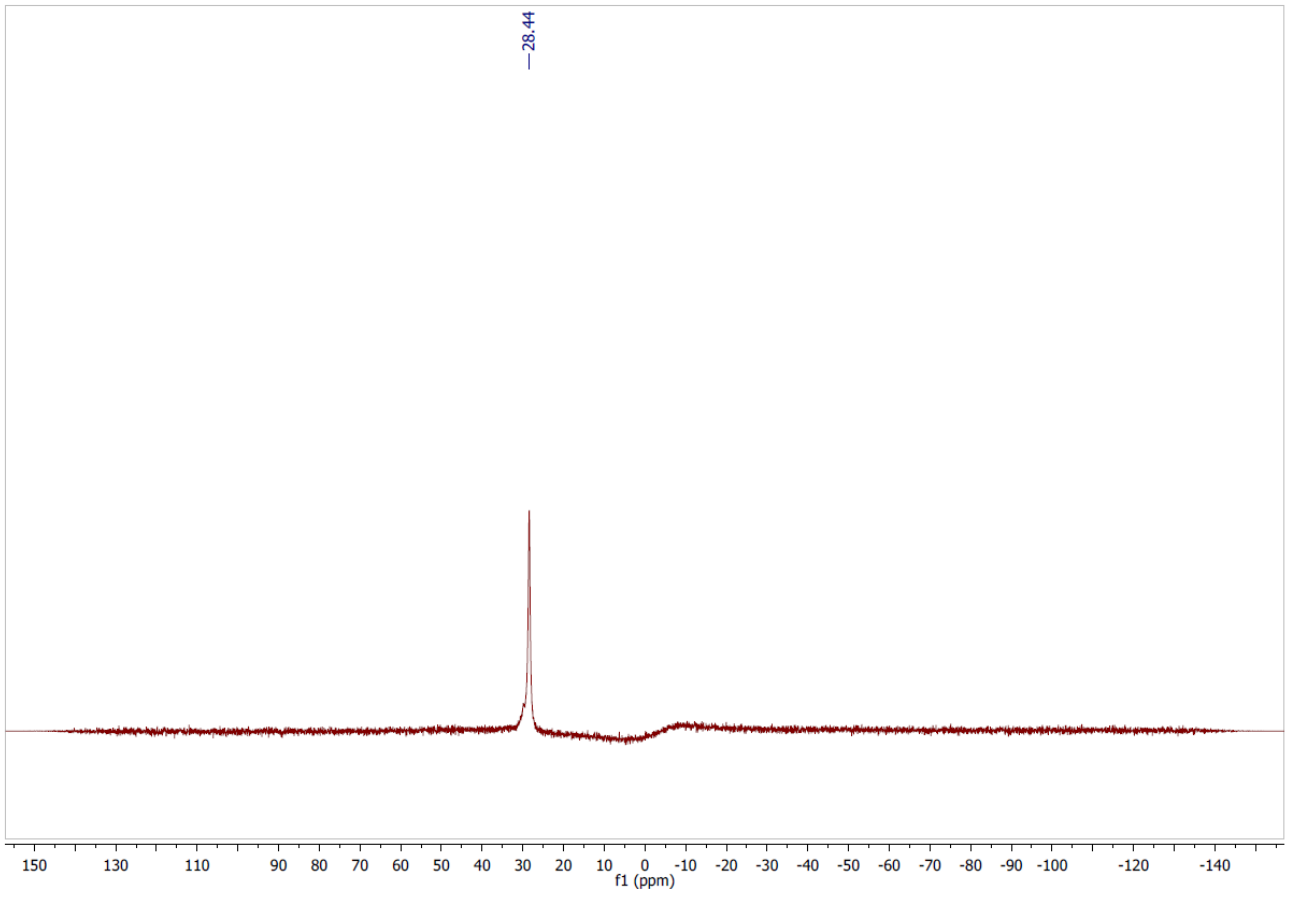
28.44
f1 (ppm)

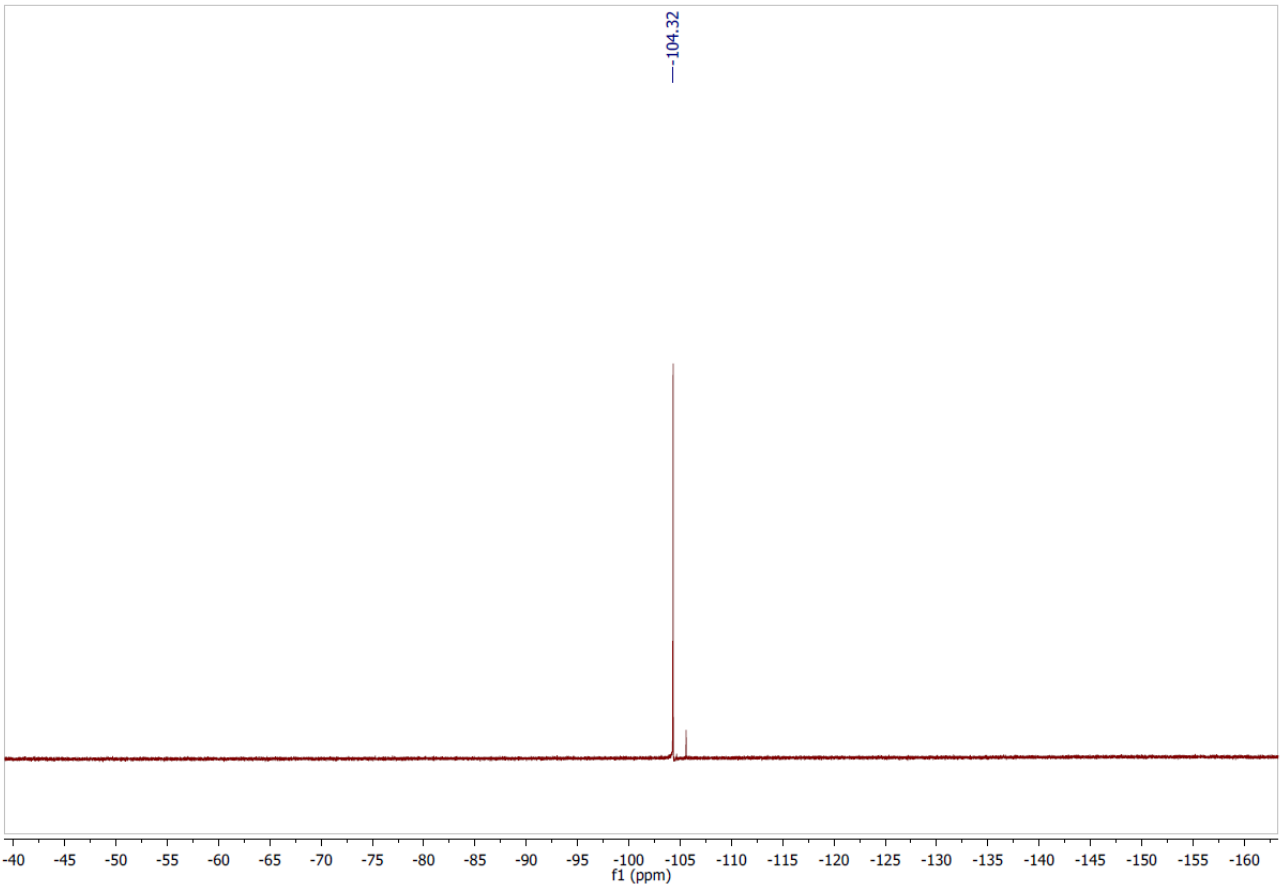

tris[2-formylphenyl]-boroxine **21**:

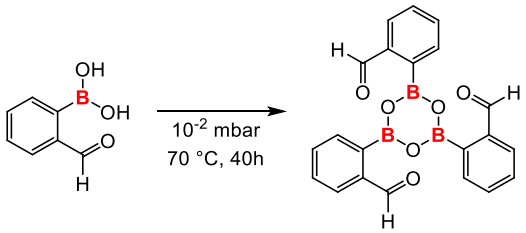

4 **21** (91 %)

In a sublimator appartus, (2-formylphenyl)boronic acid **4** (1.07 g, 7.16 mmol) was heated under reduced pressure (6 mbar) at 70 °C during 40h. The unsublimated product was collected in the glovebox and correspond to the title product.

White solid (2.5g, yield = 91 %).

M.p. ($CHCl_3$): 159-164°C

^{1}H NMR (500 MHz, $CDCl_3$) δ (ppm) =10.3 (s, 1H), 7.92 (dd, *J* = 11.8, 4.0 Hz, 6H) 7.76-7.60 (m, 3H), 7.56 (td, *J* =8.5, 0.9 Hz, 3H)

^{11}B NMR (160 MHz, $CDCl_3$) δ (ppm) = 26.4 (br)

^{13}C NMR (126 MHz, $CDCl_3$) δ (ppm) = 195.9, 140.7, 134.7, 133.5, 130.3, 129.3. The carbon atoms directly attached to the boron atom on the boroxine core were not detected, likely due to quadrupolar relaxation.

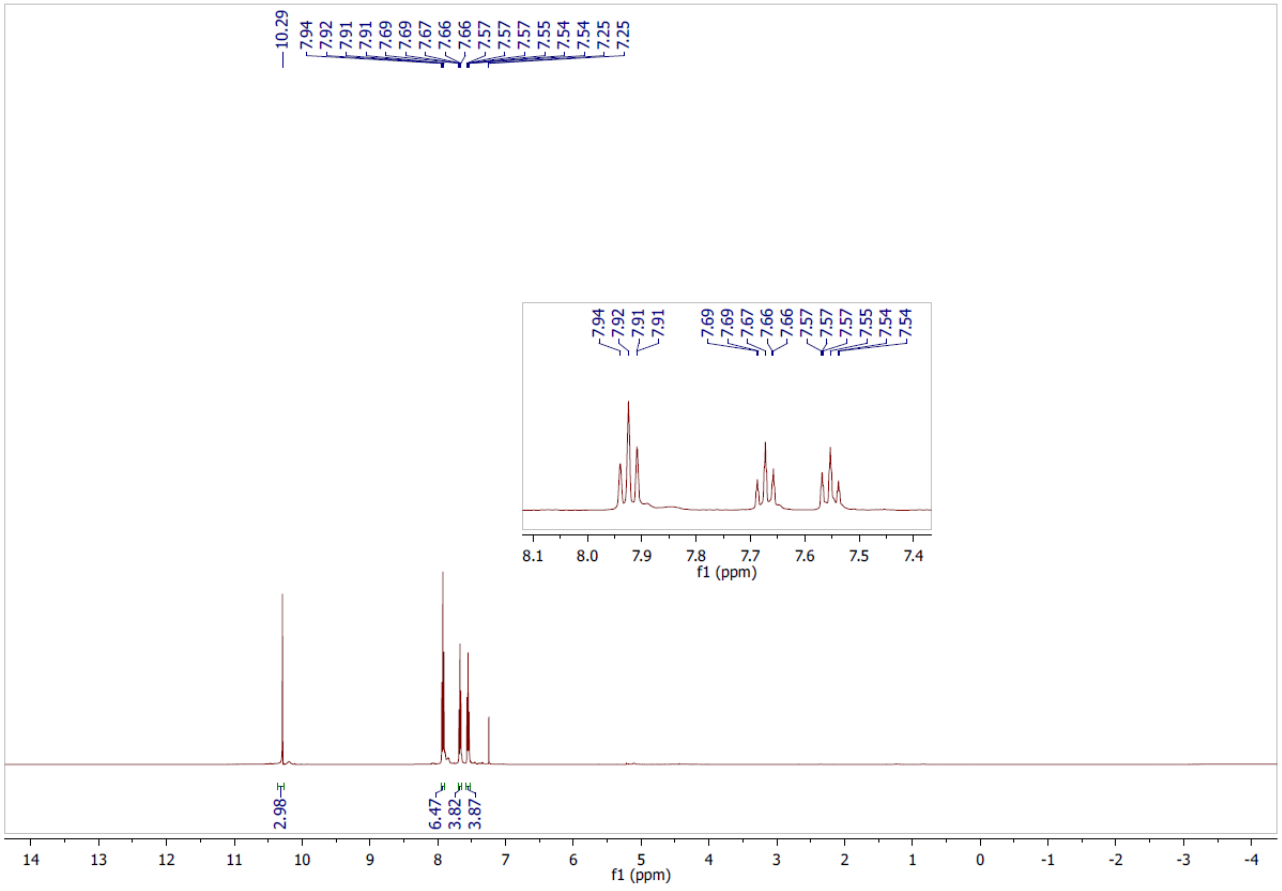

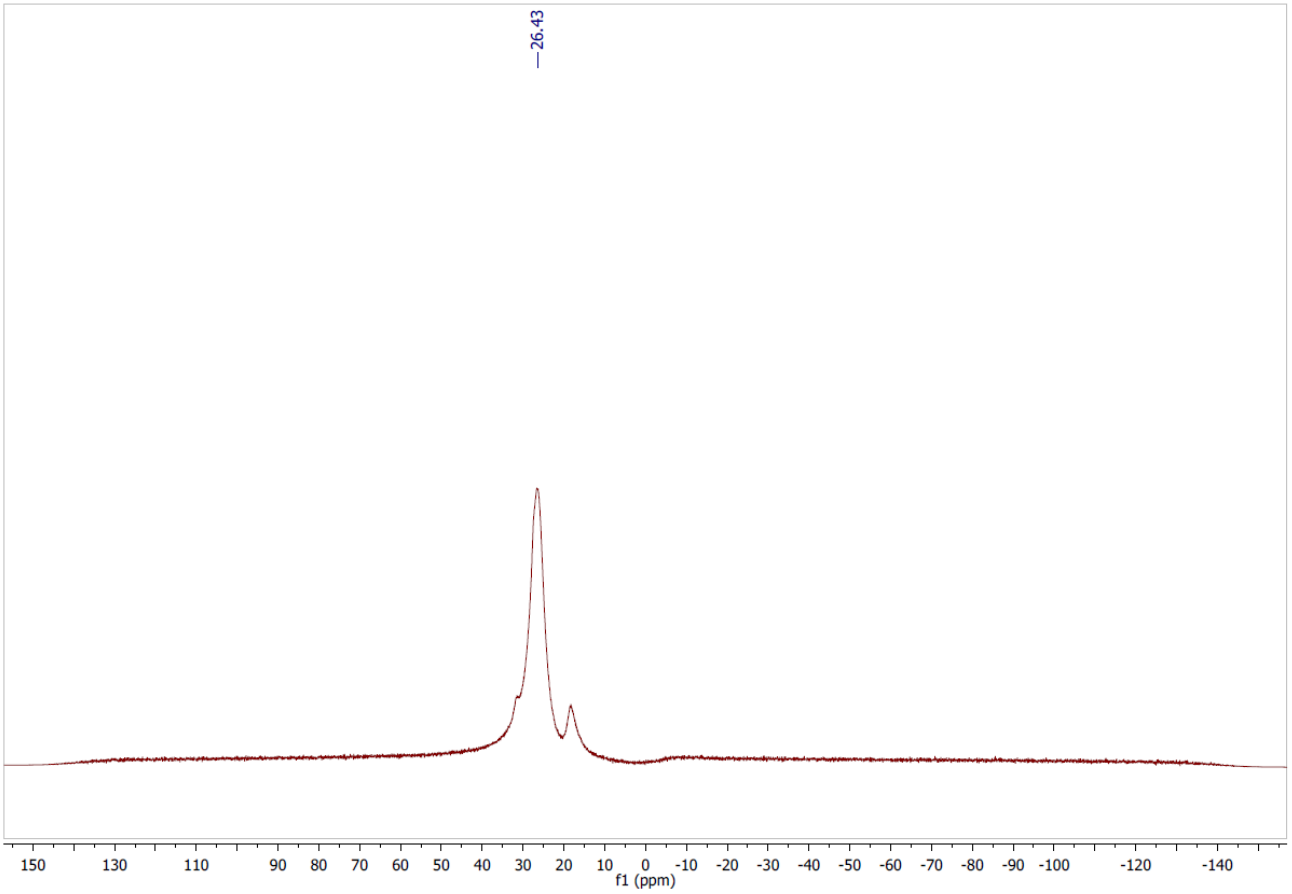
26.43
150 130 110 90 80 70 60 50 40 30 20 10 0 -10 -20 -30 -40 -50 -60 -70 -80 -90 -100 -120 -140
f1 (ppm)

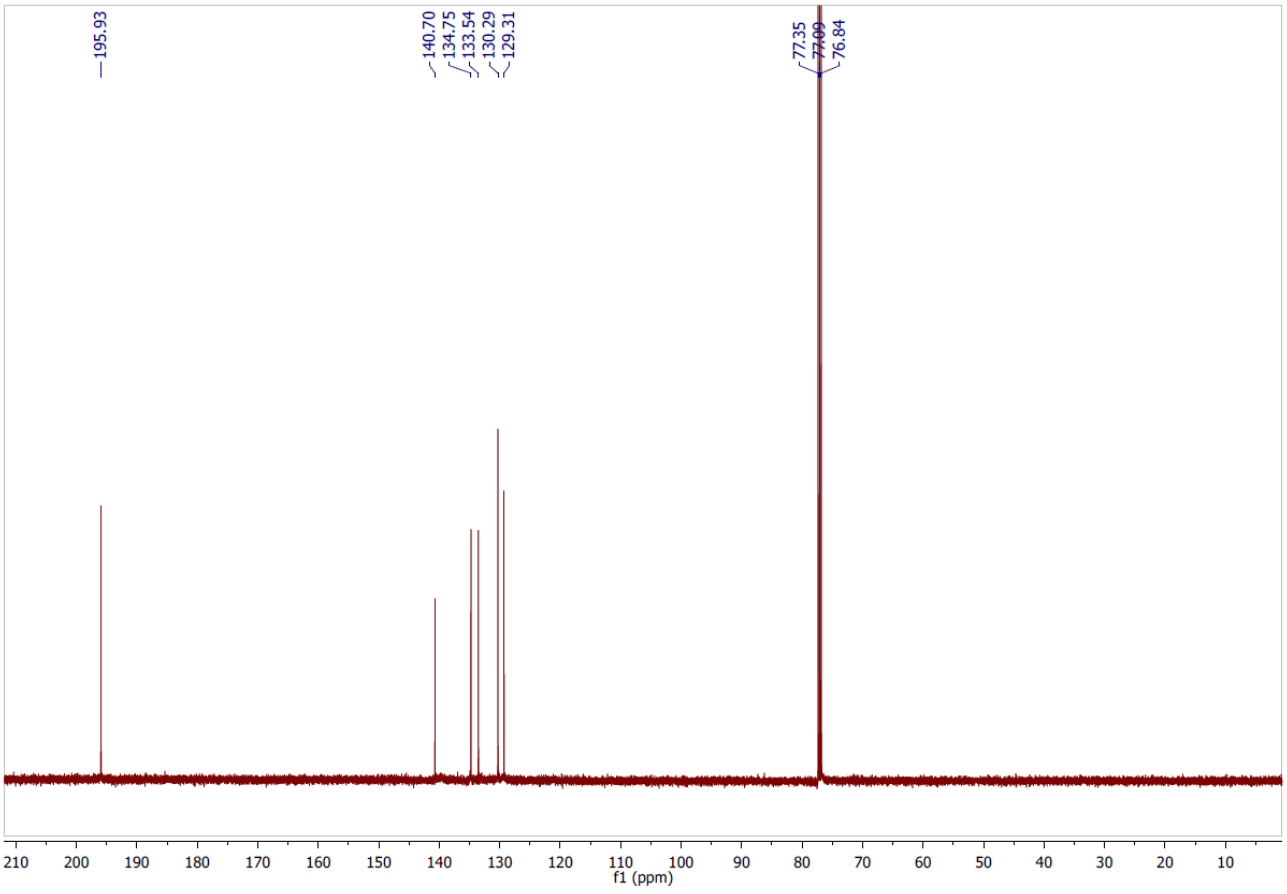
195.93
140.70
134.75
133.54
130.29
129.31
77.35
77.09
76.84
210 200 190 180 170 160 150 140 130 120 110 100 90 80 70 60 50 40 30 20 10
f1 (ppm)

tris[5-tert-butyl-2-formylphenyl]-boroxine **22**:

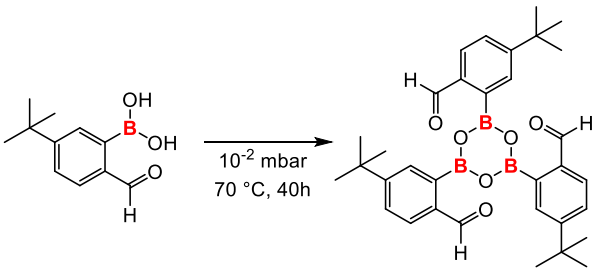

12 **22** (n.d.)

In a sublimator appartus, (5-tert-butyl-2-formylphenyl)boronic acid **12** (0.10 g, 0.49 mmol) was heated under reduced pressure (10^{-2} mbar) at 70 °C during 40h. Thermal induced degradation has been observed and no pure product has been isolated.

tris[3-fluoro-2-formylphenyl]-boroxine **23**:

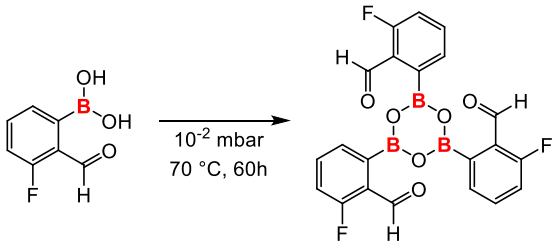

19 **23** (79 %)

In a sublimator, (3-fluoro-2-formylphenyl)boronic acid **19** (2.00 g, 11.9 mmol) was heated under reduced pressure (10^{-2} mbar) at 70 °C during 60h. The unsublimated product was colected in the glovebox and correspond to the title product.

Yellow solid (1.37 g, yield = 79 %).

M.p. ($CHCl_3$): 150-161°C

^{1}H NMR (500 MHz, $CDCl_3$) δ (ppm) =10.3 (s, 1H), 7.65 (ddd, *J* = 8.2, 7.4, 5.1 Hz, 3H) 7.55 (d, *J* = 7.2 Hz, 3H), 7.56 (ddd, *J* = 10.0, 8.3, 0.8 Hz, 3H)

^{11}B NMR (160 MHz, $CDCl_3$) δ (ppm) = 25.9 (br)

^{19}F NMR (476 MHz, $CDCl_3$) δ (ppm) = -119.8 (d, *J* = 5.2 Hz)

^{13}C NMR (126 MHz, $CDCl_3$) δ (ppm) = 190.5 (CH), 163.5 (d, *J* = 261.5 Hz, Cq), 137.8 (d, *J* = 8.4 Hz, CH), 127.2 (d, *J* = 3.6 Hz, CH), 127.1 (Cq), 116.4 (d, *J* = 19.8 Hz, CH). The carbon atoms directly attached to the boron atom on the boroxine core were not detected, likely due to quadrupolar relaxation.

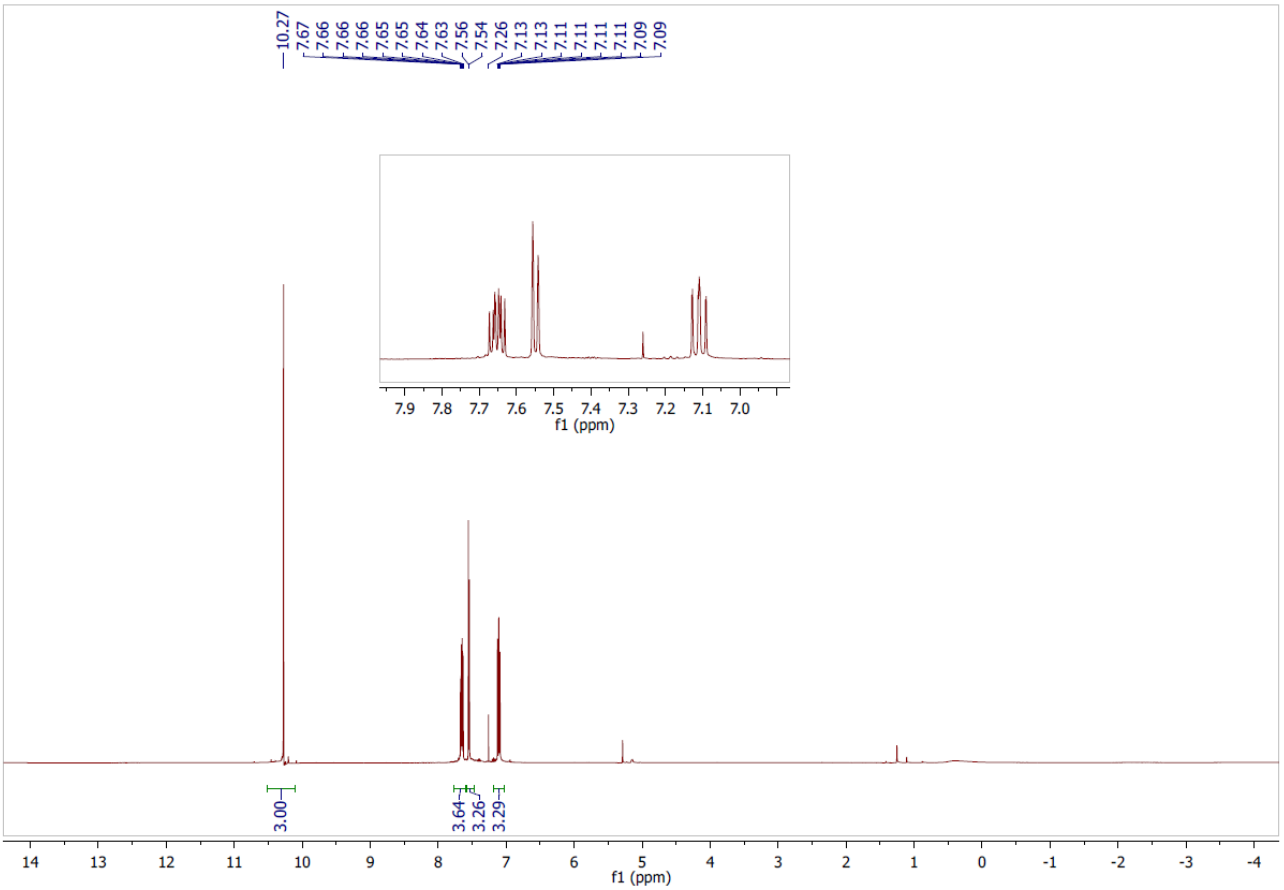

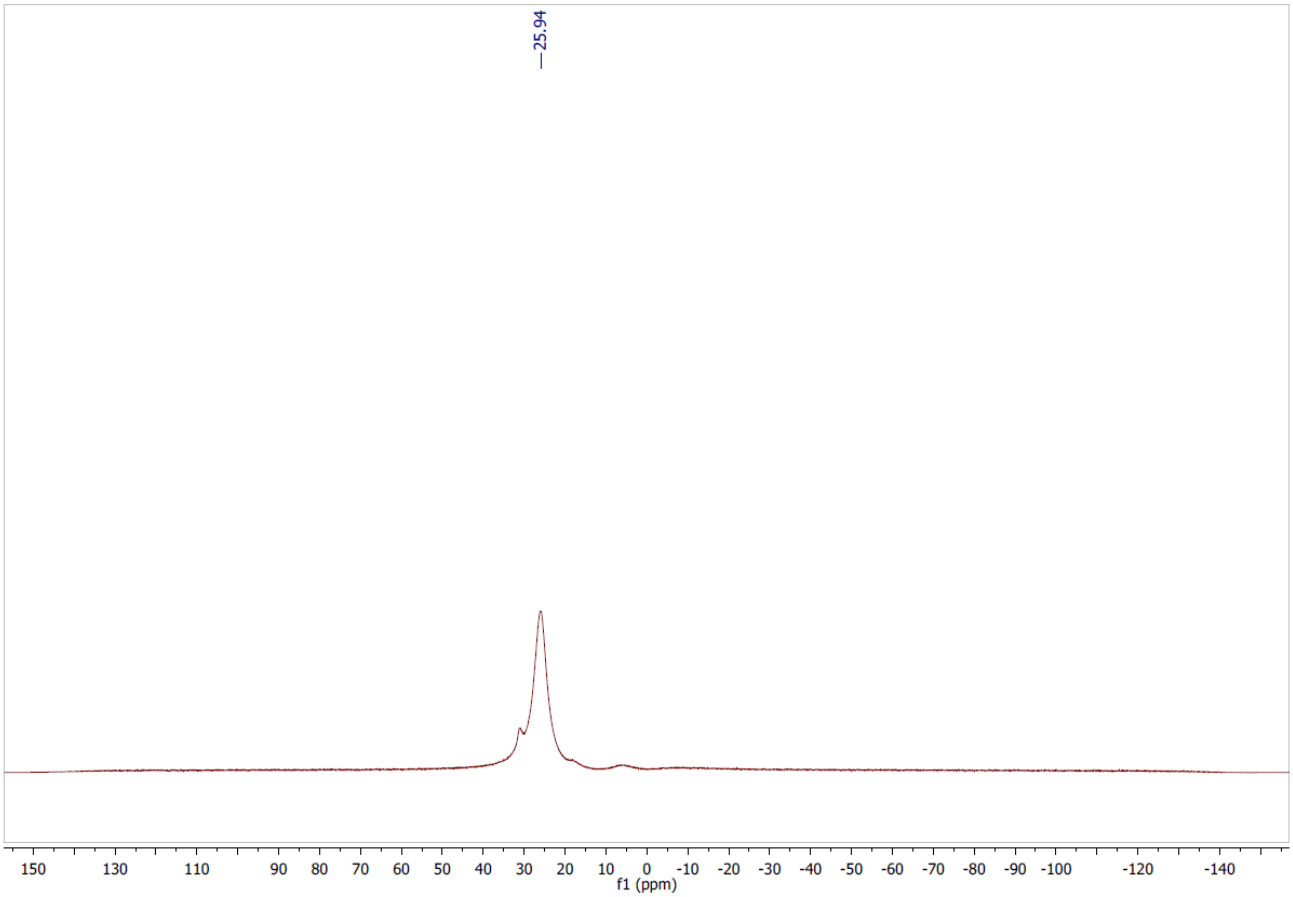
25.94
150 130 110 90 80 70 60 50 40 30 20 10 0 -10 -20 -30 -40 -50 -60 -70 -80 -90 -100 -120 -140
f1 (ppm)

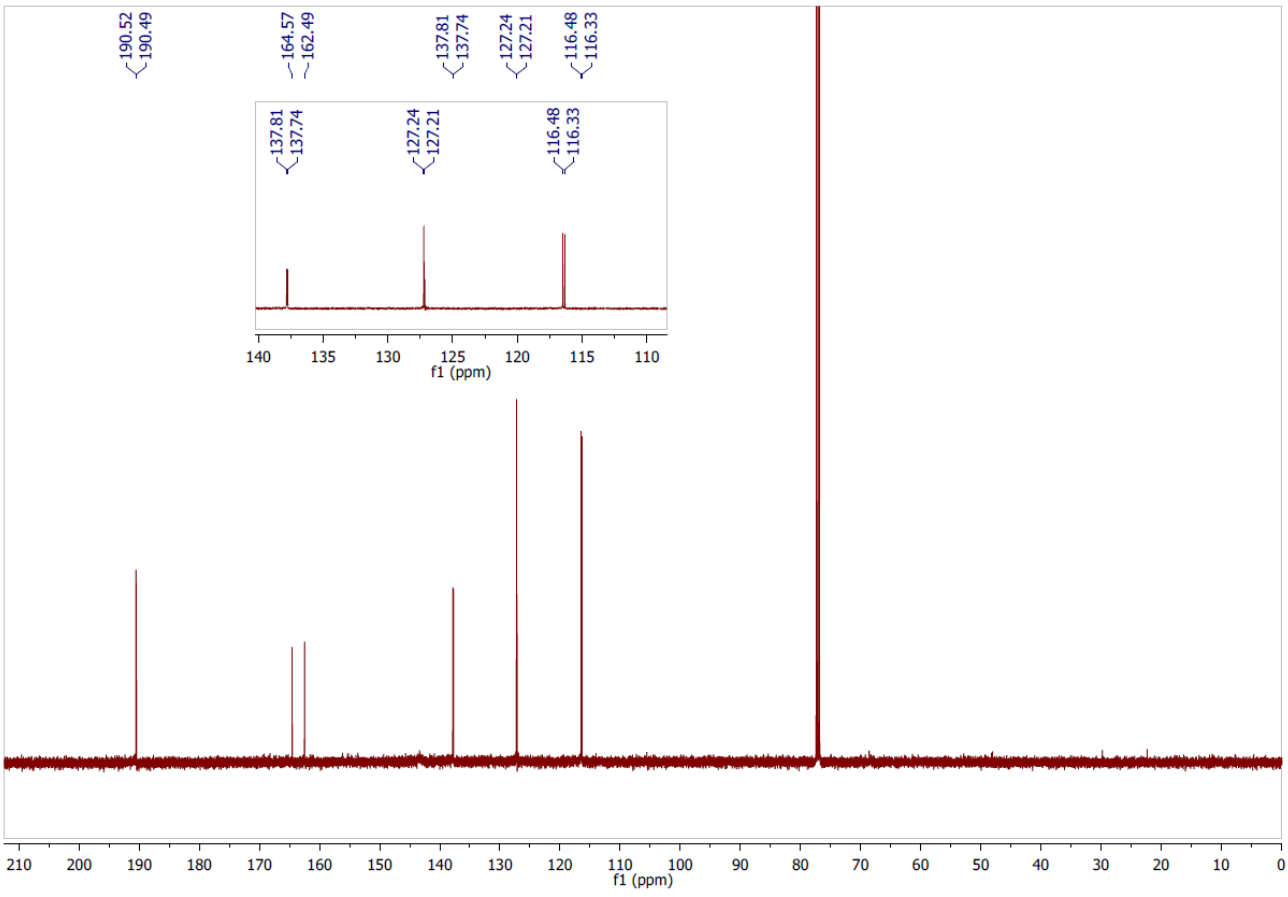
190.52
190.49
164.57
162.49
137.81
137.74
127.24
127.21
116.48
116.33
137.81
137.74
127.24
127.21
116.48
116.33
140 135 130 125 120 115 110
f1 (ppm)
210 200 190 180 170 160 150 140 130 120 110 100 90 80 70 60 50 40 30 20 10 0
f1 (ppm)

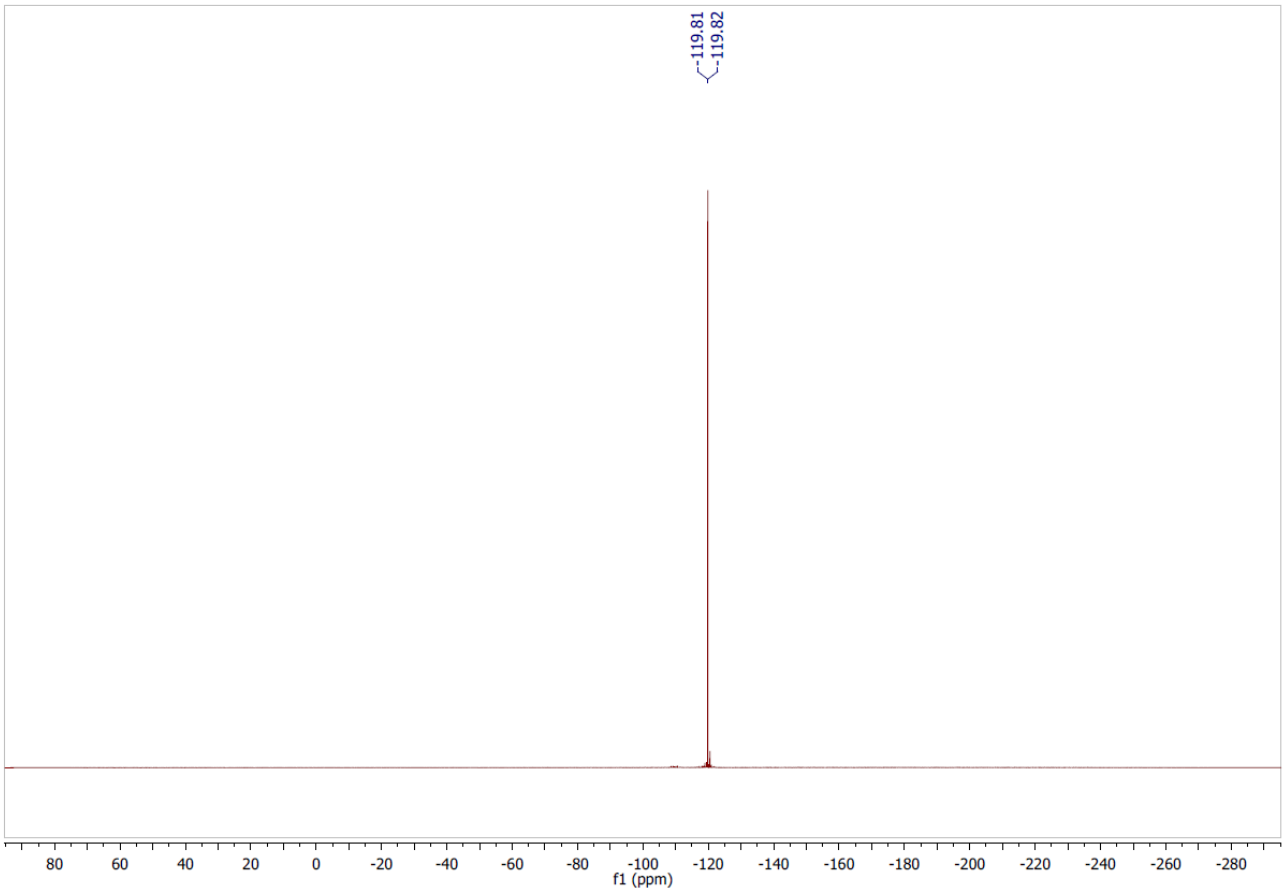

tris[5-fluoro-2-formylphenyl]-boroxine **24**:

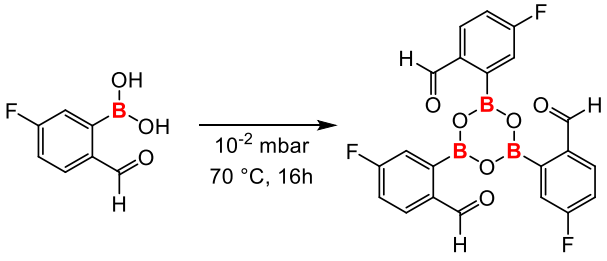

18 **24** (90 %)

In a sublimator, (5-fluoro-2-formylphenyl)boronic acid **18** (3.00 g, 17.9 mmol) was heated under reduced pressure (10^{-2} mbar) at 70 °C during 16h. The unsublimated product was recollected in glovebox and correspond to the boroxine. The unsublimated product was colected in the glovebox and correspond to the title product.

White solid (2.44 g, yield = 90 %)

M.p. ($CHCl_3$): 165-169°C

^{1}H NMR (500 MHz, $CDCl_3$) δ (ppm) =10.1 (s, 1H), 7.96 (dd, *J* = 8.5, 5.1 Hz, 3H) 7.57 (dd, *J* = 8.5, 2.5 Hz, 3H), 7.39-7.10 (m, 3H)

^{11}B NMR (160 MHz, $CDCl_3$) δ (ppm) = 23.9 (br)

^{19}F NMR (476 MHz, $CDCl_3$) δ (ppm) = -100.2 (br)

^{13}C NMR (126 MHz, $CDCl_3$) δ (ppm) = 194.6 (d, *J* = 3.0 Hz, CH), 167.4 (d, *J* = 260.6 Hz, Cq), 136.6 (d, *J* = 1.9 Hz, Cq), 132.3 (d, *J* = 9.8 Hz, CH), 120.3 (d, *J* = 21.1 Hz, CH), 117.3 (d, *J* = 22.9 Hz, CH). The carbon atoms directly attached to the boron atom on the boroxine core were not detected, likely due to quadrupolar relaxation.

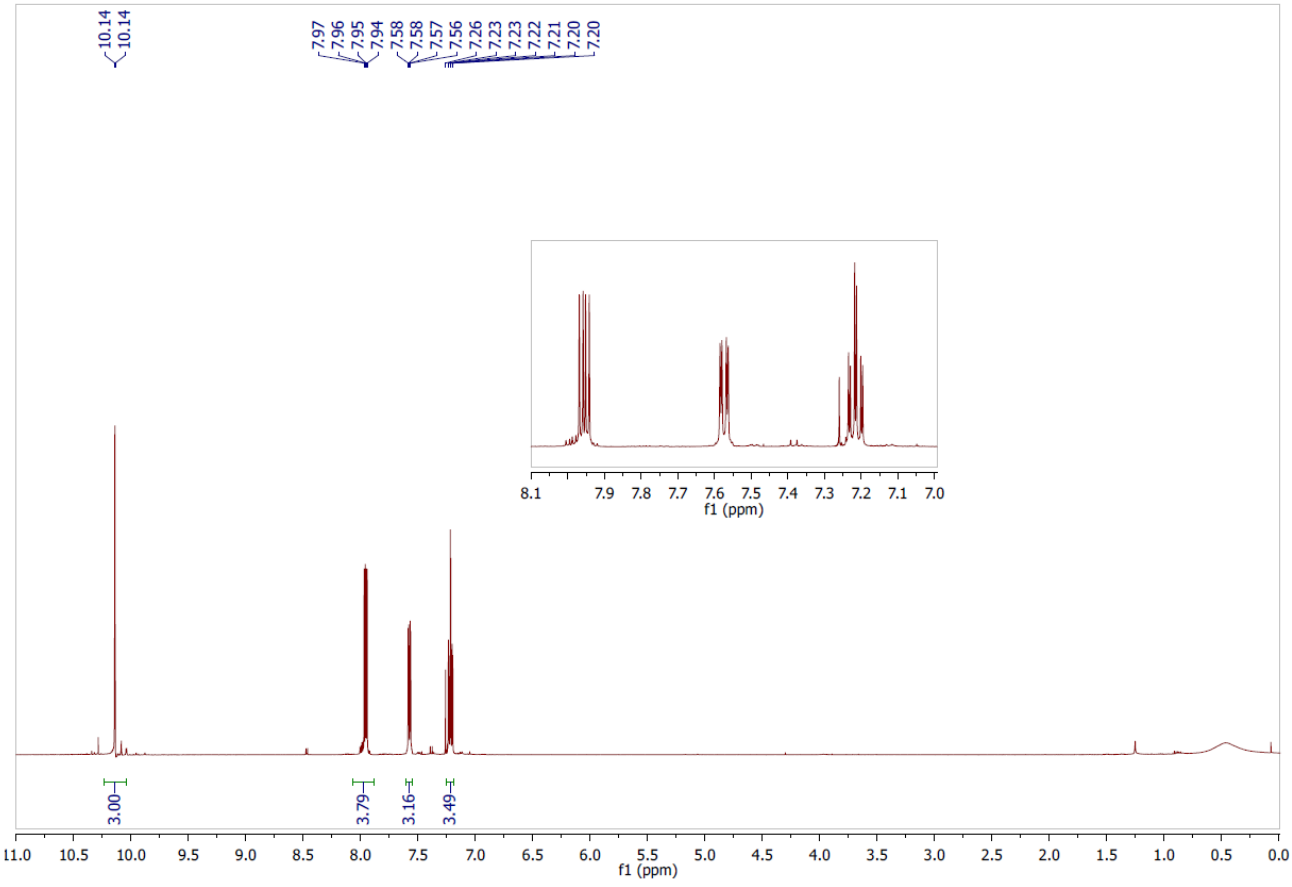

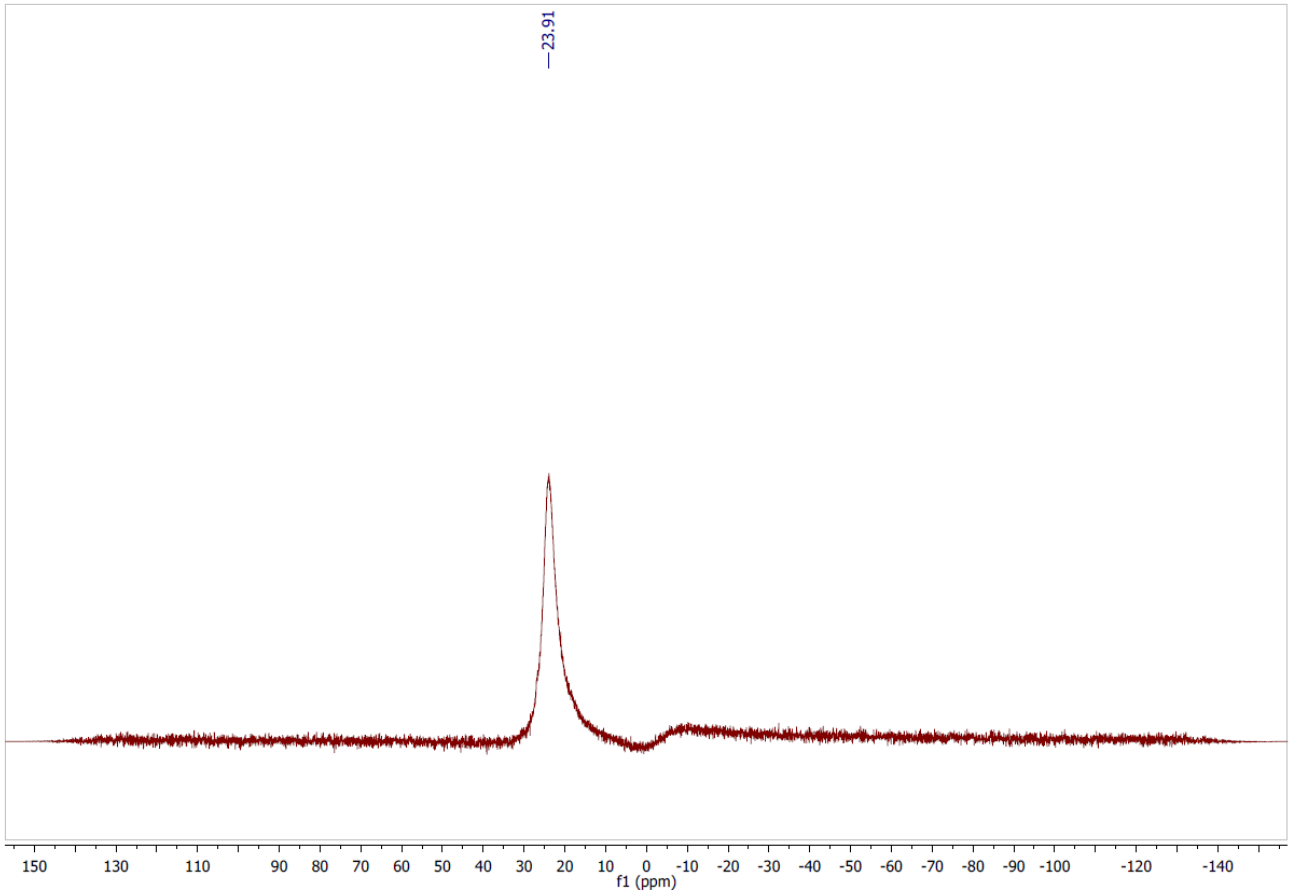
23.91
150 130 110 90 80 70 60 50 40 30 20 10 0 -10 -20 -30 -40 -50 -60 -70 -80 -90 -100 -120 -140
f1 (ppm)

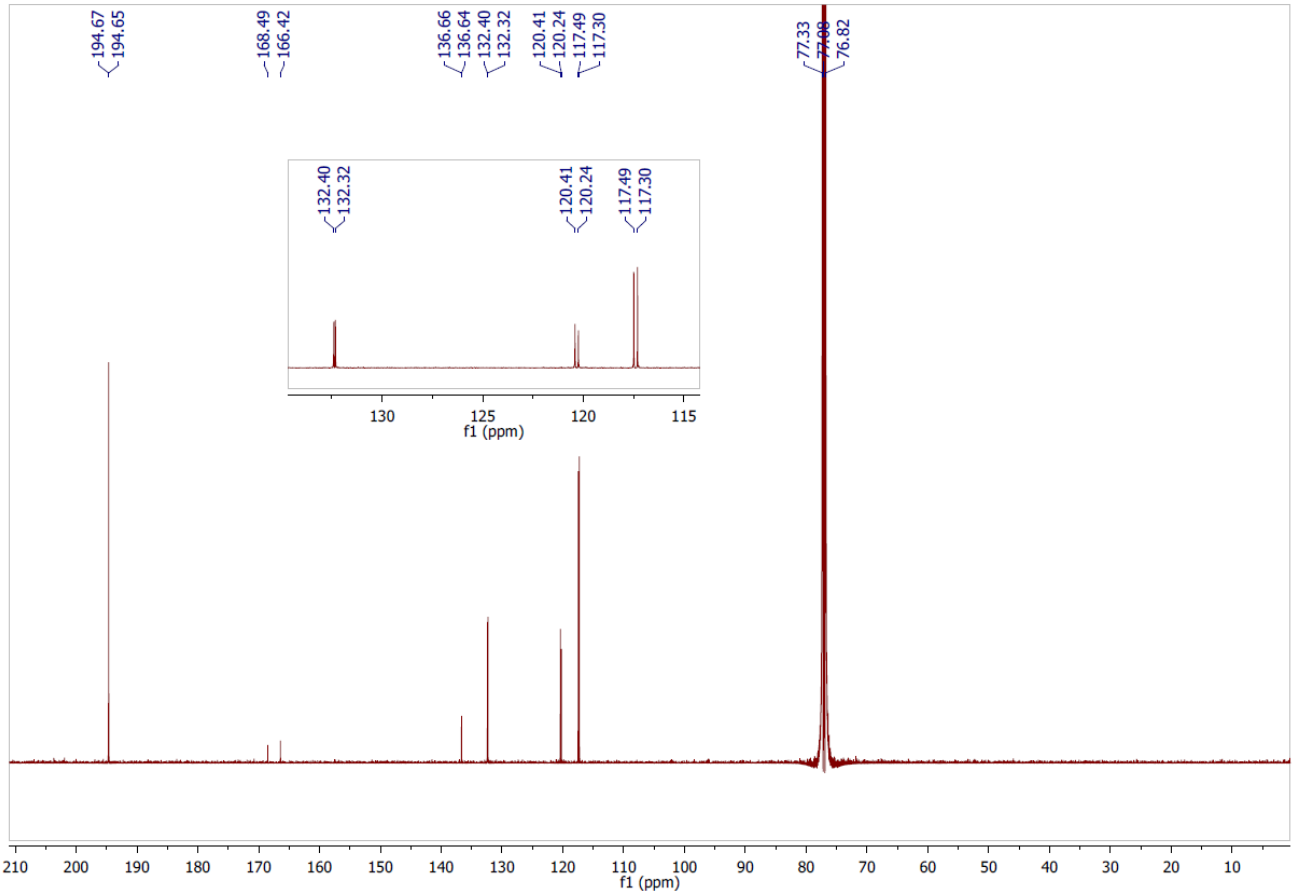
194.67
194.65
168.49
166.42
136.66
136.64
132.40
132.32
120.41
120.24
117.49
117.30
77.33
77.08
76.82
132.40
132.32
120.41
120.24
117.49
117.30
130 125 120 115
f1 (ppm)
210 200 190 180 170 160 150 140 130 120 110 100 90 80 70 60 50 40 30 20 10
f1 (ppm)

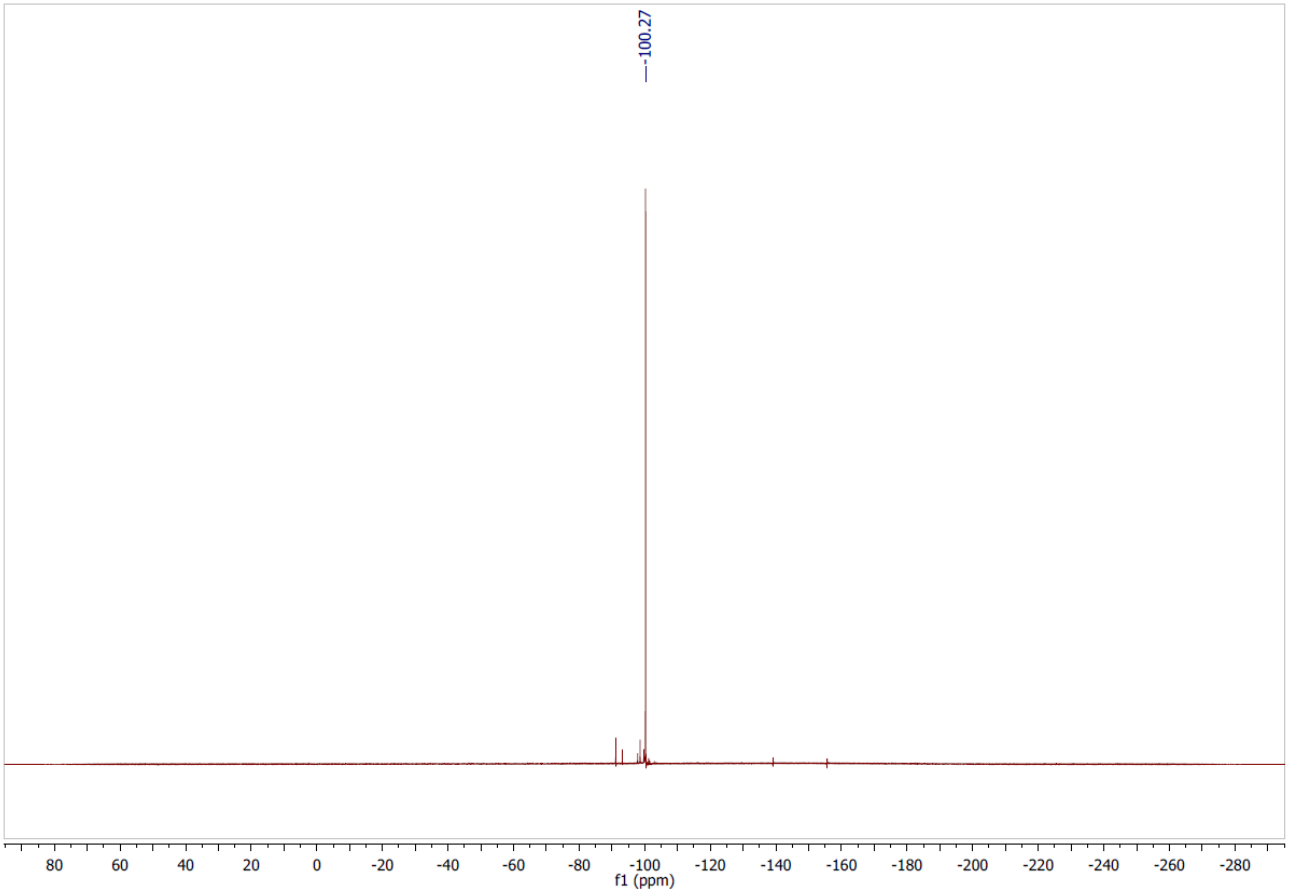

triphenyl boroxine **26**:

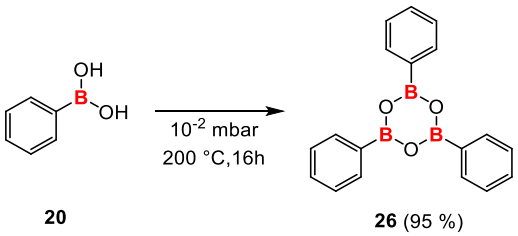

20 **26** (95 %)

In a sublimator appartus, phenyl boronic acid **20** (0.40 g, 3.3 mmol) was heated under reduced pressure (10^{-2} mbar) at 200 °C during 16h. The sublimated product was collected in glovebox and correspond to the title compound. The ^{1}H and ^{11}B NMR data are consistent with those reported in the literature.

White solid (974 mg, yield = 95 %)

^{1}H NMR (500 MHz, $CDCl_3$) δ (ppm) = 8.25 (dd, 8.0, 1,4 Hz, 6H), 7.69 (ddd, *J* = 6.8, 5.2, 3.4 Hz, 3H) 7.57-7.36 (m, 6H).

^{11}B NMR (160 MHz, $CDCl_3$) δ (ppm) = 29.0 (br)

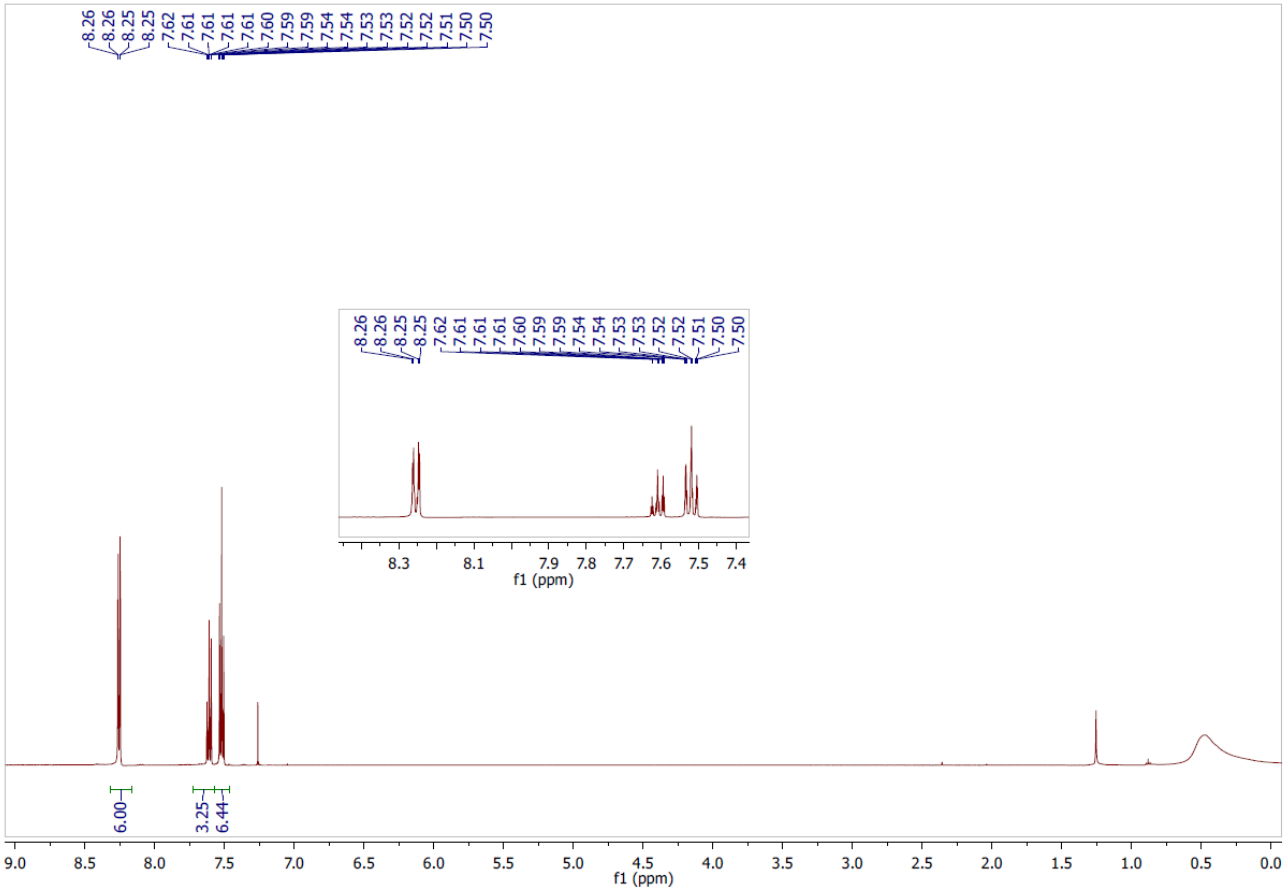
8.26
8.26
8.25
8.25
7.62
7.61
7.61
7.61
7.61
7.60
7.59
7.59
7.54
7.54
7.53
7.53
7.52
7.52
7.51
7.50
7.50
8.3
8.1
7.9
7.8
7.7
7.6
7.5
7.4
f1 (ppm)
6.00
3.25
6.44
9.0
8.5
8.0
7.5
7.0
6.5
6.0
5.5
5.0
4.5
4.0
3.5
3.0
2.5
2.0
1.5
1.0
0.5
0.0
f1 (ppm)

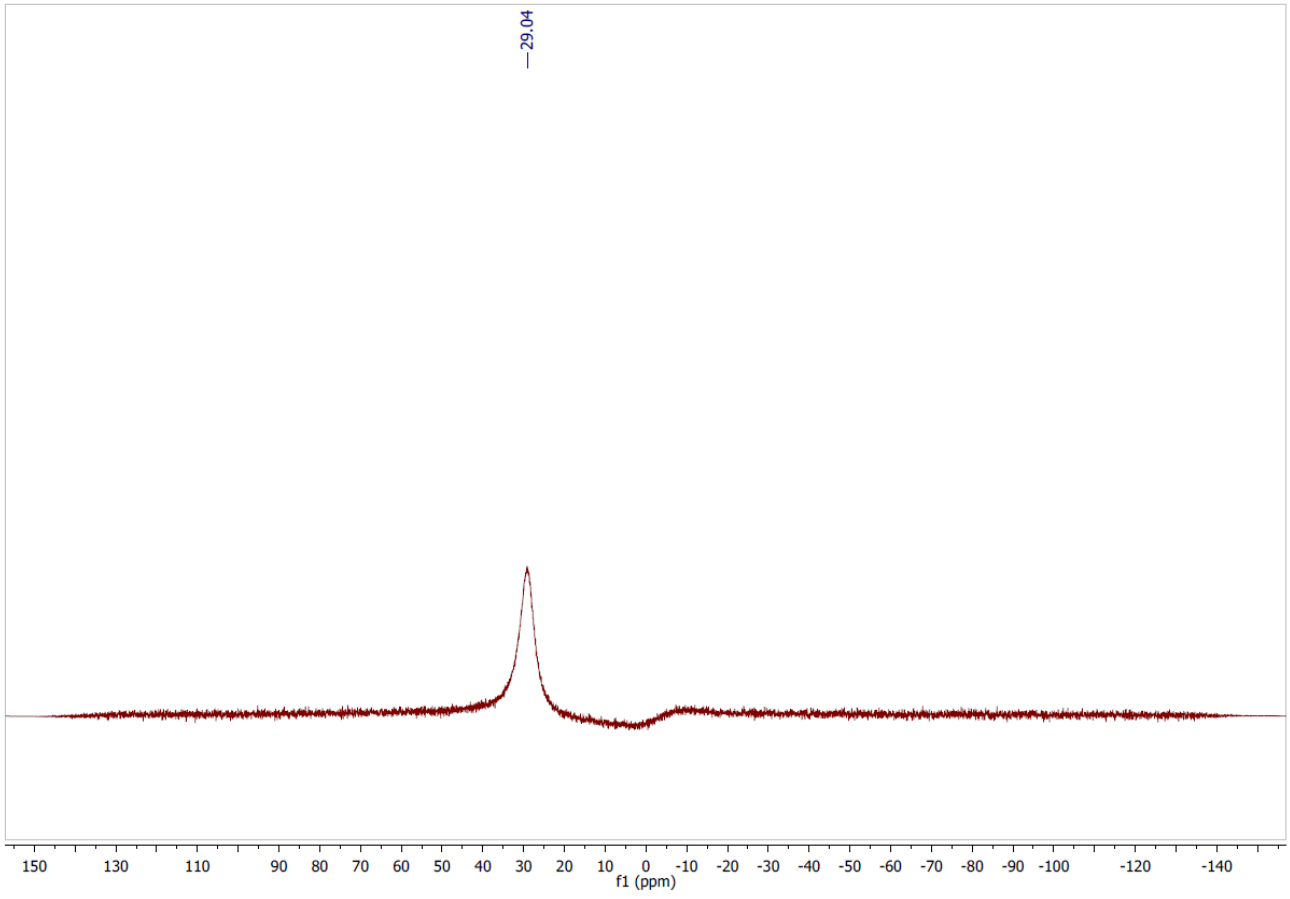
29.04
150
130
110
90
80
70
60
50
40
30
20
10
0
-10
-20
-30
-40
-50
-60
-70
-80
-90
-100
-120
-140
f1 (ppm)

Triphenyl boroxine/DMAP adduct formation **29**:

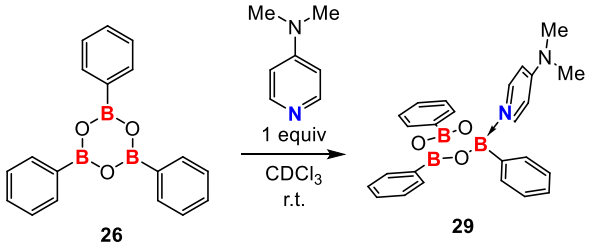

In a glovebox, triphenyl boroxine **26** (10 mg, 0.032 mmol, 1 equiv) and DMAP (4 mg, 0.032 mmol, 1 equiv) was mixed together in a small flask in $CDCl_3$ at room temperature, mixed manually and transferred in a NMR tube.

tris[2-[(n-butylimino)methyl]phenyl]-boroxine **32**:

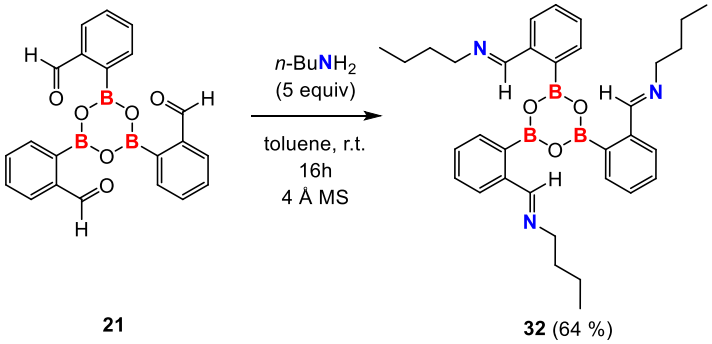

*n*Butylamine (0.10 mL, 1.0 mmol, 5 equiv) was added to tris[2-formylphenyl]-boroxine **21** (0.082 g, 0.20 mmol, 1 equiv) in dry toluene on molecular sieves under argon atmosphere and stirred 16h at room temperature. The solution was then filtered through syringe filter (0.2 µm) under argon and the solvent evaporated under reduced pressure.

Slightly yellow solid (71 mg, yield = 64 %).

^{1}H NMR (500 MHz, $CDCl_3$) δ (ppm) =8.48 (s, 3H), 7.68 (d, *J* = 7.2 Hz, 3H) 7.58 (d, *J* = 7.6 Hz, 3H), 7.39 (t, *J* = 7.3 Hz, 3H), 7.25 (dd, *J* = 8.0, 6.9 Hz, 3H), 3.68 (t, *J* = 7.4 Hz, 6H), 1.76 (m, 6H), 1.40-1.35 (m, 6H, partially overlapped with water), 0.86-0.82 (m, 9H, partially overlapped with water)

^{11}B NMR (160 MHz, $CDCl_3$) δ (ppm) = 14.3 (br)

^{13}C NMR (126 MHz, $CDCl_3$) δ (ppm) = 165.1, 138.6, 131.6, 131.0, 129.1, 128.3, 127.7, 125.8, 52.3, 29.8, 20.4, 13.9

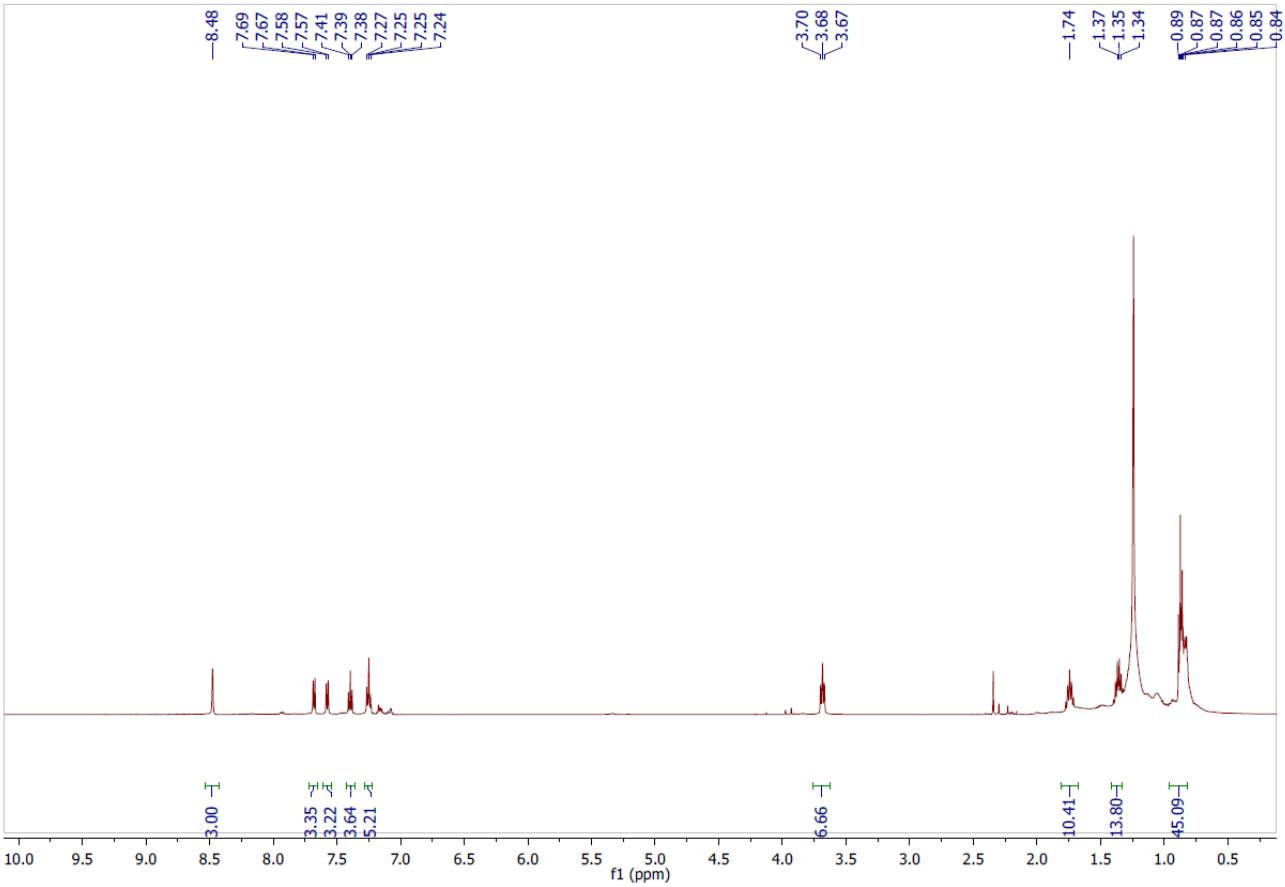

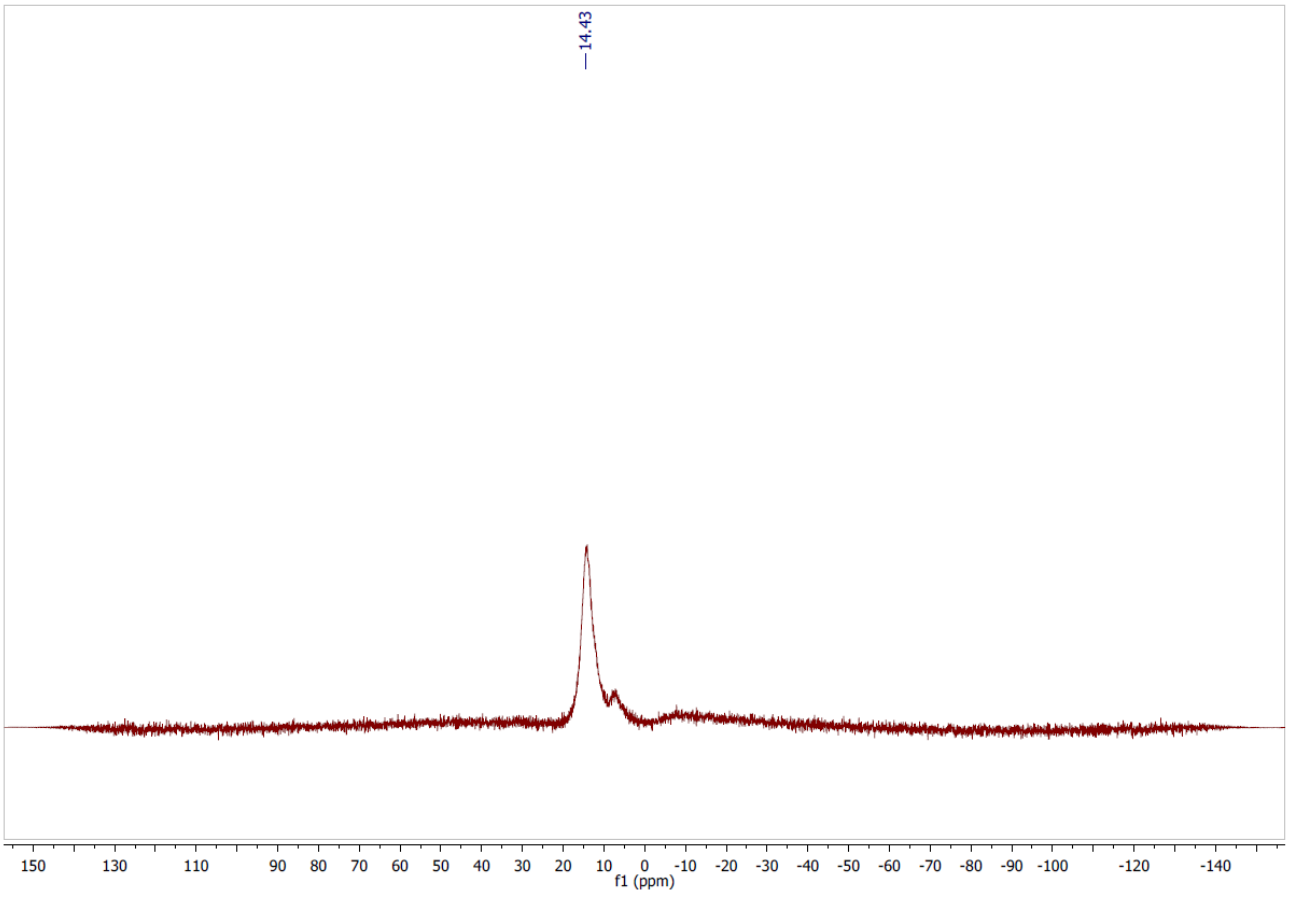
14.43
150 130 110 90 80 70 60 50 40 30 20 10 0 -10 -20 -30 -40 -50 -60 -70 -80 -90 -100 -120 -140
f1 (ppm)

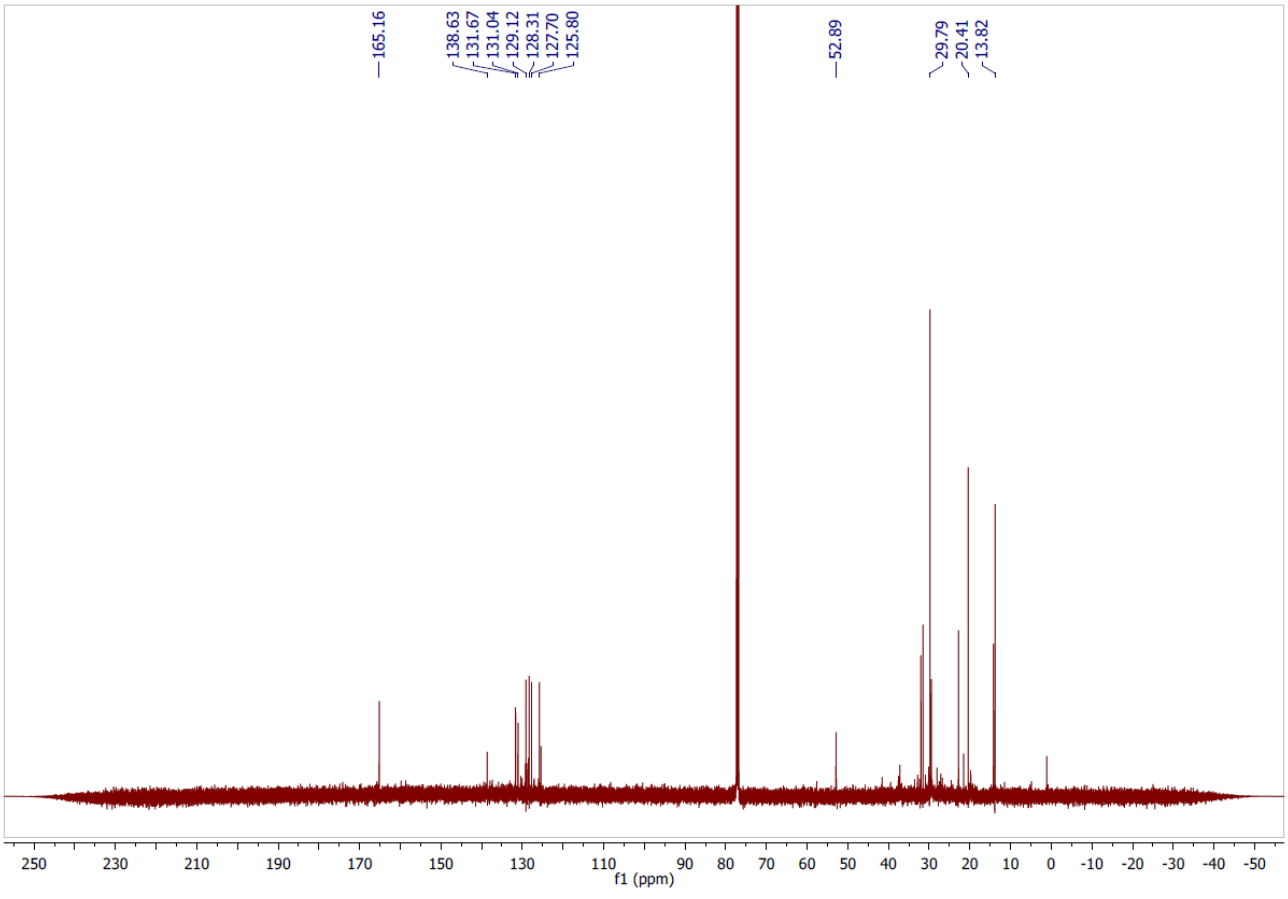
165.16
138.63
131.67
131.04
129.12
128.31
127.70
125.80
52.89
29.79
20.41
13.82
250 230 210 190 170 150 130 110 90 80 70 60 50 40 30 20 10 0 -10 -20 -30 -40 -50
f1 (ppm)

[2-[(phenylimino)methyl]phenyl]-boroxine **33**:

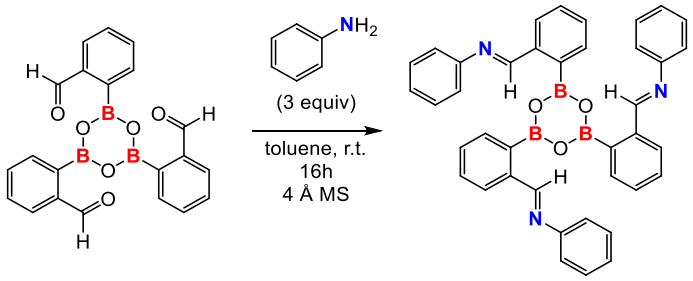

21 **33** (69 %)

Aniline (0.05 mL, 0.55 mmol, 3 equiv) was added to tris[2-formylphenyl]-boroxine **21** (0.082 g, 0.20 mmol, 1 equiv) in dry toluene on molecular sieves under argon atmosphere and stirred 16h at room temperature. The solution was then filtered through syringe filter (0.2 µm) under argon and the solvent evaporated under reduced pressure.

White solid (86 mg, yield = 69 %)

^{1}H NMR (500 MHz, $CDCl_3$) δ (ppm) =8.72 (br, 3H), 7.74 (br, 3H) 7.32 (br, 6H), 7.27 (br, 15H), 7.05 (br, 3H)

^{11}B NMR (160 MHz, $CDCl_3$) δ (ppm) = 17.2 (br)

^{13}C NMR (126 MHz, $CDCl_3$) δ (ppm) = 165.2, 147.7, 138.6, 132.4, 131.8, 129.3, 128.3, 127.3, 126.6, 122.3. The carbon atoms directly attached to the boron atom on the boroxine core were not detected, likely due to quadrupolar relaxation.

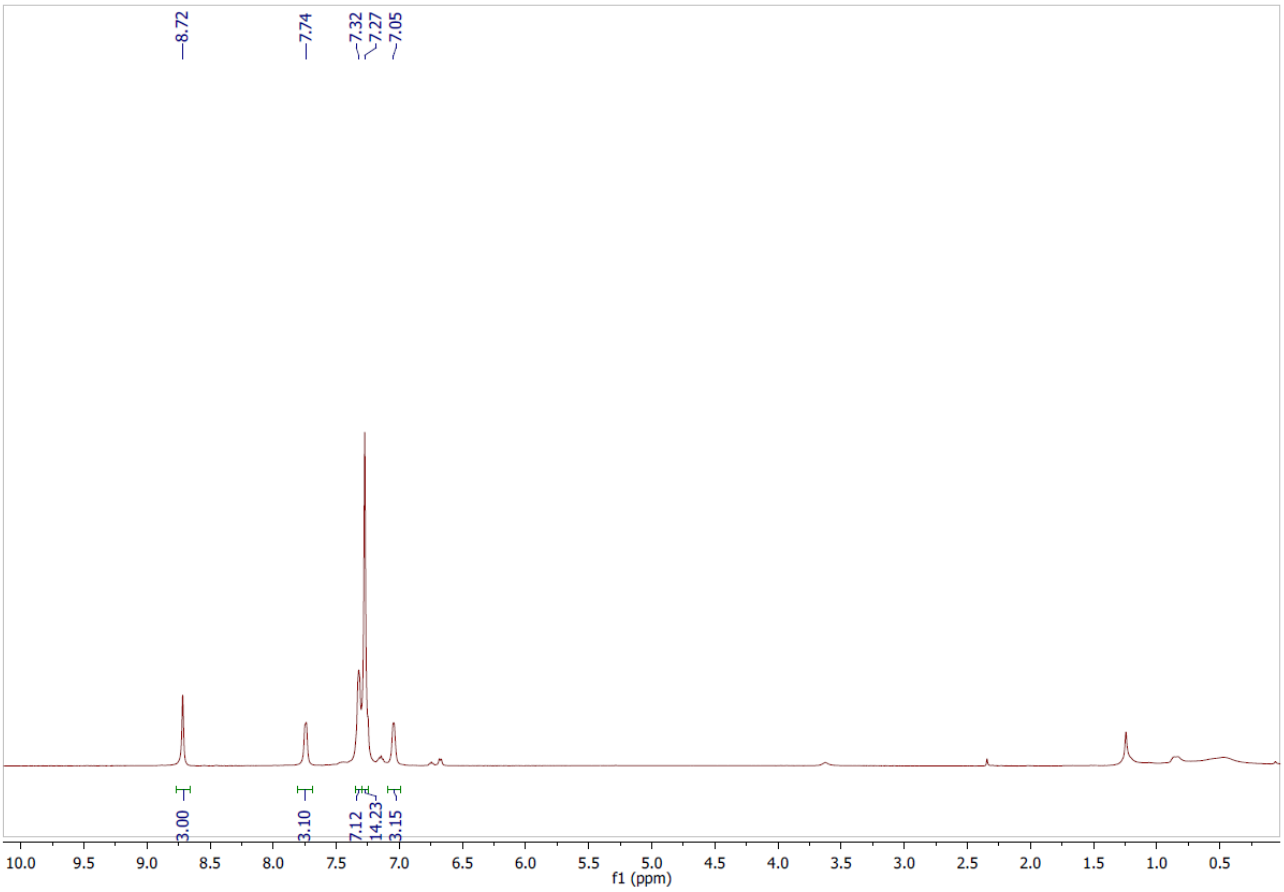
8.72
7.74
7.32
7.27
7.05
3.00
3.10
7.12
14.23
3.15
10.0 9.5 9.0 8.5 8.0 7.5 7.0 6.5 6.0 5.5 5.0 4.5 4.0 3.5 3.0 2.5 2.0 1.5 1.0 0.5
f1 (ppm)

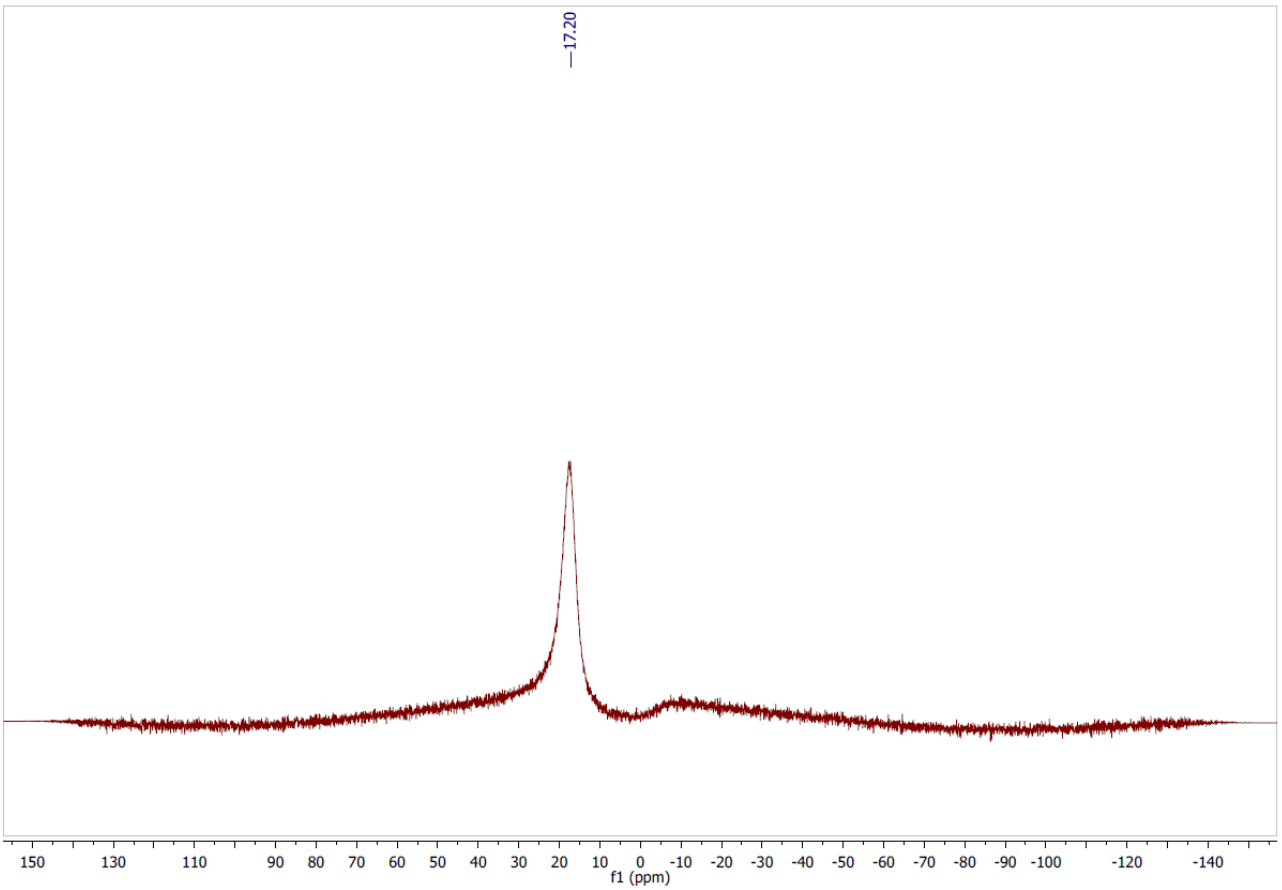
17.20
150 130 110 90 80 70 60 50 40 30 20 10 0 -10 -20 -30 -40 -50 -60 -70 -80 -90 -100 -120 -140
f1 (ppm)

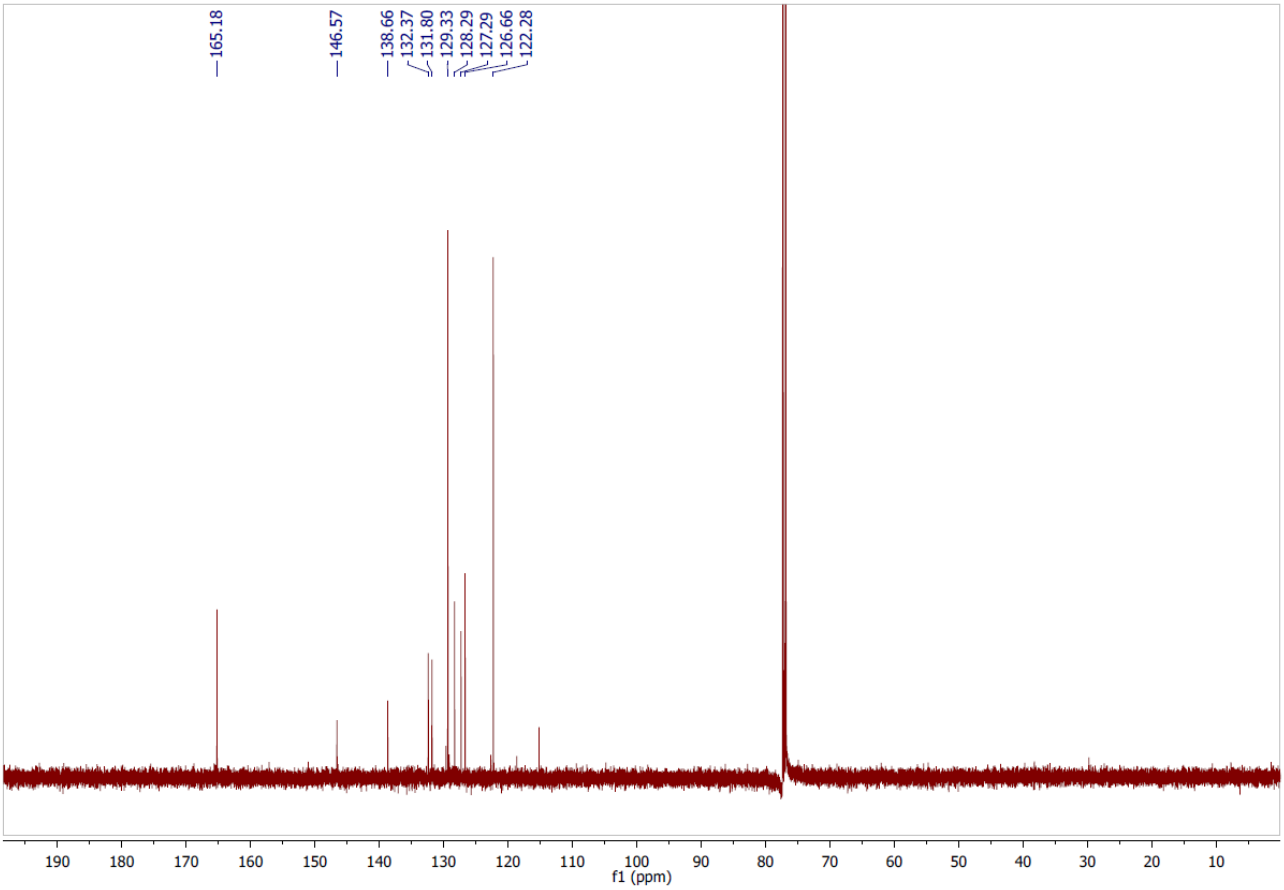

tris[2-[(tert-butylimino)methyl]phenyl]-boroxine **34**:

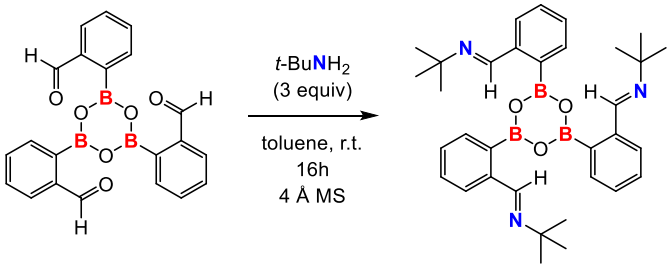

21 **34** (60 %)

tert-Butylamine (0.05 mL, 0.55 mmol, 3 equiv) was added to tris[2-formylphenyl]-boroxine **21** (0.073 g, 0,18 mmol, 1 equiv) in dry toluene on molecular sieves under argon atmosphere and stirred 16h at room temperature. The solution was then filtered through syringe filter (0.2 µm) under argon and the solvent evaporated under reduced pressure.

White solid (60 mg, yield = 60 %)

^{1}H NMR (500 MHz, $CDCl_3$) δ (ppm) =8.84 (s, 3H), 7.89 (d, *J* = 6.9 Hz, 3H) 7.83-7.63 (m, 3H), 6.16-6.11 (m, 6H), 1.26 (s, 27H).

^{11}B NMR (160 MHz, $CDCl_3$) δ (ppm) = 20.6 (br)

^{13}C NMR (126 MHz, $CDCl_3$) δ (ppm) = 161.6, 140.8, 133.2, 130.6, 129.4, 126.2, 58.2. 29.9. The carbon atoms directly attached to the boron atom on the boroxine core were not detected, likely due to quadrupolar relaxation.

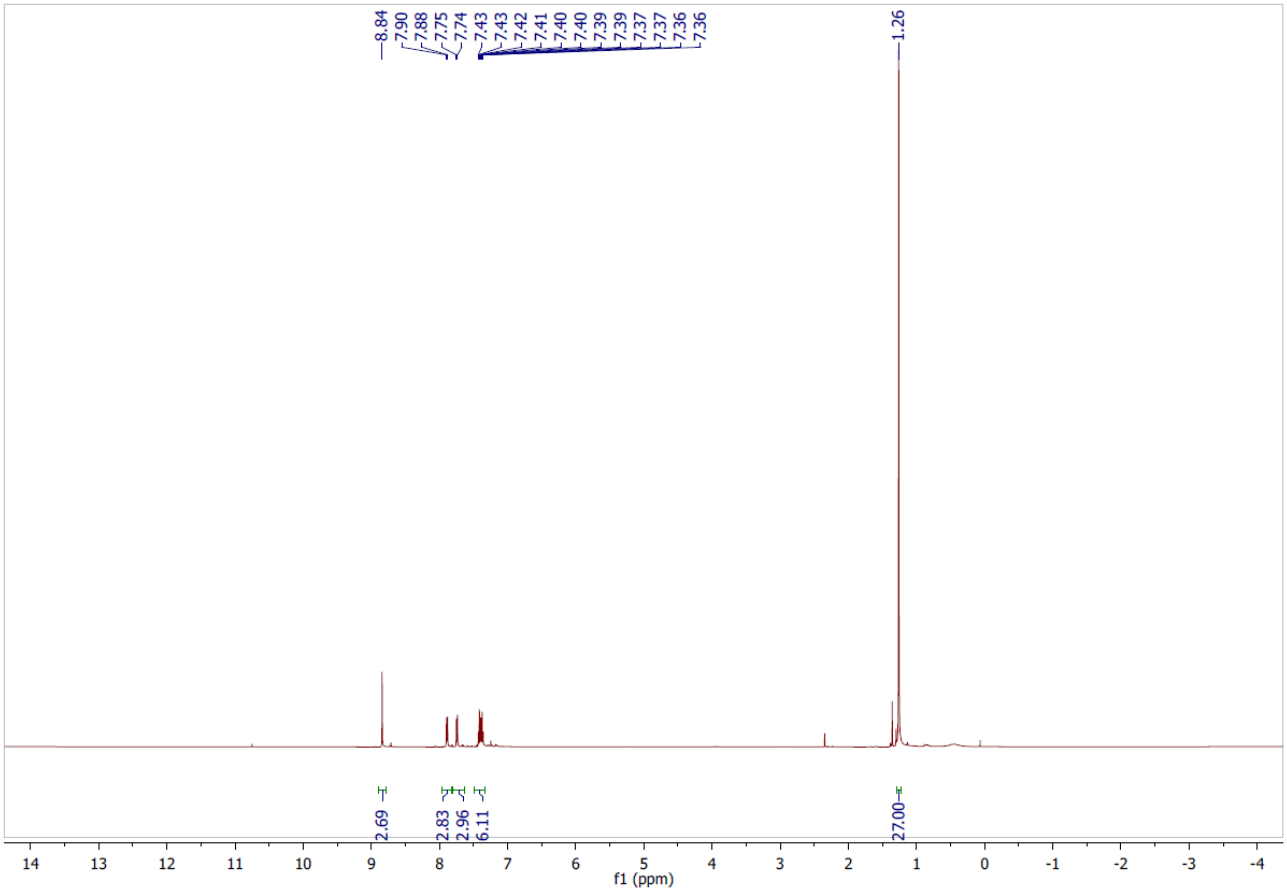

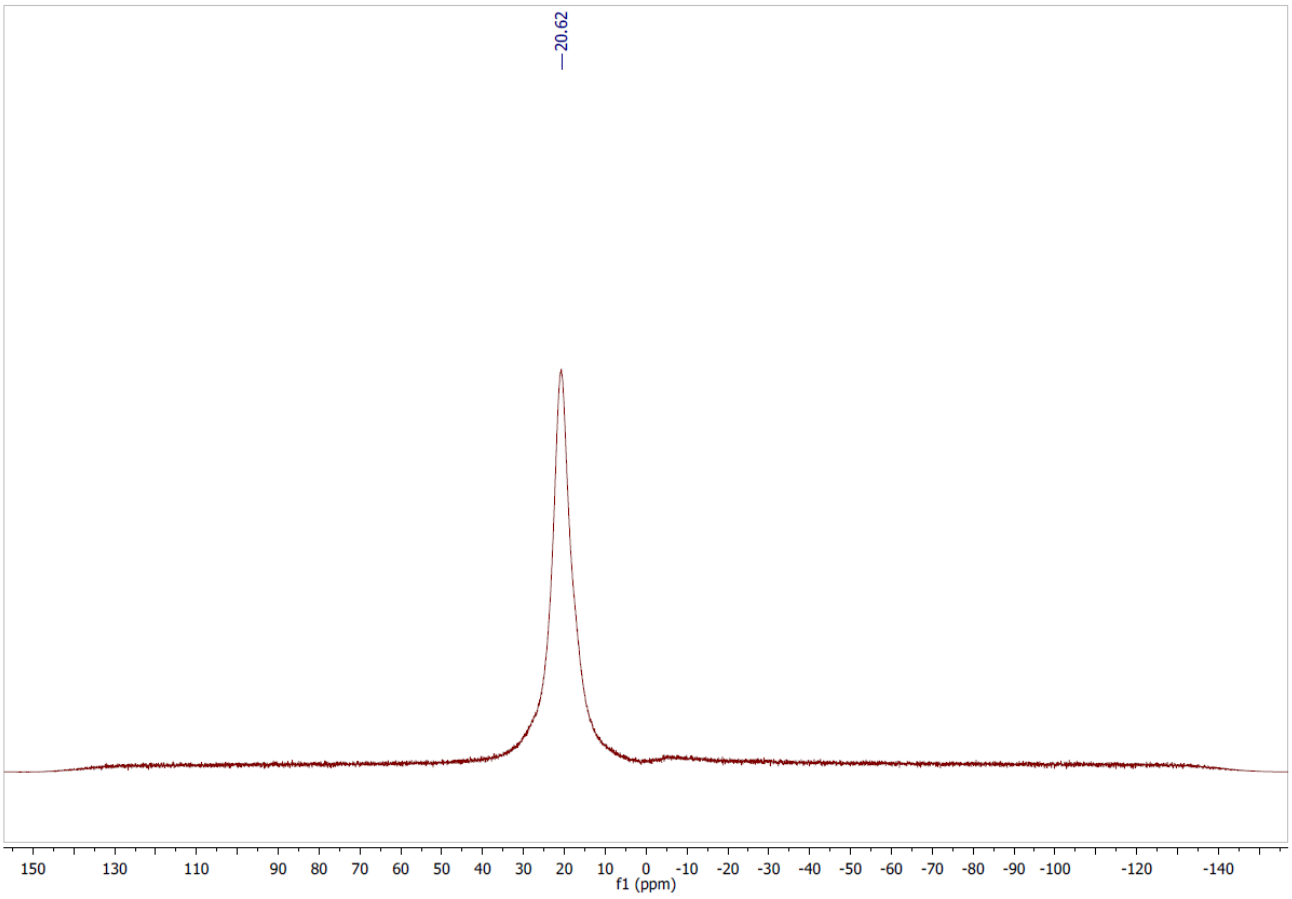
20.62
150 130 110 90 80 70 60 50 40 30 20 10 0 -10 -20 -30 -40 -50 -60 -70 -80 -90 -100 -120 -140
f1 (ppm)

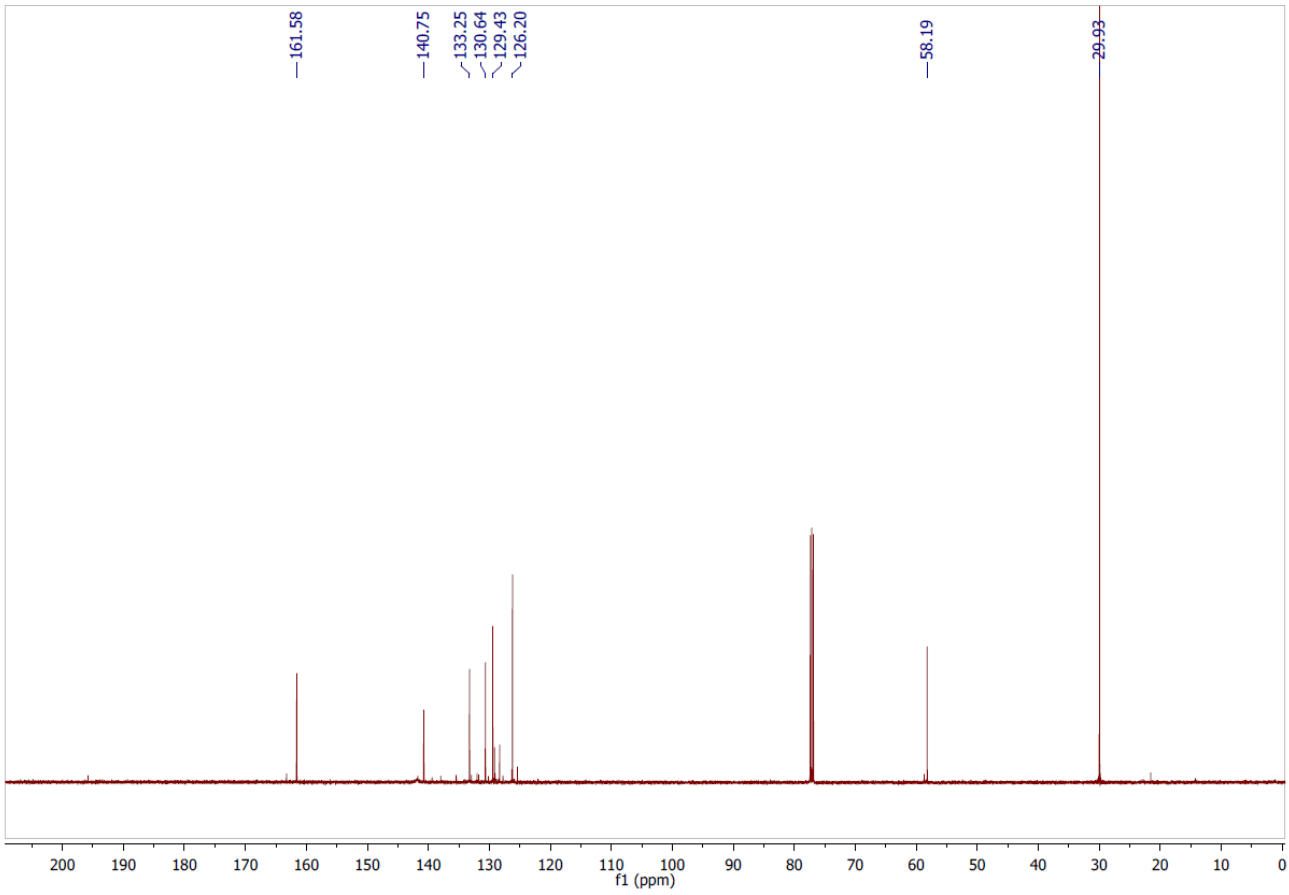
161.58
140.75
133.25
130.64
129.43
126.20
58.19
29.93
200 190 180 170 160 150 140 130 120 110 100 90 80 70 60 50 40 30 20 10 0
f1 (ppm)

tris[3-fluoro-2-[(n-butylimino)methyl]phenyl]-boroxine **35**:

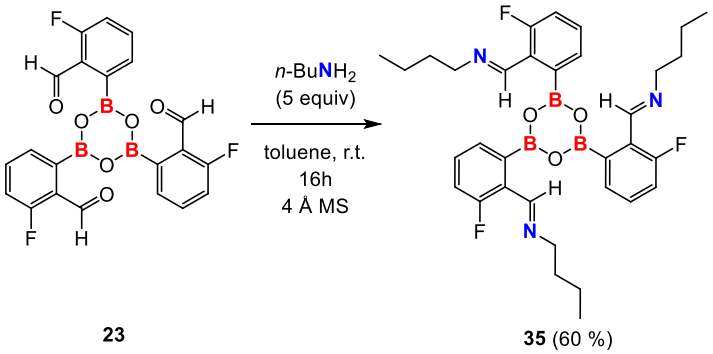

23 **35** (60 %)

n-Butylamine (0.1 mL, 1.0 mmol, 5 equiv) was added to tris[3-fluoro-2-formylphenyl]-boroxine **23** (0.0905 g, 0.20 mmol, 1 equiv) in dry toluene on molecular sieves under argon atmosphere and stirred 16h at room temperature. The solution was then filtered through syringe filter (0.2 µm) under argon and the solvent evaporated under reduced pressure.

White solid (73 mg, yield = 60 %).

^{1}H NMR (500 MHz, $CDCl_3$) δ (ppm) =8.46 (s, 3H), 7.40 (td, *J* = 7.7, 5.8 Hz, 6H), 7.00-6.77 (m, 3H), 3.77 (t, *J* = 7.5 Hz, 6H), 1.79 (t, *J* = 7.5 Hz, 6H), 1.42 (dd, *J* = 15.0, 7.5 Hz, 6H), 0.93 (t, *J* =7.4 Hz, 9H).

^{11}B NMR (160 MHz, $CDCl_3$) δ (ppm) = 13.9 (br)

^{13}C NMR (126 MHz, $CDCl_3$) δ (ppm) = 161.3, 159.2, 153.3, 133.7 (d, *J* = 7.0 Hz), 126.5 (d, J = 2.8 Hz), 125.2 (d, *J* = 8.6 Hz), 114.4 (d, *J* = 20.2 Hz), 52.3, 31.5, 20.5, 13.9

^{19}F NMR (476 MHz, $CDCl_3$) δ (ppm) = -121.6 (br)

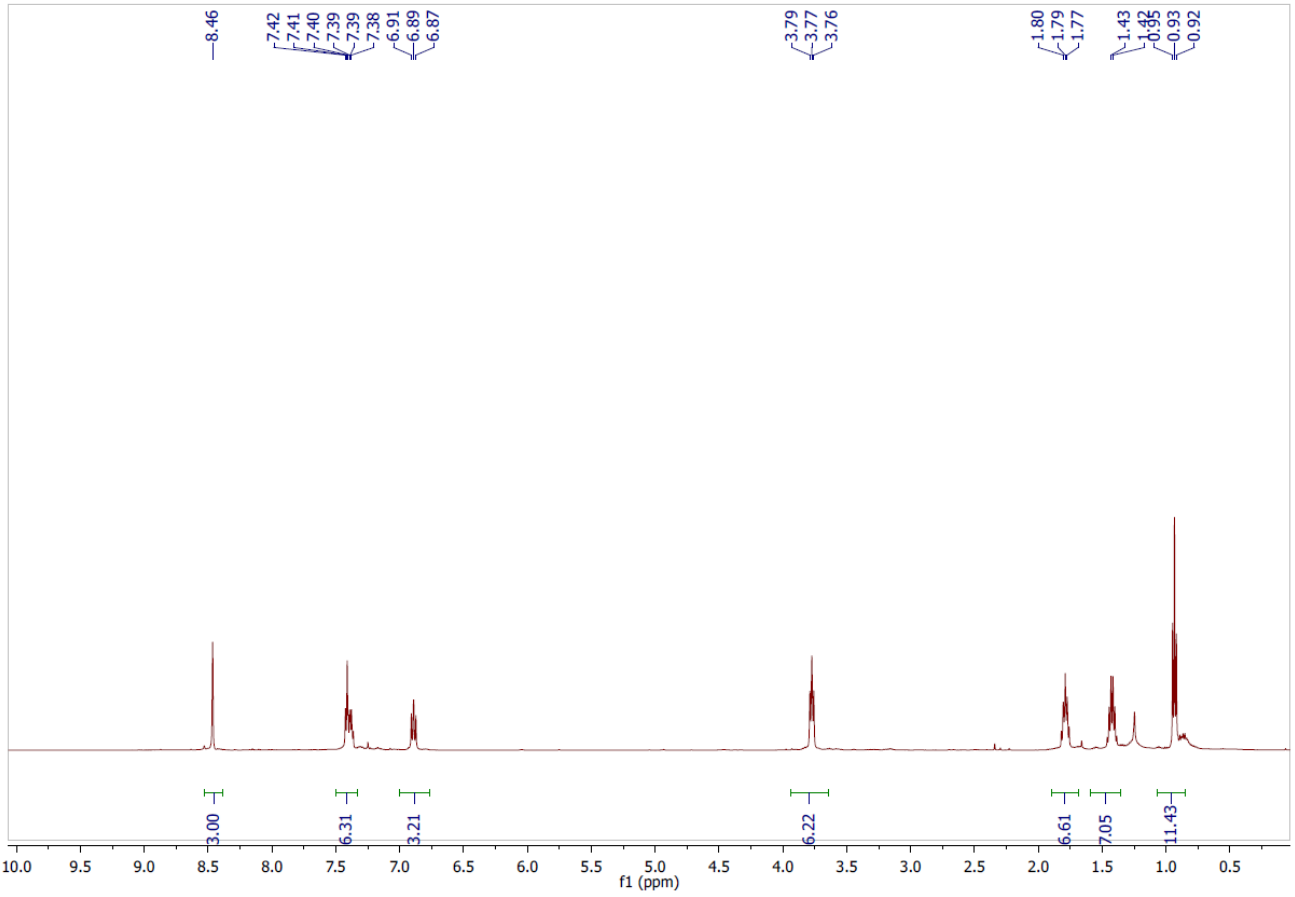
8.46
7.42
7.41
7.40
7.39
7.39
7.38
6.91
6.89
6.87
3.79
3.77
3.76
1.80
1.79
1.77
1.43
0.95
0.93
0.92
3.00
6.31
3.21
6.22
6.61
7.05
11.43
f1 (ppm)

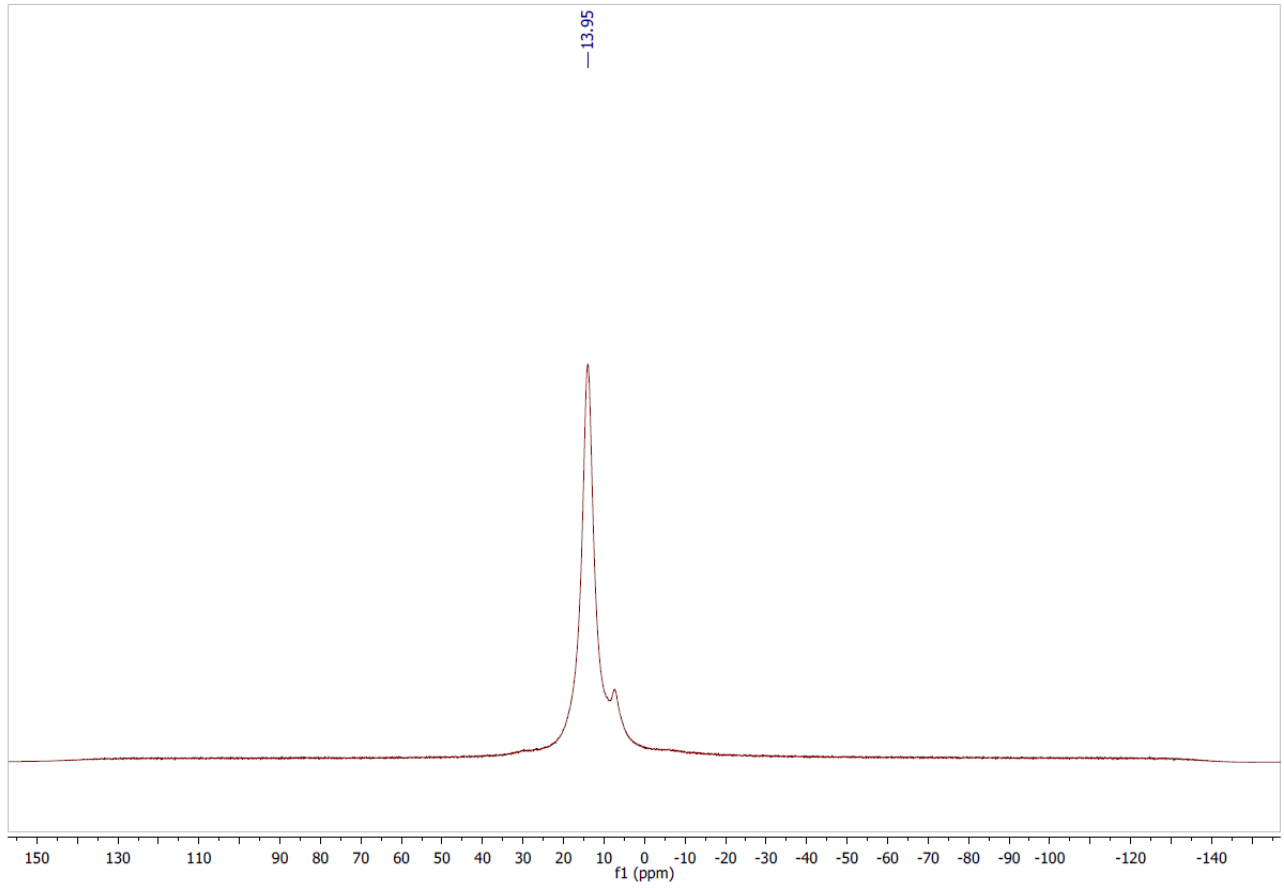
13.95
f1 (ppm)

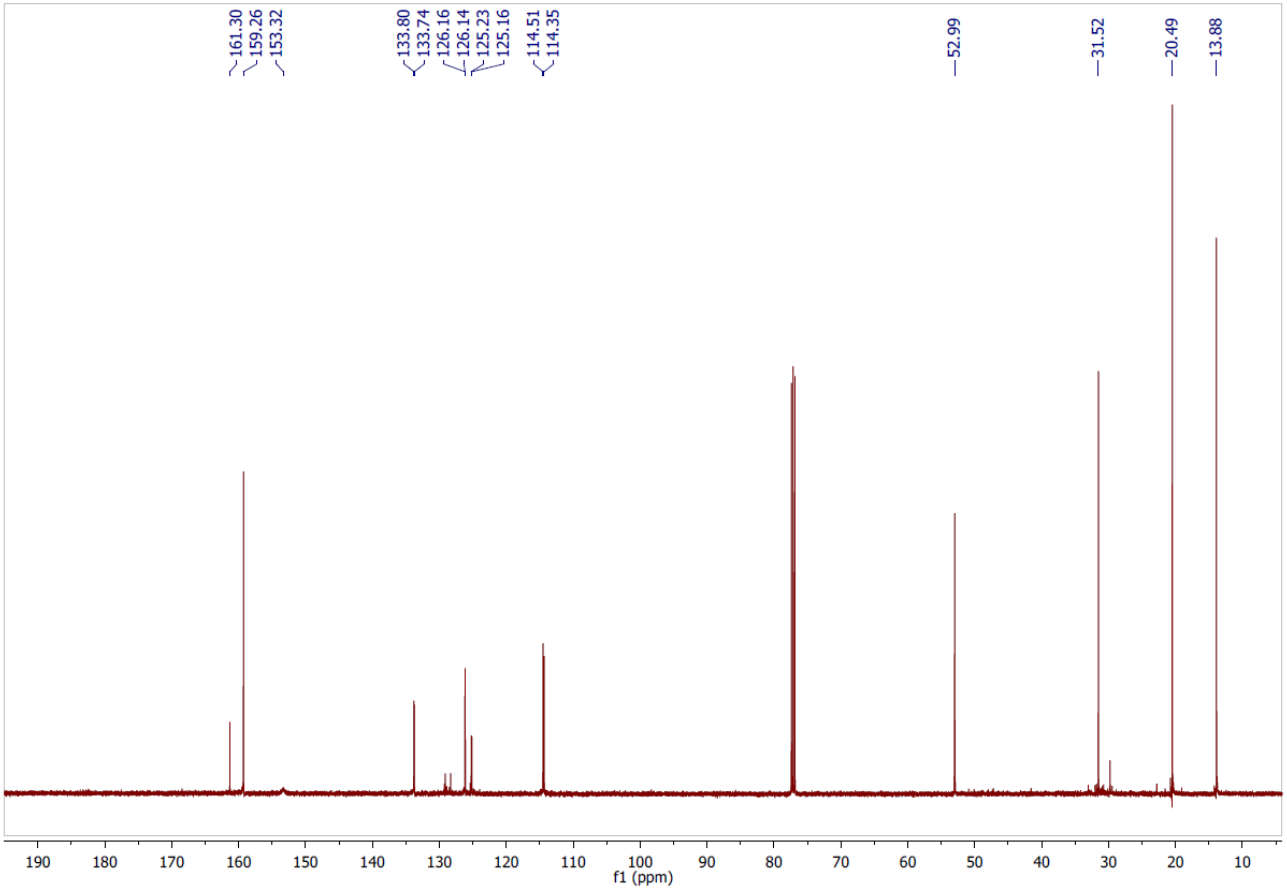
161.30
159.26
153.32
133.80
133.74
126.16
126.14
125.23
125.16
114.51
114.35
52.99
31.52
20.49
13.88
190 180 170 160 150 140 130 120 110 100 90 80 70 60 50 40 30 20 10
f1 (ppm)

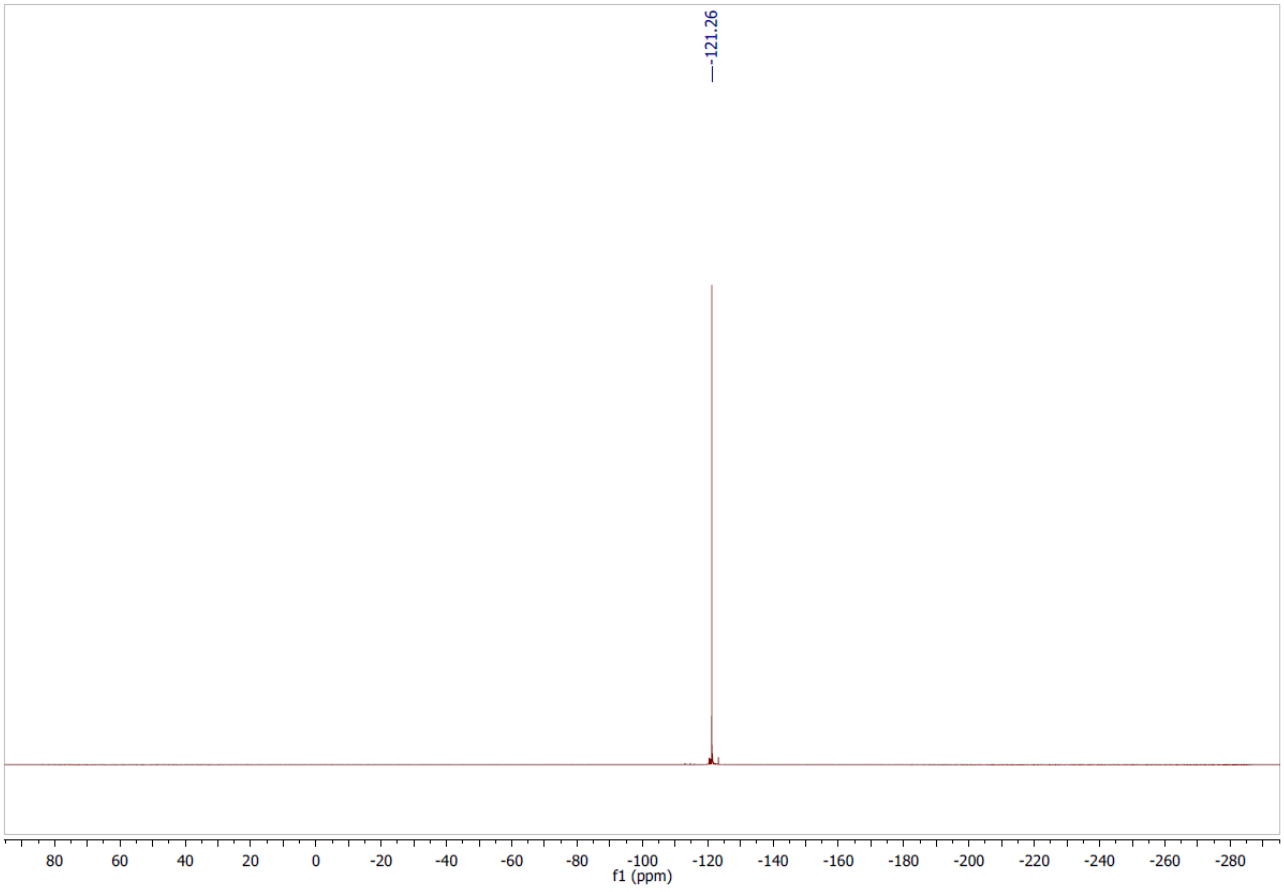
-121.26
80 60 40 20 0 -20 -40 -60 -80 -100 -120 -140 -160 -180 -200 -220 -240 -260 -280
f1 (ppm)

tris[3-fluoro-2-[(phenylimino)methyl]phenyl]-boroxine **36**:

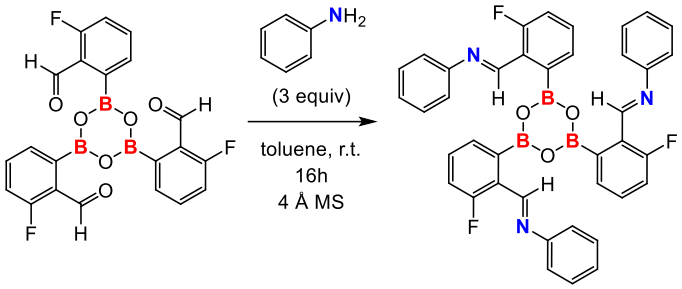

23 **36** (63 %)

Aniline (0.05 mL, 0.55 mmol, 3 equiv) was added to tris[3-fluoro-2-formylphenyl]-boroxine **23** (0.0820 g, 0.18 mmol, 1 equiv) in dry toluene on molecular sieves under argon atmosphere and stirred 16h at room temperature. The solution was then filtered through syringe filter (0.2 µm) under argon and the solvent evaporated under reduced pressure.

White solid (76 mg, yield = 63 %).

^{1}H NMR (500 MHz, $CDCl_3$) δ (ppm) =8.63 (s, 3H), 7.45-7.24 (m, 18H), 6.92 (t, *J* = 9.1 Hz, 3H), 6.73-6.59 (m, 3H).

^{11}B NMR (160 MHz, $CDCl_3$) δ (ppm) = 16.3 (br)

^{13}C NMR (126 MHz, $CDCl_3$) δ (ppm) = 160.2 (d, *J* =252 Hz), 159.9, 146.3, 134.6 (d, *J* = 7.2 Hz), 129.3, 127.6, 126.9 (d, *J* = 2.9 Hz), 122.3, 115.1, 114.2 (d, *J* = 20.0 Hz) .The carbon atoms directly attached to the boron atom on the boroxine core were not detected, likely due to quadrupolar relaxation.

^{19}F NMR (476 MHz, $CDCl_3$) δ (ppm) = -119.9 (br)

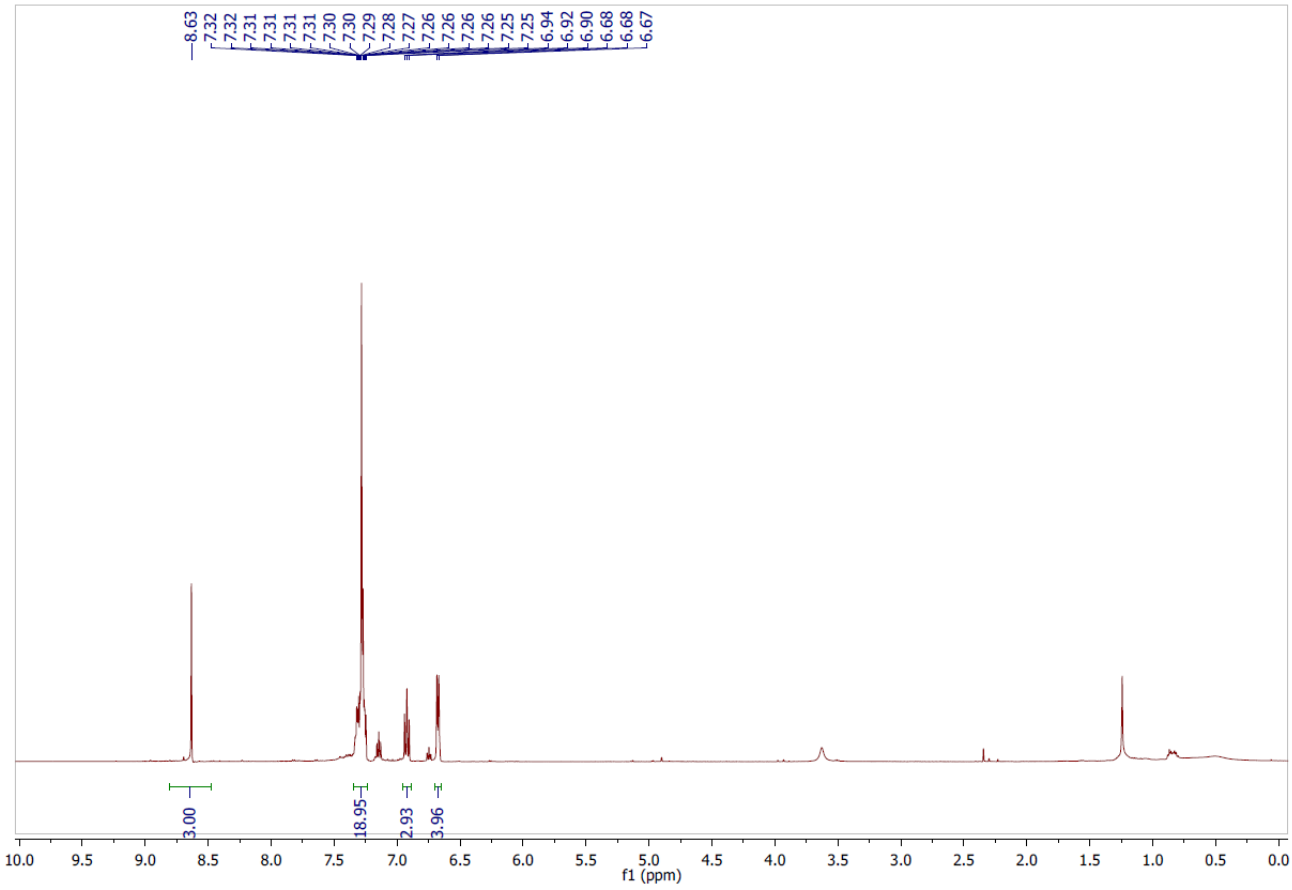
8.63
7.32
7.32
7.31
7.31
7.31
7.30
7.30
7.29
7.28
7.27
7.26
7.26
7.26
7.25
7.25
6.94
6.92
6.90
6.68
6.68
6.67
3.00
18.95
2.93
3.96
10.0 9.5 9.0 8.5 8.0 7.5 7.0 6.5 6.0 5.5 5.0 4.5 4.0 3.5 3.0 2.5 2.0 1.5 1.0 0.5 0.0
f1 (ppm)

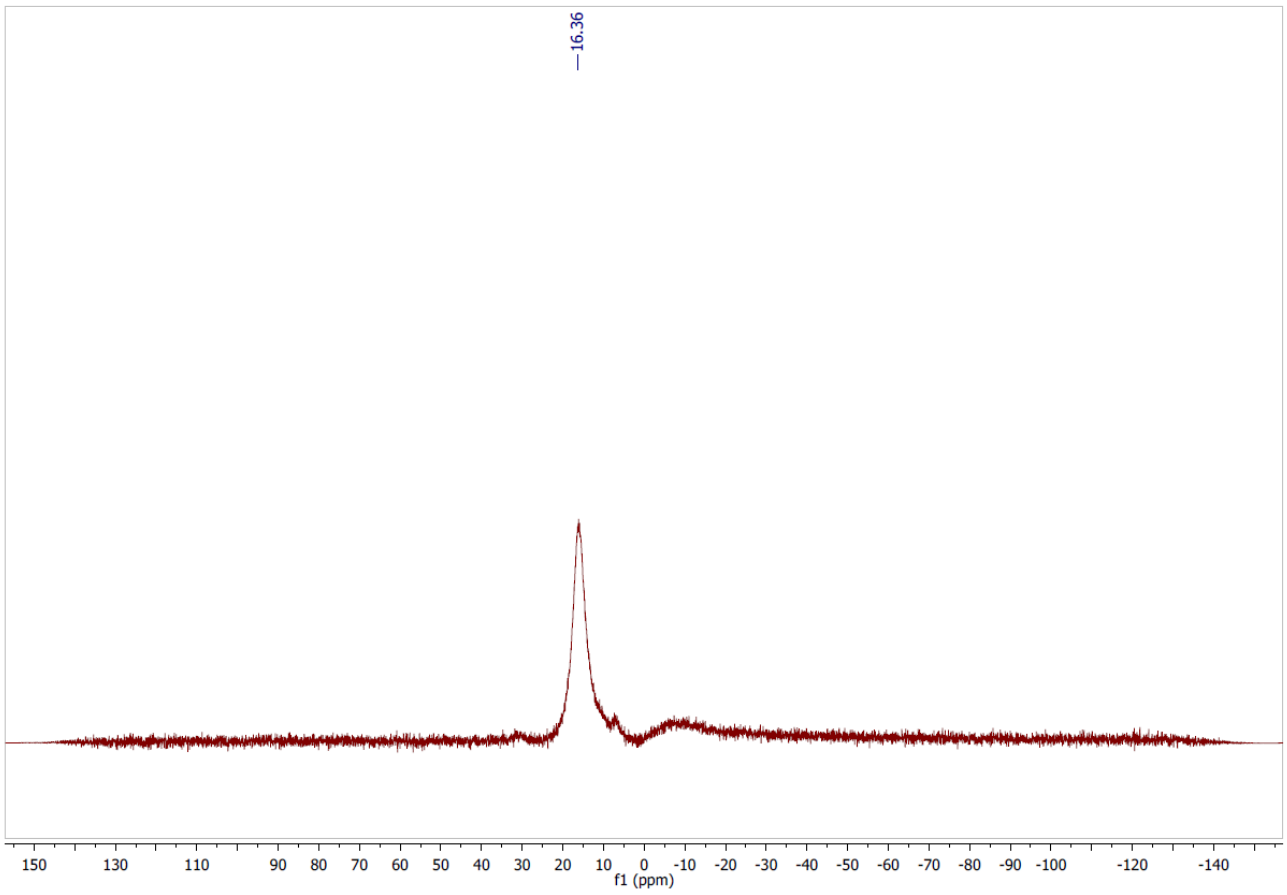
16.36
150 130 110 90 80 70 60 50 40 30 20 10 0 -10 -20 -30 -40 -50 -60 -70 -80 -90 -100 -120 -140
f1 (ppm)

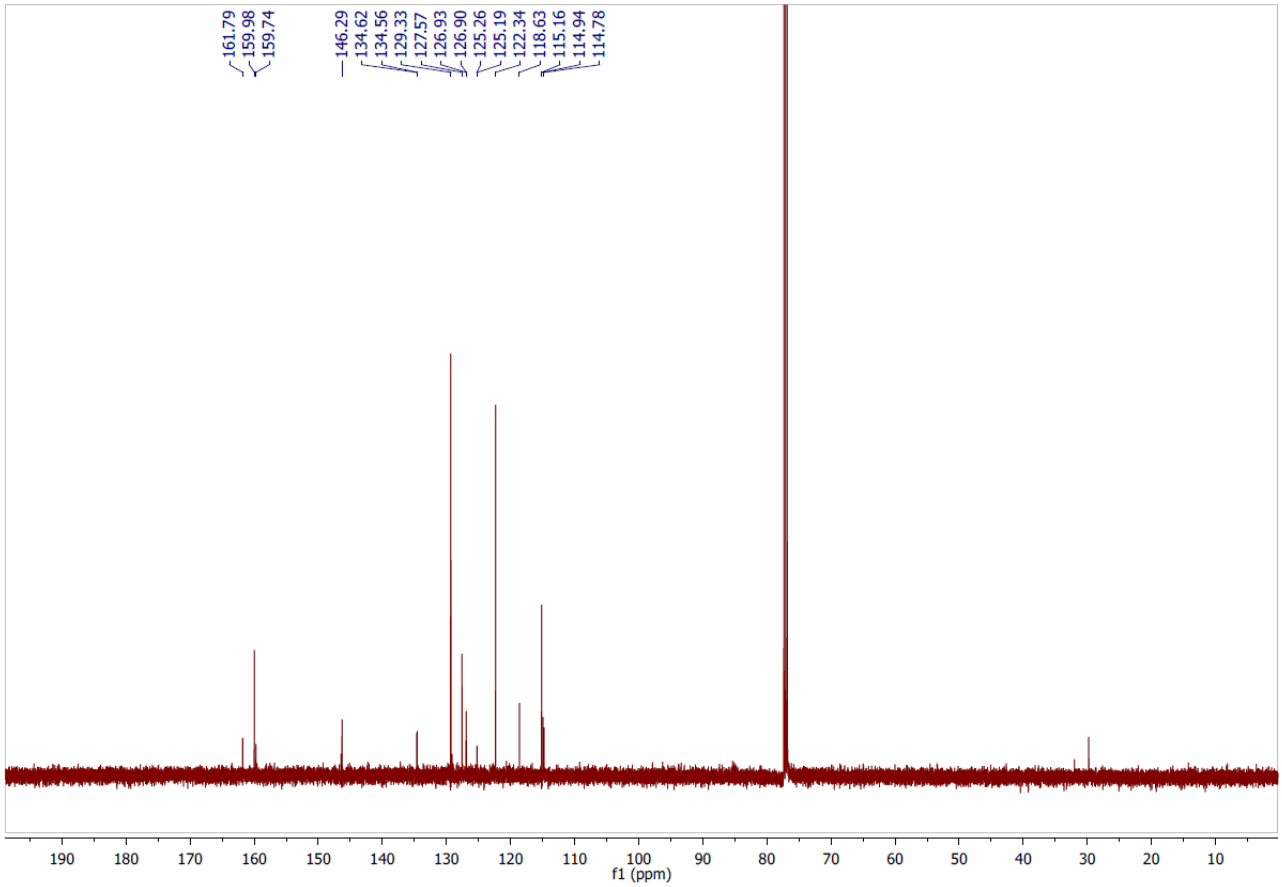
161.79
159.98
159.74
146.29
134.62
134.56
129.33
127.57
126.93
126.90
125.26
125.19
122.34
118.63
115.16
114.94
114.78
190 180 170 160 150 140 130 120 110 100 90 80 70 60 50 40 30 20 10
f1 (ppm)

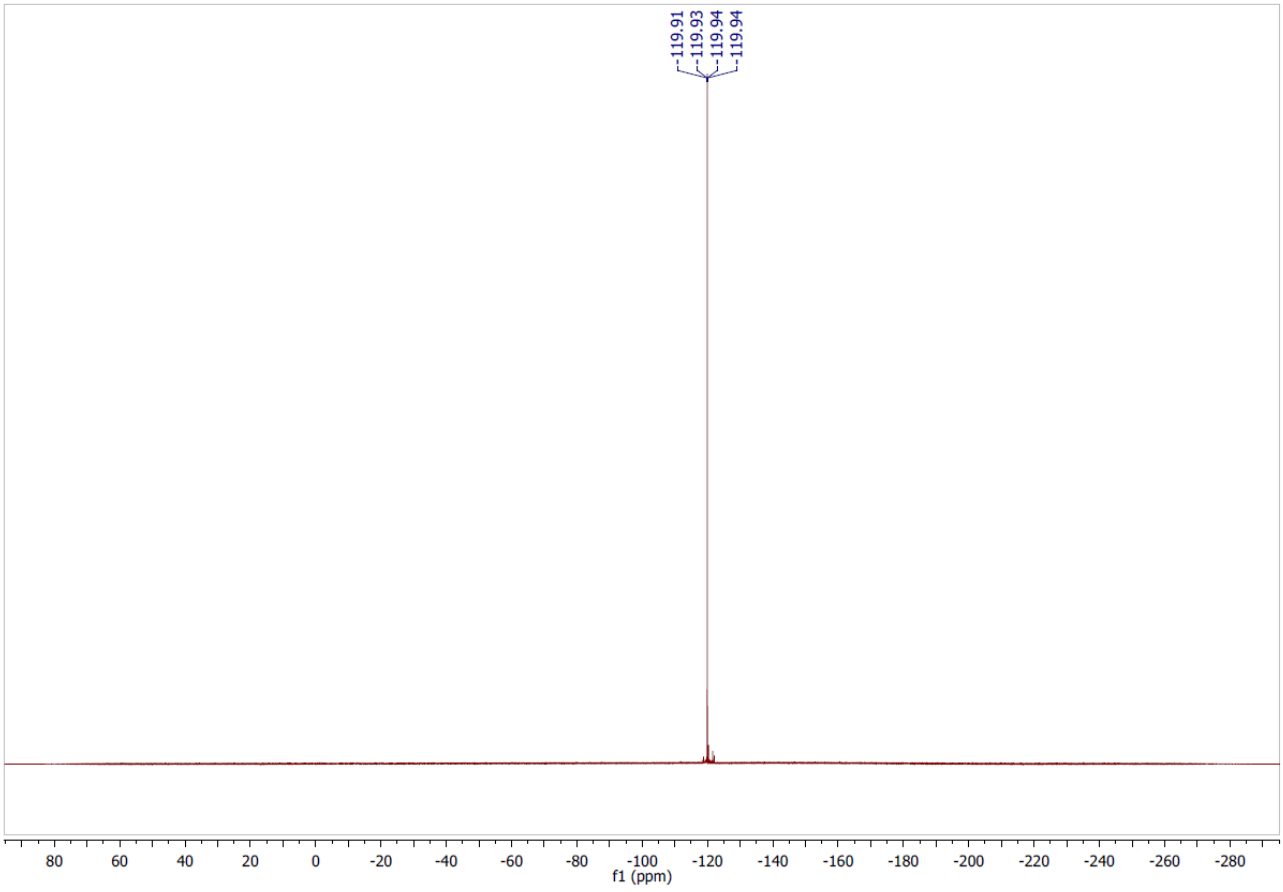
-119.91
-119.93
-119.94
-119.94
80 60 40 20 0 -20 -40 -60 -80 -100 -120 -140 -160 -180 -200 -220 -240 -260 -280
f1 (ppm)

tris[3-fluoro-2-[(tert-butylimino)methyl]phenyl]-boroxine **37**:

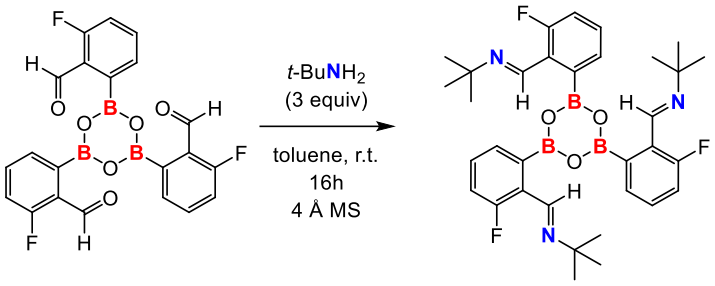

23 **37** (64 %)

tert-Butylamine (0.07 mL, 0.67 mmol, 3 equiv) was added to tris[3-fluoro-2-formylphenyl]-boroxine **23** (0.090 g, 0.20 mmol, 1 equiv) in dry toluene on molecular sieves under argon atmosphere and stirred 16h at room temperature. The solution was then filtered through syringe filter (0.2 µm) under argon and the solvent evaporated under reduced pressure.

White solid (79 mg, yield = 64 %).

^{1}H NMR (500 MHz, $CDCl_3$) δ (ppm) =8.60 (s, 3H), 7.54 (d, *J* = 7.2 Hz, 3H) 7.49 (td, *J* = 7.2 Hz, 3H), 6.97 (t, *J* = 9.1 Hz, 3H), 1.35 (s, 27H).

^{11}B NMR (160 MHz, $CDCl_3$) δ (ppm) = 18.5 (br)

^{13}C NMR (126 MHz, $CDCl_3$) δ (ppm) = 160.1 (d, *J* = 254.9 Hz), 156.3, 132.7 (d, *J* = 7.2 Hz), 128.2 (d, *J* = 3.0 Hz), 126.9, 115.6 (d, *J* = 20.5 Hz), 58.9, 29.9 carbon atoms directly attached to the boron atom on the boroxine core were not detected, likely due to quadrupolar relaxation.

^{19}F NMR (476 MHz, $CDCl_3$) δ (ppm) = -121.2 (br)

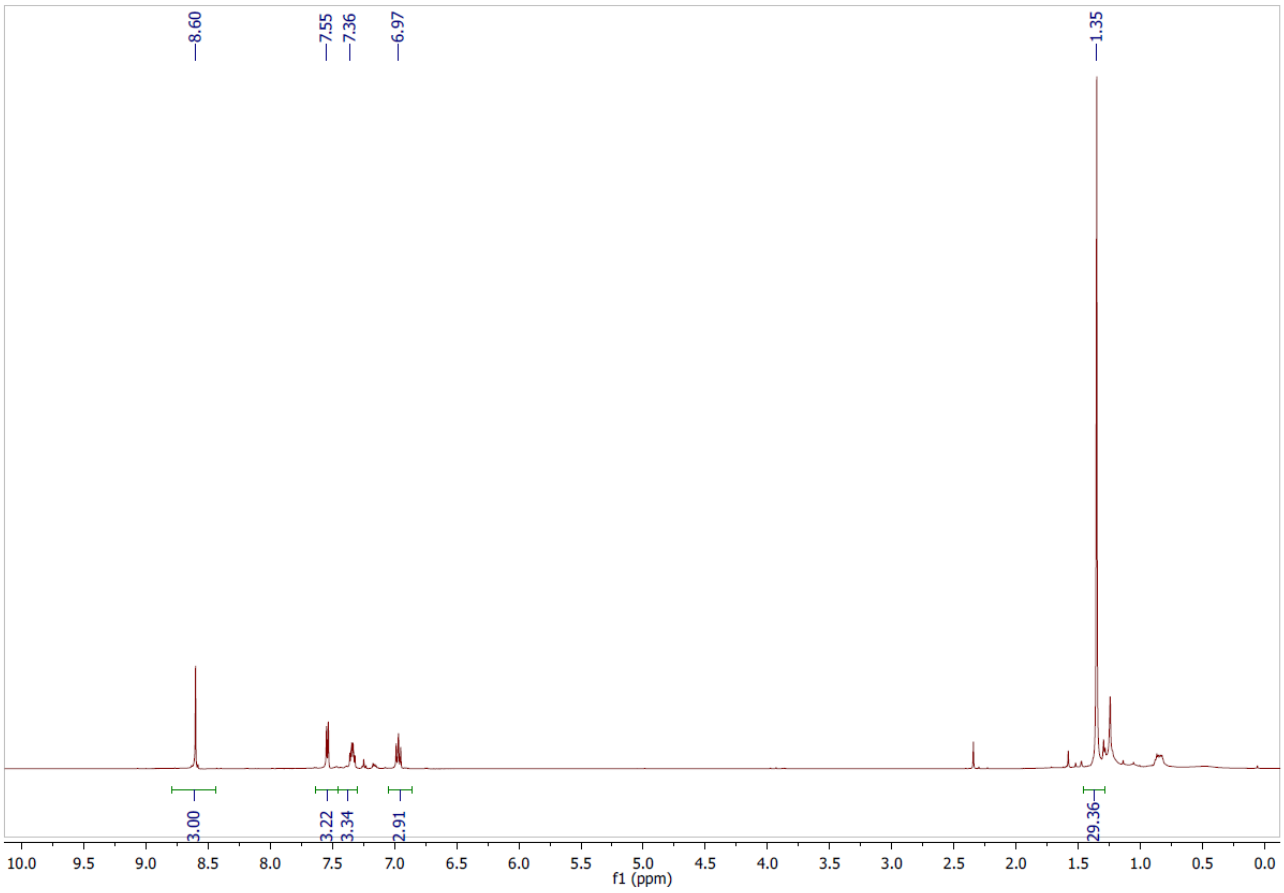
8.60
7.55
7.36
6.97
1.35
3.00
3.22
3.34
2.91
29.36
10.0
9.5
9.0
8.5
8.0
7.5
7.0
6.5
6.0
5.5
5.0
4.5
4.0
3.5
3.0
2.5
2.0
1.5
1.0
0.5
0.0
f1 (ppm)

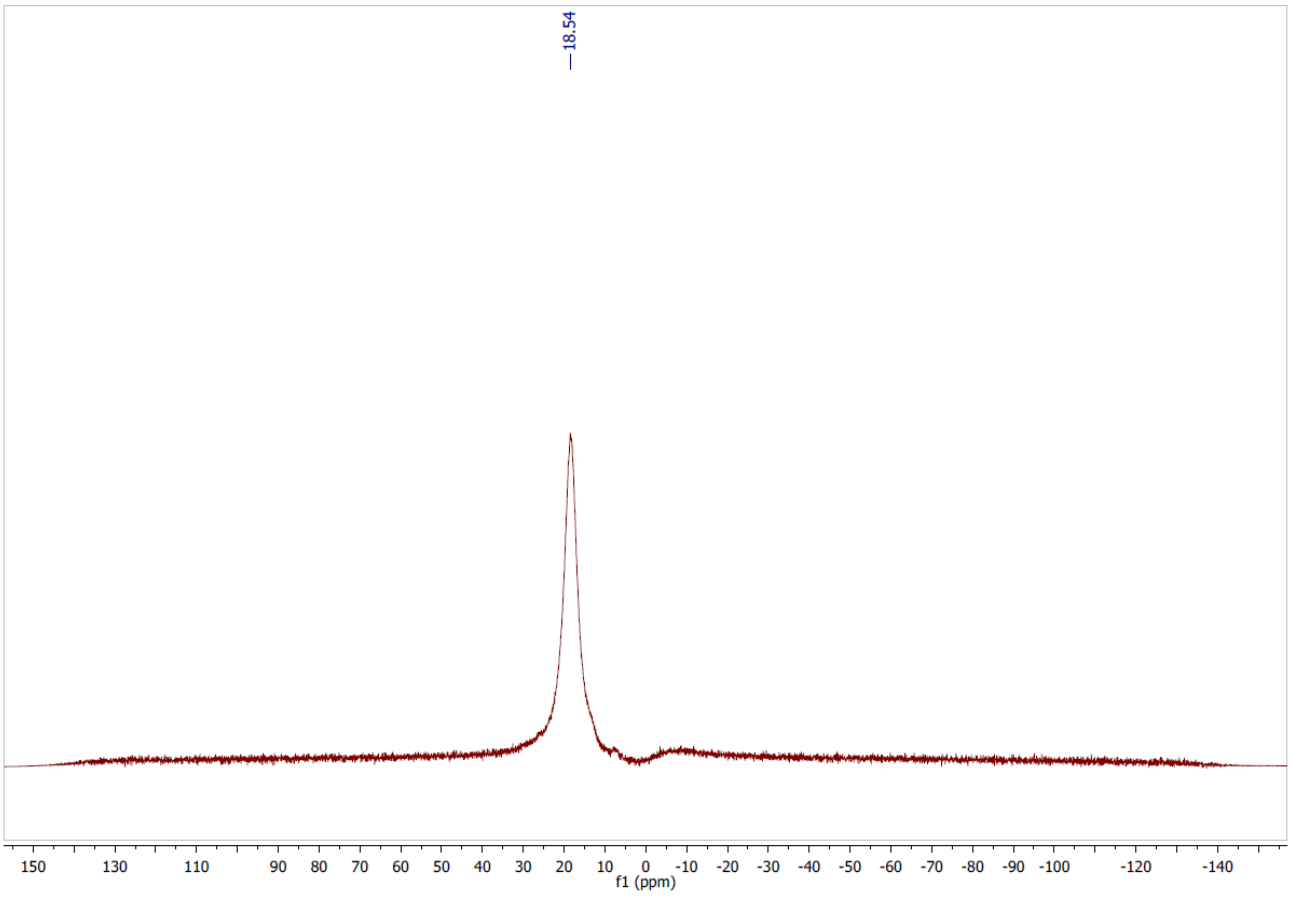
18.54
150 130 110 90 80 70 60 50 40 30 20 10 0 -10 -20 -30 -40 -50 -60 -70 -80 -90 -100 -120 -140
f1 (ppm)

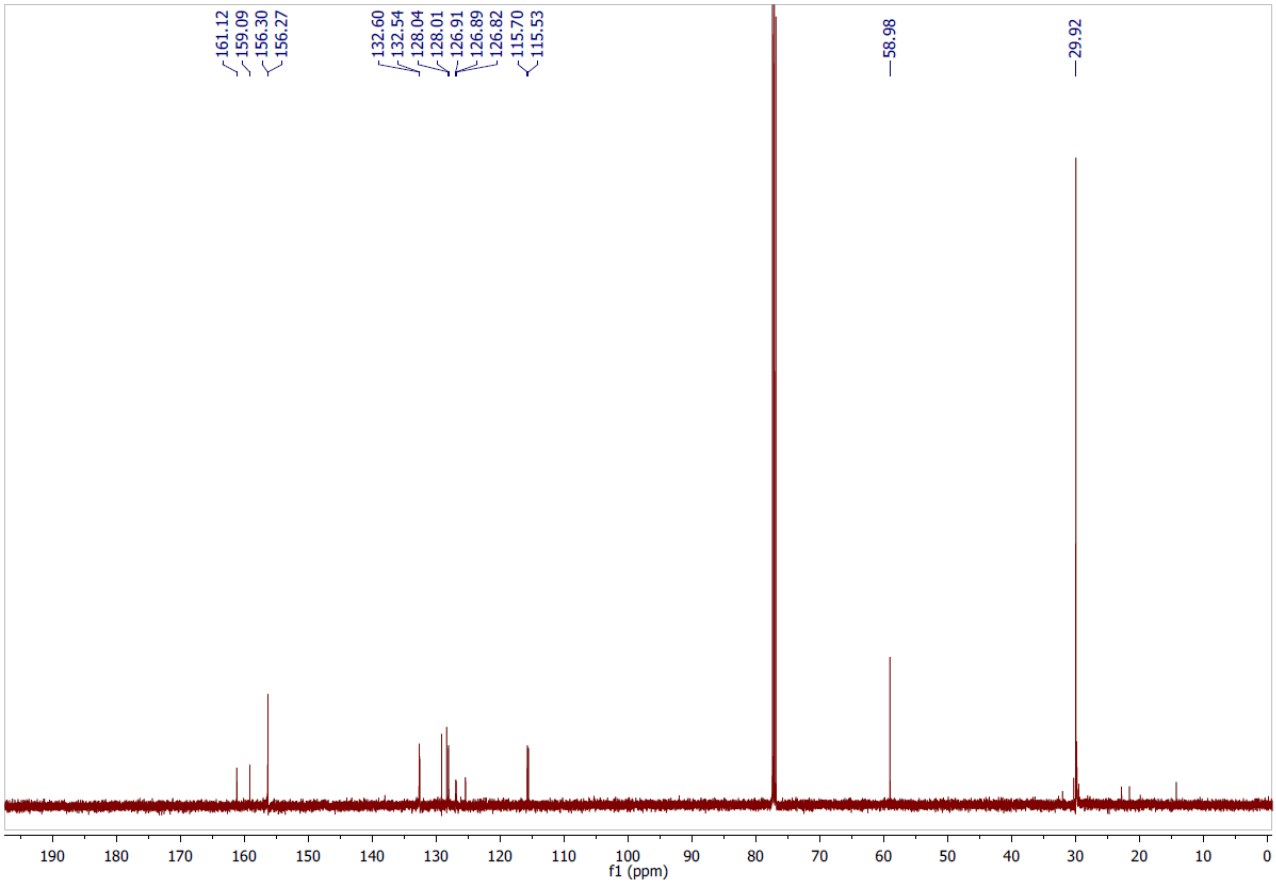
161.12
159.09
156.30
156.27
132.60
132.54
128.04
128.01
126.91
126.89
126.82
115.70
115.53
58.98
29.92
190 180 170 160 150 140 130 120 110 100 90 80 70 60 50 40 30 20 10 0
f1 (ppm)

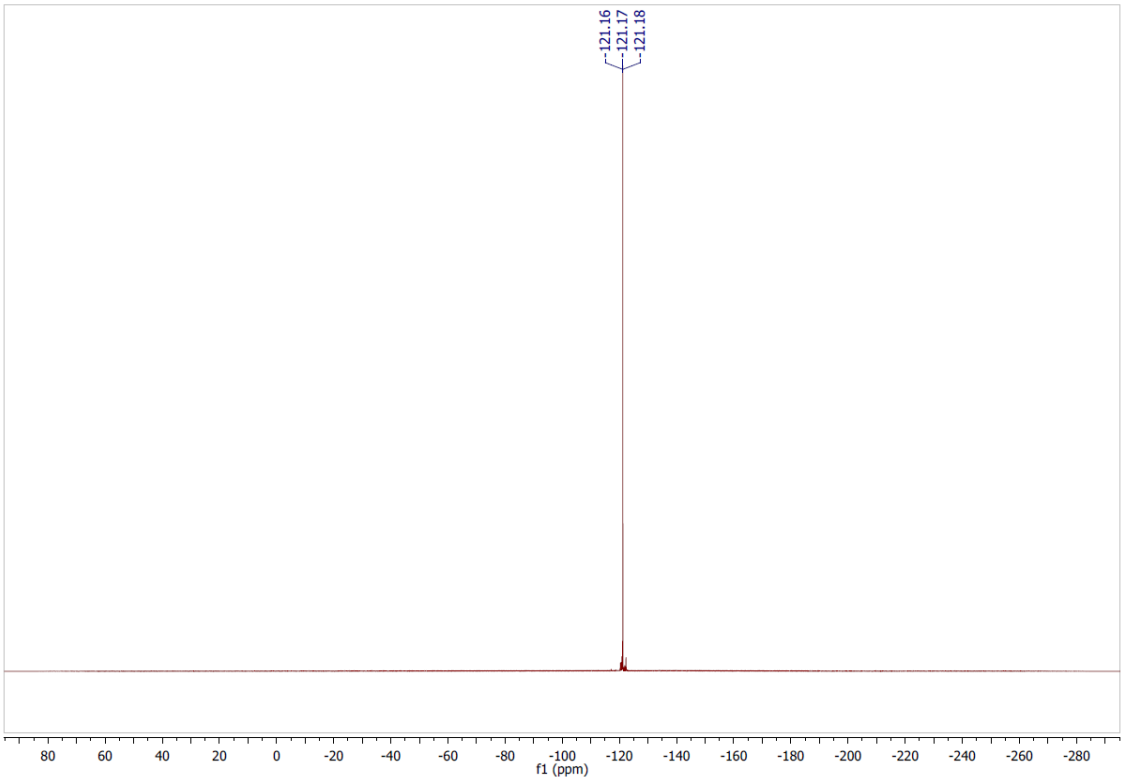

tris[5-fluoro-2-[(n -butylimino)methyl]phenyl]-boroxine **38**:

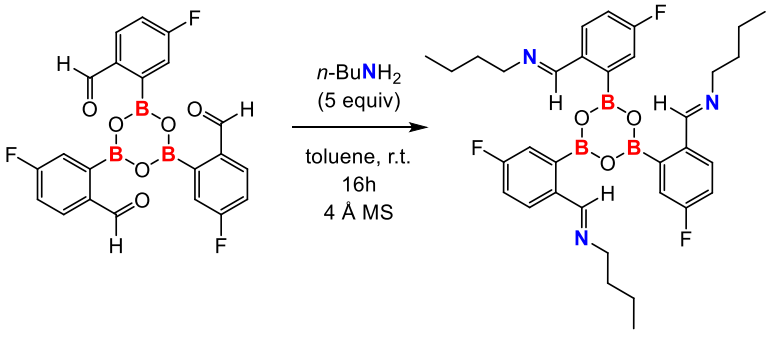

24 **38** (58 %)

*n*Butylamine (0.10 mL, 1.0 mmol, 5 equiv) was added to tris[5-fluoro-2-formylphenyl]-boroxine **24** (0.09 g, 0.20 mmol, 1 equiv) in dry toluene on molecular sieves under argon atmosphere and stirred 16h at room temperature. The solution was then filtered through syringe filter (0.2 µm) under argon and the solvent evaporated under reduced pressure.

White solid (71 mg, yield = 58 %).

^{1}H NMR (500 MHz, $CDCl_3$) δ (ppm) =8.4 (s, 3H), 7.58 (dd, *J* = 8.3, 5.0 Hz, 3H), 7.32 (d, *J* = 8.6, 2.5 Hz 3H), 7.39 (td, *J* = 8.6, 2.5 Hz, 3H), 3.67 (t, *J* = 7.4 Hz, 6H), 1.75 (dd, *J* = 8.7, 6.4 Hz, 6H), 1.38 (dd, 8.3, 5.0 Hz, 6H), 0.89 (t, *J* =7.4 Hz, 9H).)

^{11}B NMR (160 MHz, $CDCl_3$) δ (ppm) = 13.7 (br)

^{13}C NMR (126 MHz, $CDCl_3$) δ (ppm) = 165.8 (d, *J* = 253.8 Hz), 164.0, 135.6, 128.0 (d, *J* = 8.6 Hz), 117.3, 114.8 (d, *J* = 23.1 Hz), 52.9, 31.5, 20.3, 13.7.

^{19}F NMR (476 MHz, $CDCl_3$) δ (ppm) = -108.2 (br)

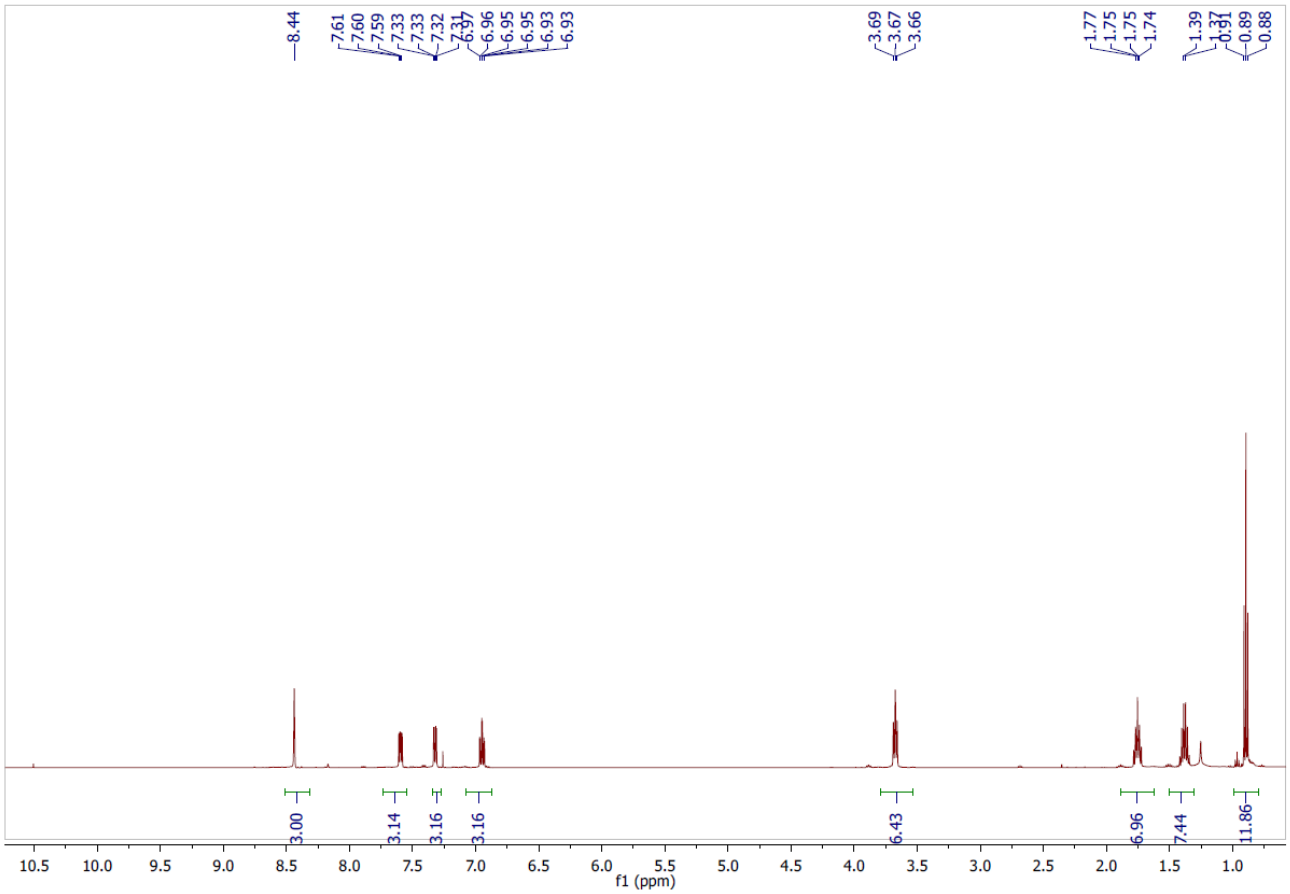

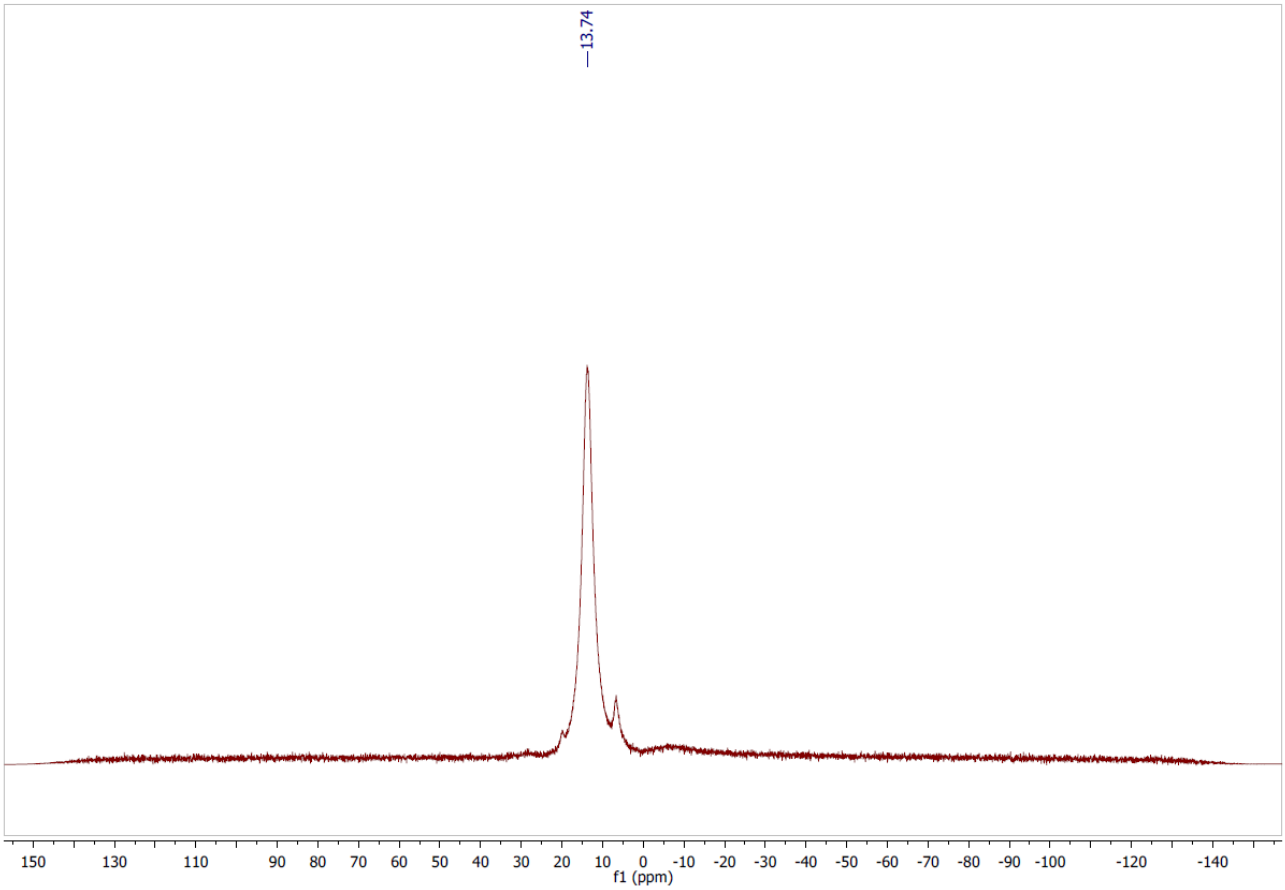
13.74
150 130 110 90 80 70 60 50 40 30 20 10 0 -10 -20 -30 -40 -50 -60 -70 -80 -90 -100 -120 -140
f1 (ppm)

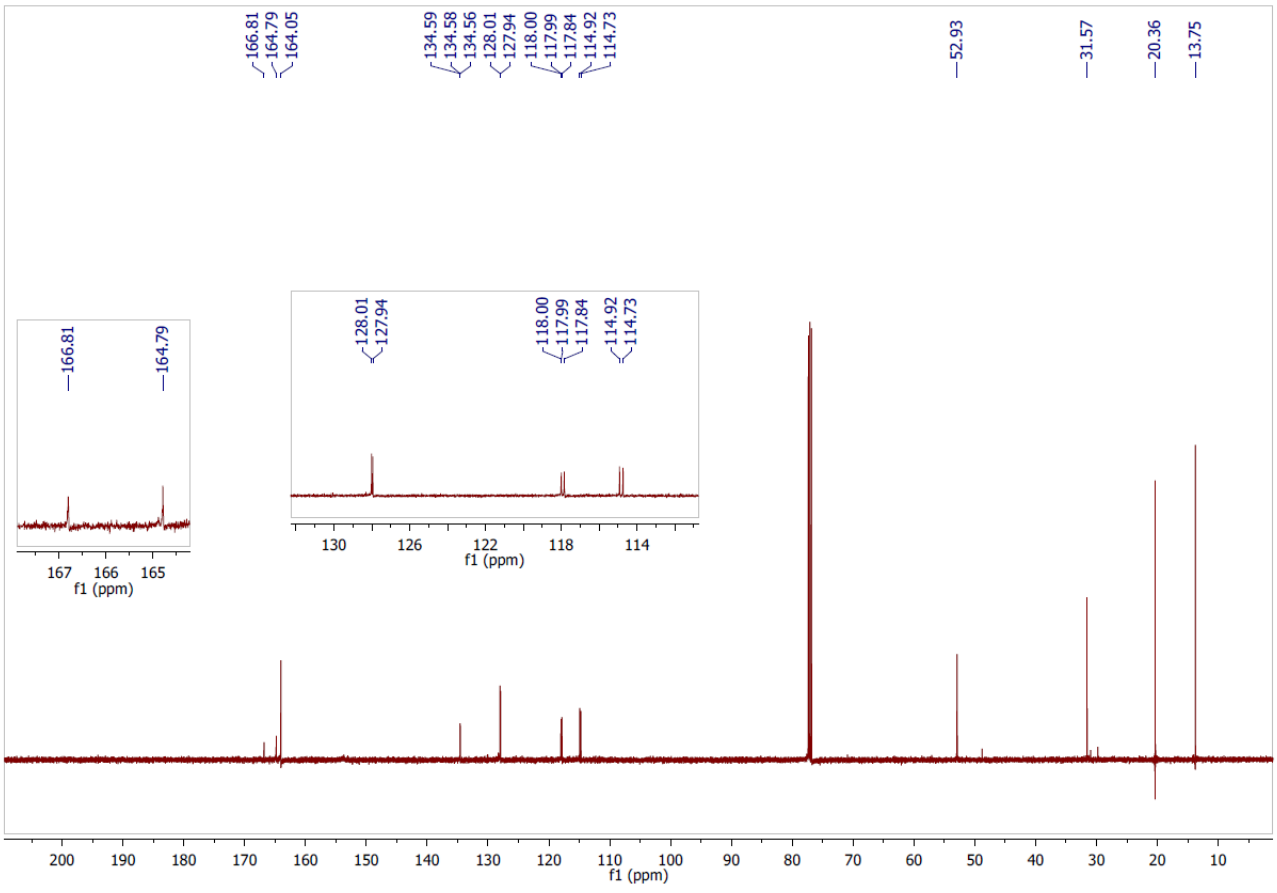
166.81
164.79
164.05
134.59
134.58
134.56
128.01
127.94
118.00
117.99
117.84
114.92
114.73
52.93
31.57
20.36
13.75
166.81
164.79
167 166 165
f1 (ppm)
128.01
127.94
118.00
117.99
117.84
114.92
114.73
130 126 122 118 114
f1 (ppm)
200 190 180 170 160 150 140 130 120 110 100 90 80 70 60 50 40 30 20 10
f1 (ppm)

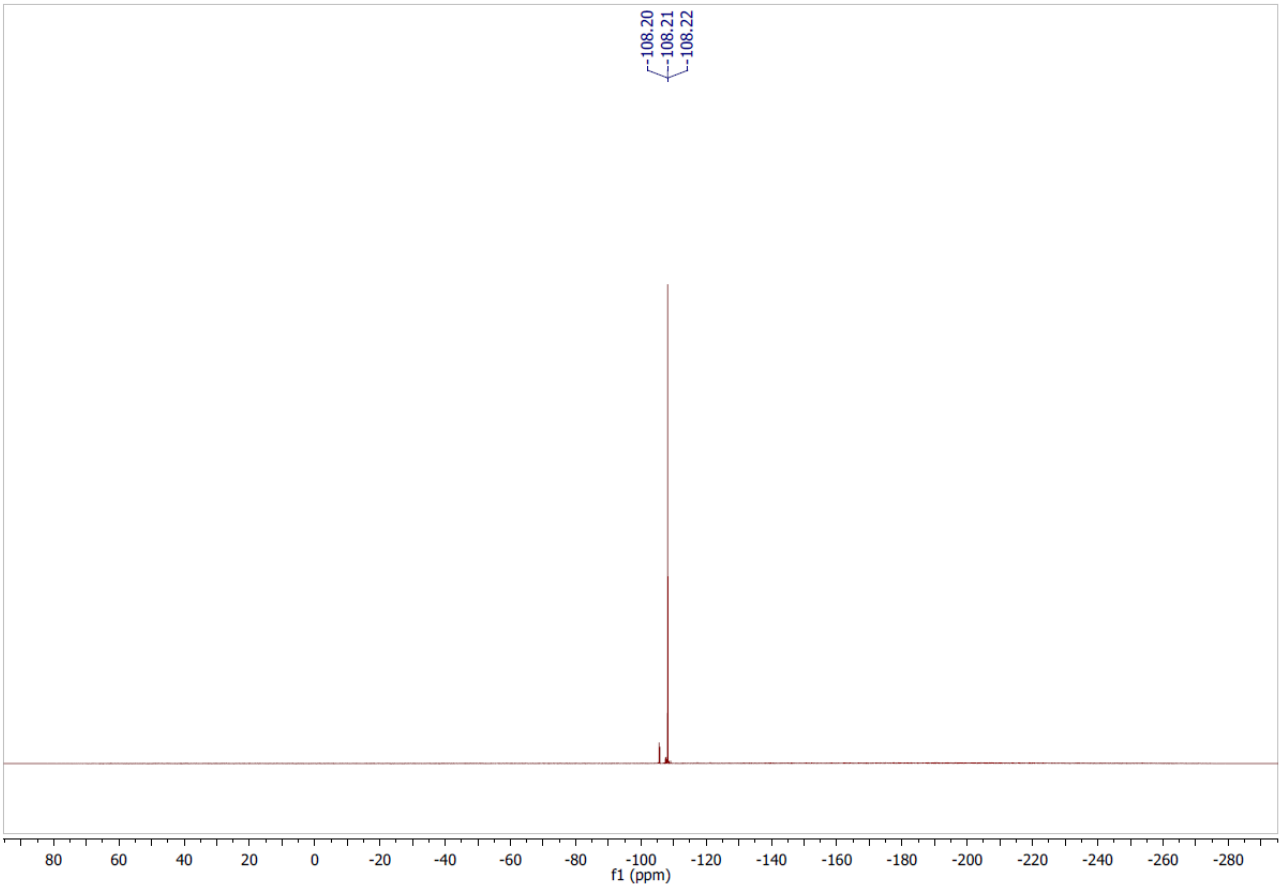

tris[5-fluoro-2-[(phenylimino)methyl]phenyl]-boroxine **39**:

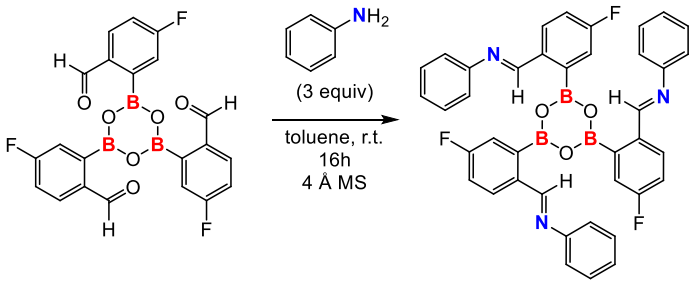

24 **39** (91 %)

Aniline (0.05 mL, 0.55 mmol, 3 equiv) was added to tris[3-fluoro-2-formylphenyl]-boroxine **24** (0.082 g, 0.18 mmol, 1 equiv) in dry toluene on molecular sieves under argon atmosphere and stirred 16h at room temperature. The solution was then filtered through syringe filter (0.2 µm) under argon and the solvent evaporated under reduced pressure.

White solid (111 mg, yield = 91 %).

^{1}H NMR (500 MHz, $CDCl_3$) δ (ppm) =8.62 (s, 3H), 7.93-7.60 (m, 3H), 7.42-7.30 (m, 9H), 7.33-7.20 (m, 6H), 6.97 (td, *J* = 8.6, 2.2 Hz), 6.66 (m, 3H).

^{11}B NMR (160 MHz, $CDCl_3$) δ (ppm) = 15.3 (br)

^{13}C NMR (126 MHz, $CDCl_3$) δ (ppm) = 165.2, 147.7, 138.6, 132.4, 131.8, 129.3, 128.3, 127.3, 126.6, 122.3. The carbon atoms directly attached to the boron atom on the boroxine core were not detected, likely due to quadrupolar relaxation.

^{19}F NMR (476 MHz, $CDCl_3$) δ (ppm) = -106.1 (br).

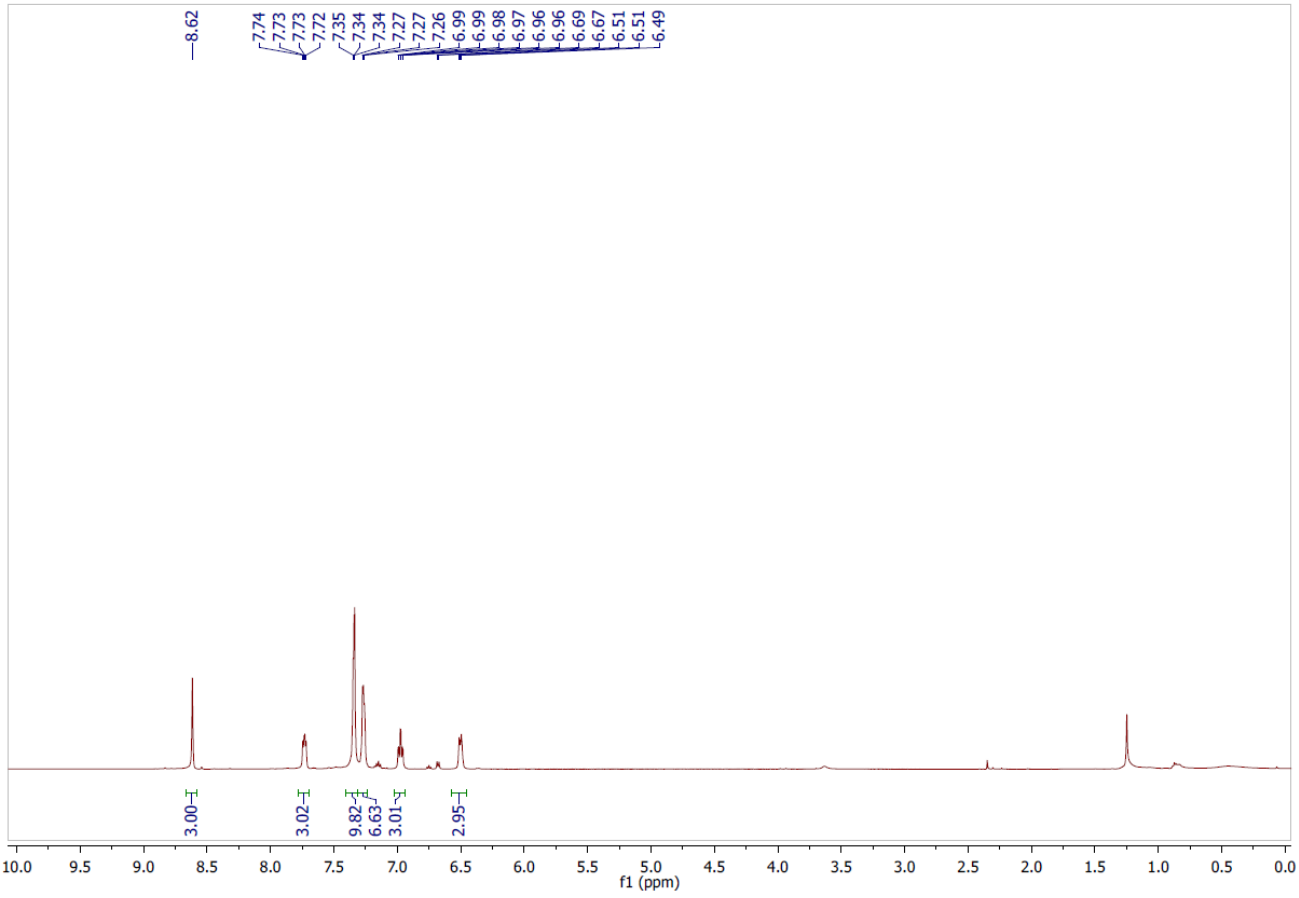

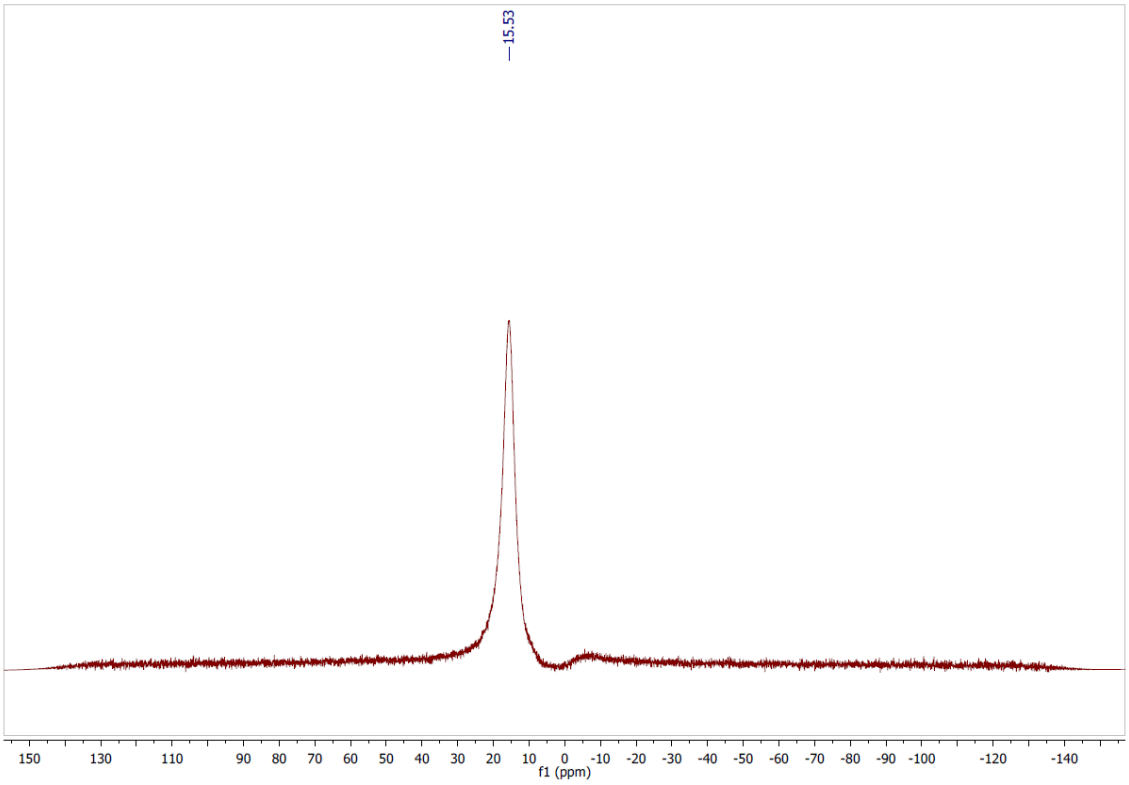
15.53
150 130 110 90 80 70 60 50 40 30 20 10 0 -10 -20 -30 -40 -50 -60 -70 -80 -90 -100 -120 -140
f1 (ppm)

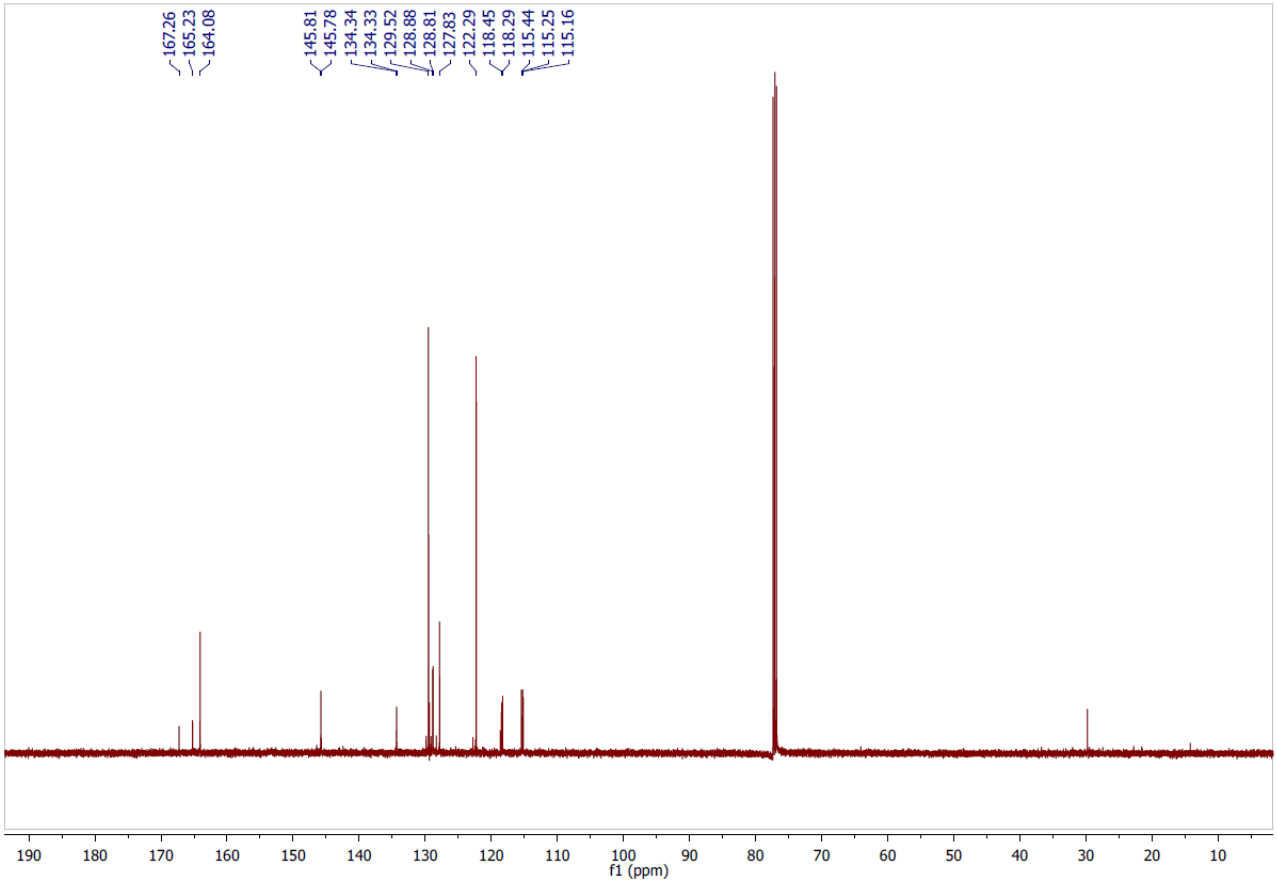
167.26
165.23
164.08
145.81
145.78
134.34
134.33
129.52
128.88
128.81
127.83
122.29
118.45
118.29
115.44
115.25
115.16
190 180 170 160 150 140 130 120 110 100 90 80 70 60 50 40 30 20 10
f1 (ppm)

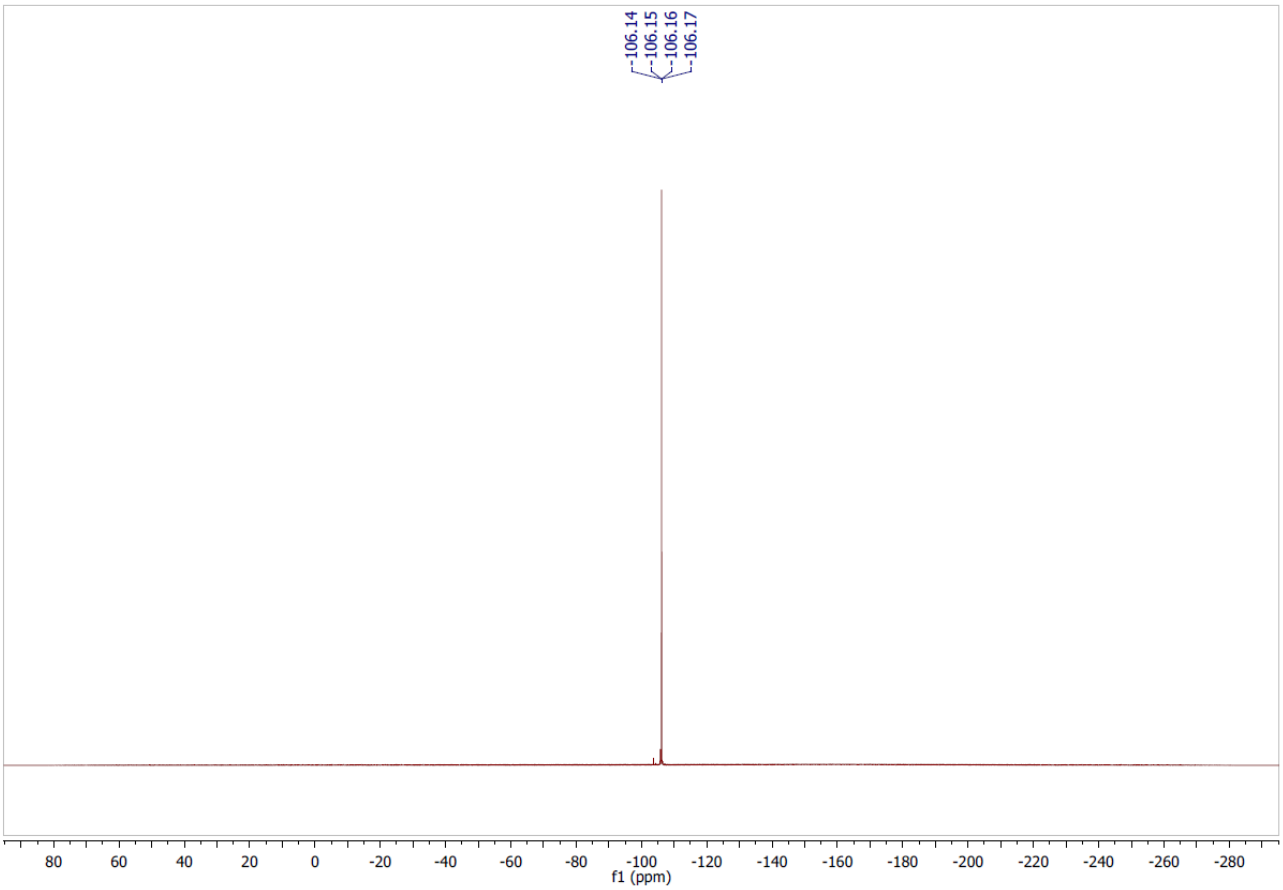

tris[5-fluoro-2-[(tert-butylimino)methyl]phenyl]-boroxine **40**:

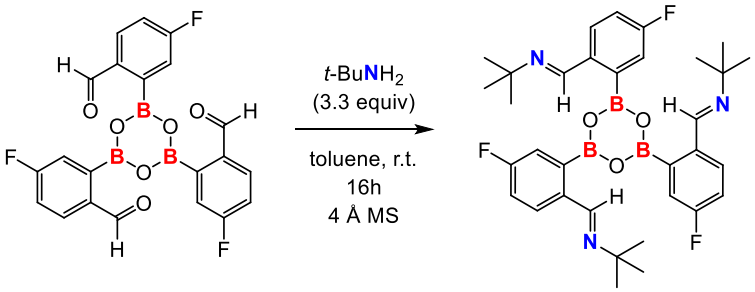

24 **40** (83 %)

tert-Butylamine (0.07 mL, 0.67 mmol, 3.3 equiv) was added to tris[3-fluoro-2-formylphenyl]-boroxine **24** (0.09 g, 0.20 mmol, 1 equiv) in dry toluene on molecular sieves under argon atmosphere and stirred 16h at room temperature. The solution was then filtered through syringe filter (0.2 µm) under argon and the solvent evaporated under reduced pressure.

White solid (102 mg, yield = 83 %).

^{1}H NMR (500 MHz, $CDCl_3$) δ (ppm) =8.67 (s, 3H), 7.70-7.61 (m, 3H) 7.49 (dd, 9.1, 2.6 Hz, 3H), 7.01 (td, *J* = 8.5, 2.6 Hz, 3H), 1.37 (s, 27H).

^{11}B NMR (160 MHz, $CDCl_3$) δ (ppm) = 18.2 (br)

^{13}C NMR (126 MHz, $CDCl_3$) δ (ppm) = 165.2 (d, *J* = 252.4 Hz), 160.7, 135.8, 128.5 (dd, *J* = 57.4, 55.2 Hz), 119.5 (d, *J* = 20.0 Hz), 115.7 (d, *J* = 22.8 Hz), 58.5, 30.0 carbon atoms directly attached to the boron atom on the boroxine core were not detected, likely due to quadrupolar relaxation.

^{19}F NMR (476 MHz, $CDCl_3$) δ (ppm) = -109.2 (br)

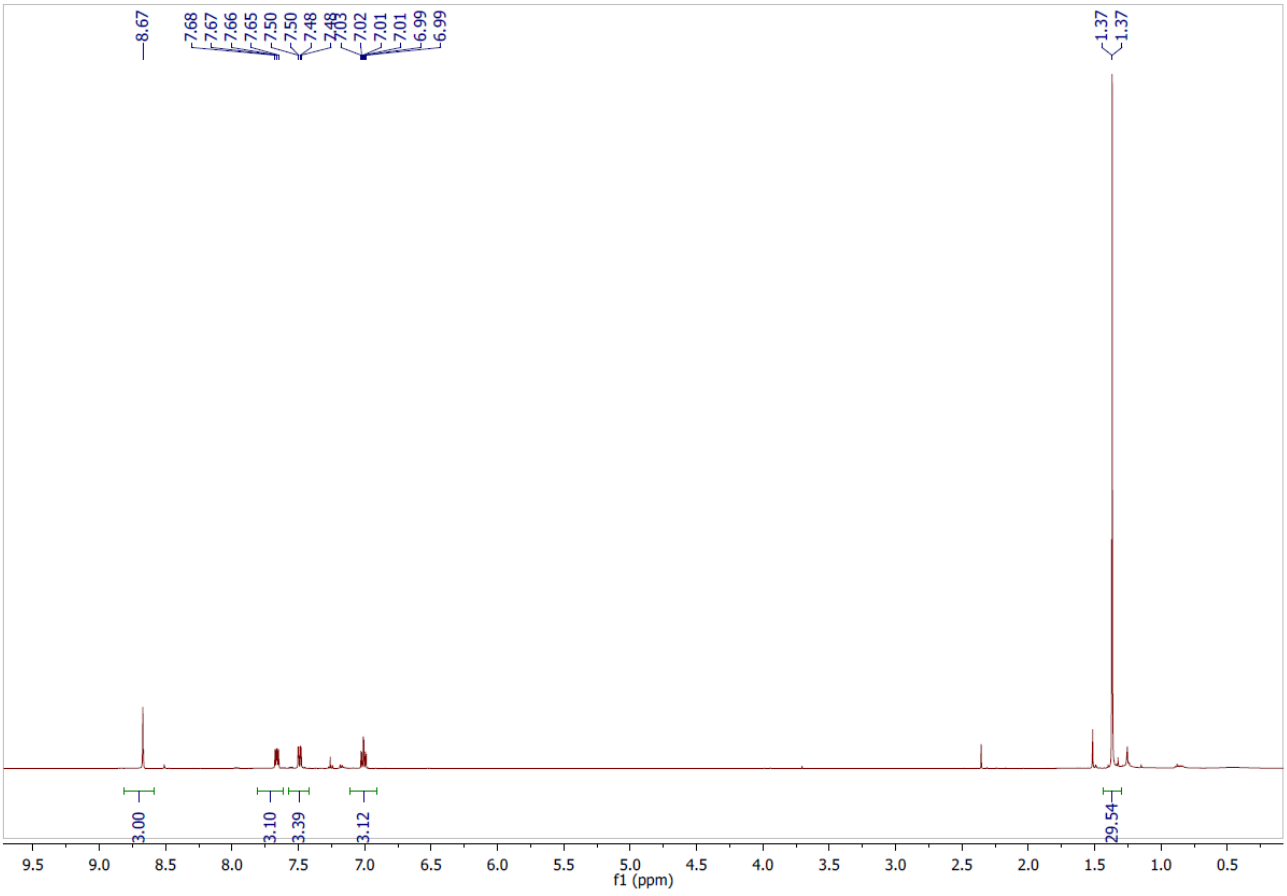

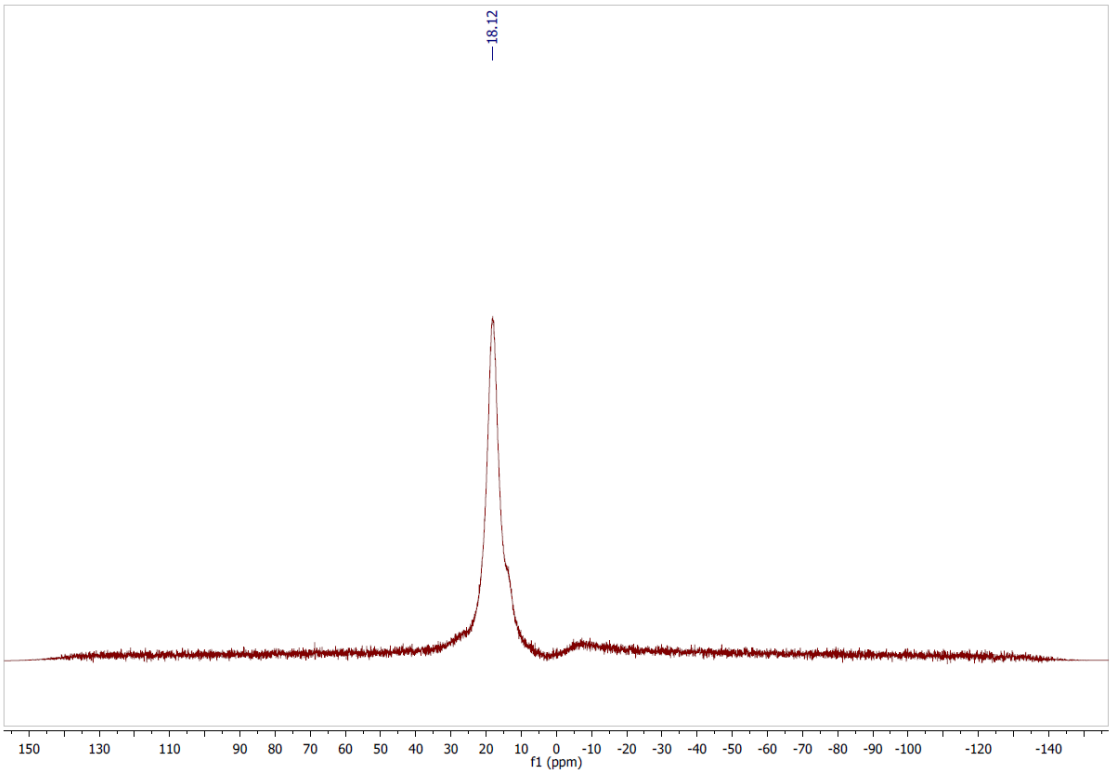
18.12
150 130 110 90 80 70 60 50 40 30 20 10 0 -10 -20 -30 -40 -50 -60 -70 -80 -90 -100 -120 -140
f1 (ppm)

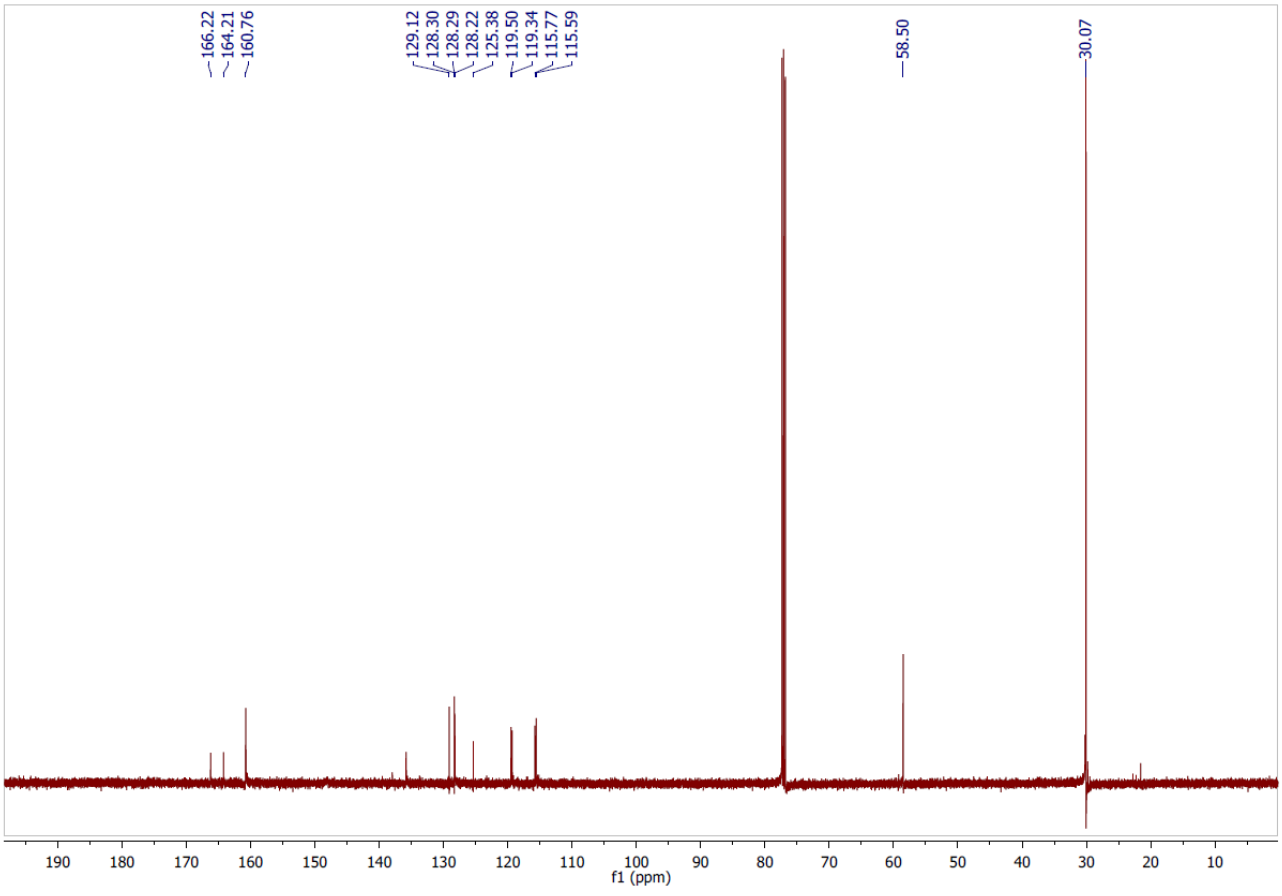
166.22
164.21
160.76
129.12
128.30
128.29
128.22
125.38
119.50
119.34
115.77
115.59
58.50
30.07
190 180 170 160 150 140 130 120 110 100 90 80 70 60 50 40 30 20 10
f1 (ppm)

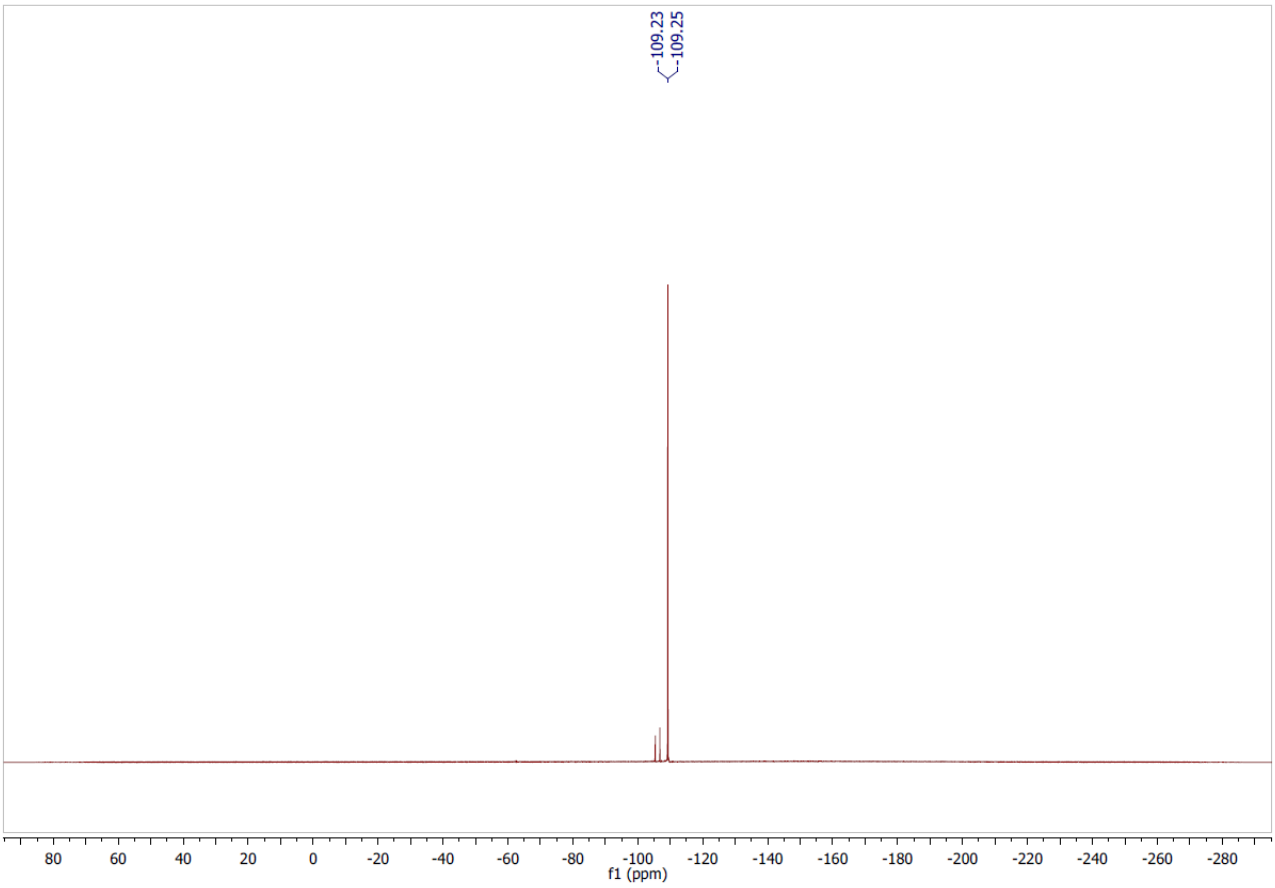
-109.23
-109.25
80
60
40
20
0
-20
-40
-60
-80
-100
-120
-140
-160
-180
-200
-220
-240
-260
-280
f1 (ppm)

tris[2-[(furfurylimino)methyl]phenyl]-boroxine **42**:

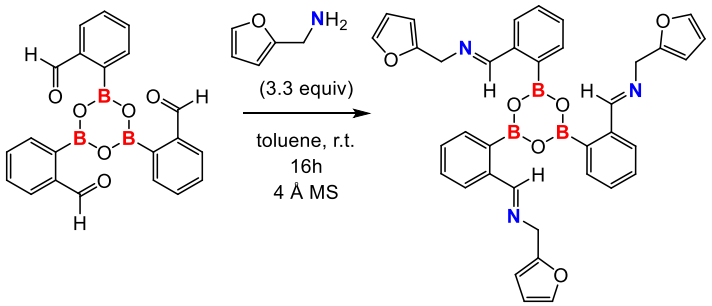

21 **42** (55 %)

Furfurylamine (0.06 mL, 0.68 mmol, 3.3 equiv) was added to tris[2-formylphenyl]-boroxine **21** (0.0804 g, 0.203 mmol, 1 equiv) in dry toluene on molecular sieves under argon atmosphere and stirred 16h at room temperature. The solution was then filtered sintered glass filter and the solvent evaporated under reduced pressure.

White solid (70 mg, yield = 55 %).

^{1}H NMR (500 MHz, $CDCl_3$) δ (ppm) =8.34 (s, 1H), 7.73 (d, *J* = 7.2 Hz, 1H), 7.57 (d, *J* = 7.5 Hz, 1H), 7.42 (t, *J* = 7.3 Hz, 1H), 7.2- (dd, *J* = 10.5, 3.5 Hz, 1H), 6.54-6.22 (m, 2H), 4.85 (s, 2H).

^{11}B NMR (160 MHz, $CDCl_3$) δ (ppm) = 14.9 (br)

^{13}C NMR (126 MHz, $CDCl_3$) δ (ppm) = 166.3, 149.5, 143.1, 138.4, 132.0, 131.2, 127.8, 126.3, 110.7, 110.0, 109.9. Carbon atoms directly attached to the boron atom on the boroxine core were not detected, likely due to quadrupolar relaxation.

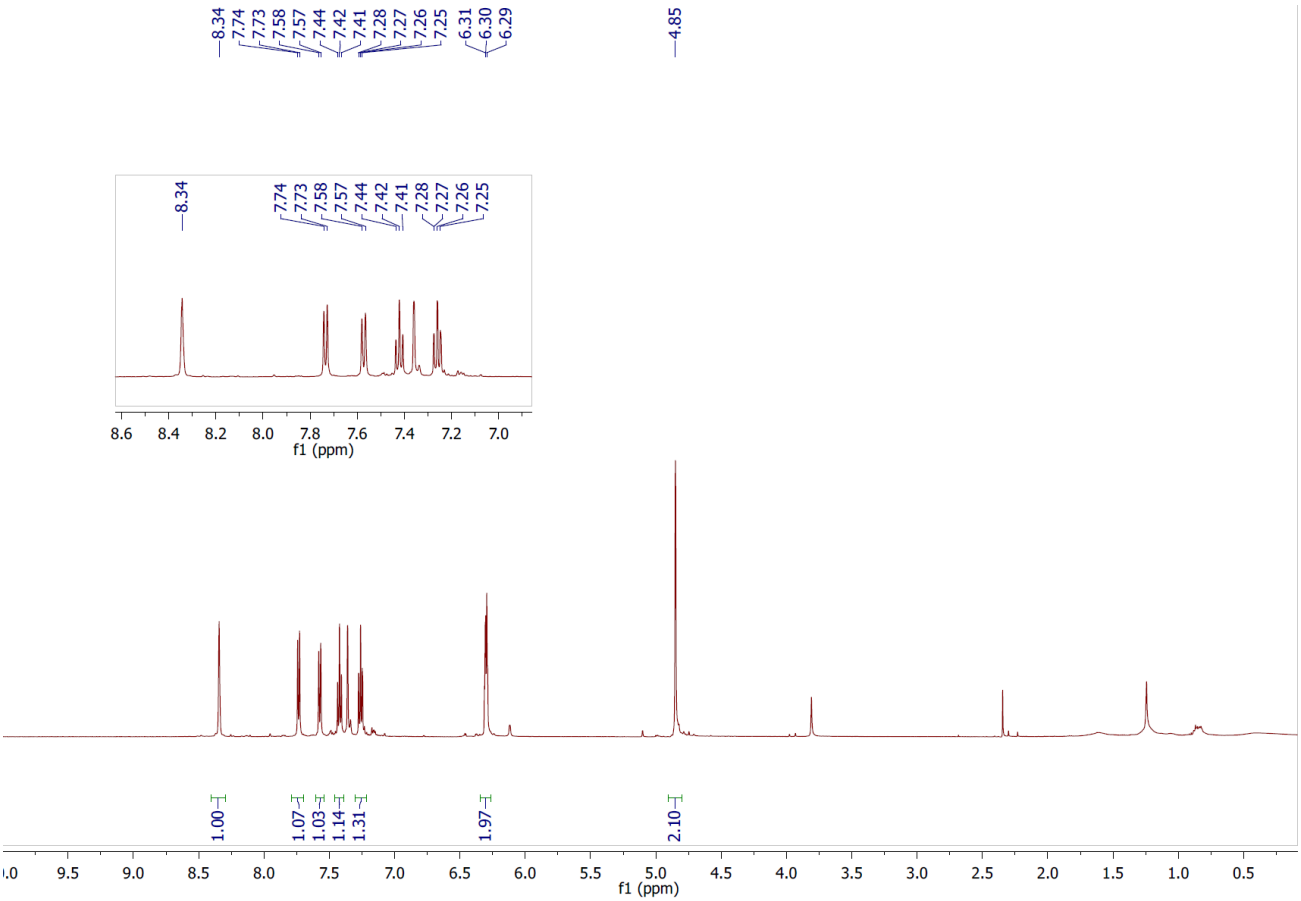
8.34
7.74
7.73
7.58
7.57
7.44
7.42
7.41
7.28
7.27
7.26
7.25
6.31
6.30
6.29
4.85
1.00
1.07
1.03
1.14
1.31
1.97
2.10
f1 (ppm)

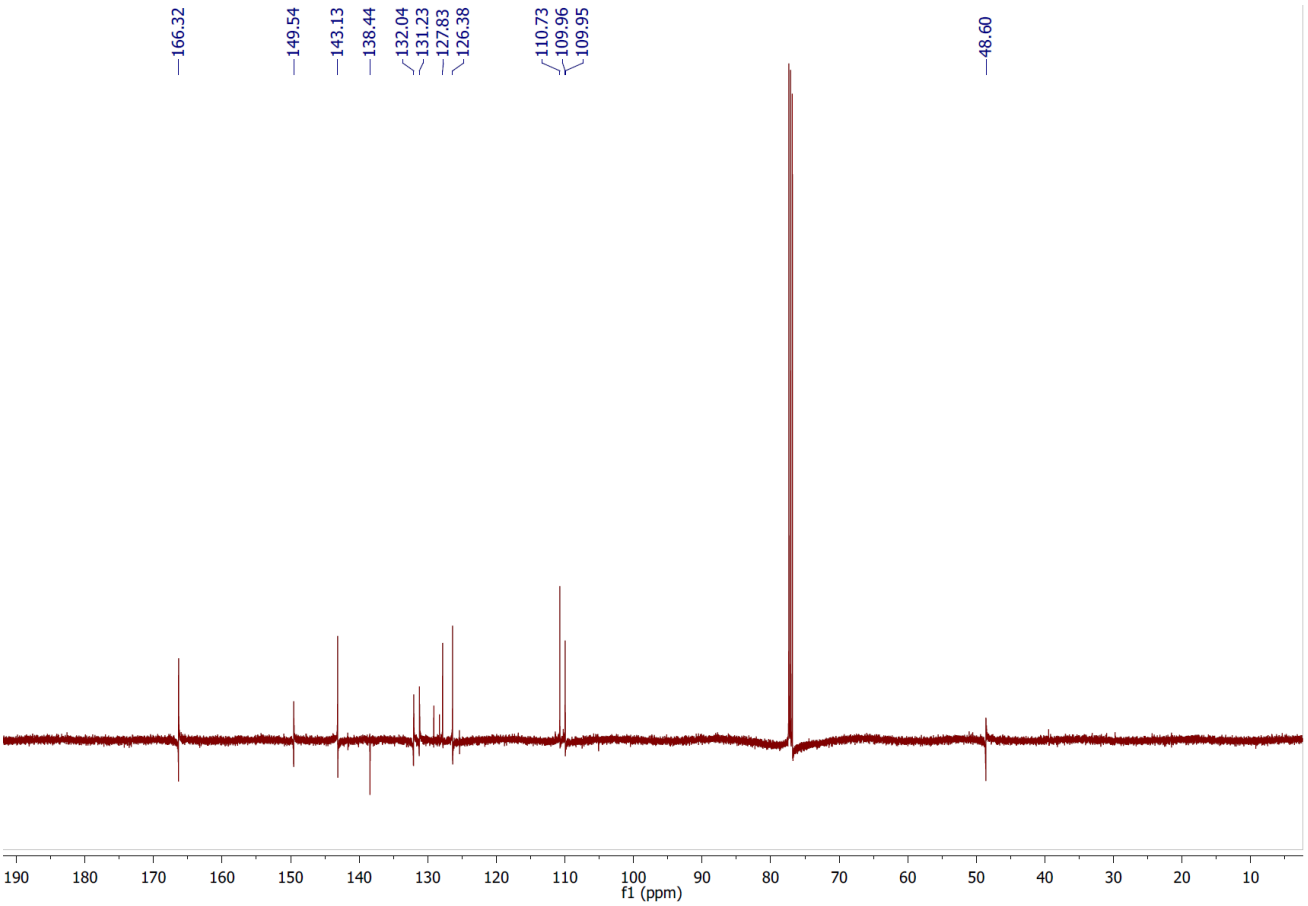
166.32
149.54
143.13
138.44
132.04
131.23
127.83
126.38
110.73
109.96
109.95
48.60
f1 (ppm)

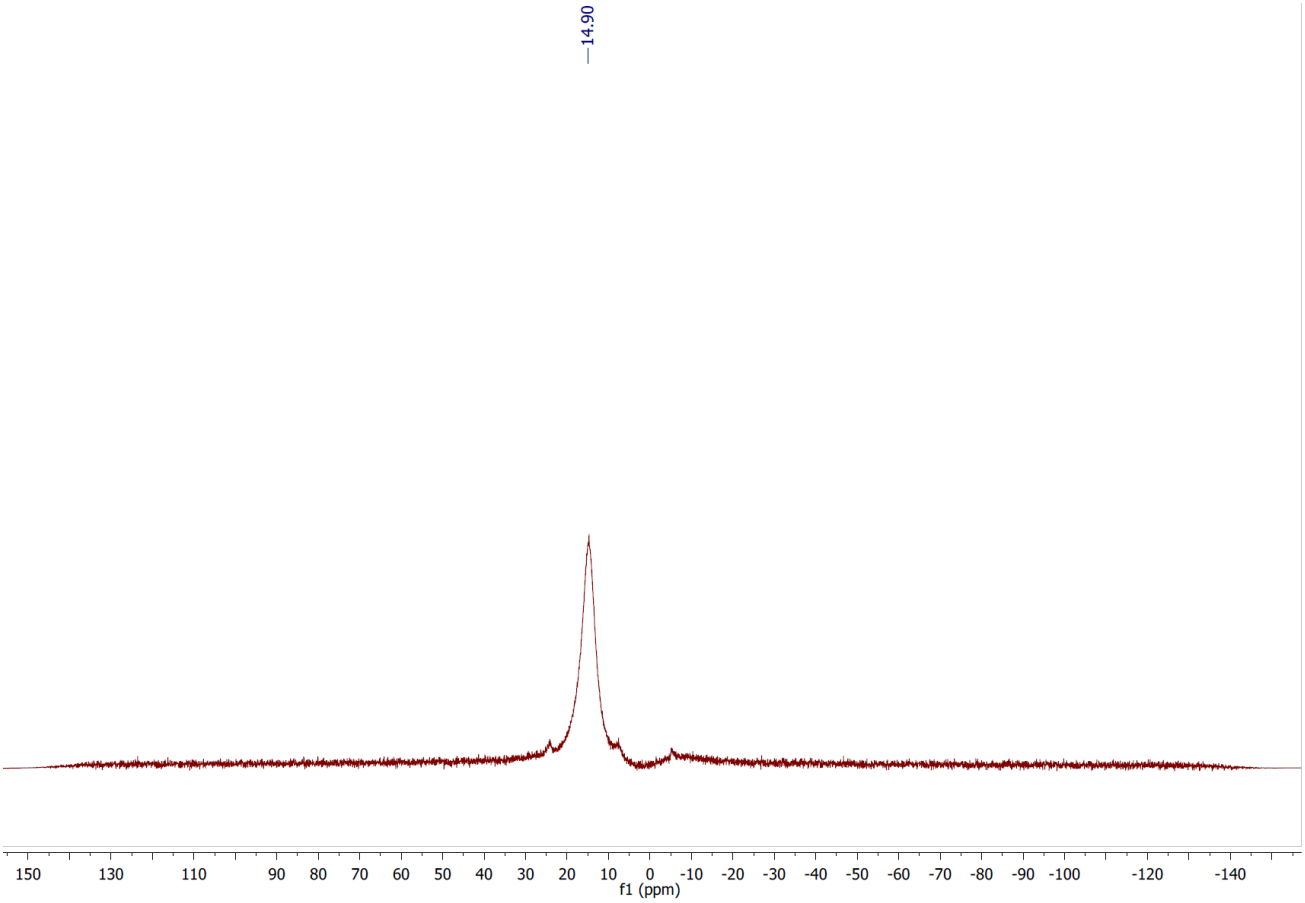

tris[2-[(tetrahydrofurfurylimino)methyl]phenyl]-boroxine **43**:

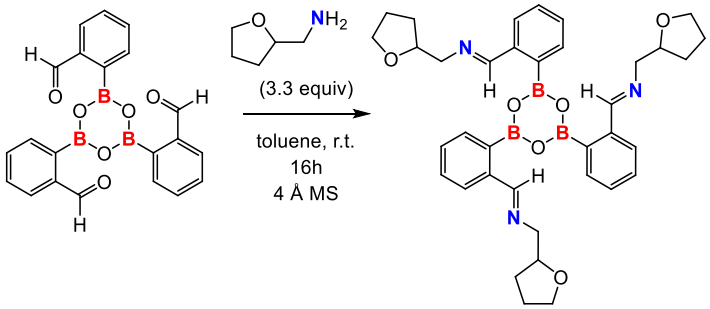

21 **43** (n.d.)

Tetrahydrofurfurylamine (0.07 mL, 0.68 mmol, 3.3 equiv) was added to tris[2-formylphenyl]-boroxine **21** (0.0805 g, 0.203 mmol, 1 equiv) in dry toluene on molecular sieves under argon atmosphere and stirred 16h at room temperature. The solution was then filtered sintered glass filter and the solvent evaporated under reduced pressure. The title compound was found to be contaminated by a substantial amount of tetrahydrofurylamine, therefore no characterisation was attempted.

tris[2-[(benzylimino)methyl]phenyl]-boroxine **44**:

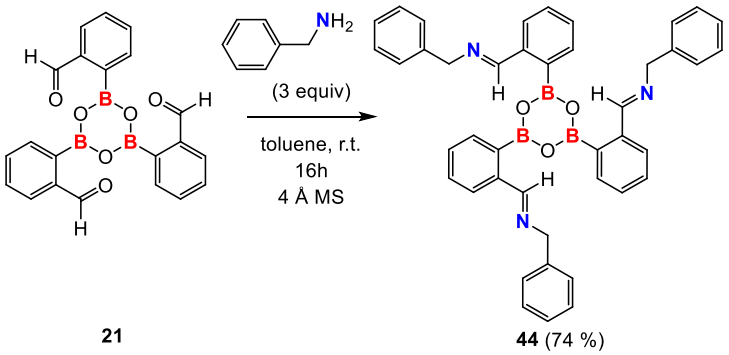

21 **44** (74 %)

Benzylamine (0.07 mL, 0.64 mmol, 3 equiv) was added to tris[2-formylphenyl]-boroxine **21** (0.0805 g, 0.203 mmol, 1 equiv) in dry toluene on molecular sieves under argon atmosphere and stirred 16h at room temperature. The solution was then filtered sintered glass filter and the solvent evaporated under reduced pressure.

White solid (100 mg, yield = 74 %).

^{1}H NMR (500 MHz, $CDCl_3$) δ (ppm) =8.27 (s, 3H), 7.76 (d, *J* = 7.2 Hz, 3H), 7.57 (d, *J* = 7.5 Hz, 3H), 7.41 (t, *J* = 7.3 Hz, 1H), 7.36-7.20 (m, 27H), 6.54-6.22 (m, 2H, partially contaminated with toluene and resulting benzylamine), 4.86 (s, 6H).

^{11}B NMR (160 MHz, $CDCl_3$) δ (ppm) = 14.9 (br)

^{13}C NMR (126 MHz, $CDCl_3$) δ (ppm) = 165.9, 150.2, 138.6, 136.0, 131.9, 131.2, 131.21, 129.4, 129.0, 128.0, 127.1, 126.3, 56.1, 46.6. Carbon atoms directly attached to the boron atom on the boroxine core were not detected, likely due to quadrupolar relaxation.

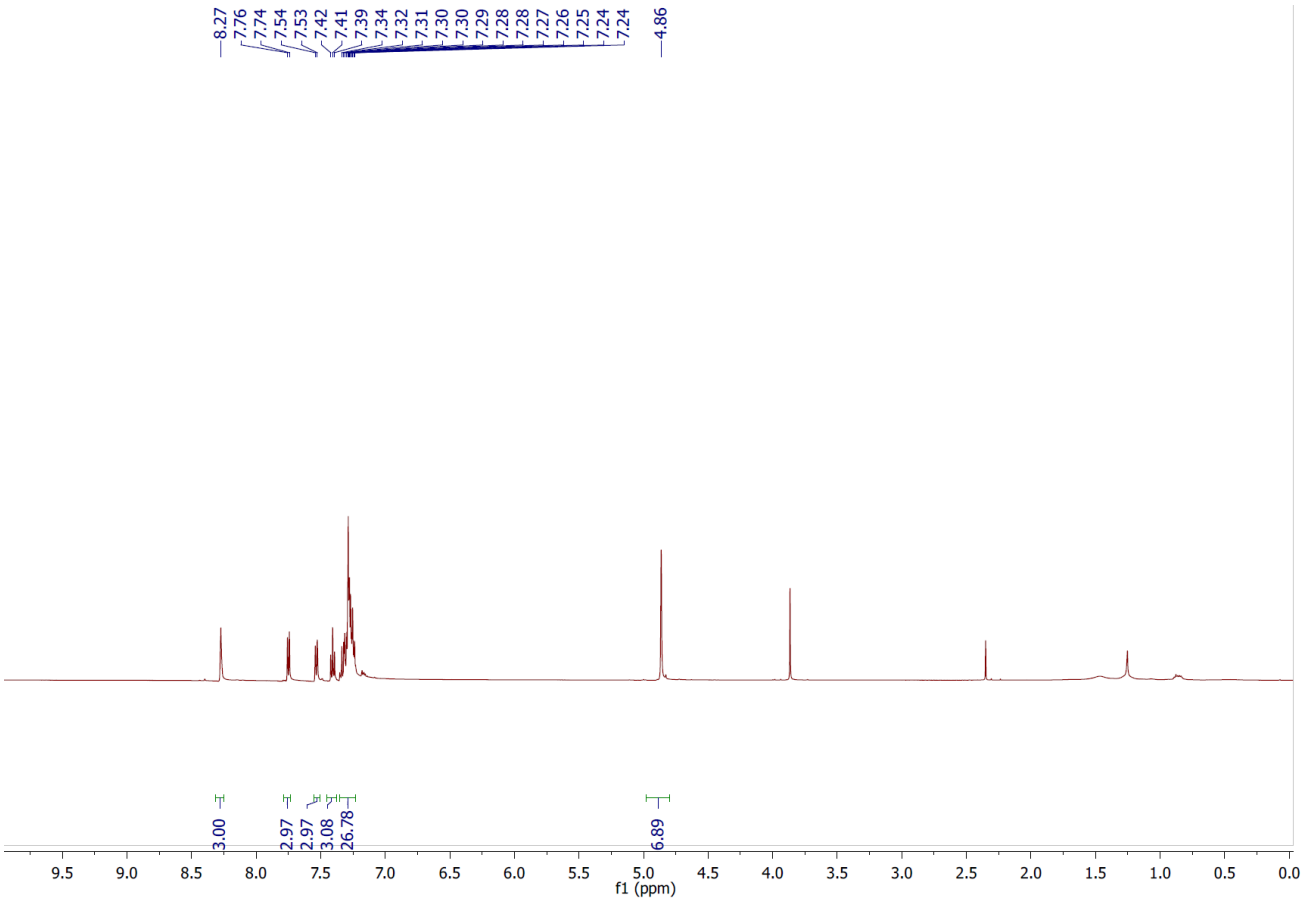
8.27
7.76
7.74
7.54
7.53
7.42
7.41
7.39
7.34
7.32
7.31
7.30
7.30
7.29
7.28
7.28
7.27
7.26
7.25
7.24
7.24
4.86
3.00
2.97
2.97
3.08
26.78
6.89
9.5
9.0
8.5
8.0
7.5
7.0
6.5
6.0
5.5
5.0
4.5
4.0
3.5
3.0
2.5
2.0
1.5
1.0
0.5
0.0
f1 (ppm)

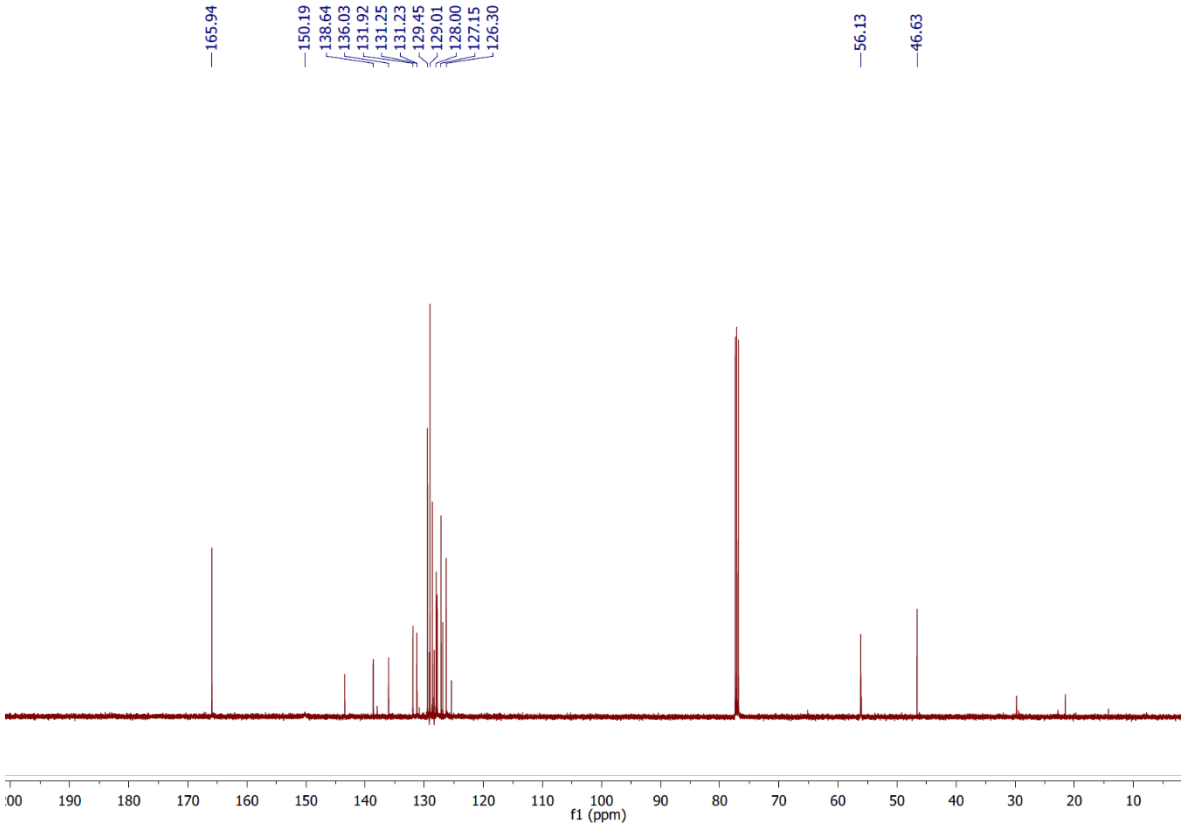
165.94
150.19
138.64
136.03
131.92
131.25
131.23
129.45
129.01
128.00
127.15
126.30
56.13
46.63
f1 (ppm)

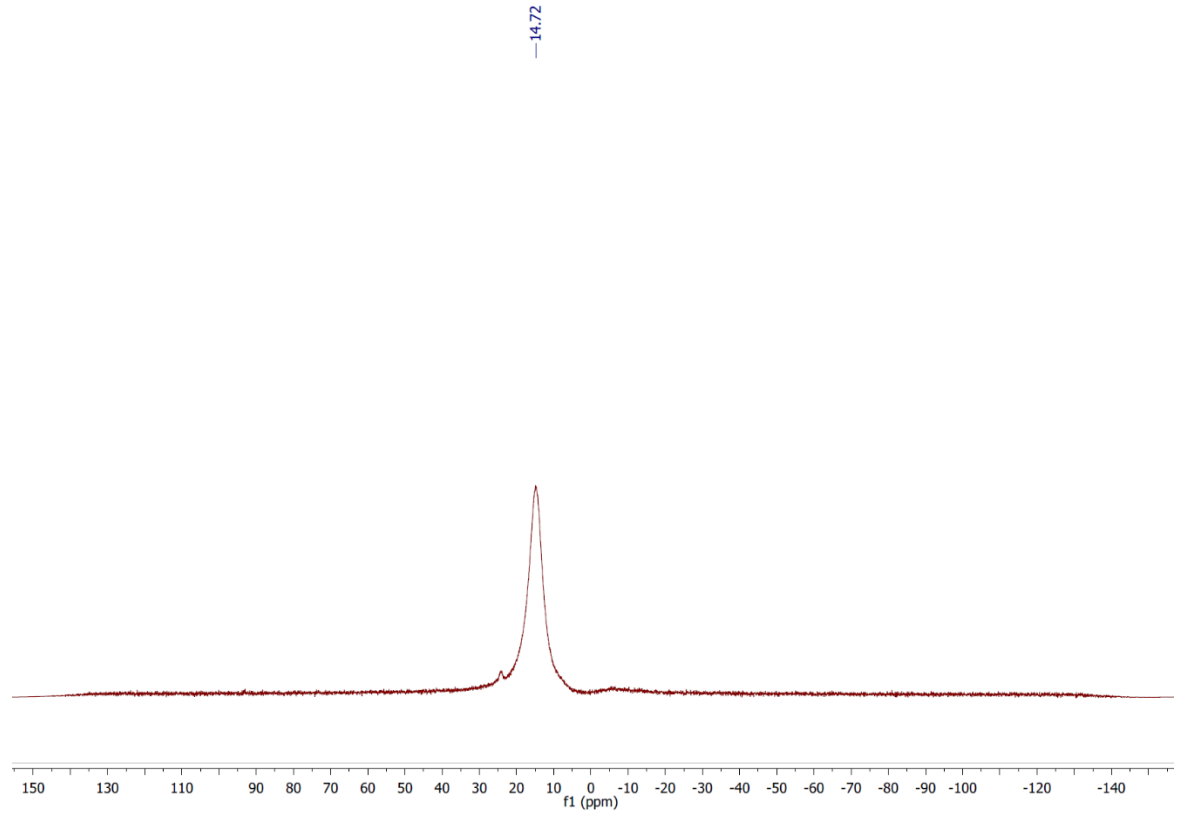
14.72
f1 (ppm)

Water-sensitive self-healing polymer networks based on the tris[2-formylphenyl]-boroxine **21** in association with 400 g.mol^{-1} poly(propylene glycol) bis(2-aminopropyl ether) **51**:

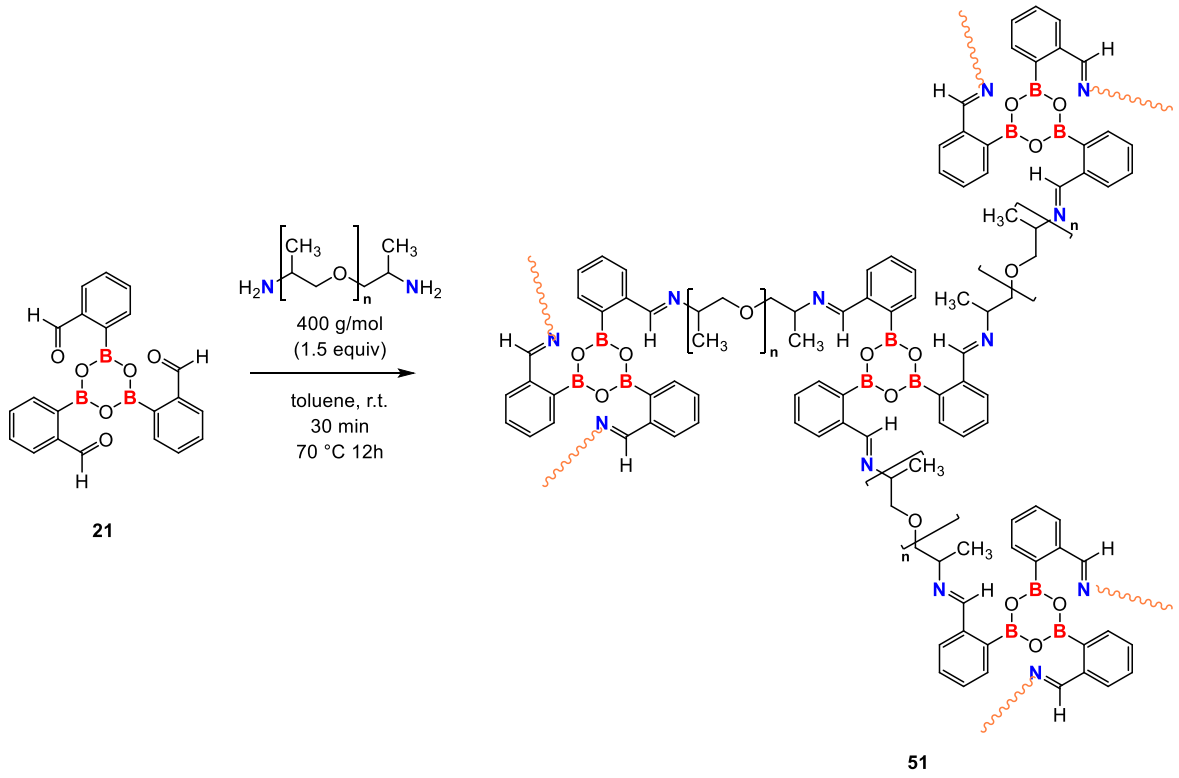

21 **51**

Poly(propylene glycol) bis(2-aminopropyl ether) (0.300 g, 0.75 mmol, 1.5 equiv) was added into a dry round-bottom flask with a solution of aryl-boroxine **21** (0.200 g, 0.50 mmol, 1 equiv) in toluene. After stirring 30 minutes under N_2 atmosphere, the reaction medium was poured into a mould and this latter was placed in oven at 70 °C for 12h to remove the solvent.

Yellow slightly sticky film.

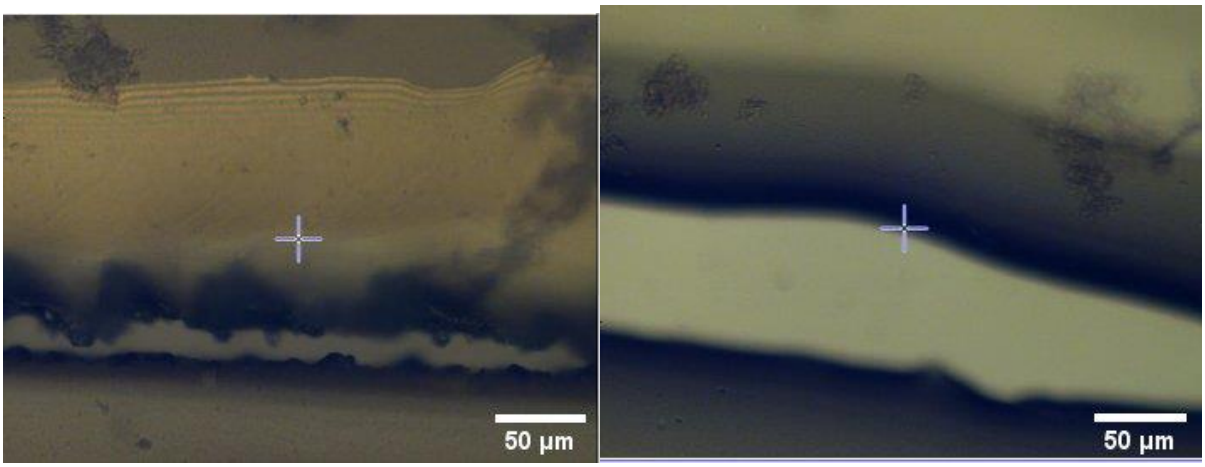

*Figure 45 – Microscope pictures of polymer **51** cut (left) and repaired after 48h exposure to ambient humidity (right) at X20 magnification*

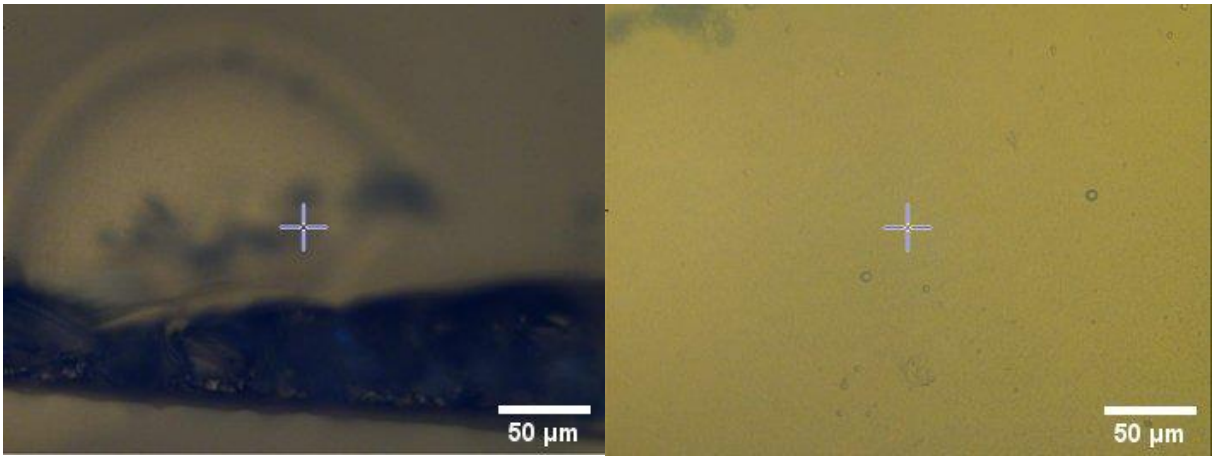

*Figure 46 - Microscope pictures of polymer **51** cut (left) and repaired after 48h exposure to 43 % relative humidity (right) at X20 magnification*

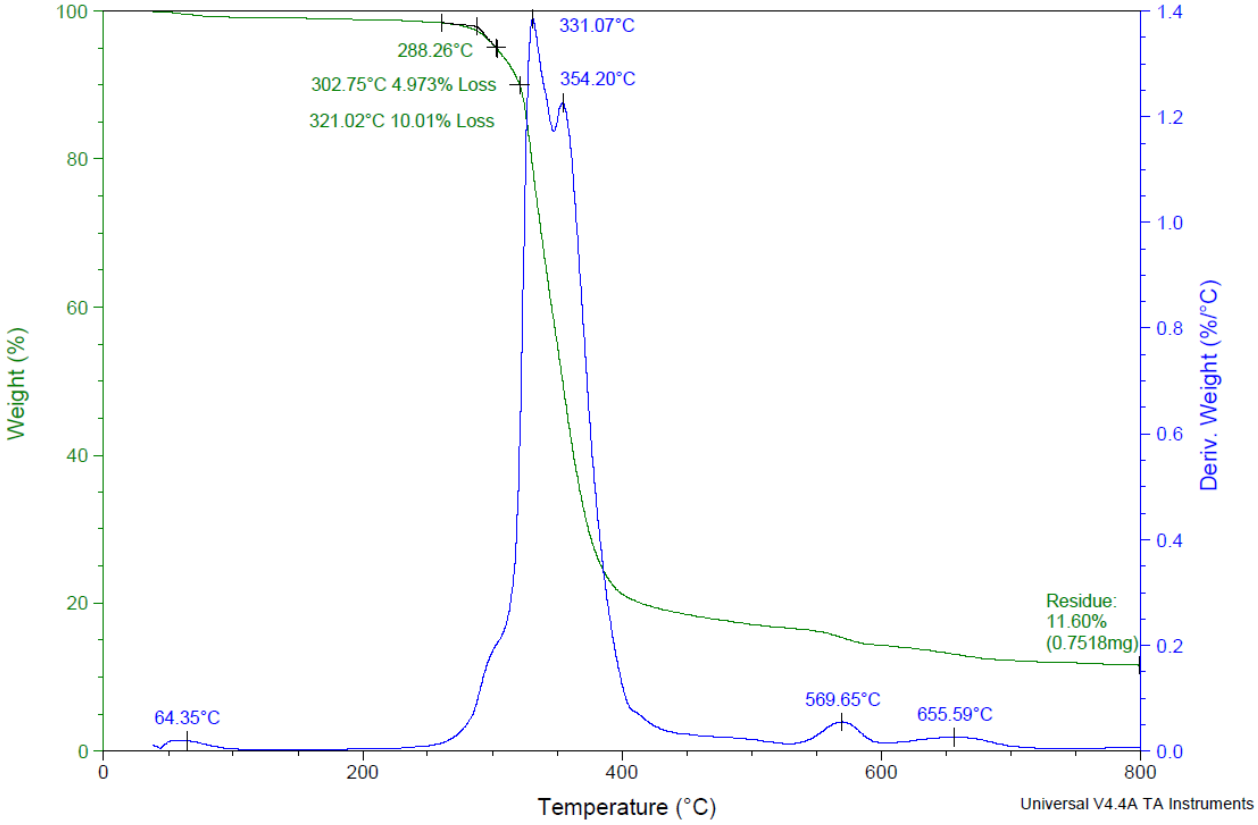

*Figure 47 - TGA curve of the evolution of the polymer **51** mass with the temperature (green) and the first derivative (blue)*

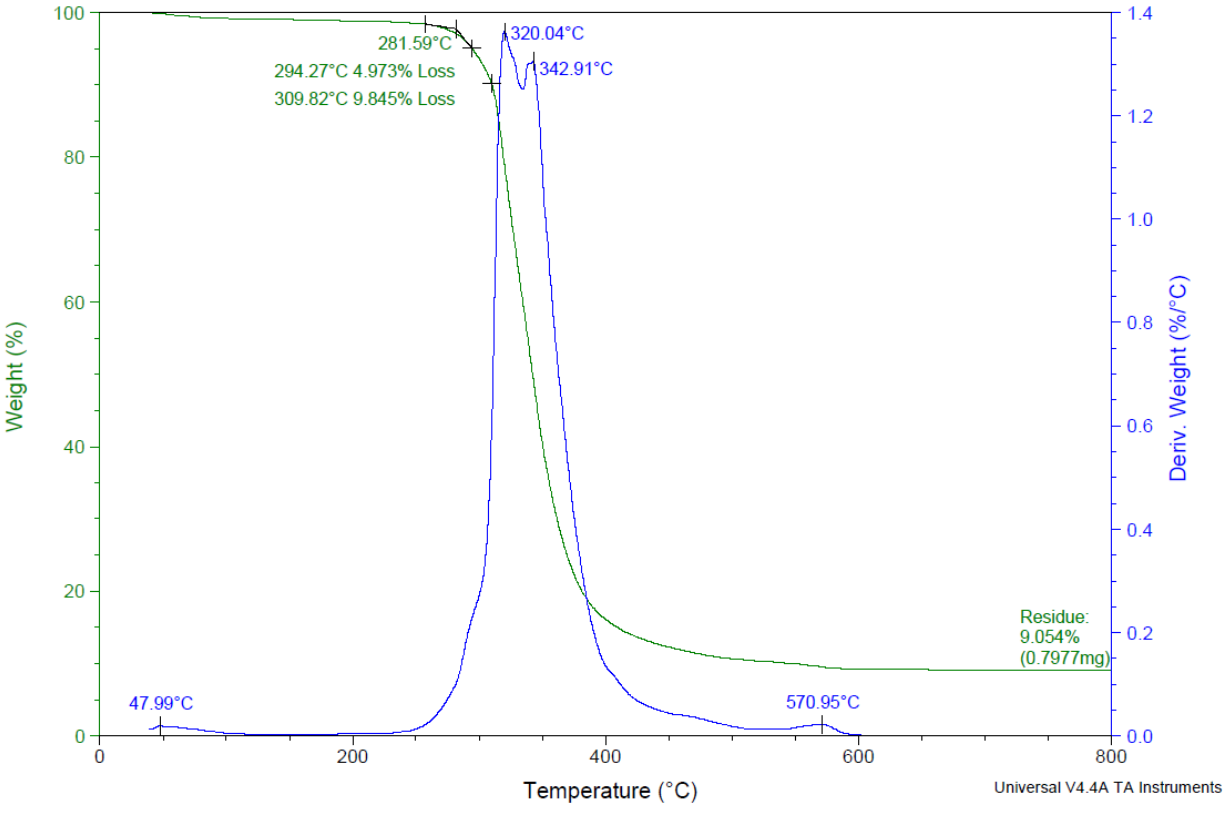

*Figure 48 - TGA curve of the evolution of the polymer **51H** mass with the temperature (green) and the first derivative (blue)*

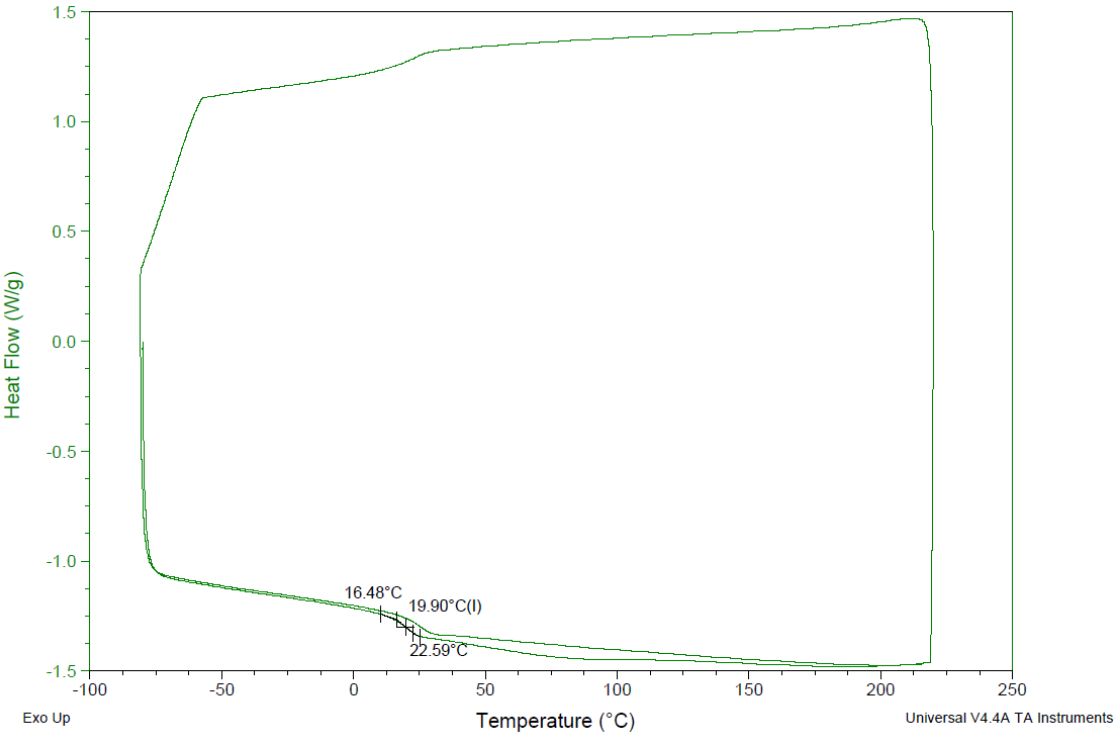

*Figure 49 - DSC curve of the evolution of the heat flow with the temperature for polymer **51***

Water-sensitive self-healing polymer networks based on the tris[3-fluoro-2-formylphenyl]-boroxine **23** in association with 400 g.mol^{-1} poly(propylene glycol) bis(2-aminopropyl ether) **52**:

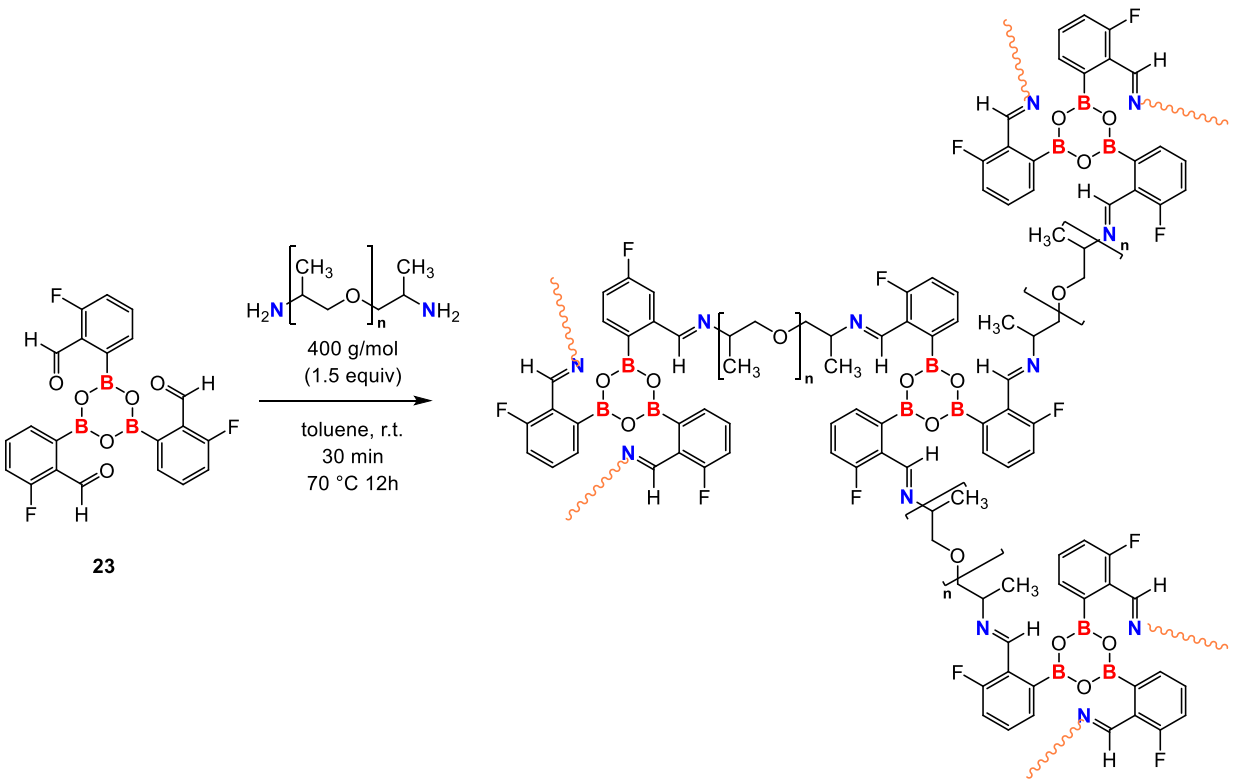

23

52

Poly(propylene glycol) bis(2-aminopropyl ether) (0.300 g, 0.75 mmol, 1.5 equiv) was added into a dry round-bottom flask with a solution of aryl-boroxine **23** (0.226 g, 0.50 mmol, 1 equiv) in toluene. After stirring 30 minutes under N_2 atmosphere, the reaction medium was poured into a mould and this latter was placed in oven at 70 °C for 12h to remove the solvent.

Brown film.

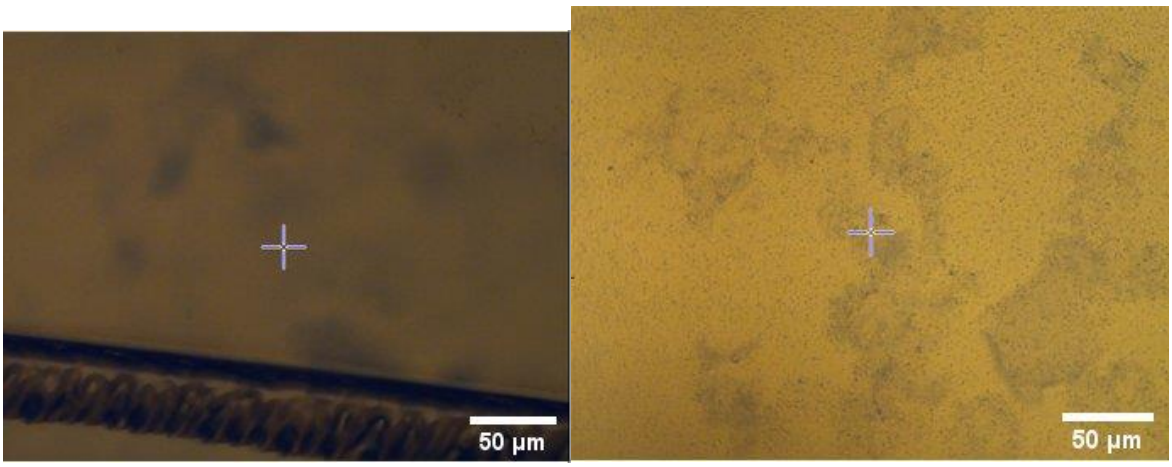

*Figure 50 - Microscope pictures of polymer **52** cut (left) and repaired after 48h exposure to ambient humidity (right) at X20 magnification*

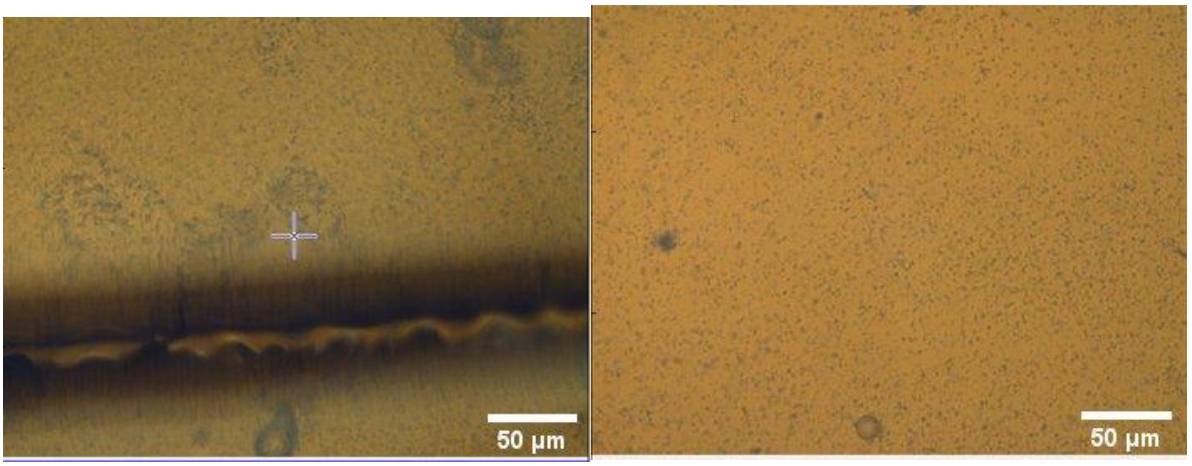

*Figure 51 - Microscope pictures of polymer **52** cut (left) and repaired after 48h exposure to 43 % relative humidity (right) at X20 magnification*

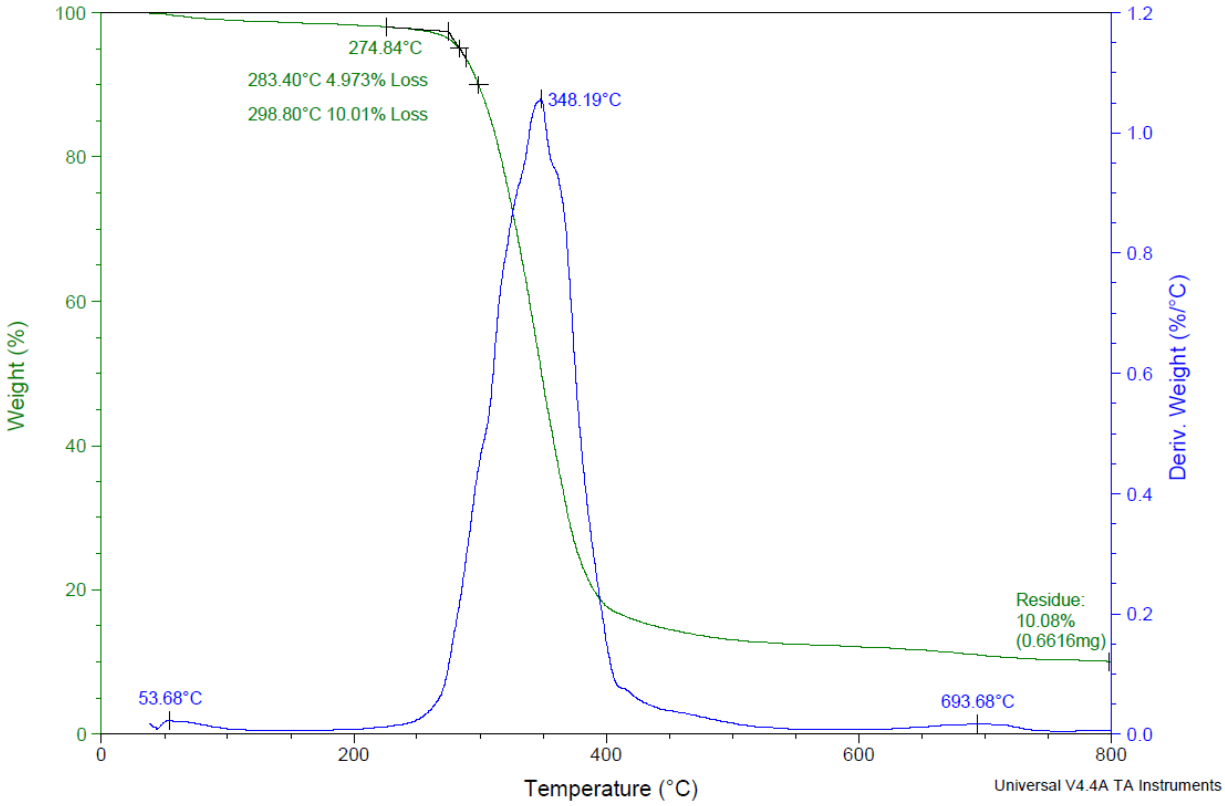

*Figure 52 - TGA curve of the evolution of the polymer **52** mass with the temperature (green) and the first derivative (blue)*

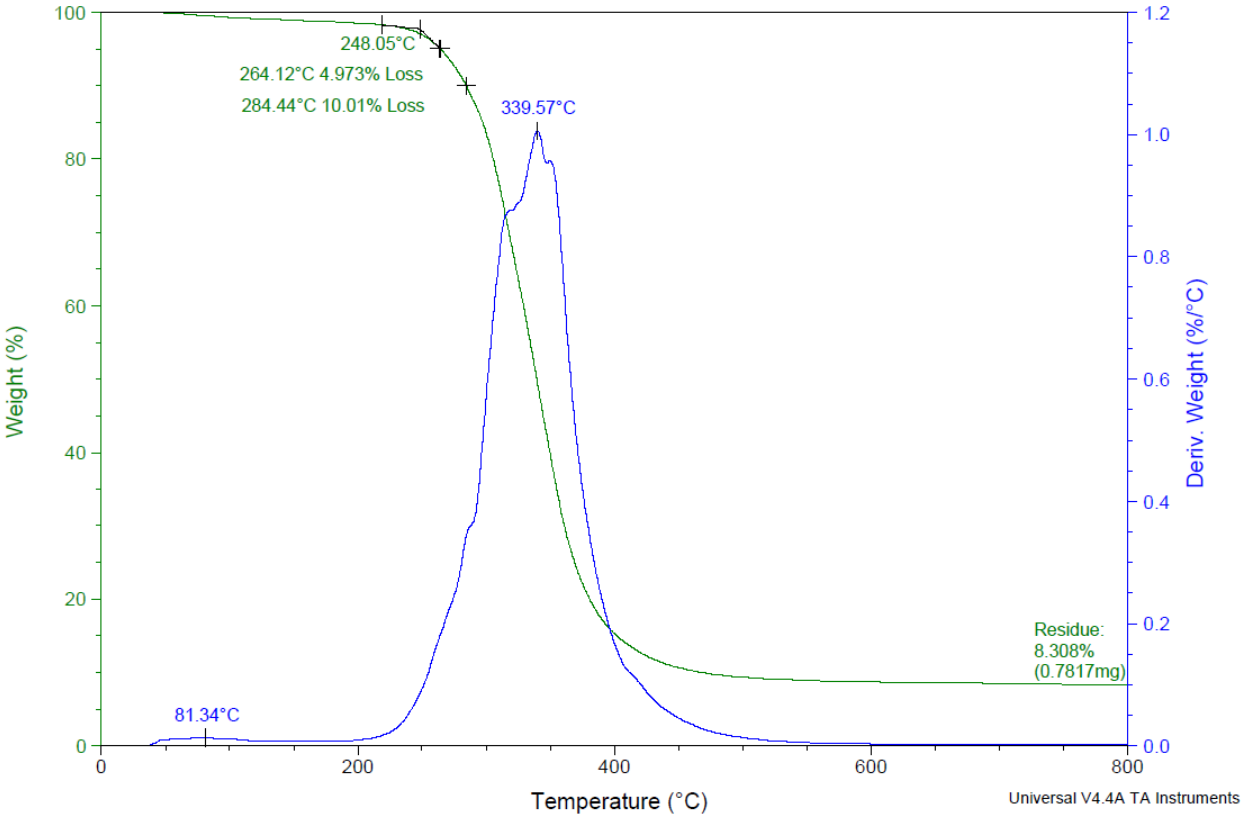

*Figure 53 - TGA curve of the evolution of the polymer **52H** mass with the temperature (green) and the first derivative (blue)*

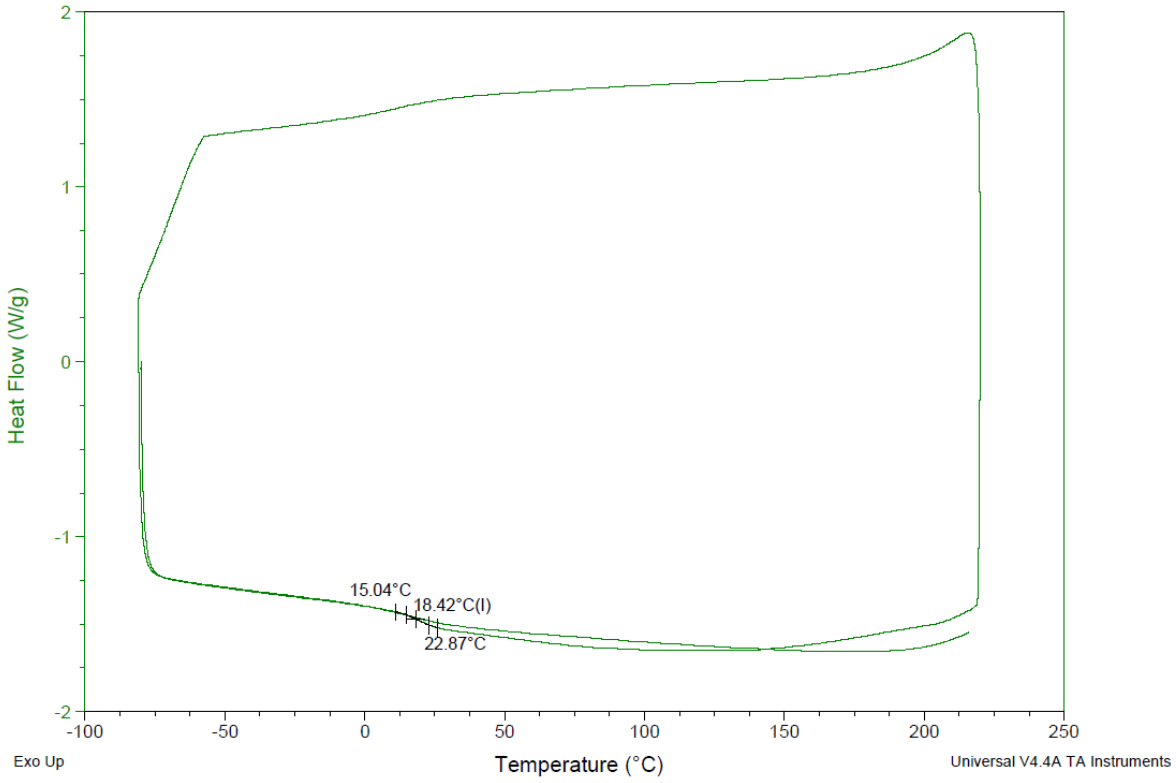

*Figure 54 - DSC curve of the evolution of the heat flow with the temperature for polymer **52***

Water-sensitive self-healing polymer networks based on the tris[5-fluoro-2-formylphenyl]-boroxine **24** in association with 400 g.mol^{-1} poly(propylene glycol) bis(2-aminopropyl ether) **53**:

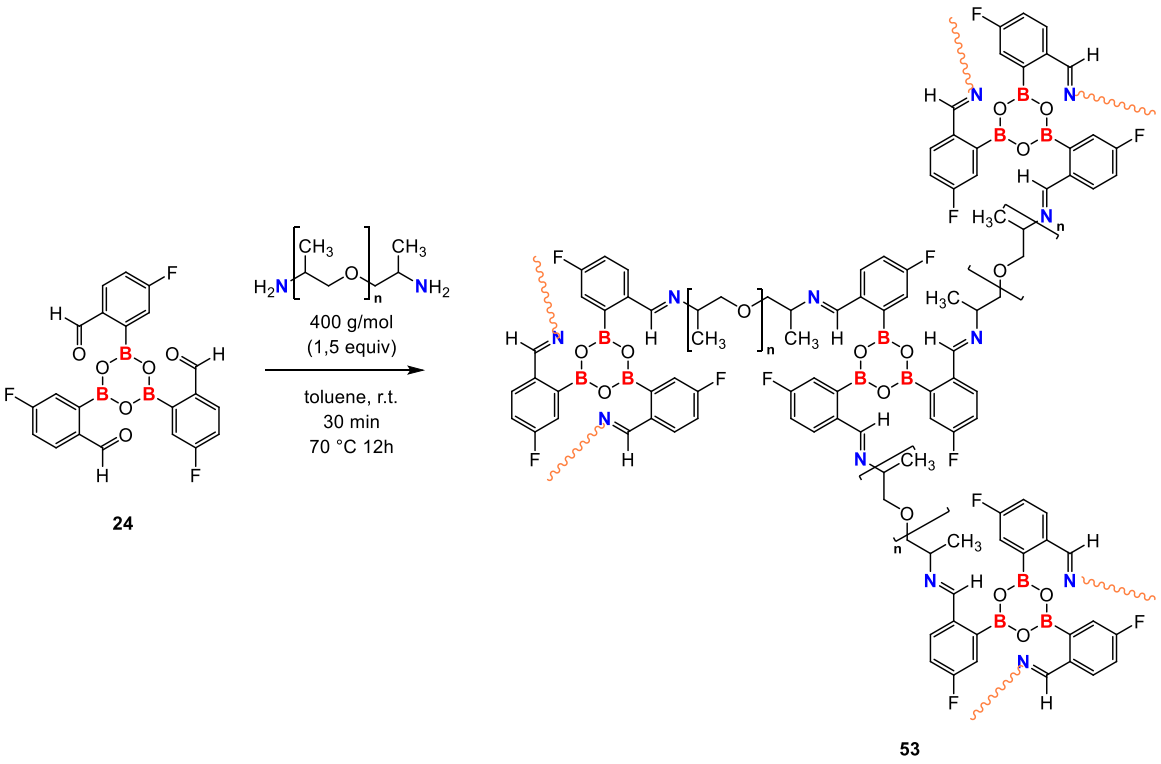

24 **53**

Poly(propylene glycol) bis(2-aminopropyl ether) (0.300 g, 0.75 mmol, 1.5 equiv) was added into a dry round-bottom flask with a solution of aryl-boroxine **24** (0.226 g, 0.50 mmol, 1 equiv) in toluene. After stirring 30 minutes under N_2 atmosphere, the reaction medium was poured into a mould and this latter was placed in oven at 70 °C for 12h to remove the solvent.

Yellow slightly sticky film.

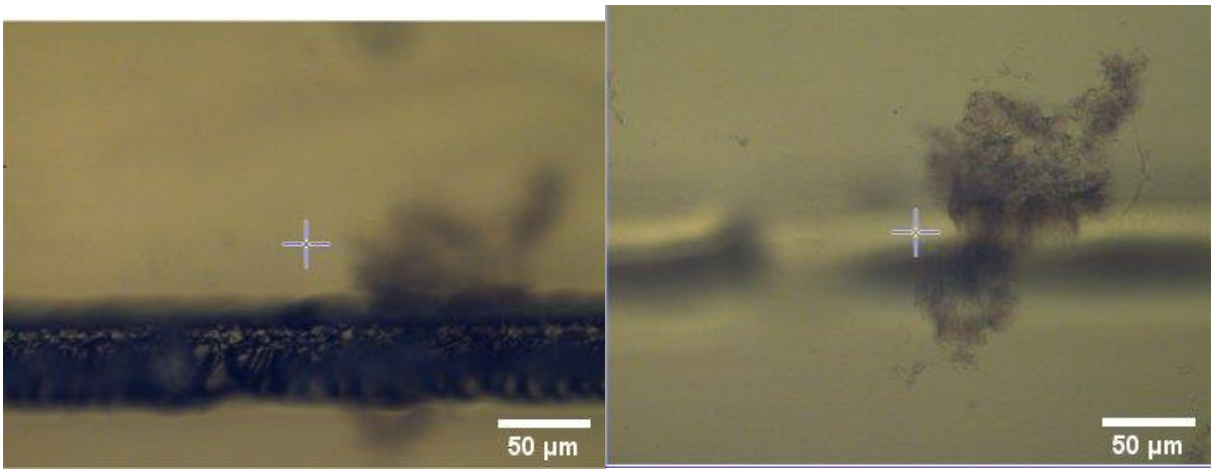

*Figure 55 - Microscope pictures of polymer **53** cut (left) and repaired after 48h exposure to ambient humidity (right) at X20 magnification*

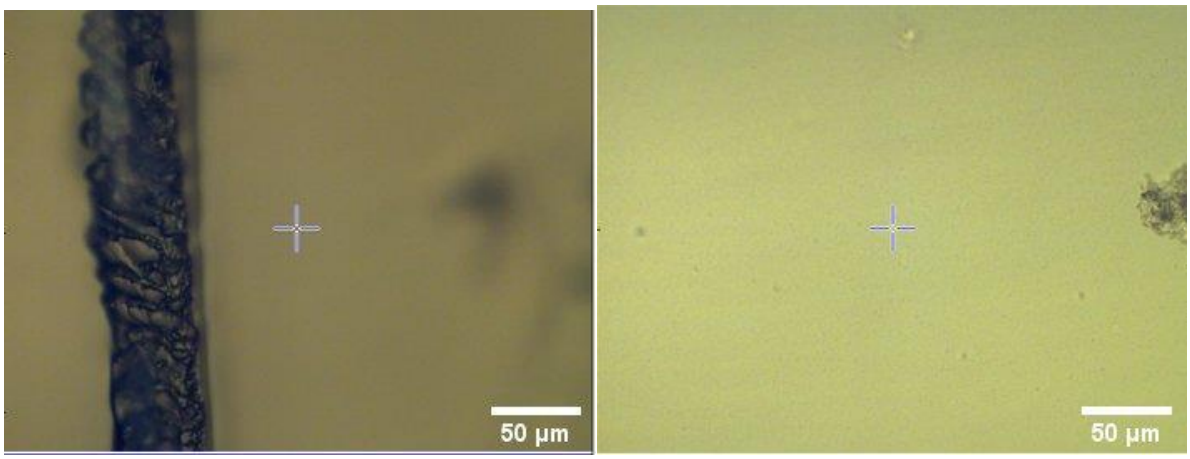

*Figure 56 - Microscope pictures of polymer **53** cut (left) and repaired after 48h exposure to 43 % relative humidity (right) at X20 magnification*

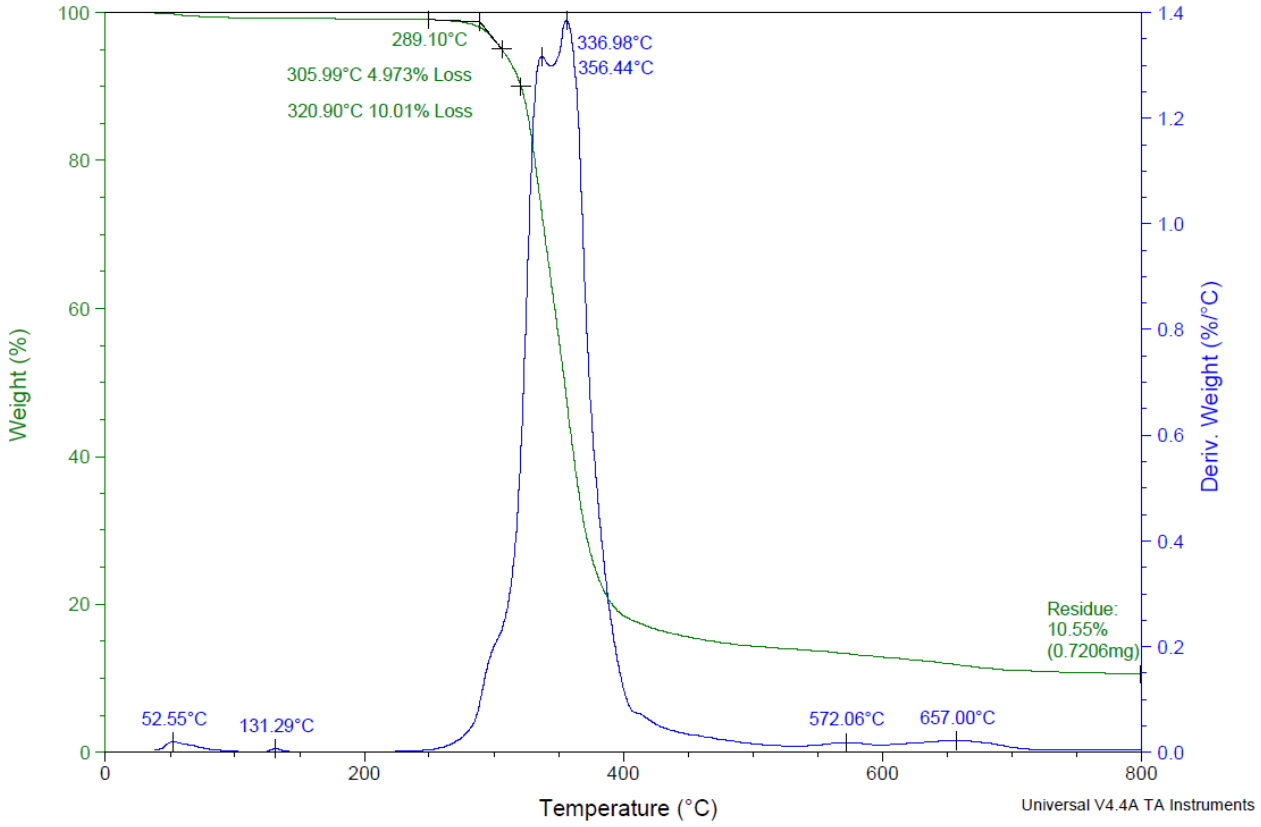

*Figure 57 - TGA curve of the evolution of the polymer **53** mass with the temperature (green) and the first derivative (blue)*

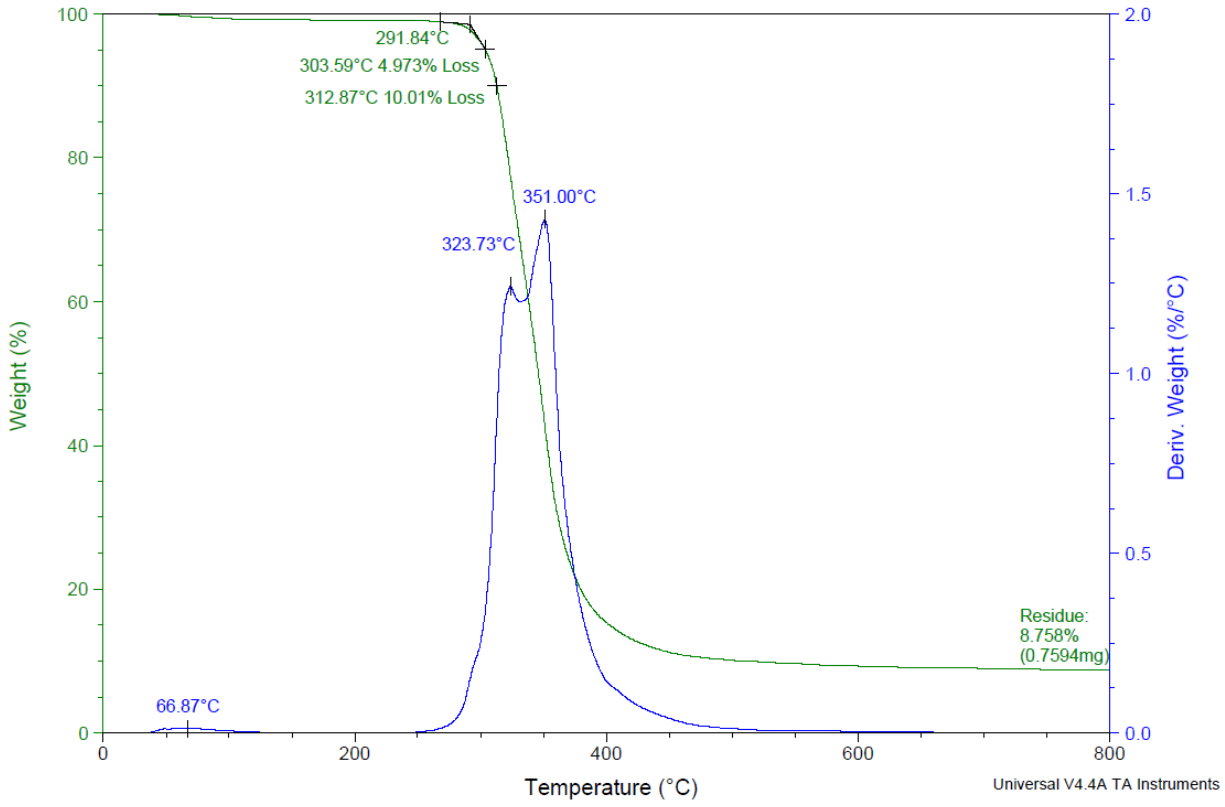

*Figure 58 - TGA curve of the evolution of the polymer **54H** mass with the temperature (green) and the first derivative (blue)*

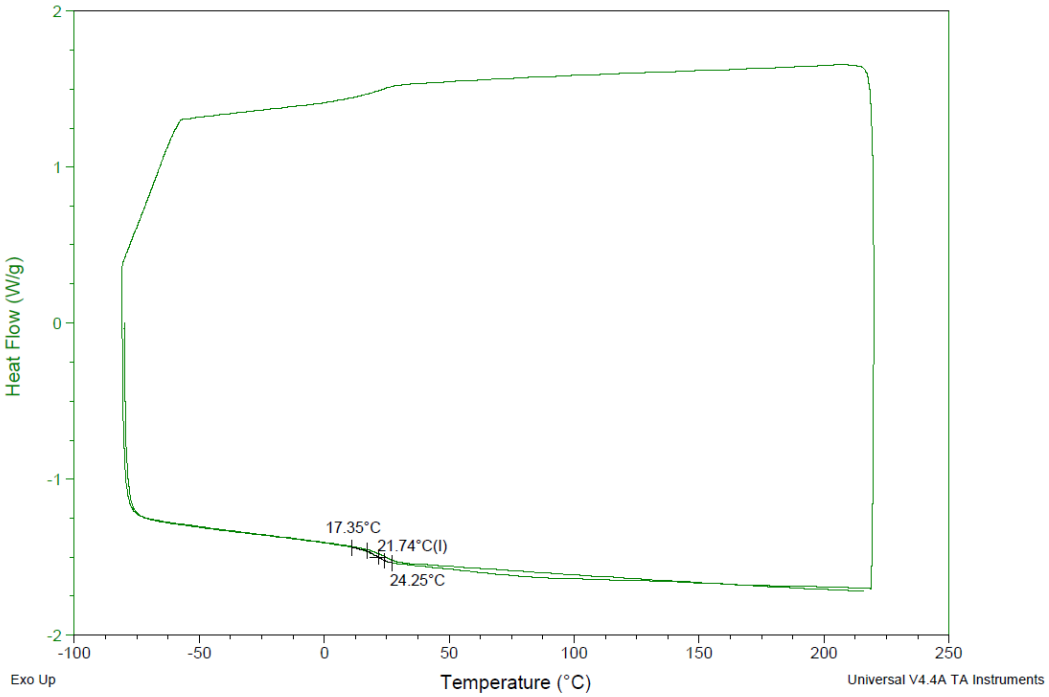

*Figure 59 - DSC curve of the evolution of the heat flow with the temperature for polymer **53***

Water-sensitive self-healing polymer networks based on the tris[2-formylphenyl]-boroxine **21** in association with 400 g.mol^{-1} poly(propylene glycol) bis(2-aminopropyl ether) **54**:

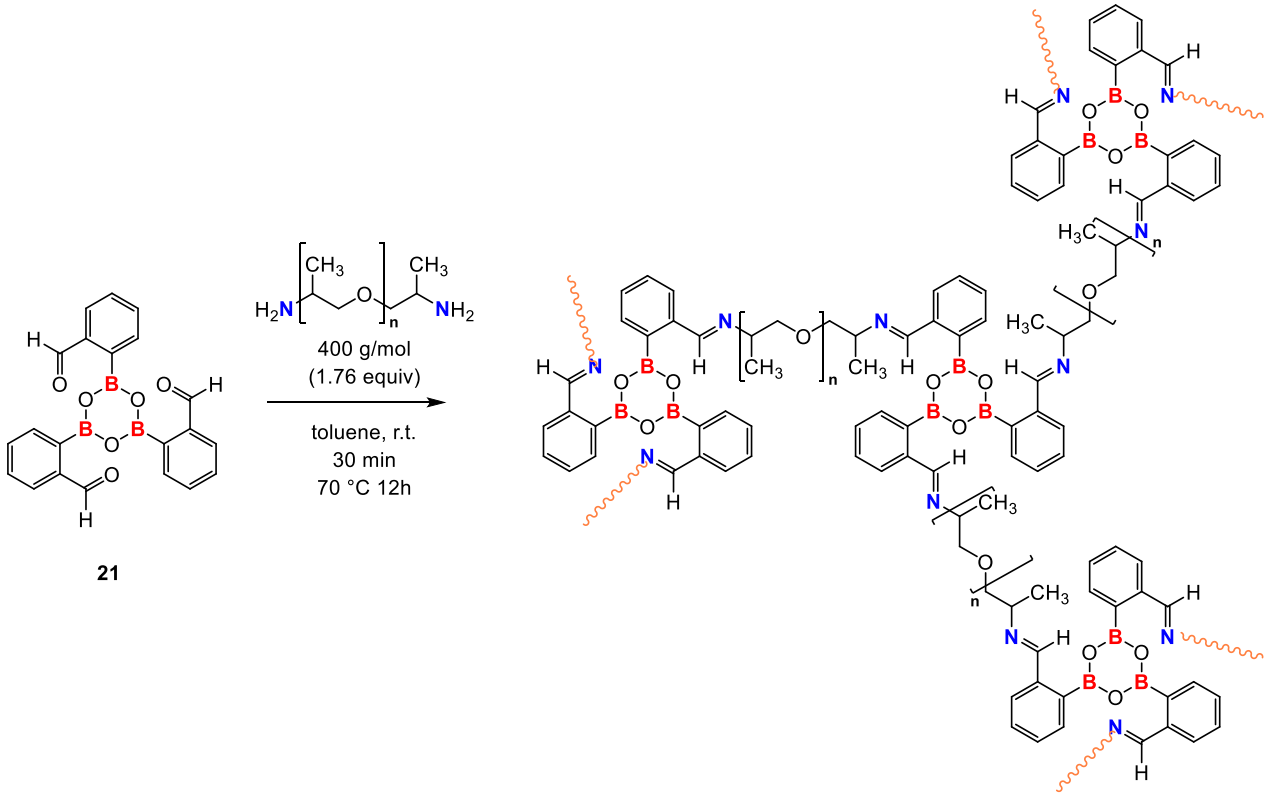

21 **51**

Poly(propylene glycol) bis(2-aminopropyl ether) (0.350 g – 0.88 mmol, 1.76 equiv) was added into a dry round-bottom flask with a solution of aryl-boroxine **21** (0.200 g, 0.50 mmol, 1 equiv) in toluene. After stirring 30 minutes under N_2 atmosphere, the reaction medium was poured into a mould and this latter was placed in oven at 70 °C for 12h to remove the solvent.

Yellow slightly sticky film.

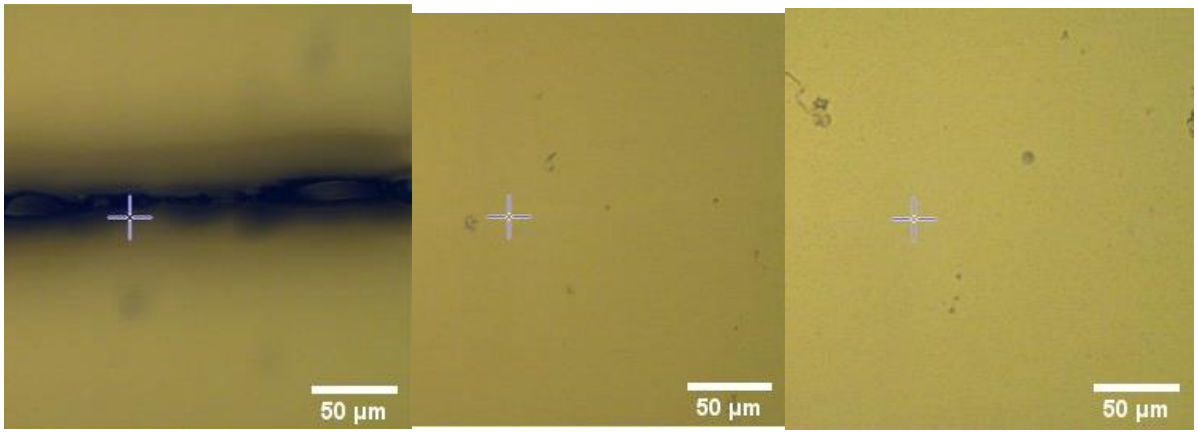

*Figure 60 - Microscope pictures of polymer **54** cut (left) repaired after 24h (centre) and 48h exposure to ambient humidity (right) at X20 magnification*

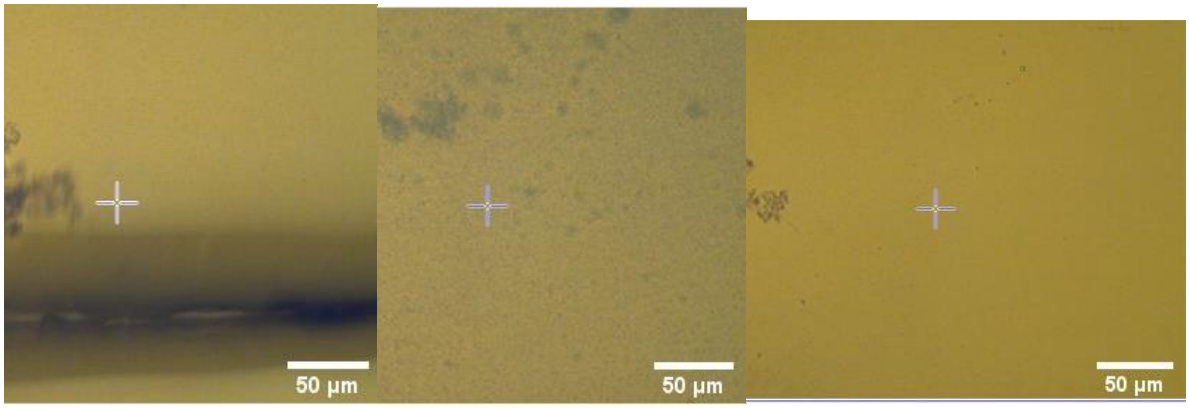

*Figure 61 - Microscope pictures of polymer **54** cut (left) repaired after 24h (centre) and 48h exposure to 43 % relative humidity (right) at X20 magnification*

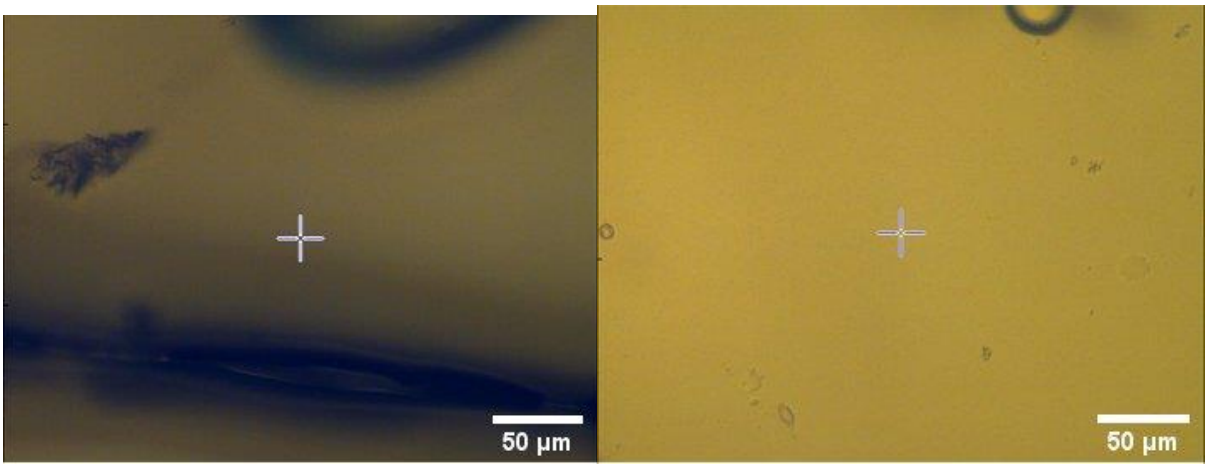

*Figure 62 - Microscope pictures of polymer **54** cut (left) and 48h exposure to 43 % relative humidity (right) at X20 magnification*

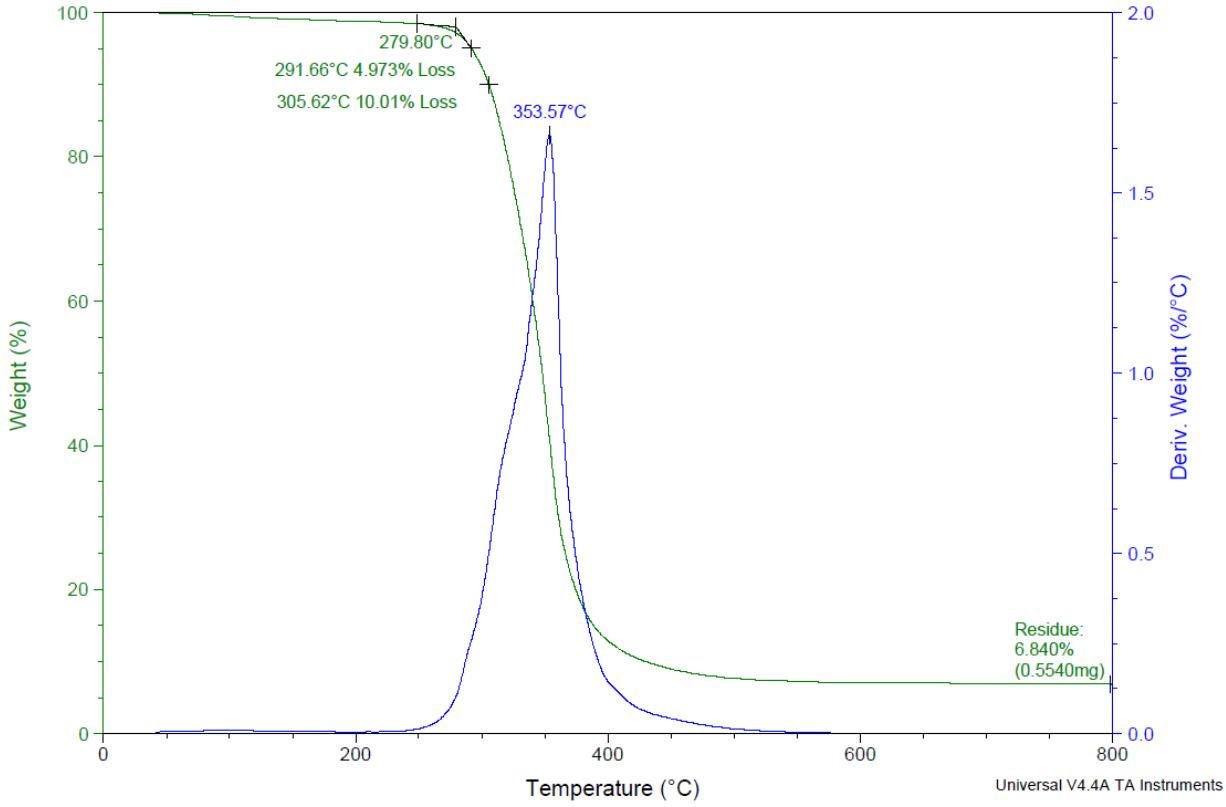

*Figure 63 - TGA curve of the evolution of the polymer **54** mass with the temperature (green) and the first derivative (blue)*

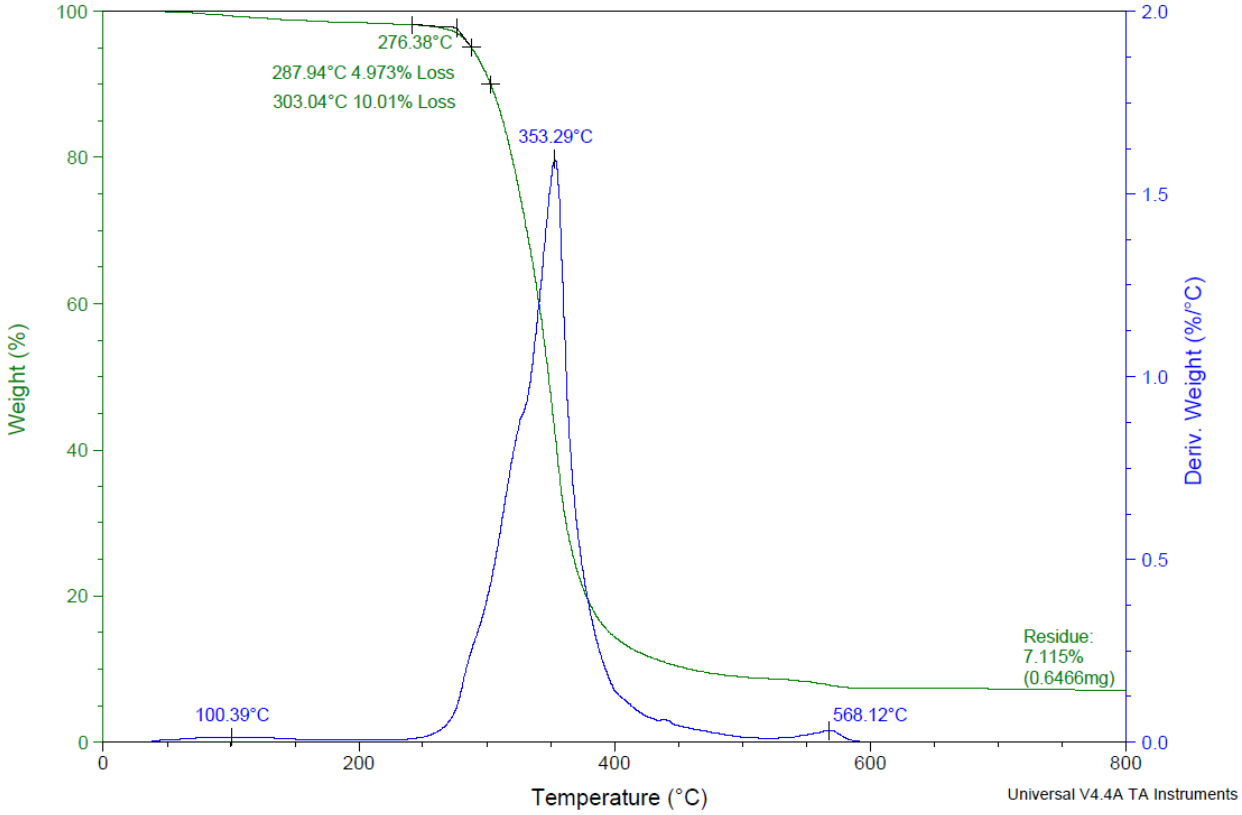

*Figure 64 - TGA curve of the evolution of the polymer **54H** mass with the temperature (green) and the first derivative (blue)*

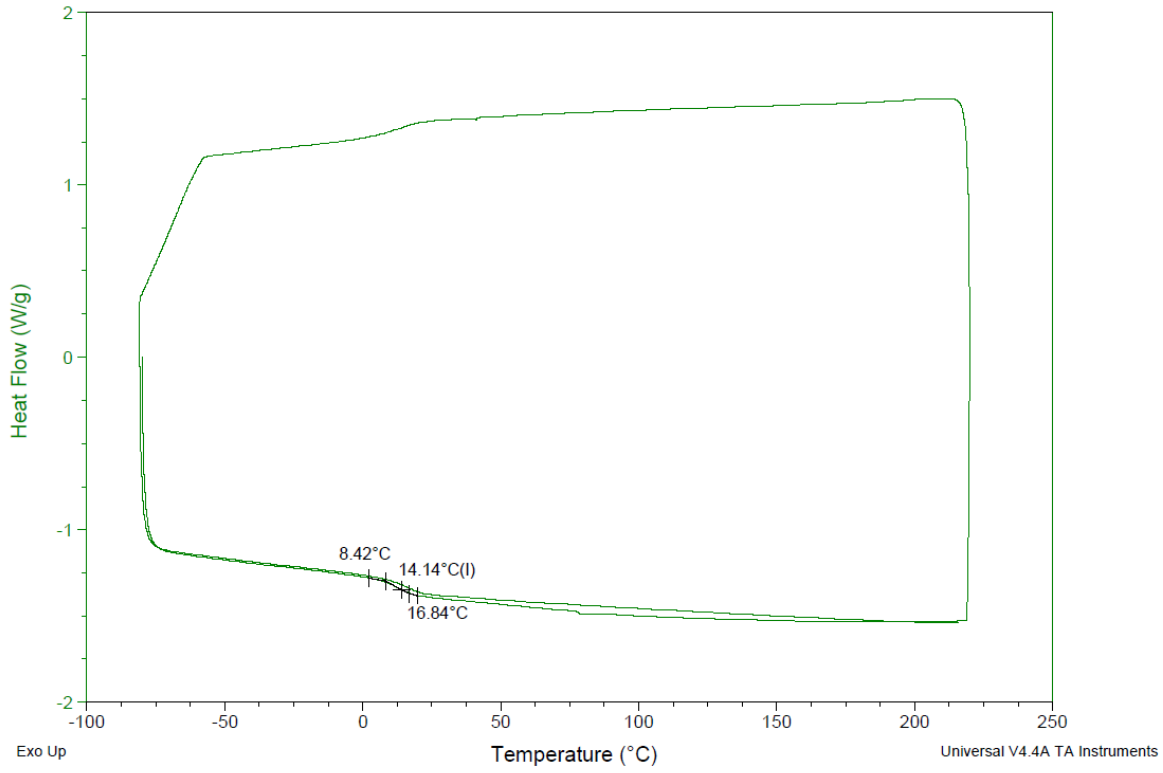

*Figure 65 - DSC curve of the evolution of the heat flow with the temperature for polymer **54***